The development of a rabies virus glycoprotein derivative for targeted nanoparticulate drug delivery across an *in vitro* blood brain barrier model

Rachel Huey

Faculty of Life and Health Sciences

Ulster University

Thesis submitted for the degree of Doctor of Philosophy

May 2019

I confirm that the word count of this thesis is less than 100,000 words excluding the title page, contents acknowledgements, summary or abstract, abbreviations, footnotes, diagrams, maps, illustrations, tables, appendices, and references or bibliography.

Declaration

I hereby declare that for 2 years following the date on which the thesis is deposited in the Research Office of the Ulster University, the thesis shall remain confidential with access or copying prohibited. Following expiry of this period I permit

1. The Librarian of the University to allow the thesis to be copied in whole or in part without reference to me on the understanding that such authority applies to the provision of single copies made for study purposes or for inclusion within the stock of another library.
2. The thesis to be made available through the Ulster Institutional Repository and/or EThOS under the terms of the Ulster e-Theses Deposit Agreement which I have signed.

Acknowledgement

I would like to extend my sincerest gratitude to those who have helped me over the last few years which has lead me to the completion of this thesis. I have deeply appreciated the help, advice and individual expertise of my supervisors, Dr Susan Hawthorne and Professor Paul McCarron. I must especially thank Susan for her endless support and encouragement during this project, who has been a pleasure to work with. I would also like to extend thanks to other members of staff within the School of Pharmacy at Ulster University who have been a great help to me. Finally, a word of thanks to my mum who has always believed in me and encouraged me to do my best.

Abstract

Parkinson's disease (PD) is a progressive neurodegenerative disorder, which has a devastating impact on the lives of patients, characterised primarily by the loss of dopamine-producing neurons in the brain. Drug delivery to the mammalian brain is notoriously difficult due to the physical and chemical restrictions presented by the blood brain barrier (BBB), a major contributing factor to the lack of disease-modifying treatments currently available for PD. This means that recovery from PD is not currently possible and clinical treatment is aimed at controlling symptom progression.

Neurotrophic factors (NTF) are promising treatments for the regeneration of dopaminergic (DA) neurons and offer the possibility of functional recovery in PD. However, the short half-life of NTF and invasive means of administration are limiting features in clinical trials of such promising treatments. Endogenous receptors expressed at the BBB and throughout the central nervous system (CNS) might present viable targets for achieving highly effective drug delivery to the brain in a non-invasive manner via peptide ligand-facilitated transport. Rabies virus-derived peptide (RDP) is a 39-amino acid derivative of the rabies virus glycoprotein (RVG) which has shown promise as an *in vivo* brain targeting ligand. RDP has gained attention for features such as neural cell targeting specificity and *in vivo* safety, making it an attractive ligand for development within brain delivery systems.

The experimental work reported herein describes the formulation and characterisation of RDP-conjugated polymeric nanoparticles (NP), which exhibited enhanced payload accumulation in neural cell types. It was demonstrated that cellular uptake was mediated by the neuronal nicotinic acetylcholine receptor (nAchR) specifically. RDP optimisation studies lead to the development of a smaller 18-amino acid analogue of RDP termed DAS, which showed enhanced serum stability whilst retaining neural-specific activity when tested in various cell types *in vitro.* A human-derived *in vitro* BBB model was designed and developed using a triple culture of brain microvascular endothelial cells (HBMVEC), astrocytes and pericytes. Transport studies using this BBB model revealed the significant targeting advantage of both RDP and DAS ligands

(compared to the unlabelled NP) in the ability to deliver a payload across this simulated biological barrier

RDP and derivatives such as DAS may offer a solution to the challenge of delivering therapeutics across the BBB. The development of a nanoparticulate drug delivery system decorated with an RDP derivative offers specific, non-invasive targeting to the brain alongside protection of unstable or sensitive cargo. Such drug delivery systems may be beneficial for the treatment of PD, as a means of depositing regenerative NTF directly to the diseased brain.

Abbreviations

°C- Degrees Celsius

BBB- Blood brain barrier

BCA- Bicinchoninic acid

bFGF- Basic fibroblast growth factor

BSA- Bovine serum albumin

CNS- Central nervous system

CPP- Cell penetrating peptides

DAS- Newly designed targeting peptide

DCM- Dichloromethane

DLS- Dynamic light scattering

DMSO- Dimethyl sulfoxide

FBS- Foetal bovine serum

FITC-dex- Fluorescein isothiocyanate–dextran

HBMVEC- Human brain microvascular endothelial cells

ICG- Indocyanine green

mg- Milligram

mL- Millilitre

mM- Millimolar

nAChR- Nicotinic acetylcholine receptor

NP- Nanoparticles

NTF- Neurotrophic factors

PBS- Phosphate buffered saline

PD- Parkinson's disease

PDI- Polydispersity index

PEG- Poly(ethylene glycol)

PLGA- Poly(D,L-lactide-co-glycolide)

PVA- Poly(vinyl) alcohol

RDP- Rabies virus-derived peptide

RVG- Rabies virus-derived glycoprotein

scDAS- Scrambled version of the newly designed targeting peptide

SD- Standard deviation

SDS-PAGE- Sodium dodecyl sulphate poly(acrylamide) gel electrophoresis

SNpc- Substantia nigra pars compacta

v/v- Volume/volume

v/w- Volume/weight

w/w- Weight/weight

µg- Microgram

µL- Microlitre

µm- Micrometre

Table of Contents

Chapter 1

Introduction

1.1. Parkinson's Disease

1.1.1. Neurodegeneration in Parkinson's Disease

In an 1817 essay, James Parkinson described a "shaking palsy" which often started in the hands and arms before spreading to the legs (Obeso et al., 2017). Nowadays, we know this condition as Parkinson's Disease (PD). In the UK, 1 in 37 people will be diagnosed with PD during their lifetime. Over 135 000 diagnoses of PD were reported for the UK in 2015, however this is projected to double by 2065 (Parkinson's UK, 2017). PD is more prevalent in the male and ageing populations, affecting 2% of those over 60 years old (Kalia & Lang, 2015) and is the second most common neurodegenerative disorder after Alzheimer's Disease (Bauer & Przedborski, 2003). PD affects the central nervous system (CNS), leading to a range of complications which progressively worsen with time.

Primarily characterised by the loss of dopaminergic (DA) neurons in the Substantia Nigra pars compacta (SNpc) region of the brain (Dawson & Dawson, 2003), this pathological event results in decreased output of the neurotransmitter, dopamine, along the nigrostriatal pathway (Figure 1.1). This pathway normally supplies the striatum region of the brain with dopamine, which is required for various functions associated with motor control. The gradual depletion in striatal dopamine causes impairment of motor function, resulting in many symptoms which can be classified as motor and non-motor symptoms. The striatum is best known for its essential role in voluntary motor control and is the major input source for the basal ganglia. However, it is also responsible for the integration of movement and reward responses in the brain, which can be linked to social behaviours (Baez-Mendoza & Schultz, 2013). Fully functioning striatal neurons in the healthy brain enable the planning, initiation and execution of movement in response to dopamine input (Tewari et al., 2016), which originates from the large, dopamine-containing neurons in the SNpc (Singer et al., 2010). It is when these cells of the SNpc are progressively depleted, that PD onset occurs. However, clinical manifestation of symptoms does not occur

until 50-70% of SNpc dopaminergic neurons are lost (Cheng et al., 2010). This greatly limits the chance of early detection in patients and is the most important factor for preventing life-threatening complications of the disease.

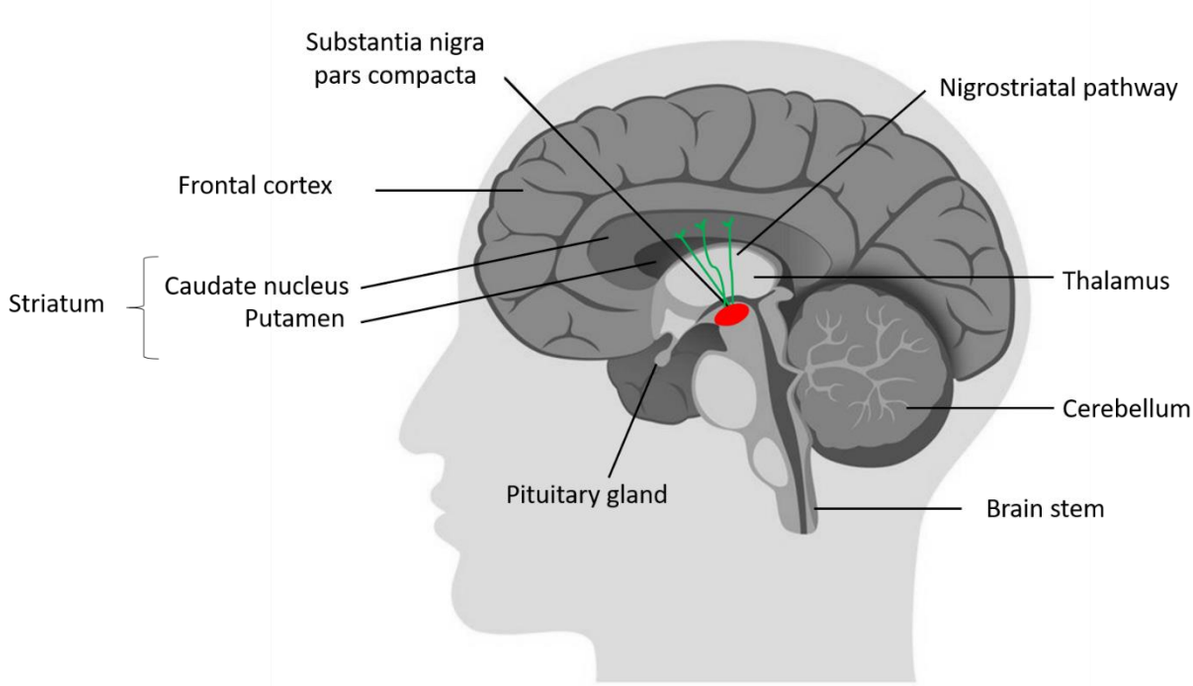

Figure 1.1. Simplified diagram of the human brain showing the anatomical location of the substantia nigra pars compacta (SNpc) (red) which is responsible for dopamine input to the striatum via the nigrostriatal pathway (green). Dopamine is a neurotransmitter in the brain involved in movement and reward pathways. Degeneration of dopaminergic (DA) neurons in the SNpc results in impaired motor control, the main symptom of Parkinson's disease.

1.1.2. PD symptoms

The symptoms of PD can be divided into two classes: motor and non-motor. Impairment of motor control, induced by considerable nigrostriatal dopamine depletion, is often the symptom first

detected by patients which leads to clinical diagnosis. This can manifest in several ways, including development of symptoms such as tremor, gait difficulties, postural instability, bradykinesia, speech impairment, stiffness and muscle rigidity (Lescaudron et al., 2012). PD is well-characterised by these motor symptoms; however non-motor symptoms often precede the onset of compromised motor control by many years (Marras & Chaudhuri, 2016). At some stage during their disease progression, 90% of patients experience loss of olfaction (sense of smell) as the most common non-movement related symptom (Pfeiffer, 2016). Other common symptoms include severe constipation and sleep disorders. In addition to this, depression and anxiety often occurs as a preceding symptom in around 30% of clinically diagnosed patients (Reijinders et al., 2009). These symptoms are difficult to detect in relation to PD and can quite easily be mistaken for many other common clinical conditions. In late stages of the disease, urinary dysfunction and orthostatic hypotension almost universally affect all patients, with a further 30-40% experiencing onset of dementia (Poewe, 2008).

In addition to parkinsonian symptoms, PD patients often suffer many debilitating side effects from current first-line treatment options such as hallucinations, psychosis, impulsive behaviours and further motor complications such as dyskinesias. Due to the widespread effects of this neurological disease throughout the whole body, quality of life can be severely compromised, particularly in the later stages. All aspects of the disease are difficult to manage, often requiring multiple medications for PD symptom control in addition to managing treatment-induced side effects. The use of polypharmacy greatly enhances the risk of adverse drug reactions. Often, risk-benefit approaches must be used to ensure the patient's quality of life is maintained as far as is practicable. Consequently, those responsible for patient care must prioritise treatment of different symptoms and patients may be required to tolerate certain side effects to maintain motor control.

1.1.3. PD pathology

Currently, the aim is to slow disease progression, however it is not reversible. At the point of clinical presentation, disease progression is believed to be too far advanced to benefit from neuroprotective treatments (Noyce et al., 2016). There is a vast range of clinical symptoms which PD patients may experience to differing extents and severities, reflecting the rate of disease progression which can be different for everyone. The complexity of this disease and its symptoms means that experts are still trying to understand the underlying pathology and what this means for patient prognosis. Recent research has suggested that disease progression may not be so random after all, as certain symptoms and factors such as age-onset have been grouped and identified to have similarities in relation to patient prognosis (Fereshtehnejad & Postuma, 2017). Developments in PD subtyping could provide better insight into which treatments may be successful and ultimately lead to better patient outcomes.

The detection of Lewy bodies in the cytoplasm of remaining SNpc DA neurons is a distinguishing feature in most cases of PD (Lo Bianco et al., 2004). Lewy bodies are aggregates of amyloid-like fibrils and cytotoxic α-synuclein protein deposited due to impaired clearance of misfolded proteins (Dawson & Dawson, 2003). Multiple mechanisms have been suggested to explain Lewy body formation, however it is generally accepted that the underlying pathology of PD is not yet entirely understood. Many contributory factors have been identified to date, including the production of reactive oxygen species (ROS). Indeed, it has been suggested that multiple mechanisms are likely to have a synergistic effect in causing PD (Yacoubain & Standaert, 2009).

PD pathology can be sporadic or genetic in nature (Timmer at al., 2007), resulting in cell apoptosis and Lewy body formation as a sign of defective cellular processes. Sporadic PD has no known cause and accounts for the majority of cases, however 15% of diagnosed patients have a family history of the disease (Deng et al., 2018). Family history is therefore a major risk factor for development of PD.

The discovery of mutations in the α-synuclein gene, SNCA, was the first indication that PD may have a genetic link. To date, six mutations in the SNCA gene, also known as PARK-1, have been identified to cause Lewy body-associated PD, although this only accounts for 2% of all PD cases (Rosborough et al., 2017). A mutation causing genomic triplication of PARK-1, can directly lead to α-synuclein accumulation and thus Lewy body formation, causing eventual neuronal cell apoptosis (Dawson & Dawson, 2003). The gene for Parkin (PARK-2) was identified second to SNCA or PARK-1 and is an E3 ubiquitin ligase, responsible for ubiquination of cellular proteins which determines their cellular fate (Klein & Westenberger, 2012). These discoveries have helped to identify more gene defects responsible for familial PD, such as DJ-1 and PINK-1. Mutations in PINK-1 (PTEN- induced kinase 1) or PARK-6, a mitochondrial kinase, can lead to loss of enzymatic activity and result in abnormal oxidative stress response (Schapira, 2009). Furthermore, PINK-1 protein works alongside Parkin to remove damaged mitochondria (Gladkova et al., 2017). DJ-1 (PARK-7) is a cellular sensor protein of oxidative stress and, along with SNCA and PINK-1, is associated with early-onset PD (Deng et al., 2018).

The aforementioned genes are associated with normal functioning of the ubiquitin-proteasomal system (UPS), otherwise known as the cell proteasome. The UPS is responsible for the detoxification and clearance of misfolded and damaged proteins (Lo Bianco et al., 2004). Mutations in genes which affect the ability of the UPS to break down protein aggregates in the cell cytoplasm, leads to α-synuclein accumulation i.e. Lewy bodies.

Another major gene associated with risk of familial PD is that for the large 268 kDa protein, LRRK2 (leucine-rich repeat kinase 2). LRRK2 (also known as PARK-8) is an enzyme involved in cell signalling with complicated regulation pathways, thought to have multiple cell functions (Price et al., 2018). Understanding of these pathways and events are important advances for PD research. Defects in LRRK2 has been identified as a causative factor in sporadic PD, as has UCH-L1 (Ubiquitin carboxy-terminal hydrolase L1), an enzyme which has stabilising functions within the UPS (Osaka et al., 2003). Ongoing enquiry into the genetic causes of PD continues to identify new mutations, such as CHCHD2, a gene which encodes a stress-response protein

involved in the negative regulation of mitochondria-mediated apoptosis (Puschmann, 2017). Indeed, many of the genes contributing to PD pathology previously discussed have also been identified in astrocytes, the most abundant glial cell of the brain (Booth et al., 2017). Further studies into the role of astrocytes in PD are required, however early investigations suggest that pathological events may occur in more than one cell type.

Two major pathological events have been identified thus far which are instrumental in causing DA neuron degeneration. Firstly, cytosolic deposits of misfolded or aggregated proteins and secondly, mitochondrial dysfunction (Dauer & Przedborski, 2003). The sequence in which these events occur is not clear and therefore it is difficult to identify cellular targets for effective treatment. Oxidative stress due to the production of reactive oxygen species (ROS) is implicated as the major cause of neurodegeneration in PD, damaging important cell proteins, DNA and organelles such as the mitochondria. ROS such as hydrogen peroxide and superoxide are produced by all tissues of the body as part of the respiratory process and signalling events in the mitochondria (Hauser & Hastings, 2013). In normal circumstances, these oxygen-derived free radicals are controlled by endogenous anti-oxidants such as glutathione and thus prevent the imbalance which causes oxidative stress (Yuan et al., 2007). It was reported by Sian et al. (1994) that reduced levels of antioxidant molecules were detected in the SNpc of PD patients compared to healthy individuals (Sian et al., 1994). Furthermore, upregulation of DNA repair enzymes has been observed in PD patients, possibly triggered due to oxidative damage (Zhang et al., 1999).

ROS can accumulate from a number of events such as impairment of mitochondrial complex 1 activity, dopamine metabolism, neuroinflammation, environmental toxins and glutamate excitotoxicity (Schapira, 2008). These pathogenic events which lead to the overproduction of ROS may also be caused by some of the genetic mutations previously mentioned. Oxidative stress caused by ROS is therefore implicated in both sporadic and familial forms of the disease. Figure 1.2 summarises the different sources of ROS production implicated in PD aetiology.

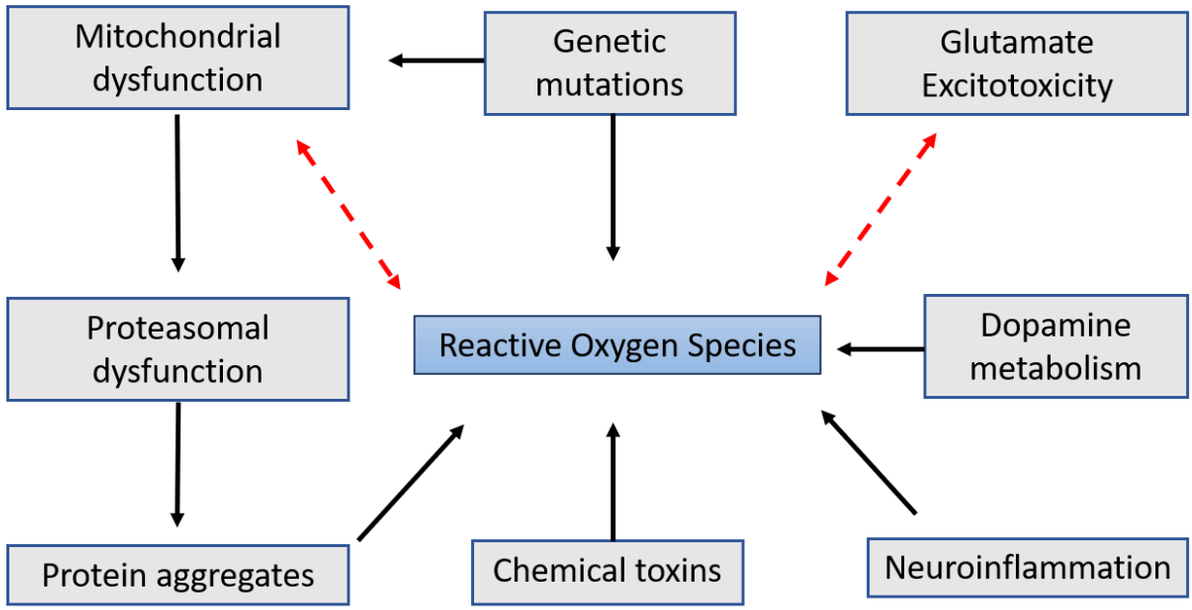

Figure 1.2. Pathogenic factors influencing the generation of reactive oxygen species (ROS) in Parkinson's disease. Overproduction of ROS results in oxidative stress, which is harmful to cellular organelles and DNA.

Mitochondrial complex 1 is a major enzyme complex involved in cellular respiration (Mimaki et al., 2012). The mitochondria are responsible for ATP (adenosine triphosphate) synthesis, a process which requires oxygen and nutrients (Fukae et al., 2007). It has been suggested that dysfunction of this complex is the major cause of oxidative stress and ROS production in non-familial sporadic PD (Schapira, 2008). ROS can induce further mitochondrial complex 1 damage, leading to a detrimental cycle of ROS production which ultimately results in cell apoptosis. Lysosomal function in neurons might also be affected in this cascade of events, affecting cellular enzyme activity (Burbulla et al., 2017). This makes PD research very challenging, as new treatments cannot be developed until these mechanisms are understood.

Glutamate transmission is responsible for most of the excitatory synaptic activity in the mammalian brain and thus is a major source of ROS (Carrillo-Mora et al., 2013). Glutamate

metabolism and ROS production are interrelated as one phenomenon can induce the other, leading to a cycling of events resulting in neurodegeneration (Gilgun-Sherki et al., 2001). Metabolism of the catecholamine neurotransmitter dopamine generates hydrogen peroxide, which in turn can produce cytotoxic hydroxyl ions (Meiser et al., 2013). It is thought that because of this, dopamine-containing neurons of the SNpc are exposed to a higher level of ROS and oxidative stress than other brain regions (Yuan et al., 2007). However, more insight is required into how this mechanism of ROS production correlates with PD onset. Dopamine may be oxidised in response to dysfunctional mitochondria, leading to deposits of the dark pigment neuromelanin (Rodriguez et al., 2015). This product of oxidised dopamine, proteins and lipids is responsible for the characteristic dark appearance of the SNpc in the mammalian brain (Beach et al., 2007), however it has also been implicated as a cause for neuroinflammation.

High density areas of microglial activation have been identified in the SNpc of both familial and sporadic PD patients (Blesa et al., 2015). Microglia, the resident immune cells of the CNS, release ROS in response to environmental stressors and neurotoxins (Block et al., 2007). Microglia normally function in a protective capacity, however in circumstances where the inflammatory response is amplified neurotoxicity is triggered (Mosley et al., 2006; Goldberg & Tansey, 2010). One cause of neuroinflammation may be the release of neuromelanin from dying dopamine-containing neurons (Zucca et al., 2004). Alternatively, chemical neurotoxins such as MPTP and 6-hydroxydopamine (6-OHDA) have been shown to induce similar responses due to ROS generation (Tansey & Goldberg, 2010). Such chemicals have consequently been associated with a higher risk of developing PD (Elbaz et al., 2009). 6-OHDA and chemical pesticides such as rotenone and paraquat can induce classic parkinsonian symptoms in animal models for preclinical studies (Dauer & Przedborski, 2003; Zeng et al., 2018). In a study by Ascherio et al. (2006), a 70% higher incidence of PD was reported in humans who had been exposed to pesticides during their lifetime, compared to those who had never been exposed. Environmental exposure to pesticides used mainly in cereal and potato crops were reported to increase the risk of developing PD in a study by Brouwer et al. (2017).

1.2. PD treatments

1.2.1. Current PD treatments

Current pharmacological management of PD is focused on providing symptomatic relief of motor symptoms, so that patients can maintain enough functional ability to carry out daily activities. Clinical management of PD is not yet at the stage where restoration of neurons or prevention of disease progression is possible, however current research is geared towards achieving this. The National Institute for Health and Care Excellence (NICE) advises that dopamine therapy should be prescribed as a first line treatment for PD patients with motor symptoms. This approach which aims to replenish striatal dopamine levels has been rather successful in achieving reasonable control of motor symptoms in the early to mid-stages of the disease. NICE clinical guideline 71 (NICE, 2017) recommends levodopa and if necessary, a dopamine agonist or monoamine oxidase-B (MAO-B) inhibitor as an adjunctive treatment for first line therapy for the treatment of troublesome motor symptoms. Levodopa is a prodrug of dopamine, capable of crossing the BBB where it is then metabolised to dopamine (Khor & Hsu, 2007). The most common pharmaceutical preparation of levodopa is co-beneldopa, a combination of levodopa and benserazide, a peripheral aromatic amino acid decarboxylase inhibitor (Kim et al., 2017). Despite the improvement in motor control and ability to carry out daily activities afforded by levodopa therapy, it does cause complications with prolonged use (Tomlinson et al., 2010). Long-term effects of levodopa therapy can cause dyskinesias, which are abnormal, repetitive involuntary movements commonly affecting the facial, oral and neck muscles (Fox & Lang, 2008). Dystonic posturing of the limbs can often occur during peak concentration of levodopa dose (Jankovic, 2005). In addition to this, impulsive control disorder (Starkstein et al., 2012) and excessive sleepiness (Chaudhuri & Logishetty, 2009) are also common side effects.

Dopamine agonists such as ropinirole and pramipexole activate the dopamine receptor to induce the same physiological response as endogenous dopamine (Bonuccelli & Pavese, 2006). MAO-

B inhibitors such as selegiline prevent the breakdown of dopamine in the brain, maximising the availability of this neurotransmitter to neurons (Elmer & Bertoni, 2008). Dopamine agonists and MAO-B inhibitors are less likely than levodopa to cause motor complications but are not as effective and therefore are rarely sufficient as stand-alone therapies (Gray et al., 2014).

Side effects of dopamine treatments can range in severity however often require pharmacological management. Psychotic symptoms such as hallucinations, delusions and depression occur in many patients (Friedman et al., 2000). Anti-psychotic drugs such as quetiapine and clozapine are recommended by NICE alongside a reduction in any dopamine agonist medication. Anti-psychotic drugs antagonise the D2 dopamine receptor and thus can worsen the symptoms of PD (Suchowersky, 2002). Treatment or a reduction in dopamine replacement therapy is also required for symptoms of dementia, sleep disturbance, restless leg syndrome and orthostatic hypotension (Pourcher et al., 2010). The clinical management of this disease therefore requires multiple drugs and introduces complex polypharmacy which often requires intense monitoring for drug interactions and risk-benefit analysis.

At late stages of the disease most dopamine replacement strategies are ineffective and cannot sufficiently manage debilitating “off periods” to allow initiation of movement on a daily basis. At such times, last resort treatments such as daily infusion of the potent dopamine agonist apomorphine is necessary (Salat et al., 2013). This is inconvenient, restrictive and expensive requiring multidisciplinary management. It is for these reasons, that the aim of current PD research is to find preventative and neuroprotective means of managing the disease (Kelly et al., 2015). Ultimately, restoration of DA neurons in the SNpc would be the optimal outcome of PD treatment. This novel approach however remains distant from the clinical setting, as significant progress in clinical trials is yet to be made.

.

1.2.2. Prospective treatments for PD

1.2.2.1. Antioxidants

New approaches aiming to preserve neurons in the SNpc and prevent disease progression are currently being investigated as an alternative to dopamine replacement initiatives. Ongoing research has identified many potential drug candidates which are targeted towards different pathological aspects of the disease. Due to the major involvement of oxidative stress in DA neuron degeneration, antioxidants were explored in the early 1990s as a potential means of containing the widespread production of ROS in PD. In theory, antioxidants may have some potential application in the treatment of PD, however clinical data to date has not provided enough evidence of efficacy (Chang et al., 2018). In a pilot study, Fahn (1992) indicated that vitamin E supplementation may delay the need for levodopa in PD patients by 2.5 years. Following this, the DATATOP trial was set up by The Parkinson Study Group (1993) as an investigation into the effect of antioxidant vitamin E. This trial however, concluded that selegiline was effective in delaying PD progression in human participants but antioxidant vitamin E was not. Since then, uric acid and selenium have also been proposed as antioxidants which may have some therapeutic benefit in PD (Yacoubian & Standaert, 2009).

In a study by Gao et al. (2008) a link was reported between high dietary uric acid and a decreased risk of PD in men. A neuroprotective effect from high levels of serum urate has been linked with a decrease in PD risk due to its potent antioxidant activity, however results thus far have been mixed. O'Reilly et al. (2010) concluded that high serum urate levels in women was not associated with a lower risk of PD. The use of this antioxidant molecule has been revisited in recent studies, showing reduced α-synuclein accumulation in transgenic mice (Sheng et al., 2017) and association with lower PD risk in both men and women (Cortese et al., 2018). Due to the risk of developing gout and cardiovascular problems from high dietary uric acid intake, Bi et al. (2018) aimed to maximise endogenous urate activity through upregulation of the Glut-9 transporter. The results from this study supported the action of urate as a neuroprotective agent in an animal model of PD.

Selenium acts a glutathione promoter and has gained attention for its neuroprotective effects in animal models of PD (Zafar et al., 2003). The antioxidant activity of selenium has also been associated with positive effects on co-ordination and speed of tasks in PD patients by Shahar et al. (2010). Dietary sources of selenium may help to reduce PD risk however direct association is yet to be established.

1.2.2.2. Anti-inflammatory agents

Attempts to reduce neuroinflammation have been made with the use of non-steroidal anti-inflammatory drugs (NSAIDS) such as ibuprofen, celecoxib, rofecoxib and naproxen with quite poor results in animal models of PD (Goldberg & Tansey, 2010; Moore et al., 2010). The dose of NSAID needed to have a significant therapeutic effect in PD may be too high for safe use, particularly due to risk of GI and cardiovascular side effects. The lipophilic tetracycline derivative minocycline has gained much attention recently for its positive effects in the SNpc of animals (Du et al., 2001; He et al., 2001; Nam et al., 2014). Recent studies have been promising as minocycline has prevented neuronal loss, partially restored neuronal function and reduced neuroinflammation in neurotoxin-induced animal models of PD (Cronin & Gready, 2017; Verma et al., 2018). Ongoing investigations using minocycline as a therapeutic agent is certainly warranted due to these promising results. Another molecule which has improved PD-like behaviours in MPTP- and rotenone-induced animal models is the plant flavone, baicalein. The neuroprotective effect of baicalein in mice may be due to various mechanisms of action including restoration of mitochondrial function (Zhang et al., 2017), reduction of neuroinflammation (Lee et al., 2014) and antioxidant activity (Cheng et al., 2008; Mu et al., 2011).

1.2.2.3. Other neuroprotective agents

Neuroprotective properties of existing and well-known drugs have been identified as potentially useful treatments for PD. The calcium channel antagonists dihydropyridine and nimodipine have been utilised to reduce NMDA receptor-mediated glutamate excitotoxicity in an animal models

(Kupsch et al., 1996 & Schapira, 2009). Furthermore, the adenosine (A_{2a}) receptor antagonist caffeine was indicated to preferentially enhance dopamine signalling amongst men, thus reducing the incidence of PD (Ascherio et al., 2001). However, following an extensive review of clinical trials by Schapira (2009), it was reported that A_{2A} antagonists in general failed to provide sufficient symptom control to be used as effective PD treatments. To date, minimal focus has been directed towards the targeting of α-synuclein deposits within DA neurons. Modulation of the stress response which occurs due to α-synuclein may be a promising approach in the treatment of PD, as enhanced activation of chaperone molecules such as heat shock protein-70 (HSP-70) can protect cells from such toxicity (Auluck et al., 2005). Geldanamycin is such a drug which may induce HSP-70 activity and reduce α-synuclein aggregation (McLean et al., 2004).

The development of these novel approaches has involved targeting many of the major factors in PD pathology including oxidative stress and neuroinflammation. In theory, therapeutic agents which target these areas could provide improvement in symptoms, slow disease progression and lower overall risk of PD. The results from these investigations however have been varied, preventing progression to large scale clinical trials. Due to this, the introduction of new and effective PD treatments has been hindered in recent years.

1.2.3. Neural stem cells

PD therapy could benefit from novel disease-modifying strategies such as DA neuron replacement. Cell replacement is the newest approach for overcoming the loss of striatal dopamine and preventing disease progression. Advances in stem cell medicine have encouraged this route, as it has been shown that human pluripotent embryonic stem cells can be induced to differentiate into motor neurons (Li et al., 2008a) and DA neurons (Stanslowsky et al., 2014) *in vitro.* Currently human induced pluripotent stem cells are gaining recognition for their ability to differentiate into somatic cell types, with the advantage of being derived from adults rather than embryos (Appelt-Menzel et al., 2017). Small molecules such as retinoic acid,

purmorphamine, sonic hedgehog and various neurotrophic growth factors can be utilised to create the environment required for the differentiation of stem cells to neurons. Cultured neurons derived from stem cell sources may be transplanted into the brain *in vivo*, however this is invasive and would involve major surgery. Furthermore, difficulties with ethical issues, tumourgenicity and unstandardised cultivation methods still surround stem cell transplant initiatives (Coutts & Keirstead, 2007).

The formation and integration of new neurons (neurogenesis) in the brain was once viewed as an event which only occurred during the embryonic stages of life. It is now accepted that new neurons are formed during adulthood but only in restricted regions and in response to environmental cues (Decimo et al., 2012). Neural progenitor cells with the ability to proliferate and differentiate to form a neuronal phenotype *in vitro* have been isolated from various areas in the brain including the olfactory bulb, hypothalamus, SNpc and the striatum (Lie et al., 2002). Despite this, there is no convincing evidence that progenitor cells found in the SNpc produce new neurons *in situ,* even in the healthy brain (Farzanehfar, 2018). It is therefore likely that the *in vivo* microenvironment inhibits the differentiation of these cells to neurons and thus DA neurons are not replaced as a natural response to PD pathology (Van der Berge et al., 2013). A deeper understanding of the nigrostriatal pathway microenvironment in the brain might offer useful insight into how the induction of neurogenesis, which has been demonstrated *in vitro,* might be replicated *in situ*.

The origins of neural progenitor cells in the human brain are still being uncovered, however two of the best characterised areas are the subventricular zone (SVZ) of the lateral ventricle wall and the subgranular zone (SGZ) of the hippocampal dentate gyrus (Decimo et al., 2012). The areas where neural stem cells reside are known as niches, where environmental stimuli determine their fate. Neural stem cell populations proliferate to form neural progenitor cells, also known as the C cells, which migrate from niches to other areas of the brain (Van der Berge et al., 2013). Following proliferation, neural progenitor cells subsequently differentiate into neuroblasts, also known as the B cells. Neuroblast formation and migration has been reported in instances of

brain injury, including formation of new neurons in the striatum in response to stroke (Arvidsson et al., 2002; Yamashita et al., 2006). Neurogenesis in the SVZ and SGZ occurs throughout adult life, however the natural proliferative potential of these cells is thought to decrease with age (Apple et al., 2017). The ability of the brain to repair is therefore reduced with age, explaining the high incidence of neurodegenerative diseases in the elderly population.

The close anatomical proximity between the SVZ and the striatum may permit the mobilisation of neural stem cells in response to certain stimuli and promote the formation of new DA neurons. This would be an attractive neurorestorative approach for PD treatment, overcoming many of the issues surrounding current treatment modalities. Naturally occurring neural progenitor cells outside the stem cell niches of the SVZ and SGZ do not normally regenerate neurons in response to injury or disease, however can produce new glial cells *in vivo* (Lie et al., 2002). In a study by Ernst et al. (2014), the integration of new neurons in the adult striatum was detected following migration from the neighbouring SVZ. The fact regeneration of neurons can occur *in situ* provides hope that therapeutic stimulation of such processes might prove beneficial in PD patients.

Many studies have shown that *in situ* neuronal regeneration is possible in response to environmental stimuli such as neurotrophic factors (NTF). Although many NTF are endogenously expressed, they may not be released in sufficient quantity to induce regeneration of neurons in toxic neurodegenerative conditions (Wang et al., 2004). Alternatively, the natural microenvironment may be inhibiting the secretion of NTF.

1.2.4. Neurotrophic factors (NTF)

NTF have important functions in the CNS and their use within PD is perhaps one of the most exciting new prospects due to positive results in animal models (Kelly et al., 2015). NTF are secretory peptides or small proteins which are involved in the development, differentiation, protection and maintenance of neurons to adulthood and thus offer the possibility of neuronal

regeneration (Hegarty et al., 2014). The ability to stop neuronal degeneration and possibly restore DA neurons in the SNpc are approaches not possible with the drug candidates discussed in section 1.1.5. NTF describe a subclass of growth factors which exert their action predominantly through tyrosine kinase signalling (Huang & Reichardt, 2001).

1.2.4.1. Recent studies of NTF in animal models

There has been considerable success in the improvement of PD symptoms following viral vector delivery of neurturin (NRTN), platelet-derived growth factor (PDGF), cerebral dopamine neurotrophic factor (CDNF) and glial cell-derived neurotrophic factor (GDNF) into the striatum of animals (Kelly et al., 2015). Significant benefit in humans however has yet to be demonstrated in clinical trials. Bartus et al. (2011) reported on the safe and effective administration of NRTN with positive outcomes in neurotoxin-induced animal models, which subsequently lead to clinical trials involving human participants. A follow-up phase II clinical trial however failed to provide enough evidence of efficacy to reach the primary endpoint of the study, which was to improve "motor-off" scores (Bartus et al., 2013). Despite this, there is still substantial evidence from studies in rodents to indicate that NRTN may be a successful treatment option in the future for PD (Herzog et al., 2013).

It was demonstrated by Zachrisson et al. (2011) how intracerebral administration of a PDGF isoform (PDGF-BB) resulted in long-term restoration of DA neurons in rodents. Increased expression of dopamine transporter sites and higher levels of tyrosine hydroxylase, the rate-limiting enzyme in catecholamine synthesis, were detected in the substantia nigra region. This study by Zachrisson et al. (2011) also detected proliferation and mobilisation of neural progenitor cells in the sub-ventricular zone of the brain *in vivo.* Furthermore, proliferation of non-neuronal cell types in the brain following PDGF-BB administration indicated that mobilisation of non-neural progenitor cells may have also have protective effects in PD.

Cordero-Llana et al. (2015) reported on the synergistic effect of cerebral dopamine neurotrophic factor (CDNF) and mesencephalic astrocyte-derived neurotrophic factor (MANF) after co-

administration to the substantia nigra of rats. The combination of both NTF was beneficial for improving control of motor symptoms in a rat model.

GDNF is perhaps the most studied neurotrophic factor with a wealth of positive results in the literature reported in animal models for its neuroprotective and restorative effect on DA neurons. GDNF has shown efficacy and safety in multiple animal models of PD, increasing dopamine levels in the striatum and diminishing motor deficits in some of the earliest investigations into NTF (Beck et al., 1995; Bowenkamp et al., 1995; Fox et al., 2001; Emborg et al., 2009). The role of GDNF in PD research has progressed from preclinical studies to clinical investigations involving human participants. A large phase II clinical trial on the use GDNF in idiopathic PD was completed in 2017 by the NHS Bristol Trust (TG Study Group, 2017). The data indicated that GDNF was safe and well-tolerated, however failed to show significant therapeutic benefit to progress to phase III studies. This trial was subsequently extended and is currently ongoing.

Basic fibroblast growth factor (bFGF), also known as FGF-2, is a multifunctional 146-amino acid polypeptide native to the CNS, which has an important role in neuronal survival at different stages of development from embryogenesis to adulthood (Abe & Saito, 2001). Endogenous bFGF has been found localised to DA neurons and glial cells in the SNpc, which expresses at least three high affinity bFGF tyrosine kinase receptors (Claus et al., 2004). Tooyama et al. (1993) reported that approximately 80% of DA neurons express bFGF in the healthy brain. The expression of bFGF in the remaining DA neurons of PD patients however is severely depleted, with only 13% of the DA neuronal population expressing this NTF. Following this, Takayama et al. (1995) demonstrated how bFGF could be utilised *in vivo* to promote the survival of transplanted embryonic DA neurons in a mouse. Since then, bFGF has gained attention for its pro-survival and mitogenic effects in regenerative stem cell medicine and in neural progenitor cell populations (Jin et al., 2005; Timmer et al., 2006)

Studies have shown that overexpression of bFGF in animal models can mobilise transplanted neural progenitor cells to migrate through injured tissue (Dayer et al., 2007) and directly stimulate neurogenesis in the dentate gyrus to form new neuronal populations *in situ* (Yoshimura et al.,

2003). In the adult brain, neurogenesis is unique to the SVZ and hippocampal dentate gyrus, however multipotent progenitor cells exist throughout different regions of the brain. These cells can be isolated and respond to environmental cues which induce differentiation. Palmer et al. (1999) induced the differentiation of multipotent progenitor cells from naturally non-neurogenic tissue within the CNS into neurons, a response which only occurred in the presence of bFGF.

Timmer et al. (2007) showed how endogenous bFGF was important for protecting DA neurons from neurotoxin injury in mouse models. Mice deficient in bFGF showed much higher susceptibility to the cytotoxic effects of 6-OHDA, illustrating the role of bFGF in neuronal repair mechanisms. A potent inducer of mitosis, bFGF has also shown regenerative potential in the peripheral nervous system due to regulation of remyelination and axonal growth of injured neurons (Jungnickel et al., 2006).

The evidence from the literature would suggest that bFGF is an ideal candidate for developing into a potential neurorestorative treatment for PD. It is unlikely that a single NTF provides the support required for neuronal replacement and development in the central and peripheral nervous systems (Grothe & Timmer, 2007), therefore bFGF could be utilised alongside some of the other NTF previously mentioned. Combinations of NTF such as bFGF and epidermal growth factor (EGF) may provide the environmental cues required to upregulate the differentiation capacity of native neural stem cell populations (Wang et al., 2004). For NTF to be successful *in vivo,* they require delivery to the brain via a suitable vehicle or targeted drug carrier to avoid peripheral metabolism.

NTF have a short half-life and are unable to cross the blood brain barrier (BBB). Most animal studies to date have used direct intracerebral infusion, bolus injections and transplant procedures as a means of effective administration. For humans, these methods are invasive, inconvenient and have raised concerns on patient safety (Kelly et al., 2015). It has also been suggested that the administration site may have an effect on the activity of GDNF (Sullivan & Toulouse, 2011). Lin et al. (2017) recently developed a biological scaffold derived from the extracellular matrix for the sustained release of bFGF, which successfully improved PD-like behavioural symptoms in

rats. Invasive transplant into the striatum was still required to overcome the BBB and achieve efficient therapeutic levels of bFGF in the brain. A delivery vehicle permitting sustained release of therapeutic agent for neuronal regeneration in the parkinsonian brain is an exciting new approach in the search for a PD cure.

1.3. The blood brain barrier (BBB)

The blood brain barrier (BBB) is the interface between the circulating blood and the brain, which tightly regulates the exchange of nutrients, cells, pathogens and metabolites (Wilhelm et al., 2011). Essential for normal function of the CNS, the BBB maintains homeostasis of the brain microenvironment and protects neural tissue from potentially harmful blood-borne substances (Schenk et al., 2016). The BBB is composed of brain microvascular endothelial cells (BMVEC) supported by a capillary basement membrane embedded with pericytes and astrocyte end-feet, as shown in Figure 1.3. Pericytes provide structural support and hence are important for barrier integrity (Sweeney et al., 2014). Astrocytes have roles in the formation, regulation, function and permeability of the BBB, cross-communicating with other cells of neurovascular unit (NVU) through secretions (Ballabh et al., 2004). The NVU is the structure formed by the basement membrane, BMVEC, neurons, pericytes and glial cells (Banks, 2016). Cells of the NVU are all involved in cross-communication to ensure regular function is maintained within the BBB regarding integrity, transport and permeability.

A healthy BBB typically only permits passive diffusion of small, hydrophobic molecules < 400 Da such as oxygen and carbon dioxide (Bhaskar et al., 2010). Exchange of large or hydrophilic molecules across the BBB is limited by the characteristic presence of tight junctions (TJ) between BMVEC, unless there is a specific receptor or carrier to mediate their passage. The highly specialised endothelial cells of the BBB uniquely express high levels of mitochondria, lack membrane fenestrae typical of peripheral endothelial cells and show low levels of pinocytosis

(Bartanusz et al., 2011). These factors result in high reliance upon energy-dependent mechanisms for transport of substances across the BMVEC layer, making delivery of drugs at therapeutic concentrations difficult. The brain endothelium expresses unidirectional protein efflux transporters which have been associated with multidrug resistance at the CNS (Shen & Zhang, 2010). P-Glycoprotein encoded by the multidrug resistance-1 (MDR-1) gene is the most studied efflux transporter present in many mammalian species (Sun et al., 2003). There are also many more members of the multidrug resistance-associated protein family, collectively known as ATP-binding cassette (ABC) transporters, which remove potentially toxic substances from the brain (Miller, 2015). ABC transporters are not unique to the BBB, but expression is much higher at the blood-brain interface than in other peripheral tissues. The protective function of the BBB is unable to differentiate between harmful and therapeutic xenobiotics, therefore should drug delivery to the brain be achieved, there is a risk it will be removed by such efflux mechanisms (Qosa et al., 2015).

(A)

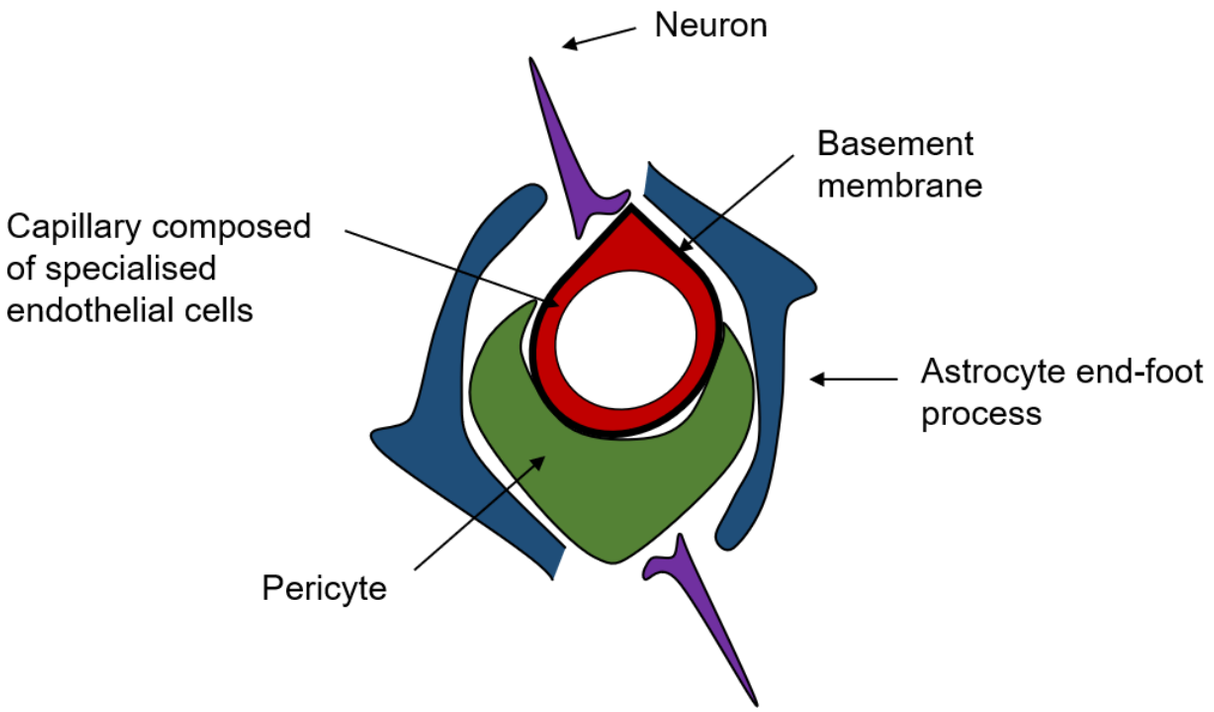

(B)

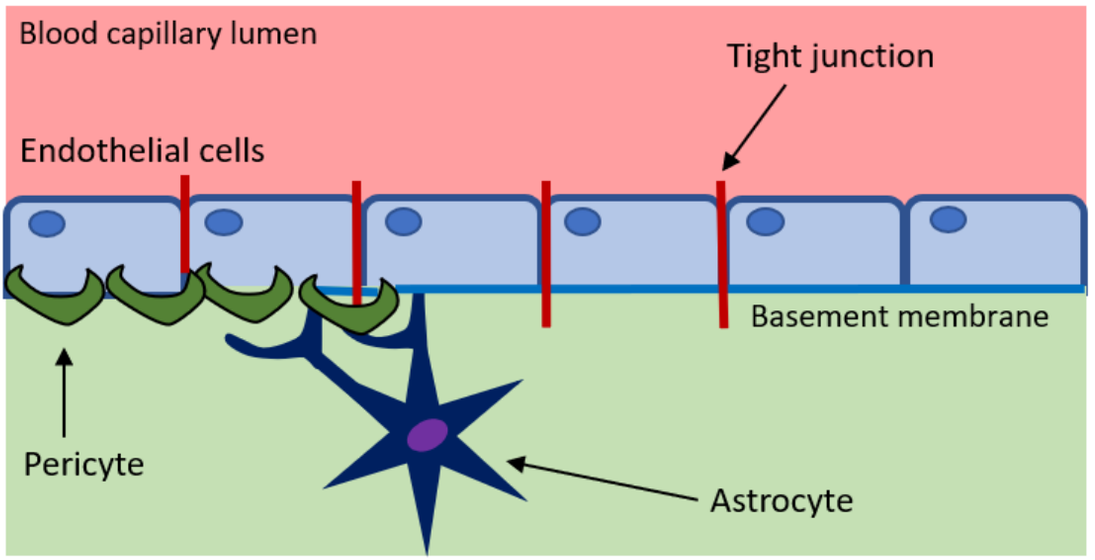

Figure 1.3. (A) A representation of the neurovascular unit and blood brain barrier (BBB) structure consisting of blood capillary endothelial cells, a basement membrane, pericytes and astrocytes. This specialised structure is responsible for the selective permeability of the brain endothelium, controlling the exchange of solutes from blood to brain. (B) A close-up representation of the BBB showing tight junction protein expression between endothelial cells, which are structurally supported by the basement membrane, pericytes and astrocytes.

TJ are responsible for high *in vivo* trans-endothelial electrical resistance or TEER (~1800 Ωcm^2) of the BBB and hence the physical restriction on paracellular movement of polar and large molecules between blood and brain (Abbott et al., 2010). TJ complexes between endothelial cells (Figure 1.4) are formed from various adheren junctions (cadherin proteins), junctional adhesion molecules (JAM), claudins, occludins and intracellular scaffold zonula-occludins (ZO) proteins (Wolfburg & Lippoldt, 2002; Abbott et al., 2010). The presence of TJ is essential for a functional *in vivo* BBB and can be used as a marker of BBB properties in endothelial cells of *in vitro* cellular models.

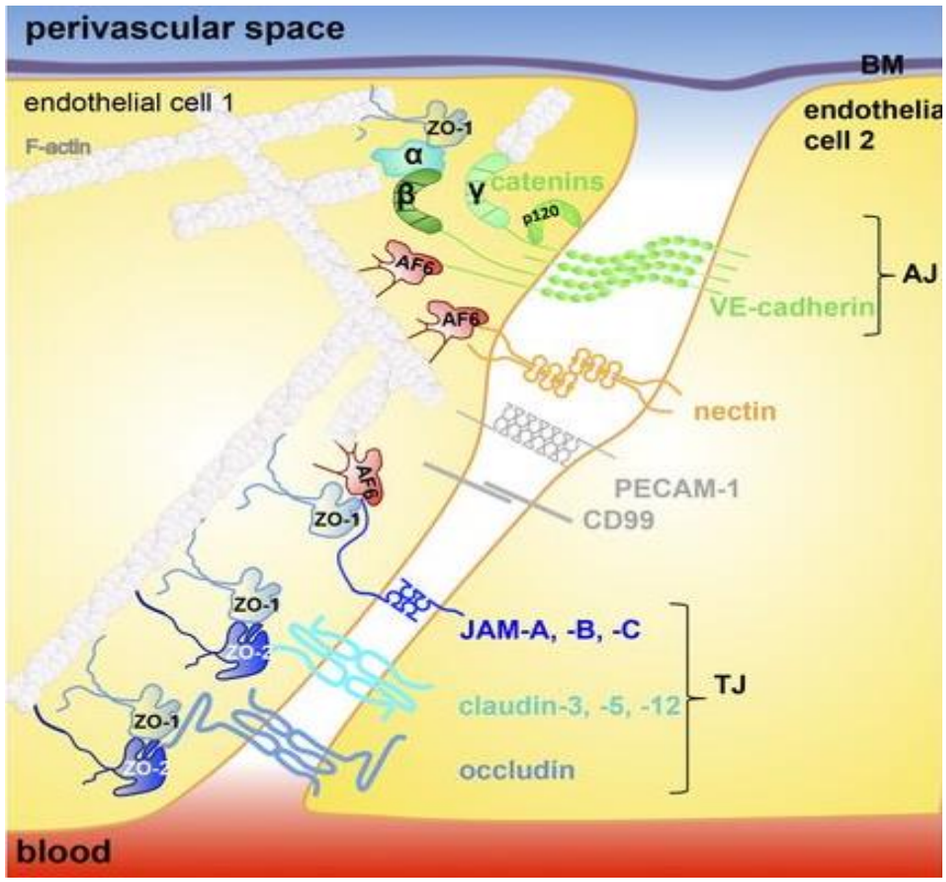

Figure 1.4. Tight junctions between brain microvascular endothelial cells of the blood brain barrier (BBB) formed from various proteins such as junctional adhesion molecules (JAM), claudins, occludin and zonula occludins (ZO). Expression of these junctional proteins are unique to the BBB structure contributing to the limited permeability of solutes between blood and brain. Image reproduced from Tietz & Engelhardt (2015) with permission of Rockefeller University Press.

The physical and chemical defences of the BBB towards foreign blood-borne substances makes drug delivery to the CNS extremely difficult. The protective function of the BBB is essential for maintenance of normal homeostasis within the CNS, however it causes many promising drug candidates for neurodegenerative conditions to fail in preclinical and clinical *in vivo* studies. The inability to achieve therapeutic levels of drug accumulation in the brain is a major concern which must be overcome in the development of any potential drug candidate for PD. Aging has been strongly associated with the onset of many neurodegenerative conditions and new research is beginning to identify how these processes are linked (Xu et al., 2018). Continuing growth of the aging population due to advances in healthcare means that the incidence of PD and other neurodegenerative diseases are also set to rise (Aron & Klein, 2011). Considering this, it is essential that suitable solutions are sought to overcome the challenge presented by the BBB in drug delivery.

Invasive means of administration have been utilised to overcome the difficulties presented by the BBB for drug delivery. Trans-cranial delivery by either intra-cerebral injection, infusion or implant has been the selected method of administration for clinical studies on NTF such as GDNF (Pardridge, 2007). These methods are extremely invasive and as such are associated with low patient acceptance, high cost and adverse events such as infection (Newland et al., 2016). Herrán et al. (2014) used a poly(lactic-co-glycolic) acid (PLGA) nanoparticulate delivery vehicle loaded with vascular endothelial growth factor (VEGF) and GDNF which was administered to rats via direct surgical injection into the striatum. This NTF delivery system achieved positive behavioural test results and increased density of neurons *in vivo*. The polymer-based nanoparticulate vehicle afforded controlled release and protection of therapeutic payload at the target site, despite requiring invasive means of administration. This neurorestorative effect was also observed by Zhao et al. (2014) when treating rats with bFGF-loaded lipid nanocarriers administered intranasally.

Trans-nasal delivery of lipid-soluble molecules is an option for achieving brain delivery of drug, however this method is not suitable for larger, hydrophilic molecules unless damage is caused

to the nasal mucosa (Merkus et al., 2003). BBB disruption may be induced with the use of hyperosmotic solutions such as mannitol (Sheikov et al., 2004) or ultrasound-induced resonance of microbubbles (Chu et al., 2018) to temporarily allow the passage of molecules from blood to brain. These methods are effective, however repeated administration may lead to the toxic leakage of plasma proteins into the brain and permanent pathology of the BBB due to damage of the brain microvasculature (Pardridge, 2007). Ongoing studies are uncovering advanced methods for achieving effective brain delivery of therapeutic agents which are not invasive and consider factors such as susceptibility to enzymatic degradation (Zhou et al., 2018).

1.4. BBB targeting ligands

The use of targeting ligands to facilitate the cellular uptake of therapeutics is a growing area of research across many disease states. This has been particularly useful in recent times for the specific targeting of drugs to the CNS, as certain ligands have the ability to traverse the BBB via various mechanisms.

1.4.1. Cell penetrating peptides (CPP)

Cell penetrating peptides (CPP) can greatly enhance the intracellular uptake of conjugated cargo across biological membranes in a non-invasive, non-disruptive manner. CPP are beneficial over conventional drug delivery methods for numerous reasons, including improved drug bioavailability at the target site, reduction of unwanted side effects and the need for less frequent dosing (Malhotra & Prakash, 2011). CPP such as TAT (transactivator of transcription) peptide, penetratin and polyarginine are among the most commonly used ligands which have the ability to transport cargos of much higher molecular weight. CPP can also be referred to as protein transduction domains, referring to the section of the parent protein domain responsible for

cellular translocation (Snyder & Dowdy, 2004). These sequences usually contain less than 30 amino acid residues and positively charged amino acid segments of lysine and arginine residues, which are essential for electrostatic interactions with the negatively-charged proteoglycans of the cell (Ul Ain et al., 2016). The exact mechanism of membrane transduction is not entirely understood, although it is thought CPP facilitate cellular uptake via energy-dependent absorption-mediated endocytosis (Zou et al., 2013).

The cell penetrating effect of TAT has been evidenced in many studies, facilitating the delivery of antibiotics (Li et al., 2008b), cancer chemotherapy (Joshi et al., 2017; Wang et al., 2018) and imaging agents (Santra et al., 2004) across the BBB *in vivo* with significantly higher efficacy than unconjugated payloads. Similarly, the CPP penetratin has also shown the ability to facilitate the brain accumulation of a conjugated cargo *in vivo* (Xia et al., 2012). The use of these CPP thus far has proved a safe approach for drug delivery. Davidson et al. (2004) used penetratin-1 to effectively deliver siRNA to primary cultures of hippocampal neurons without the disturbance caused by other classical transfection methods such as electroporation. Polyarginine is perhaps the most superior CPP for enhancing cellular uptake, with sequences containing 9 arginine resides amongst the most efficient transporters (Mitchell et al., 2000; Wender et al., 2000). One study showed how arginine-labelling of polymeric nanoparticles improved cellular uptake by 30% (Chiu et al., 2015) and when incorporated into a sequence with a specific receptor-targeting ligand, can be a very effective cellular targeting moiety (Zeller et al., 2015).

The issue presented by the use of TAT and any of the aforementioned CPP as stand-alone ligands is the lack of tissue specificity, as they do not function via a particular receptor or carrier. TAT can penetrate many tissues *in vivo* (Schwarze et al., 1999), meaning there is limited constraint on where CPP-labelled payloads might accumulate. This is potentially problematic when aiming to deliver expensive or toxic drugs. It is now becoming more common to use CPP as part of a targeting ligand sequence or dual targeted system to aid specific cellular uptake (Kumar et al., 2008).

1.4.2. Endogenous transporters and receptors

Taking advantage of endogenous transporters and receptors expressed by the BBB is an attractive approach in CNS drug delivery. Utilising ligands which are recognised by endogenous receptors at the target site is an effective way of achieving drug delivery by non-invasive means. Polysorbate-80 is a non-ionic surfactant or emulsifier which has been used as a coating on various drug delivery vehicles to facilitate brain delivery of otherwise BBB-impermeable payloads (Reimold et al., 2008). Kurakhmaeva et al. (2009) intravenously administered polysorbate 80-coated poly(butyl-cyanoacrylate) nanoparticles loaded with nerve growth factor (NGF) to rats. This study showed how polysorbate 80 facilitated the enhanced delivery of NGF across the BBB through interactions with endogenous cell surface apolipoproteins. A reduction in PD symptoms was observed in rats without the need for intracerebral administration, a significant development in achieving non-invasive and safe delivery of a NTF to the brain. Polysorbate-80 has also been used to facilitate the *in vivo* brain delivery of drugs for Alzheimer's disease (Wilson et al., 2008) and cancer (Gulyaer et al., 1999; Gelperina et al., 2002). Rempe et al. (2011) reported the development of polysorbate-80 coated PBCA NP which could permeate a porcine *in vitro* BBB model and facilitate enhanced permeability of a FITC-BSA conjugate due to temporary barrier disruption after 4 hours of exposure. Although this approach is effective in achieving enhanced accumulation of drug across the BBB, there are considerable associated risks which include long-term barrier dysfunction and passage of blood-borne neurotoxic proteins into the CNS.

Lactoferrin is a globular glycoprotein member of the transferrin family which is important for cellular absorption of iron. The lactoferrin receptor expressed on BBB endothelial cells has been used as a target to facilitate the active transport of therapeutic payloads across the BBB. Huang et al. (2010a) used lactoferrin as a targeting ligand to deliver a GDNF gene payload to a rat model of PD, which caused improved locomotor activity after repeated dosing. Hu et al. (2009) took advantage of this endogenous receptor-mediated transport mechanism to increase the accumulation of polymeric nanoparticles housing a fluorescent coumarin-6 payload in mouse brain *in vivo* following intravenous administration. In this study the lactoferrin ligand also

facilitated the *in vitro* internalisation of the fluorescent payload better in mouse brain endothelial cells than the unmodified nanoparticle treatment with low cytotoxicity (Hu et al., 2009). The anti-lactoferrin monoclonal antibody OX26 is another ligand which can be exploited to enable lactoferrin receptor-mediated transport of BBB-impenetrable peptides to the brain as shown by Penichet et al. (1999) and Aktas et al. (2005). Antibodies against receptors overexpressed by solid tumours is an effective means of specific targeting to limit the cytotoxic side effects of chemotherapy. For example, medulloblastoma is a type of primary brain tumour which overexpresses the HER2 receptor making it susceptible to anti-HER2 antibody-functionalised therapeutics (Bernardi et al., 2008). This type of targeting could be useful for overcoming the BBB, should suitable receptors be identified.

Transferrin is another iron-transporting serum glycoprotein, similar to lactoferrin, which has become a popular ligand for enabling targeted receptor-mediated transport of therapeutics at the cell surface of solid tumours (Li & Qian, 2002; Kang et al., 2009; Ulbrich et al., 2009). Overexpression of this receptor by tumours can be exploited for enhanced cytotoxicity and more effective use of expensive chemotherapeutics. Yuan et al. (2009) conjugated the transferrin ligand to a nanoparticulate vehicle loaded with anti-cancer agent for the treatment of brain glioma in rats. In this study, enhanced accumulation of drug in the tumour was facilitated by transferrin and extended the survival of rats compared to unconjugated treatment. Yuan and colleagues showed the importance of the transferrin ligand as less than 2% of unconjugated nanoparticles accumulated in the brain due to uptake by the reticuloendothelial system (RES). This shows that a targeting ligand may not only enable enhanced uptake at the target site, but also extend half-life of the therapeutic payload.

Another endogenous receptor expressed at the BBB is the low-density lipoprotein receptor (LDLR) which is also overexpressed by glioblastoma tumours (Nikanjam et al., 2007). Zhang et al. (2013) developed a novel peptide named peptide 22 which showed affinity towards the LDLR to deliver paclitaxel-loaded nanoparticles to the brain of mice for the treatment of glioblastoma multiforme. This peptide effectively reached tumour which infiltrated the brain tissue compared

to unconjugated drug vehicle, extending the survival time of glioma-bearing mice. Targeting the overexpression of LDLR, lactoferrin or transferrin receptors has been effective for increasing drug accumulation in solid brain tumours however may not be as useful for other diseases where the target is not so obvious. Whilst the BBB endogenously expresses these receptors, they are not unique to the BBB endothelium and are widely expressed throughout the peripheral tissues. In neurodegenerative conditions, this approach may not be sufficient to allow specific BBB crossing and the efficient distribution of a drug vehicle through neural tissue. It would be more beneficial in these instances, to target a receptor more uniquely expressed by the BBB endothelium and neural cells to facilitate both specific identification of the target site and subsequent internalisation of a conjugated payload with minimal dosing.

1.4.3. Toxin-derived peptides

CNS-specific peptide-based targeting ligands have been explored in recent times for the delivery of therapeutic agents to the brain. CNS-targeting peptides have had much success in animal studies, exploiting native receptors, transporters or enzymes to specifically deliver therapeutic cargo across the BBB. Many of these peptides are derivatives from natural neurotoxic agents such as tetanus toxin, neurotropic virus glycoproteins and fragments of snake, scorpion and bee venoms (Soddu et al., 2015). Taking advantage of the natural ability of these peptides to invade the CNS to achieve highly efficient drug transport across the BBB has one of the most promising brain-targeting strategies developed over the past decade. Despite this, the use of toxin or virus-derived ligands raises concerns of immune reactions and true specificity for neural cells only.

1.4.3.1. Bacteria-derived neurotoxins

Peptide derivatives of the tetanus toxin have been explored as potential CNS shuttles for the delivery of various cargo to the brain. This toxin produced by *Clostridium tetani* is responsible for the potentially life-threatening tetanus infection of the CNS. Tet-1 peptide is one such derivative which has been used to deliver a nucleic acid-polymer conjugate specifically to neural cells in mice following intraventricular injection (Kwon et al, 2010). After facile conjugation to polymeric nanoparticles, the 12-amino acid tet-1 peptide has also been used for *in vitro* uptake studies in neuronal cells (Mathew et al., 2012). The retrograde transport properties of tet-1 might prove useful for targeting of motor neurons in particular (Bhatt et al., 2017), however at present more evidence of *in vivo* efficacy is required. Tet-1 can specifically target neurons when administered directly, however it is not clear whether this peptide would be effective for BBB crossing following peripheral administration. Tetanus toxin fragment C (TTC) is another peptide derivative of tetanus toxin which may be useful for CNS targeting. It has in fact been used in combination with GDNF to target spinal cord motor neurons in mice (Larsen et al., 2006). An extensive review by Toivonen et al. (2010) on the use of TTC highlights the potential benefits of this neuron-targeting entity for conjugated therapeutics, however there are still immunogenic concerns which need to be explored in greater detail.

Cholera toxin produced by the *vibrio cholerae* bacterium contains a cell-penetrating fragment known as cholera toxin B fragment (CTB), which has potential applications as a promoter of cellular uptake. CTB is part of the cholera toxin which is responsible for cell-invasion via cell surface ganglioside GM1 receptors rather than the disease-causing metabolic effects produced by the A fragment (Vajn et al., 2013). CTB facilitated improved delivery of conjugated NGF to the brain *in vivo* utilising retrograde transport mechanisms following intranasal administration (Zhang et al., 2008). The increased brain accumulation of NGF gave rise to a greater therapeutic response in Alzheimer's disease model mice compared to treatment without CTB, including cholinergic neuron protection and improved memory ability. GM1 receptors are present in the CNS, however as they are also present in the gastrointestinal epithelium, intranasal administration of CTB-NGF was the preferred route to minimise non-specific peripheral targeting.

The diphtheria toxin (DT) is another bacteria-derived source of targeting peptide which has been explored for its cell-penetrating potential via the diphtheria toxin receptor (DTR). Although this receptor is not exclusively expressed by the CNS, DT derivatives such as CRM197 have shown efficacy in facilitating DTR-mediated endocytosis of conjugated siRNA-loaded polymeric nanoparticles to glioblastoma brain tumours in mice following systemic administration (Hobel et al., 2011).

The use of peptide derivatives from bacterial toxins has shown promise in aiding BBB crossing and brain accumulation of conjugated therapeutics due to their cell penetrating properties. Many of these targeting moieties also have affinity for peripheral receptors, which introduces the risk of non-specific targeting of drug product. Bacterial toxins may perhaps be useful for cellular uptake applications in combination with more specific neural cell-targeting ligands.

1.4.3.2. Animal-derived neurotoxins

Common to all families of the snake species, toxins are non-enzymatic proteins found in snake venom with a common three-loop structure, which have various biological effects including neurotoxicity (Kini & Doley, 2010). Snake neurotoxins are well-characterised for their ability to bind to various subtypes of the neuronal nicotinic acetylcholine receptor (nAChR) (Tsetlin & Hucho, 2004). Candoxin is a 16-amino acid derivative of the Malayan krait snake toxin which has been used to promote the brain delivery of paclitaxel-loaded polymeric micelles via the α7 nAChR subtype in mice (Zhan et al., 2011). This type of specific targeting permits maximal therapeutic effect from the drug, making treatment more efficient.

Snake toxin derivatives are perhaps the most neural-specific source of targeting moieties utilised in recent drug targeting strategies towards the CNS. Venom produced by the king cobra snake *Ophiophagus hannah* contains Toxin B, from which loop 2 residues have been identified to interact with the nAChR with high affinity. A peptide derivative from Toxin B loop 2 (KC2S) effectively enabled intracranial delivery of an attached polymeric payload following intravenous

administration in mice in a study by Zhan et al. (2010). In the same study, it was shown that KC2S preferentially targeted nAChR-expressing brain endothelial cells over non-neural HeLa cells (Zhan et al., 2010).

Neurotoxins are not only produced by species of snake, but other animals also produce such proteins. A neurotoxin produced by the scorpion species *Leiurus quinquestriatus* has been exploited for treatment of brain gliomas due to its ability to cross the BBB. Scorpion-derived chlorotoxin binds cell membrane matrix metalloproteinase-2 (MMP-2) as part of a lipid-raft anchored complex (Soddu et al., 2015). MMP-2 is overexpressed in many cancers and thus chlorotoxin has been utilised as a brain tumour-targeting ligand, enabling preferential drug accumulation in glioma cell types *in vitro* (Xiang et al., 2011) and therapeutic efficacy *in vivo* (Costa et al., 2013). Similarly, a neurotoxic peptide from bee venom known as apamin has been used to create a non-toxic derivative (ApOO) capable of crossing an *in vitro* BBB model (Oller-Salvia et al., 2013). Despite having promise as shuttles for CNS drug delivery, few *in vivo* studies have been carried out to investigate the true potential for immune reactions following repeated exposure to neurotoxin-derived peptides.

1.4.4. Virus-derived CNS targeting peptides

Viral envelope glycoproteins have the ability to initiate cell penetration via interactions with various host surface receptors. Glycoprotein derivatives from viruses such as Herpes simplex 1 and vesicular stomatitis virus (VSV) have been used to enhance the cellular uptake of conjugated payload to various cell types *in vitro,* including BBB cells. These virus-derived peptide ligands however do not confer any neural-specific targeting properties to the drug vehicle, using mainly non-specific uptake mechanisms or target receptors commonly expressed throughout numerous bodily tissues (Ammayappan et al., 2013; Guarnieri et al., 2013). The highly efficient cellular internalisation displayed by viral glycoproteins is of utmost interest in drug delivery initiatives, particularly if a more target-specific *in vivo* mechanism of action can be sought. Indeed, peptides

derived from the neurotropic rabies virus might hold the characteristics required of such a brain-targeting ligand.

1.4.4.1. Rabies-virus glycoprotein

Rabies virus is an infection of the CNS which has a high fatality rate amongst unvaccinated individuals. Starting at the neuromuscular junction of the peripheral nervous system, the virus undergoes retrograde axonal transport to infect the CNS (Cherian et al., 2015). Rabies virus infection causes various neurological symptoms manifesting as muscle spasms, respiratory problems, hallucinations or in some cases, paralysis (Jackson, 2013). In later stages of the disease, the virus spreads to various other areas of the body such as the salivary glands. The infected saliva of biting animals is the main source of rabies virus spread and hence the infective cycle is repeated (Michalicová et al., 2017). Rabies is a rod-shaped virus from the *Lyssavirus* genus of the *rhabdoviridae* family, whose genome encodes five proteins (Rupprecht, 1996). One of these proteins is the viral envelope glycoprotein, which is solely responsible for viral infection of the CNS.

Retrograde axonal transport in the direction of the cell body from the axon terminus is a natural method of cellular recycling within neurons. Rabies virus glycoprotein (RVG) is a 505-amino acid type-1 glycoprotein on the viral envelope which is responsible for BBB crossing and utilises the mechanism of retrograde axonal transport to traverse neurons of the CNS (Yan et al., 2002). Thus far, three key nerve cationic binding regions have been identified at positions 33–54, 189–214 and 330–357 of the sequence (Fu et al., 2018). Tuffereau et al. (1998) suggested that RVG interacts with a specific receptor on neural cells to allow such profound infectivity of the CNS. Nowadays, it is widely accepted that the identity of this receptor is most likely the neuronal nAChR, common to both the neuromuscular junction and neurons (Lafon, 2005; Vigerelli et al, 2014; Gooding et al, 2015). This is perhaps not surprising, as RVG shares homologous sequences with loop 2 of snake neurotoxins (Lentz, 1991).

Kumar et al. (2007) first exploited the CNS-specific action of RVG to successfully deliver siRNA to the brain in mice and subsequently observed positive therapeutic effects. Kumar and colleagues fabricated a 29-amino acid derivative of RVG, termed RVG-29, which showed evidence of specific binding to neuronal cells *in vitro* and *in vivo* via the nAChR. To enable RVG-29 conjugation to siRNA, the peptide was fixed with a 9-arginine residue tail, which would also aid cell-penetrating ability. Results from this early study on RVG-29 did not give rise to a detectable immune response in the form of antibodies or inflammatory markers, meaning drug delivery was specific, safe and non-invasive. Over the past decade, further studies on RVG-29 as a brain targeting ligand have been carried out with much success for a range of neurological disorders (Liu et al., 2009; Chen et al., 2011a; Son et al., 2011; Kuan et al., 2012; Cooper et al., 2014; Lee et al., 2017).

Liu et al. (2009) demonstrated how RVG-29 could be easily incorporated into a drug delivery vehicle of pegylated polyamidoamine dendrimers complexed with a gene payload. RVG-29 modification permitted improved transport efficiency across an *in vitro* BBB model in comparison to unlabelled dendrimers. Furthermore, *in vitro* studies presented evidence of uptake in brain endothelial cells via clathrin or calveolae-mediated endocytosis mechanisms. The neural-specific properties of RVG-29 were further demonstrated by Chen et al. (2010) when itraconazole-loaded albumin nanoparticles were preferentially targeted to mouse brain endothelial cells over non-neural Hela cells *in vitro*. Furthermore, RVG-29 facilitated greater brain distribution of itraconazole *in vivo.*

Studies on gene delivery to the brain by Son et al. (2011), Kuan et al. (2012) and Cooper et al. (2014) have exploited the activity of RVG to overcome the obstacles presented by the *in vivo* BBB. Kuan et al. (2012) used RVG-29 to deliver a therapeutic RNA payload to 6-OHDA PD model rats. The RNA payload was only detected in neural cells which expressed neuronal nicotinic acetylcholine receptors. Intravenous injection of the RVG-RNA conjugate lead to significant neuroprotection after 6-OHDA induced toxicity. RVG-29 facilitated the positive effect of the viral RNA on mitochondrial complex 1 in DA neurons, creating a potential treatment for PD

caused by mitochondrial complex 1 dysfunction. No immune response was reported following testing. The authors reported that for future development, the encapsulation of the RNA would prolong half-life and protect against degradation. Similarly, Cooper et al. (2014) achieved successful delivery of siRNA-loaded exosomes to the brain to reduce α-synuclein aggregation in a mouse model. RVG-29 is a versatile brain targeting ligand which can be used within many types of transport vehicle or therapeutic system. More recently, RVG-29 has been employed to maximise the *in vivo* distribution of silica-coated gold nanorods for photothermal therapy of brain tumours (Lee et al., 2017).

RVG-29 is derived from residues 189-214 of the parent RVG sequence, however another derivative from the 330-357 position has also gained attention for its promising brain-targeting properties (Fu et al., 2018). Rabies virus-derived peptide (RDP) has a total 39-amino acid sequence composed of the residues -KSVRTWNEIIPSKGCLRVGGRCHPHVNGGG- and fixed with an arginine (9) tail -RRRRRRRRR- at the peptide C terminal. Fu et al. (2012) used RDP to deliver different therapeutic proteins to the CNS of mice as part of a fusion protein delivery system. RDP facilitated the *in vivo* BBB crossing of the therapeutic proteins without affecting their biological activity. It was later shown in studies by Fu et al. (2013a) and (2013b) how RDP preferentially targeted different therapeutic payloads to cells of neural origin only, both *in vitro* and *in vivo*. These studies also showed the significant benefit of RDP as part of a fusion protein with the growth factor GDNF (Fu et al., 2013a) and the BDNF gene (Fu et al., 2013b) in reducing PD symptoms in mice.

It has also been proposed that the mechanism of RDP cellular uptake in neural cells is via clathrin-coated pit endocytosis, however the mechanism of cell entry is not fully understood at present. The relative ease of RDP conjugation to various therapeutics and delivery vehicles offers a wide range of applications for this peptide as a brain targeting ligand. In addition to this, investigations in animal models so far have not detected any significant toxicity or immune response, indicating that RDP may be safely used *in vivo.* In fact, RDP has already been used

for diagnostic purposes as Zhang & Fu (2015) functionalised RDP to gold nanoclusters for non-invasive brain screening in mice.

1.5. Conclusion

The difficulties presented in achieving effective drug delivery across the BBB are one of the biggest challenges faced in PD therapy. It is clear that the most beneficial solution to PD would be the restoration of DA neurons in the SNpc, however to do this non-invasively requires the mobilisation of native neural stem cells *in situ.* The potential advantages of NTF for PD are plentiful and with the correct means of brain delivery, could surely present a promising new treatment modality.

Taking advantage of native BBB receptors is a hopeful means of achieving delivery and distribution of therapeutics to the brain. Peptide ligands targeting a particular receptor have the ability to transport a conjugated drug or drug vehicle and subsequently facilitate cellular internalisation. Peptides derived from neurotoxins have perhaps presented the most desirable properties of such a ligand, particularly of the snake species, which specifically target the nAChR. It is important however that the drug vehicle is non-toxic and so far, not enough data exists on the long-term *in vivo* safety of neurotoxin derivatives.

Derivatives of RVG have emerged as lead candidates in the non-invasive, specific and safe targeting of neural cells. Many studies have provided solid evidence of *in vivo* efficacy and thus the glycoprotein derived from the rabies virus is an exciting prospect in the development of a brain delivery vehicle. It would be desirable to use a ligand such as RDP as a means of facilitating NTF delivery for the treatment of PD. RDP has shown evidence of preferential uptake by neural cell types specifically and importantly can overcome the BBB *in vivo* following systemic administration.

Polymeric nanoparticles have versatile surface characteristics which allow ligand attachment, as illustrated in Figure 1.5. Given the short half-life of NTF, encapsulation within a protective drug delivery vehicle surface-conjugated with RDP may be advantageous for increasing *in vivo* stability. Thus far, RDP has been used predominantly as part of a therapeutic fusion protein which does not offer the protection required for payloads susceptible to degradation. The benefit of growth-promoting factors on neural stem cells may be optimised to full potential following sufficient accumulation in the brain and protection from peripheral degradation.

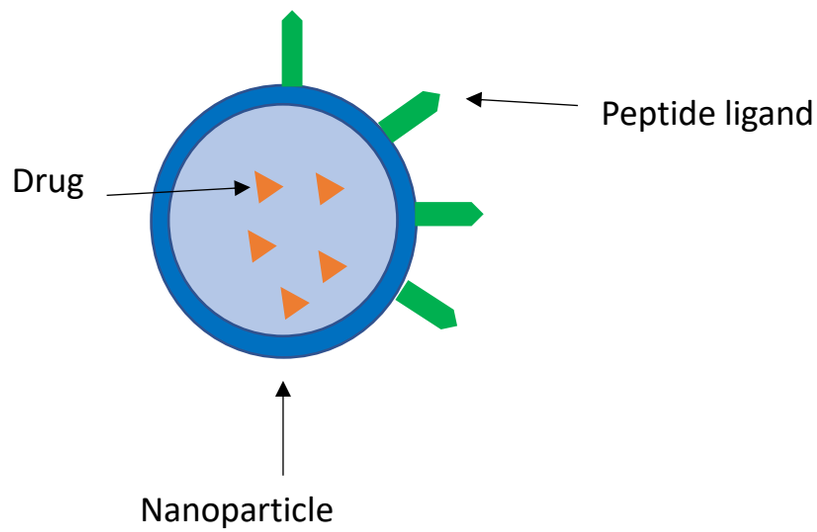

Figure 1.5. Diagrammatic representation of a targeted nanoparticle for specific drug delivery. The encapsulated therapeutic payload is protected from degradation and targeted to a specific location with peripherally attached ligand.

1.6. General aims

The general aim of this research was to develop a neural cell-specific drug delivery system capable of crossing an *in vitro* BBB model. Peptide-conjugated polymeric nanoparticles were formulated to encapsulate various model payloads, which were then tested in a range of cell-based *in vitro* studies to observe the effects of RDP as a targeting ligand. Following assessment of RDP serum stability, the sequence was optimised and assessed for targeting activity in a range of cell types. Finally, a triple culture BBB model will be established and used to assess the efficacy of peptide-conjugated nanoparticulate preparations. The aims are summarised as follows:

(1) Explore various formulation parameters to synthesise a suitable polymer-based nanoparticulate drug vehicle with surface-conjugated RDP.
(2) Test optimal RDP-conjugated nanoparticle formulation(s) on neural and non-neural cell types to assess neural-specificity of the drug delivery system.
(3) Assess RDP stability characteristics and optimise the peptide sequence.
(4) Develop an *in vitro* BBB model using three human cell types from the neurovascular unit and subsequently determine the ability of peptide-conjugated nanoparticles to traverse this model.

Chapter 2

Development of a polymeric nanoparticulate drug delivery vehicle

2.1. Introduction

2.1.1. Nanotechnology in drug delivery

Nanoparticles (NP) have been at the forefront of new drug delivery strategies over the past couple of decades. The use of NP is not exclusive to drug delivery alone, NP also have applications as diagnostic, theranostic and imaging agents *in vivo* (Lim et al., 2015; Wolfbeis, 2015). The small size and ability of NP to protect encapsulated sensitive therapeutics offers a unique advantage for controlled and targeted drug delivery (Wicki et al., 2015). Nanoparticle-based therapeutics have been researched extensively, particularly for use in targeted cancer chemotherapy, as reviewed by Sanna et al. (2014). Many cytotoxic drugs have been encapsulated within nano-sized delivery vehicles for reduction of unwanted side effects resulting from non-specific targeting and enhanced tumour retention due to their ability to permeate leaky tumour vasculature (Peer et al., 2007).

Encapsulation of drugs within NP can overcome pharmacokinetic issues associated with free drug formulations such as solubility and instability to blood enzymes (Blanco et al., 2015). Many different types of NP have been used to encapsulate therapeutics for use as drug delivery systems across a range of disease states. A plethora of research can be found in the literature for many different types of NP drug delivery vehicle, some of the most popular examples including metallic NP, stimuli-responsive NP, solid lipid NP and polymeric NP to name only a few. Therefore, only the aforementioned nanomaterials and their role in NP-mediated drug delivery are highlighted below.

2.1.2. Metallic NP

Metallic NP composed of materials such as iron oxide, gold and silver have gained recognition for their application as diagnostic and therapeutic agents (Mody et al., 2010). Iron oxide NP have been used as a contrast agent in high resolution magnetic resonance imaging (MRI), targeted drug delivery and cell tracking. Advantages of magnetic NP are mainly associated with the ability to produce a narrow particle size range and easily modify surfaces to improve cellular uptake characteristics. For example, Gupta & Curtis (2004) engineered PEG-coated iron oxide NP to improve cellular adhesion and uptake.

Silver NP have been conjugated with targeting molecules for use as nanoprobes (Mody et al., 2010) and also have shown efficacy as cytotoxic chemotherapeutic agents through anti-proliferative effects on numerous cancer cells types (Nayak et al., 2016; Barua et al., 2017). Ruan et al. (2012) used fluorescent magnetic NP-labelled mesenchymal stem cells to locate, image and treat gastric cancer *in vivo.* Dual modality contrast through fluorescence imaging and MRI enabled specific application of an external magnetic field to induce hyperthermia therapy upon cancer cells.

Silver NP are also antimicrobial in nature and thus have been incorporated into wound treatments and medical devices such as surgical instruments (Furno et al., 2004). In fact, both silver and copper NP have been utilised for their antimicrobial action through mechanisms such as cell membrane disruption and oxidative stress (Applerot et al., 2012; Herman & Herman, 2014; Le Quay & Stellacci, 2015; Meghana et al., 2015). Recently, Banik et al. (2018) detailed the preparation of bimetallic copper-silver NP which were successfully used to induce cytotoxicity in various cancer cell types through induction of apoptosis. These bimetallic NP greatly affected cancer cell viability, with much less effect on normal cells. Despite the apparent efficacy as an anti-cancer agent, these NP would be safer if they could be targeted more specifically to cancerous cells through surface modification with a targeting ligand.

Gold NP have mainly been reserved for biological imaging, particularly for cancer diagnosis (El-Sayed et al., 2005; Tong et al., 2009). They have however, been surface-conjugated with RDP for targeted brain imaging (Zhang & Fu, 2015) and gold nanorods have been utilised for targeted photothermal therapy due to their unique optical properties (Huang et al., 2010b). Much interest has been drawn to metallic NP due to their versatility for use within drug delivery systems. Classical methods of synthesis however, require costly, hazardous starting materials and energy-intensive production processes which negatively impact the environment (Thakkar et al., 2010; Edmundson et al., 2014; Mandava, 2017). Biogenic synthesis can overcome these problems, which involves natural production of metal-based NP in organisms such as bacteria, yeast and fungi (Seabra & Duran, 2015). Unfortunately, these methods are not reproducible and are difficult to scale up, as the exact method of NP synthesis is not clear.

2.1.3. Stimuli-responsive NP

NP can be synthesised to respond to one or more stimuli such as pH, temperature, magnetic fields, redox and enzymes (Chen et al., 2011b; Mura et al., 2013; Wang et al., 2016). Response to stimuli from the external or intracellular environment can be used to trigger therapeutic effect or optimise payload release characteristics, offering an element of control to *in vivo* activity (Zhang et al., 2016). These types of stimuli-responsive NP can also be coupled with a targeting ligand for enhanced specificity of drug release at the target site *in vivo* (Xiao et al., 2014).

Zhang et al. (2018) recently fabricated pH- and redox- responsive NP for drug and gene delivery through use of a cationic polymer shell and a charge reversible pullulan coating. Lee et al. (2018) also developed a NP vehicle which disintegrated in response to acidic microenvironment to release a chemotherapeutic payload for prevention of pulmonary colorectal carcinoma metastasis. Thermo-responsive nanoparticulate systems have also been utilised for therapeutic response to external stimuli such as near infrared laser irradiation (Niidome et al., 2010; Nam et al., 2012).

These systems are relatively new developments in the field of nanoparticulate drug delivery and concerns have been raised over low drug loading capability and lack of biodegradability (Cheng et al., 2013). Further research to address such issues is required for the clinical development of stimuli-responsive NP as drug delivery vehicles.

2.1.4 Solid lipid NP

Research into the use of solid lipid NP (SLN) has been on the rise since the mid-90s (Mukherjee et al., 2009). Properties such as good biocompatibility and cost effective large-scale production, without the need to use organic solvents, are a few of the advantages of this type of NP vehicle (Muller et al., 2000). SLN have been used to encapsulate a variety of drugs such as cytotoxic methotrexate (Ruckmani et al., 2006) and anti-hypertensive olmesartan medoxomil (Pandya et al., 2018), increasing the bioavailability of poorly water-soluble drugs (Hu et al., 2008).

2.1.5. Polymeric NP

Polymeric NP are a diverse group of nanocarriers in which a wealth of research has been invested for use in drug delivery strategies. Properties such as high drug loading capacity, stability, facile surface modification and manipulation of characteristics such as release kinetics, size and charge are a few of the reasons which make polymers a favourable biomaterial (Patel et al., 2012). Perhaps most importantly, evidence of *in vivo* safety in humans has contributed to the popularity of such materials (Kumari et al., 2010). This combination of features coupled with simple methods of synthesis gives incentive for developing polymer-based nanomaterials.

Polymers may be either natural or synthetic. Naturally occurring polymers such as albumin, chitosan and sodium alginate are popular due to their biocompatibility and safety in humans (El-Say & El-Sawy, 2017). Despite this, synthetic polymers are still more popular at the present time, probably due to certain formulation hurdles in the use of the natural polymers. For example,

some chitosan NP have a limited ability for controlled release due to high solubility at low pH and poor solubility at physiological pH, which often requires some form of chemical modification (Elgadir et al., 2015; Nur & Vasiljevic, 2017). Additionally, alginate is useful due to its mucoadhesive properties, however problems with low encapsulation efficiency can be experienced unless used in conjunction with another polymer (Sarmento et al., 2007). There are numerous synthetic polymers which have been made into NP such as polylactides, polyglycolides, poly(lactic-co-glycolic acid) (PLGA), polycyanoacrylate, polycaprolactone (PCL), poly(methacrylic acid) (PMAA) and poly(butyl-cyanoacrylate) (PBCA) to name only a few (El-Say & El-Sawy, 2017) .

One of the most common applications of polymeric NP to date, has been for the targeting of solid tumours. Many different polymers have been utilised for the encapsulation of cytotoxic drugs for chemotherapeutic purposes, sometimes with use of more than polymer in the same formulation. Rao et al. (2014) produced a thermally-responsive nanoparticulate system of two polymers, Pluronic® F127 and chitosan, to encapsulate curcumin for anti-cancer effects. This polymer blend was used again but for a doxorubicin payload instead, which subsequently released payload in an accelerated manner in response to the acidic tumour microenvironment (Rao et al., 2015). Most recently, Rychahou et al. (2018) formulated biocompatible poly(ethylene glycol)-ε-poly(caprolactone) (PEG-PCL) block co-polymer NP for the delivery of poorly soluble cytotoxic drug to lung metastasis. Another biodegradable polymer, poly(beta-amino ester) (PBAE), has been used to fabricate NP capable of preferentially targeting hepatocellular carcinoma cells over healthy hepatocytes *in vitro* (Zambino et al., 2017). Despite multiple reports of preferential endocytosis of PBAE-based NP in cancer cells, the underlying mechanism of this phenomenon is not yet entirely understood (Tzeng et al., 2013; Guerrero-Cázares et al., 2014).

Polymeric NP have shown the ability to cross the BBB and enter the CNS to deliver a therapeutic payload. Unlike targeting of solid tumours outside the CNS, NP often require surface modifications with targeting molecules or ligands which aid in cellular uptake mechanisms across the BBB. Kreuter et al. (1995) first achieved CNS delivery of a polymeric NP formulation through

polysorbate-80-coated PBCA NP. This NP preparation crossed the BBB in mice to deliver a therapeutic peptide which was bound to the PBCA polymer. In more recent times, a number of different polymers have been used as drug delivery vehicles to the CNS. Byeon et al. (2016) used cationic- and mannose-modified albumin NP to target brain tumours in mice through exploitation of membrane transporter molecules. Enhanced accumulation of cytotoxic drugs was achieved in glioblastoma tumours by functionalisation of pluronic-based polymeric micelles with a small cyclic Arginine-Glycine-Aspartic acid peptide in animal studies by Miura et al. (2013) and Huang at al. (2016).

Poly(lactic acid) (PLA) is another commonly used polymer for NP formulation. Liu et al. (2008) detected accumulation of poloxamer 188-coated PLA NP in the brain of mice, amongst other organs, with particle sizes of up to 300 nm. The cell penetrating peptide TAT enhanced the CNS bioavailability of the anti-HIV drug ritonavir when conjugated to PLA NP in a study by Rao et al. (2008). These non-specific NP surface ligands aid cellular uptake of polymeric NP across the BBB, but also show substantial accumulation in other major organs such as the liver. Although most commonly used polymers are non-toxic and biocompatible, it is desirable to avoid unnecessary biodistribution in other areas apart from the target organ. Emulsifiers such as poloxamers and polysorbates can promote cell uptake via temporary membrane disruption, which may be harmful in high doses and prolonged exposure (Pardridge, 2005). It is therefore preferable to attach a more specific targeting ligand to these polymeric nanocarriers, such as an RVG derivative, which utilises mechanisms such as receptor-mediated endocytosis. For example, poly(ethylenimine) was the polymer of choice to conjugate to RVG in a study by Hwang et al. (2011) for non-toxic brain targeting of mRNA in mice.

Micelles are drug carriers commonly formed from amphiphilic polymers, however they tend to be much smaller in size (<100 nm) than traditional polymeric NP. Targeted micelles have been utilised in recent times to achieve drug delivery across the BBB predominantly for the treatment of solid tumours (Wang et al., 2012; Zhu et al., 2017). The hydrophobic core formed by amphiphilic block co-polymers in aqueous solution can house hydrophobic drugs (Sezgin-

Bayindir et al., 2016), however are not the best choice for highly water-soluble or protein payloads.

2.1.5.1. Poly(lactic-co-glycolic acid) (PLGA) NP

PLGA is one of the most commonly used biodegradable synthetic polymers for drug delivery and scaffolding in tissue engineering (Burg et al., 2000; Nair & Laurencin, 2007). The popularity of PLGA over recent decades has been due to its favourable degradation properties, ability to encapsulate molecules of a large size range, solubility in many common solvents, sustained drug release characteristics and established clinical experience (Makadia & Siegel, 2011). PLGA hydrolyses *in vivo* degrading into monomer units, lactic acid and glycolic acid, which are subsequently eliminated as carbon dioxide and water by normal metabolic processes (Catiker et al., 2000; Jana et al., 2014). These by-products are toxicologically safe in humans and consequently PLGA has been approved by the Food and Drug Administration (FDA) for use in drug products (Jain, 2000). FDA-approved preparations containing PLGA already on the market include Somatuline LA (Ipsen) for acromegaly and Trelstar Depot (Pfizer) for prostate cancer (Mundargi et al., 2008).

PLGA NP formulation processes such as the double emulsion technique (w/o/w) have become a favourable choice for encapsulating highly water-soluble drugs and protein-based therapeutics (Makadia et al., 2008; Mundgardi et al., 2008). Growth factors are examples of expensive protein payloads which can be encapsulated within PLGA NP with loading efficiency for targeted drug delivery, whilst offering protection against enzymatic degradation *in vivo.* Untargeted PLGA NP can accumulate in organs such as the liver, spleen, lymph nodes and peritoneal macrophages due to their recognition by the reticuloendothelial system (RES) upon blood circulation (Anderson & Shive, 1997). This issue can be overcome by the facile surface modification of polymeric NP with a targeting ligand, which can potentially enable site-specific accumulation.

Incorporation of another polymer alongside PLGA, such as polyethylene glycol (PEG), can reduce non-specific accumulation of NP due to anti-aggregative effects and shielding of the particle surface from RES recognition (Amoozgar & Yeo, 2012; Jokerst et al., 2012). Attachment of a targeting ligand on the surface of PLGA NP can also reduce non-specific accumulation in organs (Cheng et al., 2007; Scott et al., 2007). There are examples in recent times of PLGA NP functionalisation with targeting ligands to achieve drug delivery across the BBB, either through non-specific membrane interactions (Kulkarni & Feng, 2011) or receptor-mediated mechanisms (Geldenhuys et al., 2014). Li et al. (2011) improved specificity of a PEG-PLGA NP system to the brain in mice through surface-conjugation with a 12-amino acid phage display peptide compared to unmodified NP, which accumulated at higher levels in the liver and spleen. Similarly, Li et al. (2018) recently conjugated lactoferrin to the surface of PEG-PLGA NP to enhance accumulation in mouse brain, due to high expression of the lactoferrin receptor on BBB endothelial cells, for the treatment of gliomas.

The use of a ligand-modified PLGA-based nanoparticulate vehicle is an attractive prospect for the non-invasive delivery of sensitive therapeutics to the brain. Potentially beneficial treatments, such as growth factors for the treatment of PD or other neurodegenerative conditions, may be selectively targeted to the brain where therapeutic effect can be exerted. Exploiting the neurotropism of a targeting ligand such as RDP in combination with a safe, versatile and biodegradable nanovehicle may produce such a drug delivery system.

The aims of the work reported herein were therefore to:

(1) Formulate and optimise PLGA NP preparations encapsulating various model payloads, including analysis of particle characteristics, stability and release data.

(2) Facilitate the surface-conjugation of targeting ligand RDP to optimal NP preparations via amide bond formation. Free carboxyl groups of PLGA can be activated to react with amine groups of the RDP sequence, promoting attachment of RDP to the NP.

2.2. Materials and Methods

2.2.1. Materials

Resomer® RG 502 H, Poly(D,L-lactide-*co*-glycolide) (PLGA) 50:50**,** acid terminated **(**MW 7,000-17,000), dichloromethane (DCM), poly(vinyl) alcohol (PVA) 87-89% hydrolyzed- MW 85,000-124,000, poly(ethylene glycol) methyl ether-*block*-poly(L-lactide-*co*-glycolide) (PEG-PLGA), bovine serum albumin, myoglobin, 3,3-dimethylglutaric acid (DMGA), MES hydrate, 1-ethyl-3-(3-dimethylaminopropyl)-carbodiimide (EDC), N-hydroxysuccinimide (NHS), were all purchased from Sigma-Aldrich (UK). RDP was synthesised by GL Biochem (Shanghai) Ltd. Doxorubicin hydrochloride was obtained from VWR International (Pennsylvania, USA). 4-12% Bis-Tris NuPAGE® gel, NuPAGE® MES SDS Running Buffer (20X), Coomassie Brilliant Blue R-250 dye and SeeBlue® Plus 2 pre-stained protein standard were all purchased form ThermoFisher Scientific (UK).

2.2.2. Preparation of Nanoparticles (NP)

2.2.2.1. Preparation of blank NP by a single emulsion solvent-evaporation method

Acid terminated (Resomer® 502 H) PLGA (100 mg) was dissolved in 4 mL of dichloromethane (DCM). PVA was prepared as a 1.25% solution in double distilled water (ddH_2O). The PLGA/DCM organic phase was added dropwise to 50 mL of 1.25% w/v PVA solution and homogenised on full power for 6 minutes (Silverson LST homogeniser, Silverson, USA). Solvent was evaporated from the resulting o/w emulsion by stirring overnight at room temperature. The NP emulsion was then centrifuged at 18809 *g* for 30 minutes at 4 °C, before washing the pellet with ddH_2O thrice for ten minutes each time. The final pellet was resuspended in 5 mL ddH_2O

and freeze dried using a Labconco FreeZone 4.5 plus benchtop freeze dry system on automatic mode (-40°C, 0.12 mbar) for 48 hours.

2.2.2.2. Preparation of doxorubicin-loaded NP (Dox NP) by a double emulsion-solvent evaporation technique

Doxorubicin hydrochloride was selected as a model hydrophilic drug for incorporation into PLGA NP due its cytotoxic effects, which is easy to quantify in cell-based assays. A double emulsion-solvent evaporation technique, as depicted in Figure 2.1, was initially used to fabricate drug-loaded PLGA NP according to methods similar to McCarron et al. (2008) and Kalaria et al. (2009).

Model drug, doxorubicin hydrochloride (2 mg) was dissolved in 1 mL of 2.5% w/v PVA solution in ddH_2O. This was added dropwise to a solution of 100 mg PLGA in 4 mL DCM and mechanically homogenised on full power for 2 minutes (on ice) to produce the primary w/o emulsion (VDI 12 S2 homogeniser, VWR International Ltd., USA). This w/o emulsion was then added dropwise to 50 mL of 1.25% w/v PVA solution and homogenised (on ice) for a further 6 minutes on full power to produce a w/o/w double NP emulsion. After allowing solvent to evaporate overnight at room temperature, the NP formulation was centrifuged and freeze dried, as detailed in section 2.2.2.1. Supernatant from centrifugation was retained to analyse doxorubicin entrapment efficiency (EE) using UV-Visible spectroscopy at 480 nm.

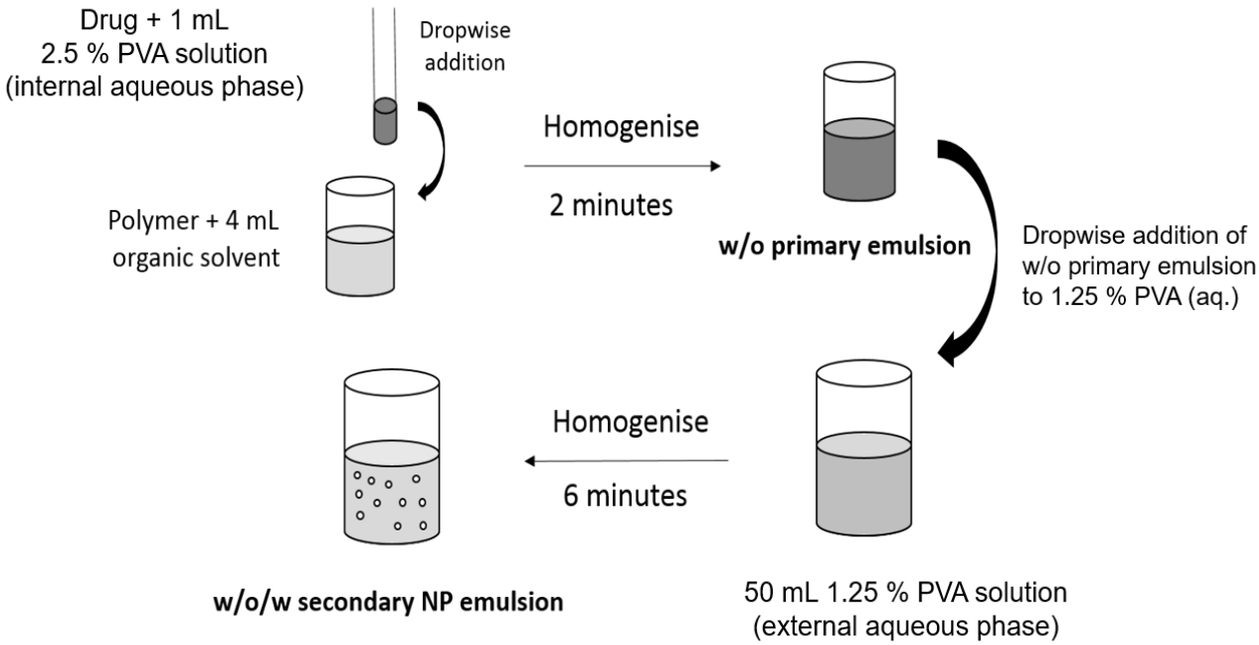

Figure 2.1. Diagrammatic representation of a double emulsion technique used to prepare drug-loaded PLGA NP.

2.2.2.3. Method development of NP preparation

To optimise the PLGA NP formulation parameters bovine serum albumin (BSA) was used as a model drug to mimic a hydrophilic protein payload (MW 66.5 kDa). Using the same double emulsion method as previously detailed in section 2.2.2.2, the addition of PEG-PLGA co-polymer (5% and 10% w/w) to PLGA was analysed along with varying the internal and external aqueous phase percentage of PVA surfactant. The effect of using different solvents in the organic phase on hydrophilic drug entrapment was subsequently investigated in comparison to DCM. The solvents used in addition to DCM were ethyl acetate, DCM/acetone 1:1, DCM/acetone 4:1 and DCM/methanol 1:1. Following these modifications, lead formulations were selected based on

best characteristics such size, PDI, zeta potential and drug entrapment. Additional adjustments such as reducing internal/external aqueous phase volumes were also explored to further optimise NP characteristics. BSA loading was maintained constant at 4% w/w (4 mg BSA per 100 mg polymer).

Finally, the effect of using a probe sonicator in small volumes rather than a mechanical homogeniser was investigated for effect on NP characteristics. The primary w/o emulsion phase was sonicated on ice with a Fisher Scientific FB50 sonicator probe (Pittsburgh, PA, USA) for 60 seconds at 80% amplitude (55 W). The second emulsion (w/o/w) was formed after sonication for a further 2 minutes, on ice, under the same conditions.

An optimised method of Dox NP formulation was subsequently developed as a result of investigations carried out in section 2.2.2.3.

2.2.2.4. Preparation of myoglobin-loaded NP (Myo NP)

Myoglobin (16.7 kDa) was selected as a second model protein payload, due its similarity in molecular weight to basic fibroblast growth factor (18 kDa). The optimal NP formulation conditions, as a result of investigations from section 2.2.2.3, were selected to fabricate myoglobin-loaded NP (Myo NP) at 4% w/w loading (4 mg drug per 100 mg polymer). Various Myo NP were prepared by the double emulsion-solvent evaporation method and characterised according to methods in section 2.2.4.

2.2.3. Determination of drug entrapment efficiency (EE)

Doxorubicin EE was calculated indirectly using supernatant from the formulation process. A standard curve of doxorubicin concentration was prepared using UV-Visible absorbance spectrometry at 480 nm (Figure 2.2). The amount of drug present in the supernatant was measured at 480 nm and calculated according to the equation from the standard calibration

curve. This value was subtracted from the total amount of doxorubicin initially added during the formulation process.

Percentage EE was subsequently calculated according to the following formula:

Equation 2.1. $$EE = \frac{Mass\ of\ drug\ added - mass\ of\ drug\ in\ supernatant}{Mass\ of\ drug\ added}\ x\ 100\%$$

For proteins payloads, BSA and myoglobin, the EE was also calculated indirectly using a BCA (bicinchoninic acid) assay. A standard calibration curve was obtained through dilutions of albumin standard (2 mg/mL) provided in the Pierce™ BCA Protein Assay Kit (ThermoFisher Scientific). Using the microplate method, 25 µL of protein solution was added per well. 200 µL of working reagent was added to protein samples in each well and subsequently incubated at 37°C for 30 minutes. After 30 minutes, UV-Visible absorbance of samples at 562 nm was measured. Protein causes the reduction of Cu^{2+} to Cu^{1+} under alkaline conditions. The cuprous cation (Cu^{1+}) is detected by bicinchoninic acid to induce a colour change of the sample from green to purple. BCA assay was carried out on supernatant from the NP formulation process of either BSA or myoglobin payload. Protein concentration was calculated according to the standard calibration curve (Figure 2.3) and EE was subsequently obtained according to Equation 2.1 above, as for doxorubicin.

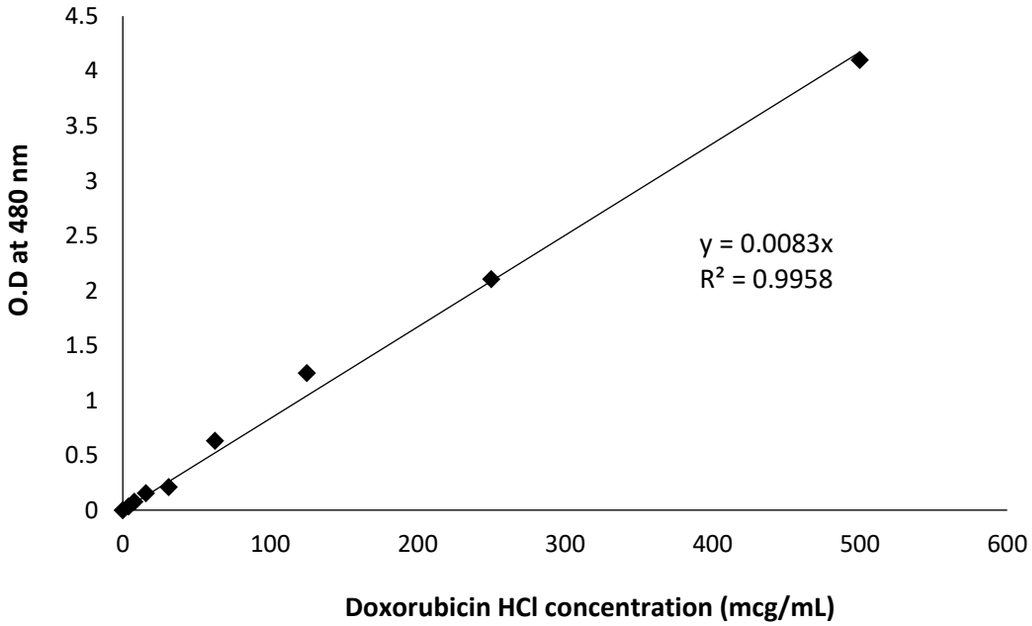

Figure 2.2. Calibration curve of doxorubicin hydrochloride using UV-Visible spectroscopy at 480 nm, used to calculate doxorubicin entrapment efficiency in PLGA NP.

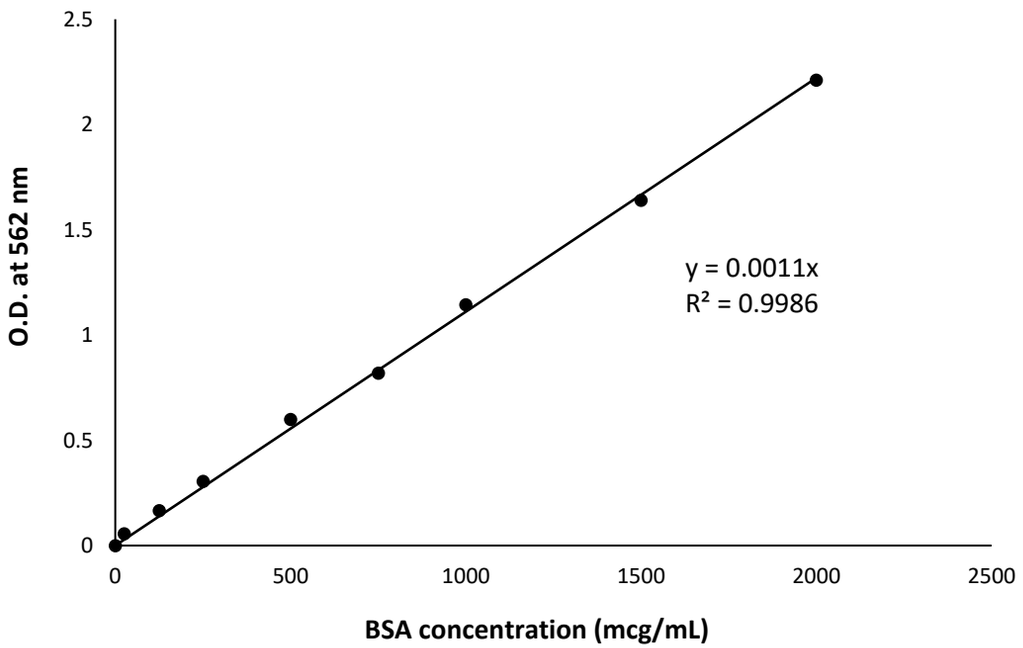

Figure 2.3. BCA assay calibration curve of bovine serum albumin (BSA) using UV-Visible spectroscopy at 562 nm, used to calculate protein drug entrapment efficiency in PLGA NP.

2.2.4. Dynamic Light Scattering (DLS)

NP were characterised for size, zeta potential (ZP) and polydispersity index (PDI) by dynamic light scattering (DLS) analysis using a Malvern Zetasizer (Nano-series, Malvern Instruments, UK). Prior to DLS analysis, 1 mg of NP were dispersed in 1 mL of ddH_2O for measuring size and PDI. For ZP measurements, NP were dispersed in 1.0 mM KCl, pH 7.5, to maintain a constant ionic strength. NP suspensions were filtered using a using a 0.45 µm sterile filter prior to analysis to remove aggregated material. Results were taken as an average of three measurements and reported as average ± standard deviation (SD).

2.2.5. Drug release studies

Release of doxorubicin and myoglobin from leading NP formulations was measured at 37 °C in both 0.1 M PBS at pH 7.4 and 0.01 M dimethylglutaric acid (DMGA) buffer at pH 4.5, according to a method similar to Betancourt et al. (2007). The acidic environment in DMGA buffer mimics the pH conditions of endocytic vesicles during cellular uptake, as late endosomes/lysosomes can have a pH of around 4.5 (Sorkin & von Zastrow, 2002).

DMGA buffer (0.01 M) was prepared by addition of 3, 3-dimethylglutaric acid (6 mM), sodium hydroxide (3.9 mM) and sodium chloride (150 mM) to ddH_2O. Sodium hydroxide (2 M) was used to adjust the buffer to pH 4.5. PBS was prepared by dissolving one PBS tablet per 100 mL of distilled water. Dox NP or Myo NP (15 mg) were added to a centrifuge tube and dispersed in 10 mL of either PBS or DMGA buffer before being incubated at 37 °C in an orbital shaker at 100 RPM. Drug release was measured at various time points over 7 days by centrifuging the respective NP samples at 18809 *g* for 12 minutes and then transferring 200 µL aliquots of supernatant to a 96-well plate. 200 µL of fresh buffer was replaced to maintain sink conditions.

Doxorubicin UV-Visible absorbance was measured at 480 nm (FLUOstar Omega microwell plate reader, BMG Labtech, Germany). The amount of drug in the supernatant was calculated using

a standard curve for doxorubicin. Doxorubicin release was calculated as a percentage of maximum total doxorubicin in the NP, determined from the EE, with results expressed as percentage cumulative release. The same process was used to calculate myoglobin release; however, a BCA assay was used to determine myoglobin concentration in the collected samples.

2.2.6. NP and payload stability studies

2.2.6.1. Scanning electron microscopy (SEM) imaging of NP morphology

Blank PLGA NP preparations were prepared and re-suspended in ddH_2O. Samples were incubated at 37 °C for 0, 1, 4, 10, 30 and 60 days prior to freeze drying, to assess changes in polymeric NP characteristics at normal body temperature (36.5-37.5 °C). Small quantities of NP were mounted onto an aluminium stub and sputter coated in a Polaron E5100 sputter coater equipped with a gold/palladium target, prior to imaging under high vacuum in secondary electron mode (F.E.I Quanta Environmental). The use of ddH_2O was preferred over phosphate buffered saline (PBS) or indeed cell culture media, due to the possibility of salt deposits or other residual material causing decreased SEM image quality.

2.2.6.2. Assessment of myoglobin payload stability using SDS-PAGE

The stability of the NP payload on dry storage over 6 months was evaluated using sodium dodecyl sulphate- polyacrylamide gel electrophoresis (SDS-PAGE). Freshly prepared myoglobin-loaded NP were lyophilised prior to storage at room temperature in a desiccator and protected from light. At various time points, NP (1 mg) were added to 1 mL of ddH_2O and vortexed to aid dispersion. 50 µL of NP sample was immediately added to 10 µL Laemmli treatment buffer (5x) and boiled for 10 minutes to denature NP and protein payload. Denatured samples were frozen and stored until required.

Approximately 30 µL of myoglobin samples and 10 µL of SeeBlue® Plus2 protein markers (Invitrogen, UK) were loaded onto a 4-12% Bis-Tris NuPAGE® gel in MES SDS running buffer (1x). Gel electrophoresis was carried out in a Novex XCell SureLock™ Mini-Cell electrophoresis system (Life Technologies, USA) over 45 minutes and subsequently stained for 2 hours with a gel stain containing Coomassie Brilliant Blue dye. The gel was destained overnight under gentle agitation at room temperature. Formulas of treatment buffer and staining reagents are given in Appendix 1.

2.2.7. Conjugation of peptide to Dox NP

RDP was surface-conjugated to Dox NP via NHS/carbodiimide-mediated amide bond formation between peptide and free PLGA carboxyl groups, as shown in Figure 2.4 (Scott et al., 2008; Mathew et al., 2012; Liu et al., 2017a). Firstly, 10 mL of 25 mM MES buffer (pH 5-6) containing 30 mg/mL EDC and 60 mg/mL NHS was prepared as one solution. This was added to 10 mL of a 30 mg/mL suspension of Dox NP, also in MES buffer (25 mM), to produce a total volume of 20 mL. This suspension was stirred at room temperature for one hour to activate free carboxyl groups of the acid terminated PLGA using EDC/NHS chemistry. The activated Dox NP suspension was centrifuged at 18809 *g* for 30 minutes at 10°C, before washing the pellet thrice with ddH_2O to remove excess EDC/NHS. The activated Dox NP were resuspended in a small volume of PBS and 1 mL of peptide solution containing 3 mg RDP was added (500 mcg RDP per 5 mg NP). The Dox NP/peptide mixture was initially incubated overnight at 4 °C to allow peptide conjugation to activated carboxyl groups. However, upon method development to improve conjugation efficiency, this step was subsequently altered. Instead, Dox NP/peptide were agitated gently on an orbital shaker (75 RPM) at room temperature for 8 hours. Finally, the Dox NP were recovered by centrifugation as before and resuspended in PBS to produce RDP-labelled Dox NP (RDP Dox NP). The supernatant was collected to assess peptide conjugation efficiency (CE) using a BCA assay and UV-Vis spectrometry at 562 nm.

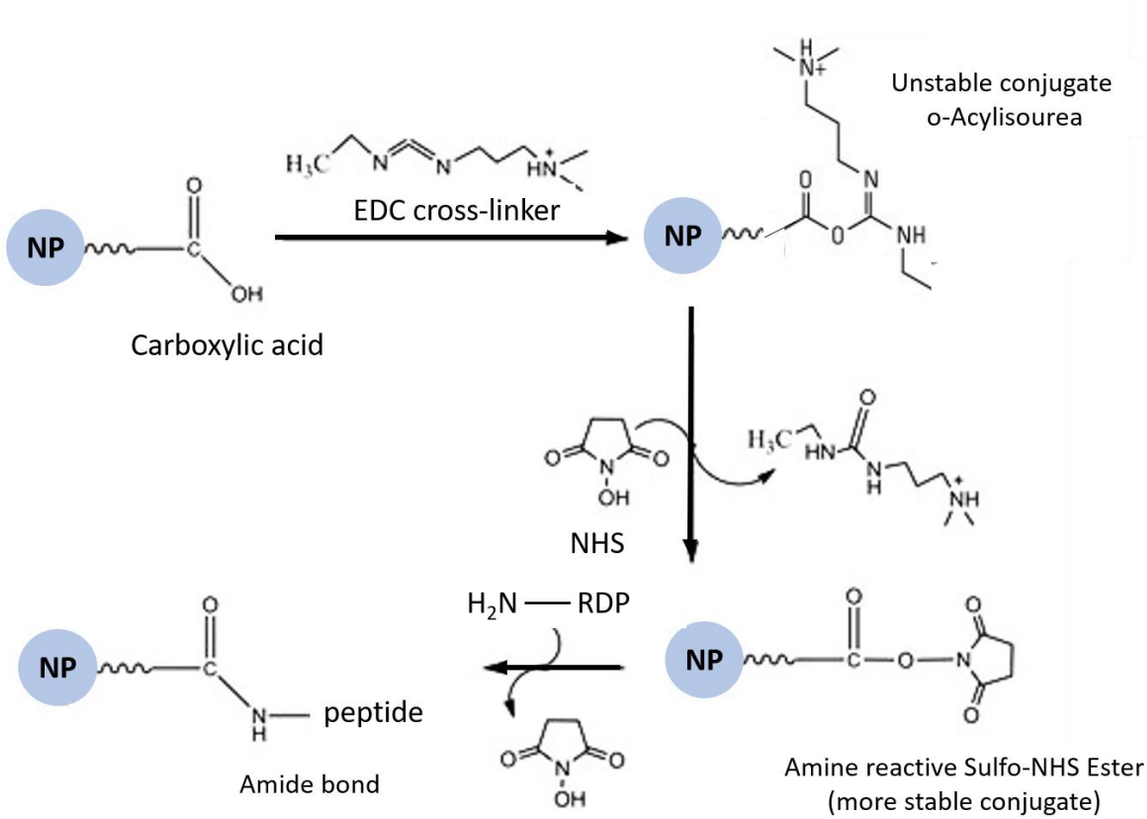

Figure 2.4. Schematic diagram of amide bond formation between PLGA NP and RDP via EDC/NHS chemistry. Free carboxyl groups of PLGA are activated by formation of two reactive intermediates, which are then able to form the amide bond with free primary amine groups on RDP.

2.2.8. Determination of RDP conjugation efficiency (CE)

RDP CE to PLGA NP was determined indirectly by a BCA assay. A standard curve was prepared from absorption of albumin standards at 562 nm as before, allowing the amount of unconjugated RDP in the supernatant from the peptide conjugation process to be determined. Using this value, the amount of RDP conjugated to NP was calculated indirectly, based on the total amount added during formulation.

The peptide CE was calculated according to the following formula:

Equation 2.2. $$CE = \frac{Mass\ of\ peptide\ added - Mass\ of\ peptide\ in\ supernatant}{Mass\ of\ peptide\ added}\ x\ 100\%$$

2.2.9. Statistical Analysis

All results reported were statistically analysed using either an unpaired two-tailed t-test or a one/two-way ANOVA with or without post-hoc tests. A P-value of < 0.05 was considered statistically significant.

2.3. Results & Discussion

2.3.1. NP formulation using a double emulsion-solvent evaporation method

NP were formulated according to a double emulsion-solvent evaporation method and characterised for size, zeta potential (ZP) and polydispersity index (PDI) using dynamic light scattering (DLS). Table 2.1 shows the results of NP characterisation studies and entrapment efficiency of cytotoxic model drug doxorubicin. Doxorubicin was selected as a model payload as its cytotoxic effects are easy to detect and is relatively inexpensive compared to other drugs. PDI, reflecting the homogeneity of particle size, was 0.26 ± 0.04 for blank PLGA NP indicating a relatively narrow size range (scale 0-1). It was determined that blank PLGA NP had an average

particle diameter of 240.2 ± 14.7 nm and a zeta potential of -18.4 ± 1.82 mV. PLGA NP are often sized between 200-300 nm, even after drug loading (Azizi et al., 2013).

Table 2.1. Characterisation properties of blank PLGA NP and doxorubicin-loaded PLGA NP formulated in a pilot study using the double emulsion-solvent evaporation method.

Formulation	Size (nm)	PDI [a]	ZP [b] (mV)	Dox EE [c] (%)
Blank NP	240.2 ± 14.7	0.26 ± 0.04	-18.4 ± 1.8	-
Dox NP	242.7 ± 18.6	0.23 ± 0.01	-14.6 ± 1.3	35.5

[a] Polydispersity index ± standard deviation (SD), n=3; [b] Zeta potential (mV) ± SD, n=3; [c] Percentage drug entrapment efficiency (EE). Following drug EE of 35%, drug content = 7 µg per 1 mg NP.

NP size is important as it can affect cellular uptake ability and *in vivo* distribution (He et al., 2010). Polymeric NP of around 50 nm are most efficiently internalised by cell endocytosis (Jiang et al., 2008). *In vivo* however, small particles (<100 nm) can non-specifically accumulate in many areas of the body. Alternatively, uptake in target cells is difficult to achieve when particles are too large (> 500 nm) for most endocytosis mechanisms (Iversen et al., 2011) and are eventually sequestered by the liver (Cheng et al., 2007). It is difficult to predict how size of NP will affect their biodistribution *in vivo*, as this can vary with different body organs (Cheng et al., 2007). Conjugation of NP to a specific targeting ligand such as RDP, would help to control *in vivo* biodistribution despite particle size. Nevertheless, NP size of around 240 nm as reported in Table 2.1, is ideal for drug targeting.

Incorporation of a doxorubicin payload caused a negligible effect on average NP diameter (242.7 ± 18.6 nm) and PDI (0.23 ± 0.01) compared to the blank NP formulation as P values were 0.86 and 0.28 respectively (two-tailed T-test, statistically significant if < 0.05). The zeta potential of

the Dox NP however increased to -14.64 ± 1.32 mV, which was a statistically significant change compared to the blank NP (P value 0.04). Doxorubicin encapsulation caused NP zeta potential to become less negative, possibly due to drug molecules at the NP surface as well as in the core of the NP, affecting surface charge. Zeta potential is important for the stability of a NP emulsion, as charge at the NP surface means particles are less likely to aggregate through electrostatic repulsion (Honary & Zahir, 2013). Additionally, this can aid cellular uptake through electrostatic interactions at cationic and anionic sites of the cell membrane (Frohlich, 2012). It is desirable that NP zeta potential holds a value between +/- 10-30 mV (Clogston & Patri, 2011) as particles which are too positive can cause membrane damage and those which have a large negative charge risk being repelled from the largely anionic cell membrane. Due to these reasons, it is preferable to formulate NP which are not of neutral zeta potential, unless modified with a targeting ligand.

Doxorubicin entrapment efficiency (EE) was determined indirectly using UV-Visible spectroscopy and was calculated to be 35.5%, using the original formulation method described in section 2.2.2.2. This meant that 0.7 mg of doxorubicin was encapsulated in 100 mg of PLGA polymer from a theoretical maximum of 2 mg (2% w/w drug loading). The difficulty in achieving a high entrapment of doxorubicin is possibly owing to the high water solubility of doxorubicin hydrochloride. Indeed, highly hydrophilic drugs are generally difficult to encapsulate, due to rapid diffusion of drug into the external aqueous phase during formulation. Different factors such as organic phase solvent, surfactant content and phase volumes may all affect how much drug is encapsulated and thus these parameters were investigated herein.

2.3.2. NP formulation development studies

2.3.2.1. BSA formulation studies

The NP size, zeta potential and PDI shown in Table 2.1 are satisfactory characteristics of a drug-targeting nanoparticulate delivery vehicle. However, the poor EE of hydrophilic drug could be

improved for better therapeutic efficiency and reduction of expense due to drug wastage. Considering this, certain formulation parameters from the original method were modified to investigate the effect on drug encapsulation, whilst maintaining good size and zeta potential properties. The ideal payload, such as basic fibroblast growth factor, is a protein and much larger than doxorubicin. Growth factors however are expensive and therefore for optimisation of NP formulation, bovine serum albumin (BSA) was used as a model payload to identify lead formulations. Table 2.2 shows the formulation parameters tested in the first stage of investigations. BSA loading (4% w/w), phase volumes, surfactant type and homogenisation times were kept constant for Formulations 1-10 (Table 2.2).

Table 2.2. Preliminary investigation of NP formulation parameters to optimise hydrophilic drug encapsulation. Ten different NP formulation conditions are detailed, varying solvent, PEG-PLGA content and PVA concentration of the aqueous phases. All other conditions are as previously described for the original formulation.

Formulation	Solvent	PEG-PLGA (%)	W1 PVA (%)	W2 PVA (%)
1	DCM	0	2.5	1.25
2	DCM	0	4	2
3	DCM	5	2.5	1.25
4	DCM	5	4	2
5	DCM	10	2.5	1.25
6	DCM	10	4	2
7	Ethyl acetate	0	2.5	1.25
8	DCM & Methanol 1:1	0	2.5	1.25
9	DCM & acetone 1:1	0	2.5	1.25
10	DCM & acetone 4:1	0	2.5	1.25

Constant formulation conditions- 4% drug loading, internal aqueous phase (W1) 1 mL, external aqueous phase (W2) 50 mL, full power mechanical homogenisation 2 min (w/o) & 6 min (w/o/w).

Surfactants such as PVA in the external aqueous phase are necessary for the formation of NP emulsions. PVA acts as a stabilising agent, reducing surface tension and thus preventing coalescence between newly-formed particles (Rao & Geckeler, 2011). Surfactant inclusion in the inner aqueous phase (W1) has been reported to further decrease particle size and aids drug entrapment in PLGA NP prepared by double emulsion-solvent evaporation methods (Chen et al., 2008; Yan et al., 2010; Mobarak et al., 2013). Chen et al. (2008) prepared peptide-loaded PLGA NP using similar formulation parameters to the methods described in this work. Chen and colleagues reported poor entrapment of peptide when surfactant was not used in the inner aqueous phase and a larger particle size. PVA was therefore also included in the original formulation in the W1 phase, at a concentration of 2.5% (w/v). It was subsequently investigated whether increasing PVA concentration to 4% (Formulations 2, 4 & 6) would improve drug entrapment efficiency, results of which are shown in Table 2.3.

Table 2.3. Results of characterisation studies for the 10 formulations detailed in Table 2.2. Dynamic light scattering analysis was used to obtain size, PDI and zeta potential measurements. Entrapment efficiency of protein model drug, BSA, was measured by BCA assay.

Formulation	Size (nm)	PDI [a]	ZP [b] (mV)	BSA EE [c] (%)
1	177.4 ± 6.8	0.29 ± 0.01	-15.6 ± 0.0	11.0
2	203.5 ± 4.0	0.43 ± 0.02	-9.6 ± 0.7	0
3	258.8 ± 18.4	0.53 ± 0.05	-12.0 ± 0.7	16.6
4	256.5 ± 0.5	0.28 ± 0.02	-6.6 ± 0.5	0
5	315.0 ± 39.2	0.35 ± 0.06	-2.5 ± 0.0	10.0
6	324.7 ± 17.3	1.00 ± 0.00	-2.5 ± 0.0	0
7	108.3 ± 55.5	0.61 ± 0.40	-8.6 ± 0.3	0
8	131.3 ± 3.8	0.29 ± 0.03	-8.6 ± 0.1	0
9	178.2 ± 9.6	0.28 ± 0.01	-24.4 ± 2.8	0
10	137.1 ± 4.6	0.35 ± 0.03	-5.6 ± 0.3	0

[a] Polydispersity index ± standard deviation (SD), n=3; [b] Zeta potential (mV) ± SD, n=3; [c] drug entrapment efficiency (%). Statistical analysis between groups was carried out using a one-way ANOVA with Tukey's HSD post-hoc test.

No BSA entrapment was detected in Formulations 2, 4 and 6 containing 4% (w/v) PVA (W1). Despite low entrapment efficiency, some BSA was encapsulated when W1 contained 2.5% w/v PVA in Formulations 1, 3 and 5. In this instance, higher W1 PVA content did not improve encapsulation of drug and therefore remained at 2.5% (w/v) to investigate the effect of using more water-miscible solvents in the organic phase (Formulations 7-10). PEG-PLGA co-polymer was introduced as part of the polymer blend at either 5% or 10% (w/w) in combination with different PVA concentrations (Formulations 3-6). It has been well established in the literature the potential advantages of including PEG in NP formulations, mainly due to its shielding effect from the reticuloendothelial system and ultimately prolongation of *in vivo* half-life (Choi et al., 2011).

From the NP formulations which did show some BSA encapsulation, the size ranged from 177.4 ± 6.8 nm (Formulation 1) to 315.0 ± 39.2 nm (Formulation 5). The only difference in these three formulations was the PEG-PLGA content, which appeared to significantly increase average BSA-loaded NP diameter when results were statistically analysed using a one-way ANOVA (P value 0.0016) and Tukey's HSD post-hoc test (all P values < 0.05). Increasing PEG-PLGA content also significantly affected surface charges between Formulations 1, 3 & 5 (P value < 0.05). The 10% PEG-PLGA in Formulation 5 caused zeta potential to become less negative and closer to neutral (-2.5 mV) compared to 5% PEG-PLGA in Formulation 3 (-12.0 mV) and no PEG in Formulation 1 (-15.6 mV).

The organic phase was altered to contain more water-miscible solvents such as ethyl acetate, methanol and acetone (Formulations 7-10). The primary emulsion from section 2.3.1 was produced using the water immiscible solvent, DCM, which might encourage rapid partition of doxorubicin hydrochloride into the outer aqueous phase during formulation of the second emulsion. Use of a different solvent, which is more water miscible, could perhaps improve the amount of doxorubicin entrapped in the inner organic phase as suggested by Cohen-Sela et al. (2009). This was investigated as the most likely factor to affect drug entrapment and so to compare effect, PVA and polymer composition were kept the same as the original formulation.

Ethyl acetate has been used previously as the organic phase in the formulation of drug-loaded PLGA NP (Song et al., 2006; Mobarak et al., 2013), however did not improve BSA EE of Formulation 7 (Table 2.3). Liu et al. (2010) introduced acetone to the organic phase alongside DCM in a ratio of 1:4, which improved entrapment efficiency of hydrophilic daunorubicin from 26% to 81%. This organic phase composition was tested in different ratios (Formulations 9 &10) and once again, no BSA was encapsulated. Introduction of water miscibility to the organic phase was not successful for protein encapsulation in these studies, despite some desirable NP size, PDI and zeta potential measurements (Table 2.3). Bilati et al. (2005a) similarly found DCM preferable over ethyl acetate for encapsulation of BSA in PLGA NP. However, in a different study, Bilati et al. (2005b) also showed that choice of solvent is protein-dependent. Bilati and colleagues achieved high entrapment of insulin using DCM as the organic phase, however tetanus toxoid and lysozyme were more efficiently entrapped in PLGA NP using ethyl acetate (Bilati et al., 2005b). Drug encapsulation is most essential and therefore higher PVA content and water-miscible solvents were excluded at this stage from further studies.

DCM is an organic solvent associated with environmental and health risks due to its mutagenic potential (Schlosser et al., 2015). The International Committee for Harmonisation limit of residual DCM detection in pharmaceuticals is no more than 600 ppm (Hu & Liu, 2011). Han et al. (2012) reported that residual DCM in NP prepared by solvent evaporation method can be reduced to around 300 ppm when NP are washed thrice after preparation and aqueous phase PVA concentration remains around 1% (w/v). Given the NP prepared in this study were washed thrice as detailed in section 2.2.2.1, DCM was selected as the organic phase to be used for further *in vitro* studies without major concerns of toxicity. The residual DCM was not analysed for the NP reported herein, however should be considered as a potential limitation of future use *in vivo.*

Since no improvements to the original NP formulation process were identified through this pilot study, further parameters were explored as shown in Table 2.4.

Table 2.4. Varying formulation parameters during the second phase of NP formulation development. Optimal conditions identified from results of Table 2.3. were chosen to remain constant whilst varying the volume of the internal (W1) and external (W2) aqueous phases. The effect of removing PVA surfactant from the internal aqueous phase (W1) was also investigated.

Formulation	W1 volume (mL)	W2 volume (mL)	W1 PVA (%)
11	1.0	50	0
12	1.0	20	0
13	1.0	20	2.5
14	0.5	20	0

Constant formulation conditions- 4% drug loading, DCM solvent, 0% PEG-PLGA, 1.25% PVA in external aqueous phase (W2), full power mechanical homogenisation 2 min (w/o) & 6 min (w/o/w).

Due to observations of better BSA encapsulation with less PVA (Table 2.3.), the effect of removing PVA from the internal aqueous phase (W1) was explored during the second stage of NP formulation development (Table 2.4.). Additionally, reduction in PVA content would be preferable for reducing the risks associated with residual DCM in the NP. Furthermore, the effect of changing the aqueous phase volumes was also observed for Formulations 11-14 (Table 2.4.). Mao et al. (2007) found that reducing both the internal aqueous phase (W1) and external aqueous phase (W2) volumes during PLGA NP formulation had minimal effect on particle size, however improved hydrophilic drug entrapment efficiency. Mao and colleagues hypothesised that reduced phase volumes would lead to a more profuse organic phase, which might reduce the rate of drug diffusion from W1 to W2 during solvent evaporation. Drug loading, solvent and polymer composition (no PEG-PLGA) were kept constant for these studies, results of which are shown in Table 2.5.

Characterisation of Formulation 11 in Table 2.5 shows the effect of removing PVA surfactant from the internal aqueous phase (W1), which improved BSA EE (36.9%) compared to the original formulation conditions used in Formulation 1 (11% EE). A considerable improvement in BSA encapsulation was observed for Formulation 12 (67.5% EE), which was formulated with a

reduction in external aqueous phase (W2) volume to 20 mL (from 50 mL), with no W1 PVA. Feczko et al. (2011) reported a reduction in particle size when the volume of W2 phase was reduced, simply due to higher power density per unit volume during emulsification. Formulations 13 & 14 (Table 2.5) both have significantly smaller average particle sizes with 20 mL W2 phase volume compared to 50 mL with Formulation 11, as P values of < 0.05 were obtained following one-way ANOVA analysis with Tukey's post-hoc test. The reduced phase volume however did not decrease the particle size of Formulation 12, with the marginally larger measurement compared to Formulation 11 being of nil significance (Tukey's post-hoc test P value- 0.6185). Once again, it is shown in Formulation 13 that inclusion of 2.5% (w/v) PVA in W1 is detrimental to BSA EE (34.5%), even with reduced W2 phase volume. Based on these results, future NP formulation procedures would include a smaller volume of external aqueous phase (20 mL or less) and remove the inclusion of PVA in the internal aqueous phase when formulating the primary emulsion (w/o).

Table 2.5. Results of characterisation studies of the four formulations detailed in Table 2.4. The effect of varying phase volumes and presence of PVA surfactant in the aqueous phase primary emulsion (W1) is reflected by dynamic light scattering analysis and determination of BSA entrapment efficiency.

Formulation	Size (nm)	PDI [a]	ZP [b] (mV)	EE [c] (%)
11	390.2 ± 5.8	0.33 ± 0.09	-18.5	36.9
12	401.3 ± 4.7	0.24 ± 0.02	-15.9	67.5
13	311.5 ± 6.1	0.39 ± 0.06	-10.1	34.5
14	226.9 ± 19.6	0.36 ± 0.03	-8.7	73.7

[a] Polydispersity index ± standard deviation (SD), n=3; [b] Zeta potential (mV) ± SD, n=3; [c] drug entrapment efficiency (%). Statistical analysis between groups was carried out using a one-way ANOVA with Tukey's HSD post-hoc test.

Substantial improvement in BSA encapsulation was achieved by varying the external phase volume (W2), therefore the effect of also reducing the internal aqueous phase (W1) volume was investigated for Formulation 14. Interestingly, compared with Formulation 12, reduction in W1 volume from 1 mL to 0.5 mL maintained favourable BSA EE (73.7%) and decreased NP size from 401.3 nm to 226.9 nm. The particle size of NP Formulation 14 is more favourable in this instance, as sizes of 400 nm may be too large for cellular internalisation. NP sized around 200 nm are still large enough to avoid non-specific uptake and accumulation, hence in combination with a specific receptor-targeting ligand, would be ideal drug delivery vehicles.

The zeta potential of Formulation 14 is higher at -8.7 mV compared to Formulation 12 at -15.9 mV. It is not clear why a smaller W1 volume might affect the zeta potential, however it could be due to location of drug within the polymer matrix during the formulation process. The PDI was mostly unaffected by changes in the formulation procedure. Following this second stage in NP formulation development, the lead formulation conditions identified from the results displayed in Table 2.5 are a reduction in the external aqueous phase volume and elimination of PVA from the internal aqueous phase. Favourable NP characteristics were also identified after reducing internal aqueous phase volume to 0.5 mL, therefore both lead NP Formulations, 12 & 14, were selected for further investigation.

Due to the reduction in phase volumes, it was decided that the use of a probe sonicator may be more appropriate in the formulation process than a mechanical homogeniser. The use of high intensity sonication bursts can reduce particle size and agglomeration and thus is an essential step in the production of a homogenous, nanoparticulate emulsion (McCall & Sirianni, 2013).

Formulations 12 & 14 were prepared using a probe sonicator to test whether sonication of the w/o/w emulsion would result in the successful formation of BSA-loaded NP with favourable characterisation properties (Table 2.6).

Table 2.6. The characterisation properties of Formulations 12 & 14 (Table 2.4) using probe sonication to form uniform BSA-loaded NP emulsions.

Formulation	Size (nm)	PDI [a]	ZP [b] (mV)	EE [c] (%)
12	330.1 ± 5.71	0.26 ± 0.05	-12.6 ± 0.78	70.7
14	173.0 ± 11.27	0.31 ± 0.05	-15.2 ± 0.40	76.7

[a] Polydispersity index ± standard deviation (SD), n=3; [b] Zeta potential (mV) ± SD, n=3; [c] drug entrapment efficiency (%). All formulation conditions are as detailed in Table 2.4 apart from use of a probe sonicator (55 W, 80% amplitude) for 1 min (w/o) and 2 min (w/o/w) and reduction of W2 volume to 15 mL. Statistical analysis was carried out using a two-tailed Student's T-test.

Results from Table 2.6 show that sonicating the NP formulation significantly reduces average particle size compared to the previous method (Table 2.5). Sonication reduced particle size to 330.1 nm from 401.3 nm for Formulation 12 (P value < 0.01), whilst Formulation 14 reduced from 226.9 nm to 173.0 nm (P value < 0.05). Furthermore, the zeta potential of Formulation 14 was much improved from -8.7 mV previously, to a more negative value of -15.2 mV. Again, the PDI largely remained at a similar value to previous results, which is acceptable for these studies. The BSA EE following sonication is above 70% for both Formulations 12 & 14, further supporting the use of these formulation parameters and showing a vast improvement from the formulation conditions used in Table 2.3.

2.3.2.2. Myoglobin formulation studies

Following the identification of various modifications to the formulation process that improved the encapsulation of a protein payload, the optimal formulation conditions were selected to fabricate myoglobin-loaded NP (Myo NP). Myoglobin is a 16.7 kDa protein which is similar in molecular weight to basic fibroblast growth factor (18 kDa). Myoglobin therefore more closely represents a model growth factor payload than BSA (66.5 kDa).

Myo NP were prepared according to the lead formulation conditions (Table 2.7) and characterised as for previous NP formulations, the results of which are shown in Table 2.8. Addition of PEG-PLGA and different internal aqueous phase volumes were investigated whilst the solvent (DCM), external aqueous phase (W2) volume (15 mL) and PVA content (1.25% w/v W2 only) remained constant for the sonicated NP preparations (Table 2.7). W2 volume was further reduced from 20 mL to 15 mL during Myo NP formulation in accordance with manufacturer recommendations on use of the probe sonicator.

Table 2.7. The lead formulation parameters identified from previous investigations (Tables 2.2-2.6) were used to formulate myoglobin-loaded PLGA NP. Model drug, myoglobin (16.7 kDa), was loaded at 4% (w/w). The effect of varying PEG-PLGA content and internal aqueous phase volume were investigated.

Formulation	PEG-PLGA (%)	W1 volume [a] (mL)
15	0	0.5
16	0	1
17	5	0.5
18	5	1
19	10	0.5
20	10	1

[a] Internal aqueous phase (W1) volume (mL). Formulation conditions- DCM solvent, W2- 15 mL (1.25% PVA), 4% drug loading, sonication (55 W, 80% amplitude) for 1 min (w/o) and 2 min (w/o/w).

Table 2.8 shows the successful preparation of Myo NP, with Formulation 15 achieving 79.2% EE and favourable size, when W1 phase volume was 0.5 mL and PEG was not included in the formulation. Again, it is shown that a W1 phase volume of 1 mL results in a larger particle size, which was statistically significant (P value < 0.05) between the preparations containing 0% PEG-

PLGA (Formulations 15 & 16) and 10% PEG-PLGA (Formulations 19 & 20). Considering this, 0.5 mL was selected as the W1 phase volume for future NP formulation in this work.

The inclusion of PEG-PLGA in the polymer caused slightly less myoglobin to be incorporated into the NP, especially at 10% (w/w) (Formulations 19 & 20). There was no significant effect of increasing PEG concentration on the NP size between Formulations 15, 17 & 19 (P values > 0.05), however it did seem to cause a significant increase in PDI and reduction in zeta potential (P values < 0.05) between Formulations 15 (0% PEG-PLGA) & 19 (10% PEG-PLGA). The inclusion of 5% and 10% (w/w) PEG-PLGA in the polymer blend may be beneficial and thus Formulations 15, 17 & 19 were selected for further studies.

Table 2.8. Characterisation properties of myoglobin-loaded PLGA NP preparations. Entrapment efficiency of myoglobin (16.7 kDa) is consistent with previous protein payload, BSA (66.5 kDa), despite being smaller in molecular weight.

Formulation	Size (nm)	PDI [a]	ZP [b] (mV)	EE [c] (%)
15	254.6 ± 27.8	0.29 ± 0.08	-8.5 ± 0.5	79.2
16	319.0 ± 28.1	0.33 ± 0.11	-7.5 ± 1.2	73.3
17	227.7 ± 15.4	0.31 ± 0.02	-9.3 ± 0.9	70.2
18	263.5 ± 12.4	0.31 ± 0.03	-7.7 ± 0.9	66.0
19	242.9 ± 14.8	0.40 ± 0.04	-11.4 ± 0.4	51.0
20	384.1 ± 21.8	0.42 ± 0.02	-10.3 ± 1.0	60.5

[a] Polydispersity index ± standard deviation (SD), n=3; [b] Zeta potential (mV) ± SD, n=3; [c] drug entrapment efficiency. Statistical analysis between groups was carried out using a one-way ANOVA with Tukey's HSD post-hoc test.

2.3.2.3. Doxorubicin formulation studies

Using the new formulation parameters, doxorubicin-loaded NP (Dox NP) were prepared once again prior to surface-conjugation with RDP. The new Dox NP formulations were characterised as previously detailed and results of these studies are shown in Table 2.9.

Table 2.9. Doxorubicin NP characteristics showing improved doxorubicin encapsulation and incorporation of PEG-PLGA co-polymer following formulation with a modified double emulsion-solvent evaporation method.

PLGA-PEG (%)	Size (nm)	PDI [a]	ZP [b] (mV)	Dox EE [c] (%)
0	293.5 ± 18.8	0.27 ± 0.02	-13.8 ± 1.2	55.0
5	283.8 ± 17.7	0.21 ± 0.02	-16.6 ± 2.6	59.8
10	268.2 ± 4.8	0.43 ± 0.06	-11.0 ± 2.8	56.5

[a] Polydispersity index ± standard deviation (SD), n=3; [b] Zeta potential (mV) ± SD, n=3; [c] drug entrapment efficiency (%). Formulation parameters- doxorubicin loading at 2%, sonication (55 W, 80% amplitude) for 1 min (w/o) and 2 min (w/o/w), DCM solvent, internal aqueous phase volume 0.5 mL (0% PVA), external aqueous phase volume 15 mL (1.25% PVA). Statistical analysis between groups was carried out using a one-way ANOVA with Tukey's HSD post-hoc test.

The average particle size of all three preparations shown in Table 2.9 narrowly range between 268.2 ± 4.8 nm (10% w/w PEG-PLGA) and 293.5 ± 18.8 nm (no PEG). In contrast to the BSA-loaded NP in Table 2.3, increasing PEG content in this instance slightly decreased Dox NP size however this was not significant following one-way ANOVA statistical analysis (P value 0.2). It has been suggested that PEG reduces co-polymer chain length and hence causes NP size to decrease, as the hydrophobic core is smaller (Lin et al., 2003).

The zeta potential measurements of Table 2.9 vary slightly amongst preparations (not significant), however remain adequately negative for stability and cell targeting. The PDI is significantly higher for the Dox NP containing 10% PEG-PLGA when compared to the 0% and 5% PEG-PLGA groups (P values < 0.01), suggesting a larger range of particle sizes. Most importantly, the doxorubicin EE improved from the original formulation (Table 2.1) to over 50% in all three instances, regardless of PEG content. Similar to the BSA payload, hydrophilic doxorubicin was better encapsulated following the changes in formulation parameters.

2.3.3. NP Stability studies

2.3.3.1. Scanning electron microscopy (SEM)

Blank PLGA NP were imaged by SEM to visualise NP morphology and the effects of incubating in ddH_2O at 37°C over various periods of time. All SEM images shown in Figure 2.5 were captured at x24 000 magnification. Freeze dried sample with no prior incubation in Figure 2.5A shows that NP are spherical in shape, with the presence of many sub-micron particles in the unfiltered sample. Despite some of the largest particles within the sample measuring approximately 1 µm in size, the majority are 200-300 nm, supporting the data obtained from previous DLS analysis in sections 2.3.1 and 2.3.2. Figures 2.5 (B)-(F) show NP which have been incubated at 37 °C for 1, 4, 10, 30 and 60 days in ddH_2O respectively.

It is evident that incubation for 1 day caused the NP to swell and become slightly larger in diameter, with early signs of degradation due to minor surface pitting, as indicated in Figure 2.5B. There were some changes in shape and aggregation of material highlighted in Figure 2.5C, suggesting that after 4 days incubation at 37 °C, degradation processes were underway within the sample. After 10 days of incubation, much larger and aggregated particles were present within the sample, with more signs of structure irregularity in Figure 2.5D. By 30 days of incubation, in Figure 2.5E, most particles increased in size into the micrometre scale. There was continued loss of the regular spherical morphology of individual particles, with agglomeration more apparent. These larger particles were susceptible to breakdown under the beam of the microscope. Finally, in Figure 2.5F after 60 days of incubation, there was complete loss of NP within the sample. Evidence of remaining larger spherical structures are highlighted in Figure 2.5F, as the remainder of the image shows only amorphous residual material.

Obvious NP swelling caused by water absorption through the polymer matrix lead to a progressive increase in NP diameter from time 0 through 30 days (Figure 2.5A- 2.5F). Figures 2.5B and 2.5C are representative of how NP incubated for 1 and 4 days respectively, started to show signs of breakdown through emergence of surface pitting (2.5B) and loss of regular

spherical shape (2.5C). This was minimal at the 1 and 4-day time points, suggesting that despite degradation processes being initiated early, they are perhaps slow. Major differences are observed in Figures 2.5D and 2.5E at 10 and 30 days incubation respectively. At these time points larger and aggregated particles are visible, with loss of regular morphology. Despite the appearance of these irregular particles, there was little to no debris or breakdown material visible, unlike the sample imaged in Figure 2.5F. It is apparent that a gradual degradation is occurring over time and that NP structure is relatively stable over the specified conditions for at least 4 days, with complete loss of nano-sized particles at 60 days.

PLGA is composed of repeating poly lactic acid and poly glycolic acid units. Both poly glycolic acid and poly-L-lactic acid are crystalline solids (Makadia & Siegel., 2011), which may explain the presence of crystal-like deposits among the amorphous breakdown material in Figure 2.5F. A similar SEM image of degraded PLGA NP was reported by Hamoudeh et al. (2008). Between 30 and 60 days in water at 37 °C, the PLGA NP appear to have undergone complete degradation. This degradative process induced by hydrolysis of ester bonds in the polymer matrix, is further autocatalysed by the formation of acidic breakdown products, lactic and glycolic acid, which can be excreted *in vivo* (Catiker et al., 2000). Catiker et al. (2000) found that this hydrolytic activity was quicker in the presence of bovine serum albumin, a major blood protein, than in PBS. It could therefore be hypothesised that complete NP degradation would occur quicker than 30-60 days in the presence of serum, rather than ddH_2O used in this study. This is advantageous, as the ideal drug delivery vehicle would not accumulate in the body over a long period of time. Nevertheless, these NP have shown the ability to swell, form aggregates and develop pits, following a similar pattern of degradation to those imaged by Panyam et al. (2003), Stevanovic et al. (2007) and Hussein et al. (2013). This shows that the PLGA polymer is biodegradable, which is why it is already approved for use as a drug carrier by the Food and Drug Administration (FDA).

(A)

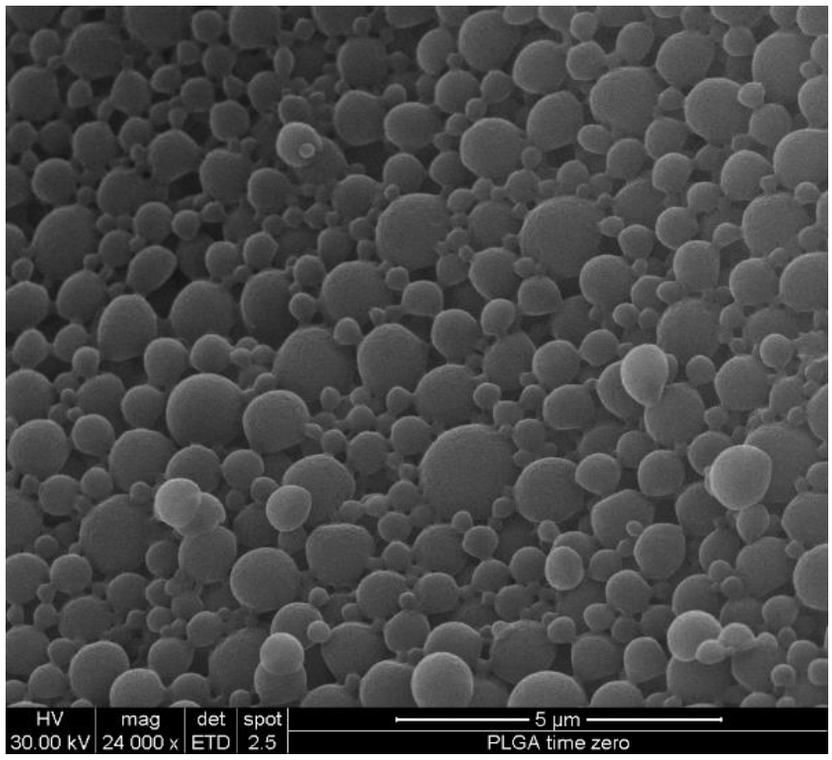
HV
30.00 kV
mag
24 000 x
det
ETD
spot
2.5
5 µm
PLGA time zero

(B)

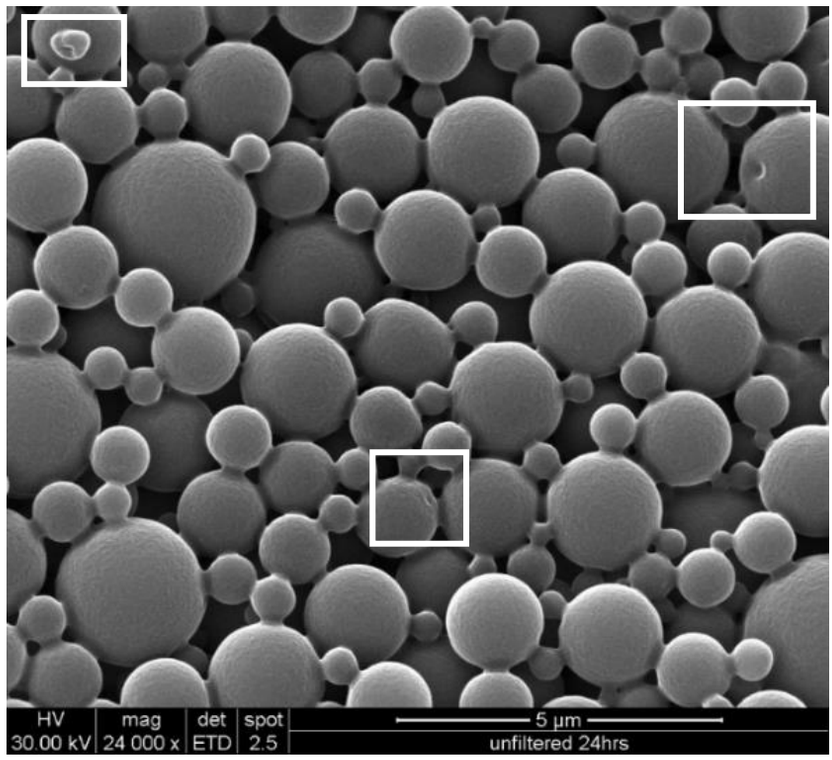
HV
30.00 kV
mag
24 000 x
det
ETD
spot
2.5
5 µm
unfiltered 24hrs

(C)

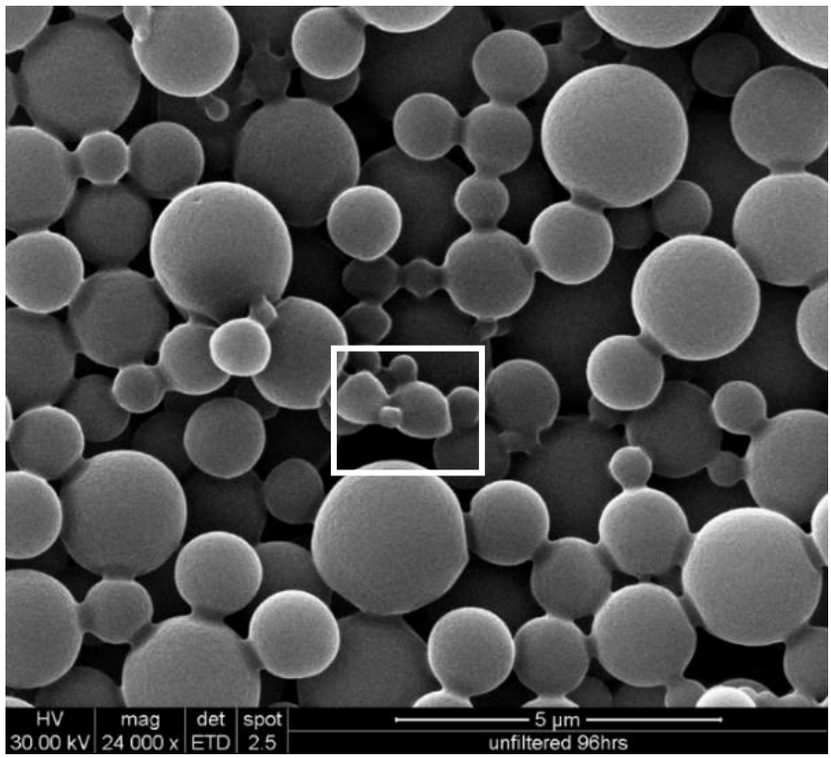
HV
30.00 kV
mag
24 000 x
det
ETD
spot
2.5
5 µm
unfiltered 96hrs

(D)

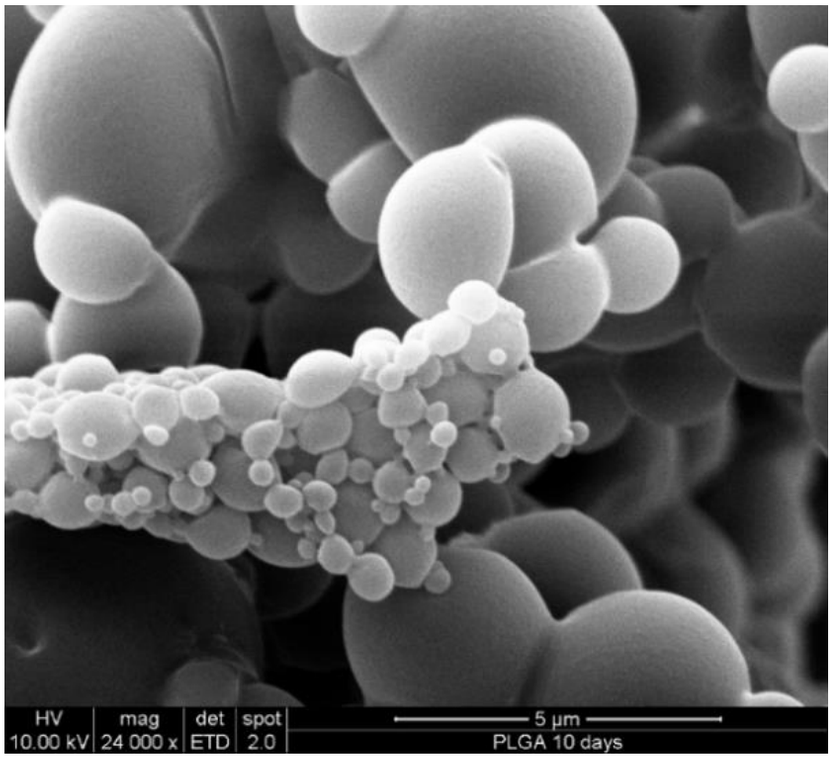
HV
10.00 kV
mag
24 000 x
det
ETD
spot
2.0
5 µm
PLGA 10 days

(E)

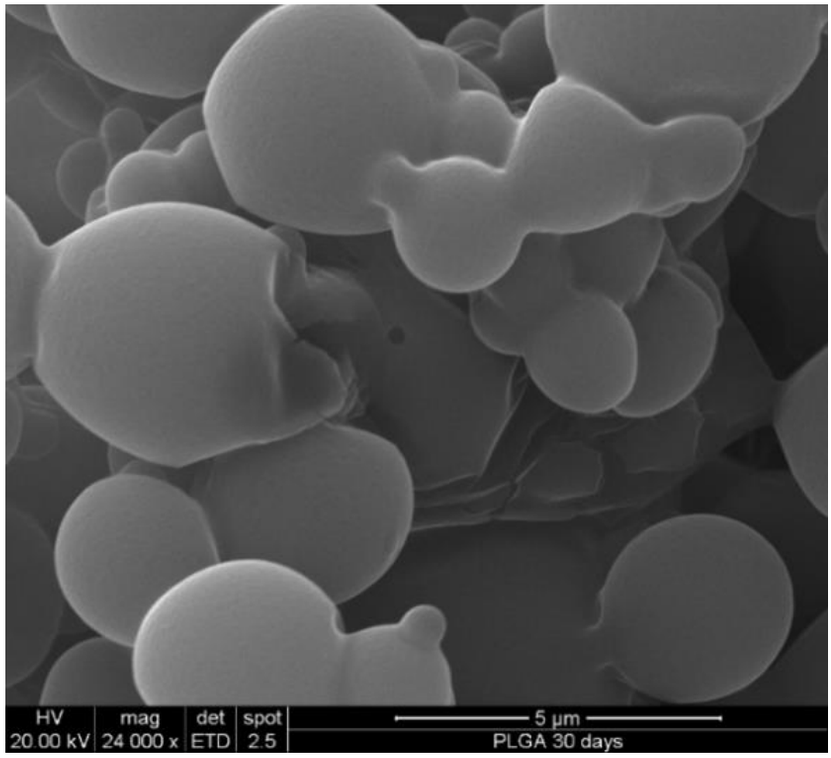

(F)

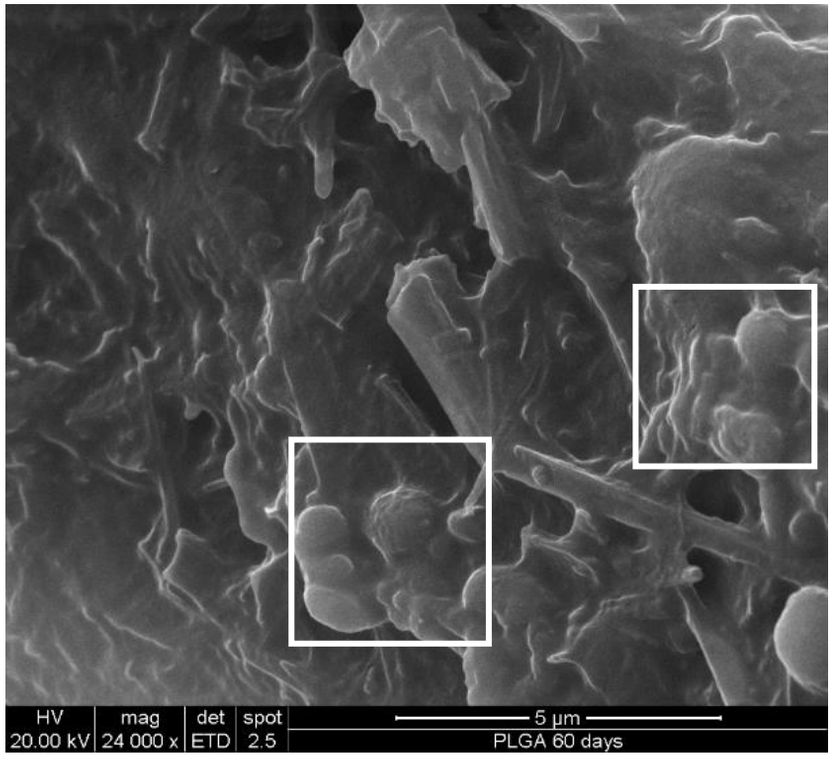

Figure 2.5. SEM images of (A) lyophilised PLGA NP at room temperature and lyophilized PLGA NP after incubation at 37°C in ddH_2O for 1 day (B), 4 days (C), 10 days (D), 30 days (E) and 60 days (F). Evidence of pitting on the NP surface (B) and loss of spherical morphology (C) are highlighted. Traces of spherical NP after 60 days incubation are highlighted in image (F). All SEM images are at x24 000 magnification.

2.3.3.2. Payload stability study using SDS-PAGE

The stability of myoglobin-loaded NP (Myo NP) upon dry storage at room temperature was investigated to assess long-term payload stability. Myo NP were stored over 6 months under the aforementioned conditions in section 2.2.6.2 and samples were taken at various time intervals. Myoglobin payload or potential myoglobin breakdown products were separated and detected using SDS-PAGE. Figure 2.6 shows the bands detected for myoglobin near the 18 kDa marker. Lane 1 shows myoglobin at time zero, detected from freshly prepared freeze-dried NP. All bands in Figure 2.6 are approximately of equal size and no myoglobin breakdown products were detected on the gel, even in lane 8 which represents 6 months of storage. This suggests that the myoglobin payload was stable within the NP structure under such conditions, which is important when utilising expensive drugs and for therapeutic efficacy. As shown with the SEM images in Figure 2.5, degradative processes begin when NP are exposed to an aqueous environment and higher temperature (37°C).

Despite no evidence of myoglobin breakdown, it cannot be determined from these results whether model payload activity would be affected over the observed experimental period. Myoglobin has no measurable activity *in vitro* or *in vivo*, however the ideal growth factor payload could be tested for subsequent activity after storage under the same conditions.

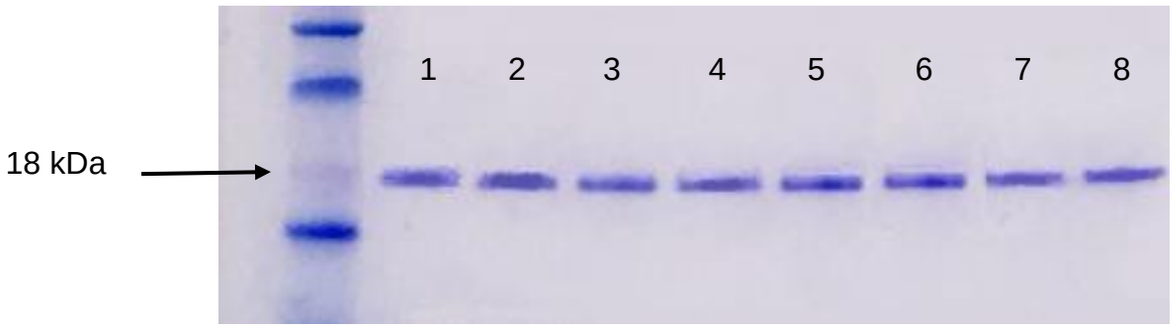

Figure 2.6. Image of an SDS-PAGE gel showing myoglobin (16.7 kDa) payload stability on dry storage of myoglobin-loaded NP at room temperature over a 6-month period. Lanes 1-8 indicate storage times of 0, 1, 2, 4, 6, 16, 20 and 24 weeks respectively. A marker for approximately 18 kDa is indicated.

2.3.4. Drug release studies

The release profiles of lead NP formulations encapsulating either doxorubicin or myoglobin as model drugs are shown in Figures 2.7- 2.12. Ligand-facilitated uptake of NP is largely considered to occur via energy-dependent endocytosis mechanisms (Danhier et al., 2012). Indeed, receptor mediated endocytosis is the proposed mechanism of RDP cellular uptake (Fu et al., 2013a). In order to resemble endocytic conditions, drug release was measured under two different pH environments, to assess how NP payload release would be affected. This would also further assess the stability of the PLGA NP and suitability as part of a targeted drug delivery system.

NP were exposed to two different buffers to reflect drug release under the harsher conditions of the endocytic process at 37°C and cumulative release was measured over 10 days. 10 mM PBS buffer at pH 7.4 provided conditions similar to the extracellular environment, whereas DMGA buffer at pH 4.5 would mimic the acidic environment of the late endosome or indeed the lysosome. Figure 2.7 shows the release of myoglobin from NP in both PBS and DMGA buffer over 5 hours (Figure 2.7A) and 10 days (Figure 2.7B). It can be seen that release in both pH environments is similar for the first four hours, at which point release in DMGA buffer accelerates until 78% of the payload is released after 10 days. This is in contrast to the 35% of myoglobin released in PBS at pH 7.4. Following the first 24 hours, myoglobin release was significantly higher for every time point in DMGA than PBS until day 10 (P values < 0.001). It has previously been shown by Colzani et al. (2016) that 100% cumulative myoglobin release from PLGA NP can take up to 60 days in PBS.

Myoglobin release in PBS is biphasic, with an initial burst phase in the first 5 hours followed by a slower sustained phase over the following days. This is a typical characteristic of PLGA NP, as many reports of a biphasic release profile exist in the literature (Fonseca et al., 2002; Ma et al., 2010; Surolia et al., 2012; Zhu & Braatz, 2015), even when the polymer is pegylated (Park et al., 2009; Yalcin et al., 2018). Contact between the release medium and soluble drug at the NP

surface can affect release rate in the burst phase, therefore location of drug within the NP matrix is one factor which may influence how much drug is initially released (Makadia & Siegel, 2011).

A different release profile is observed in Figure 2.8 when NP contain 5% PEG-PLGA polymer composition. Release in DMGA buffer at pH 4.5 follows a very similar pattern to PBS for the first 4 days, after which drug release in DMGA accelerates to 100% payload release on day 10. The difference between release in PBS and DMGA was not significant until days 7-10 of incubation (P values <0.01). Following 10 days, myoglobin release from 5% PEG-PLGA NP in PBS is 39%, closely resembling results from the Myo NP without PEG in Figure 2.7. The biphasic release pattern in PBS is also evident for 5% PEG-PLGA Myo NP in Figure 2.8B.

In Figure 2.9, 10% PEG-PLGA Myo NP display a release profile in DMGA (pH 4.5) comparable to the 5% PEG-PLGA Myo NP in Figure 2.8, with 93% of myoglobin payload released by day 9 at 37°C (Figure 2.9B). In Figure 2.9A, myoglobin release in DMGA is slower in the first 5 hours than in PBS. Interestingly, 47% cumulative release of myoglobin was measured after 10 days of incubation in PBS. This is slightly more than was observed for Myo NP and 5% PEG-PLGA Myo NP in Figures 2.7 and 2.8 respectively, over the same time period. Once again, release in DMGA buffer was significantly higher than PBS after 5 days (P values < 0.01).

For NP loaded with model protein payload, myoglobin, release in DMGA of all preparations was much greater than in PBS over 10 days. In all cases, around twice as much myoglobin was released in total after incubation in an acidic pH environment. Release of myoglobin in PBS was representative of a biphasic release profile. Release in DMGA however, could perhaps be more appropriately described as triphasic. The initial burst release is followed by a slower phase until a final accelerated release phase occurs for all Myo NP preparations in DMGA buffer (pH 4.5). A triphasic release profile is more uncommon than biphasic, however it is an indication of heterogenous polymer erosion (Xu et al., 2017). The polymer is probably undergoing faster degradation under acidic conditions (Fredenberg et al., 2011), which might explain the acceleration of myoglobin release in DMGA buffer.

PEG content in the polymer appeared to slow down pH-induced myoglobin release in DMGA to the same level as in PBS for the first 4 days of incubation. The stabilising effects of PEG can reduce particle-particle interactions and also polymer surface reactions (Jokerst et al., 2011), which might explain why myoglobin release did not accelerate rapidly until day 5 in DMGA buffer.

Figure 2.10 shows the release of doxorubicin from PLGA NP in PBS and DMGA buffer. Notably, release in DMGA was much more rapid than in PBS, achieving 86% release after 1 day and 100% release after 7 days of incubation at 37°C. Following an initial burst phase where 20% of payload was released in the first 5 hours (Figure 2.10A), doxorubicin release in PBS was slowly continuous until 54% release was detected after 10 days (Figure 2.10B). Compared with the larger myoglobin payload, doxorubicin release from PLGA NP was quicker in both pH environments, but particularly so at pH 4.5. After 1 hour, doxorubicin release in DMGA was significantly higher than in PBS at every time point until day 10 (P value < 0.001).

A similar release profile was observed for 5% PEG-PLGA Dox NP in Figure 2.11. After 2 days of incubation, 98% of the doxorubicin payload was released in DMGA buffer (Figure 2.11B). In PBS, an initial burst release of less than 20% was observed in the first 5 hours of incubation as shown in Figure 2.11A. This was followed by a slow, controlled release of doxorubicin until 62% of the NP payload was cumulatively detected by day 10 (Figure 2.11B). Once more, the difference in release between PBS and DMGA was significant after just one hour of incubation (P values < 0.001). This was also the case for doxorubicin release from 10% PEG-PLGA Dox NP as shown in Figure 2.12. The presence of 10% PEG-PLGA caused slightly less doxorubicin release (47%) after 10 days in PBS in Figure 2.12B than was observed in Figures 2.10B and 2.11B. Again, this is possibly due to the stabilising effect of PEG at the polymer surface or indeed due to hydrophilic interactions between PEG and doxorubicin. Release of doxorubicin from NP in both pH environments followed biphasic patterns. This would suggest that polymer erosion was not a factor in doxorubicin release from PLGA in DMGA, unlike observations made for myoglobin NP.

(A)

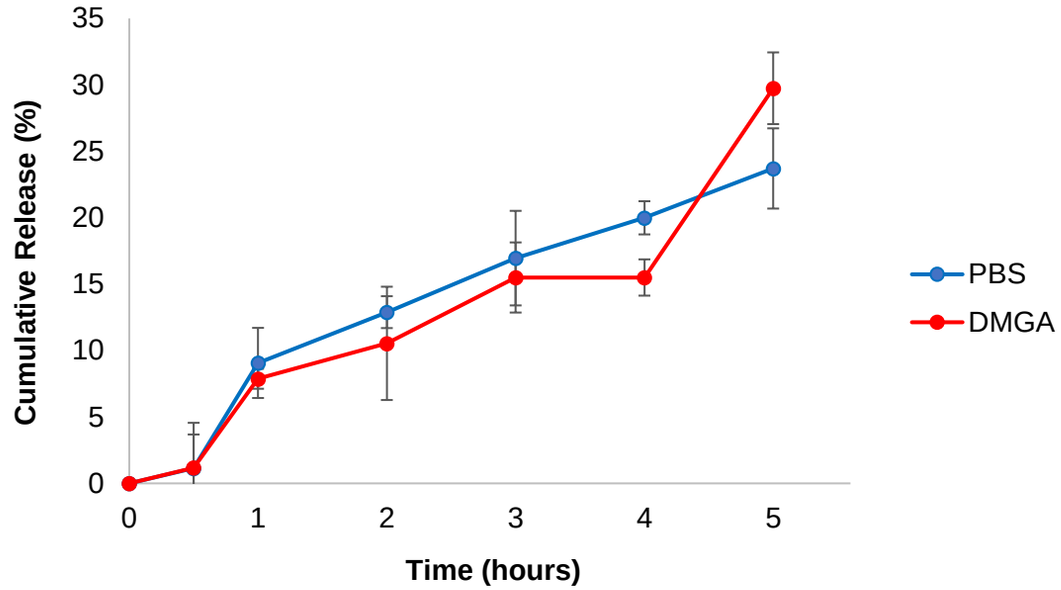

(B)

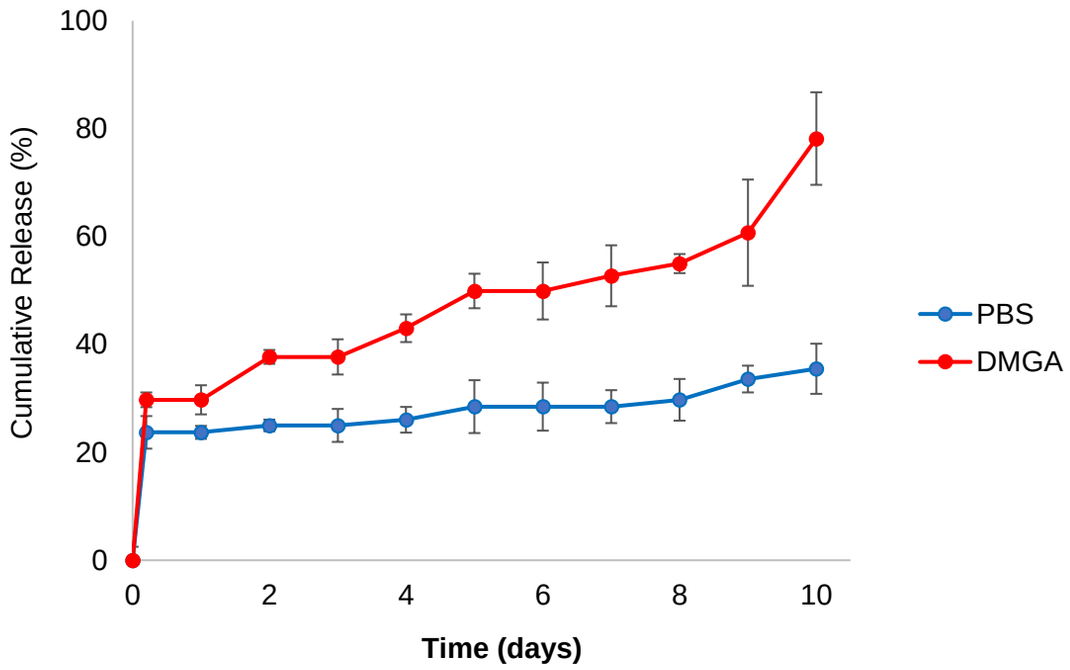

Figure 2.7. Release profile of myoglobin-loaded PLGA NP at 37 °C in PBS (pH 7.4) and DMGA buffer (pH 4.5) over (A) 5 hours and (B) 10 days. Error bars represent ± SD (n=3). Statistical analysis was performed using a two-way ANOVA with Bonferroni post-hoc tests to compare individual time points between PBS and DMGA. A P value < 0.05 was considered statistically significant.

(A)

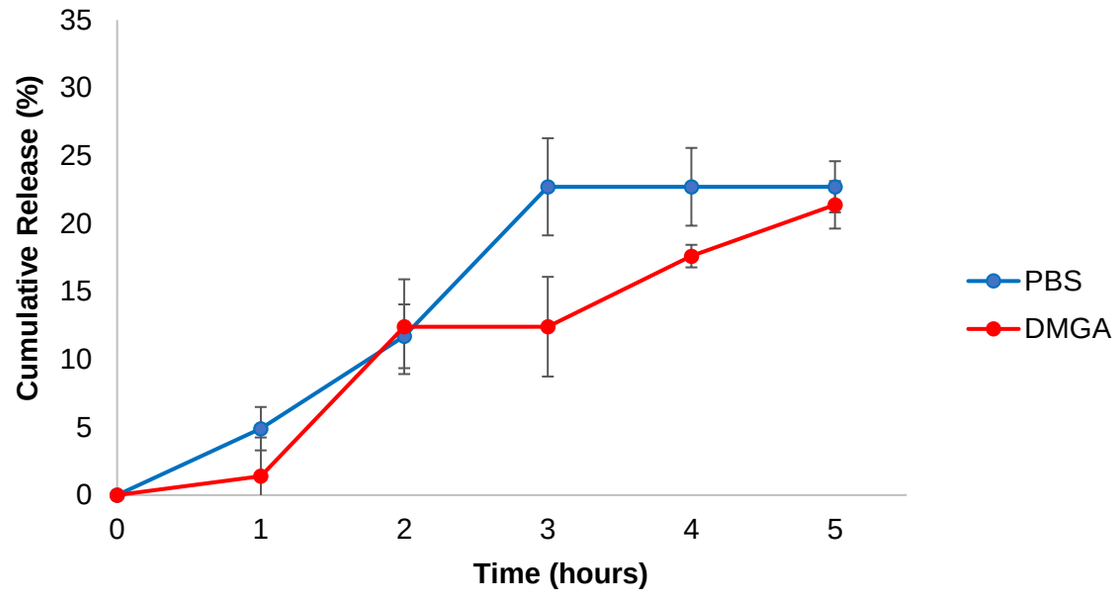

(B)

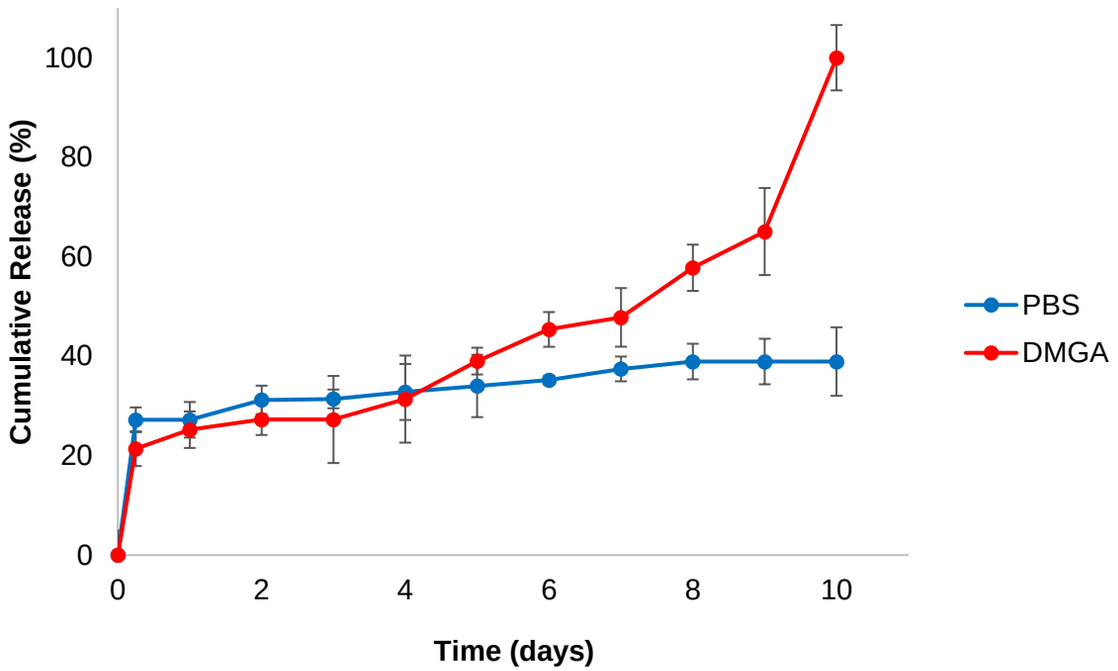

Figure 2.8. Release profile of myoglobin-loaded PLGA NP formulated with 5% PEG-PLGA co-polymer blend at 37 °C in PBS (pH 7.4) and DMGA buffer (pH 4.5) over (A) 5 hours and (B) 10 days. Error bars represent ± SD (n=3). Statistical analysis was performed using a two-way ANOVA with Bonferroni post-hoc tests to compare individual time points between PBS and DMGA. A P value < 0.05 was considered statistically significant.

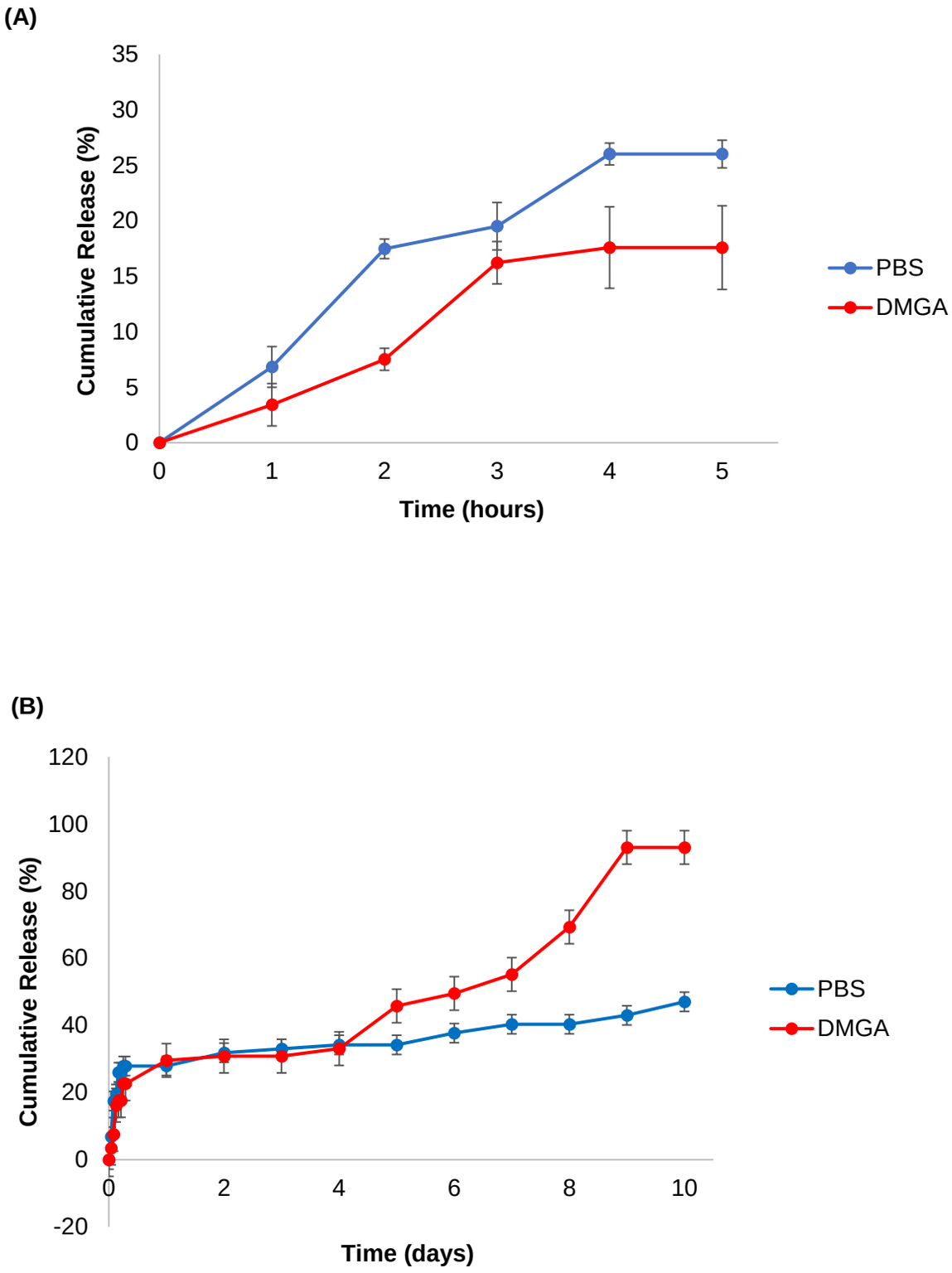

Figure 2.9. Release profile of myoglobin-loaded PLGA NP formulated with 10% PEG-PLGA co-polymer blend at 37 °C in PBS (pH 7.4) and DMGA buffer (pH 4.5) over (A) 5 hours and (B) 10 days. Error bars represent ± SD (n=3). Statistical analysis was performed using a two-way ANOVA with Bonferroni post-hoc tests to compare individual time points between PBS and DMGA. A P value < 0.05 was considered statistically significant.

(A)

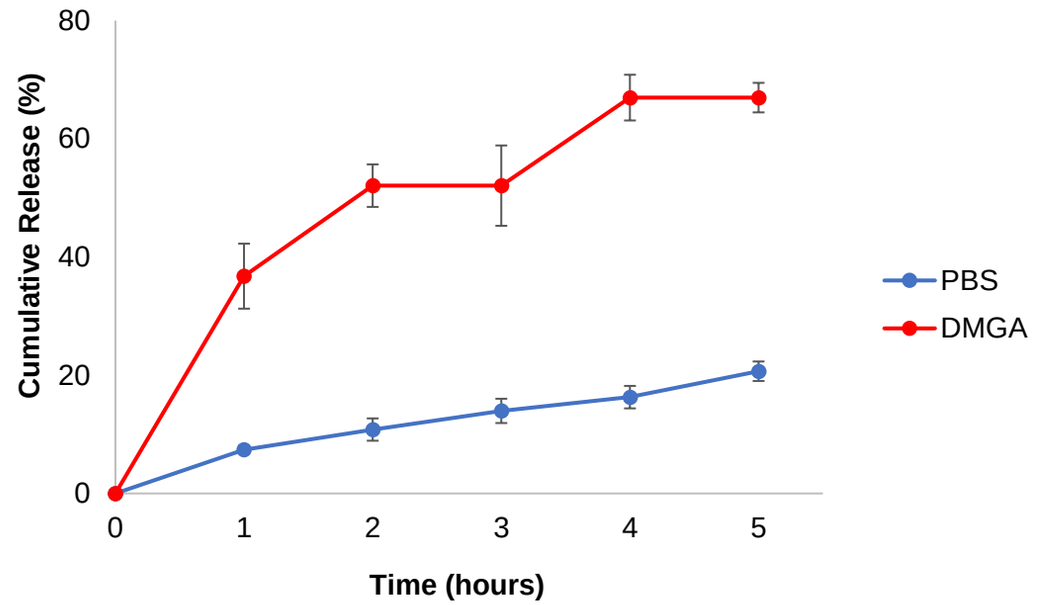

(B)

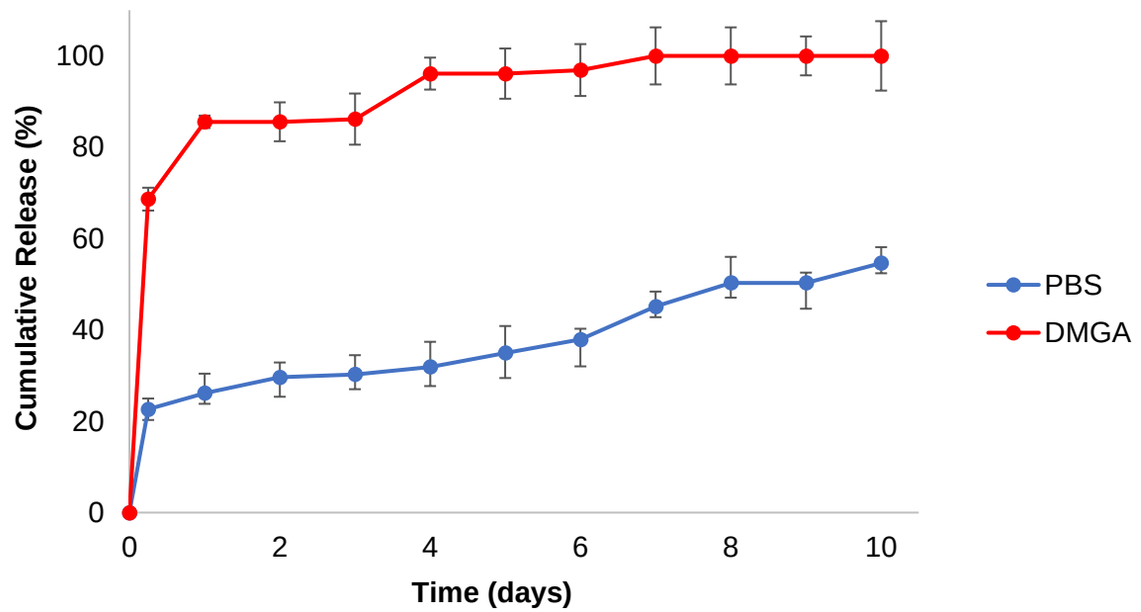

Figure 2.10. Release profile of doxorubicin-loaded PLGA NP at 37 °C in PBS (pH 7.4) and DMGA buffer (pH 4.5) over (A) 5 hours and (B) 10 days. Error bars represent ± SD (n=3). Statistical analysis was performed using a two-way ANOVA with Bonferroni post-hoc tests to compare individual time points between PBS and DMGA. A P value < 0.05 was considered statistically significant.

(A)

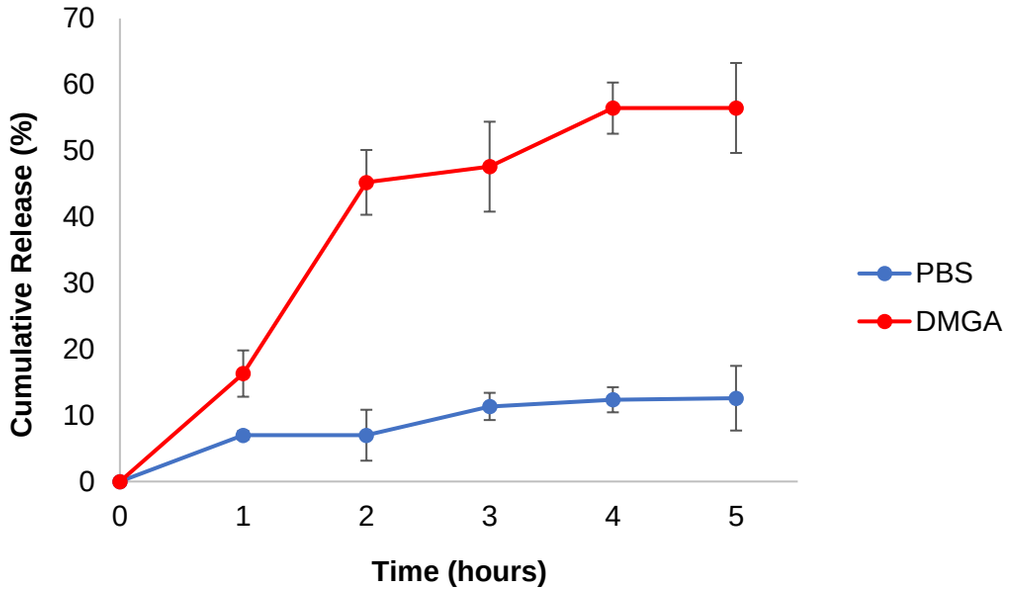

(B)

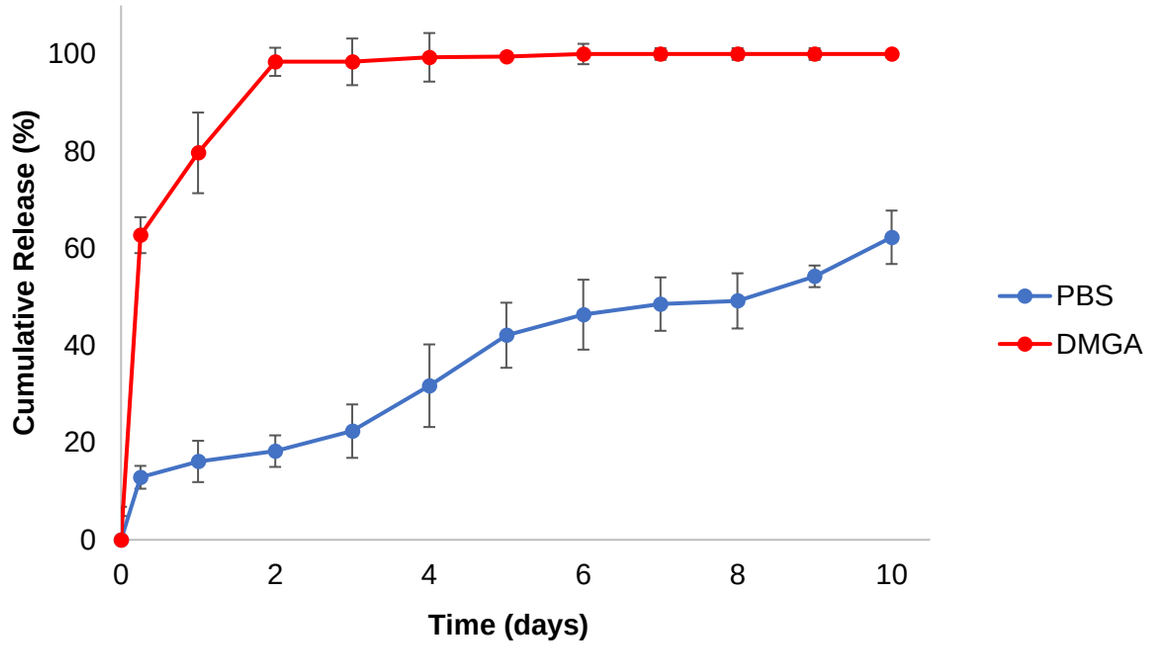

Figure 2.11. Release profile of doxorubicin-loaded PLGA NP formulated with 5% PEG-PLGA co-polymer blend at 37 °C in PBS (pH 7.4) and DMGA buffer (pH 4.5) over (A) 5 hours and (B) 10 days. Error bars represent ± SD (n=3). Statistical analysis was performed using a two-way ANOVA with Bonferroni post-hoc tests to compare individual time points between PBS and DMGA. A P value < 0.05 was considered statistically significant.

(A)

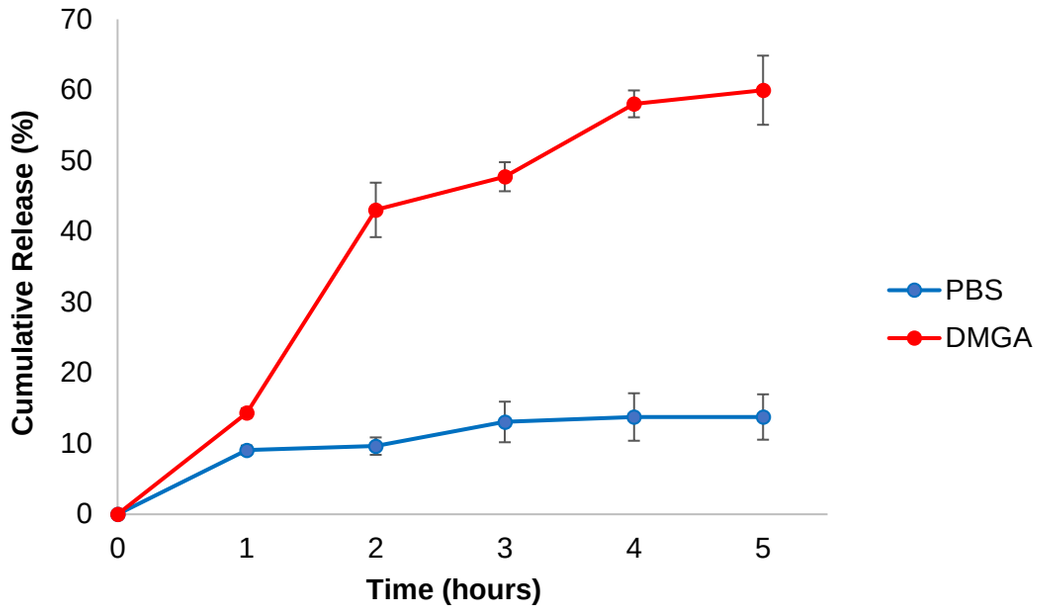

(B)

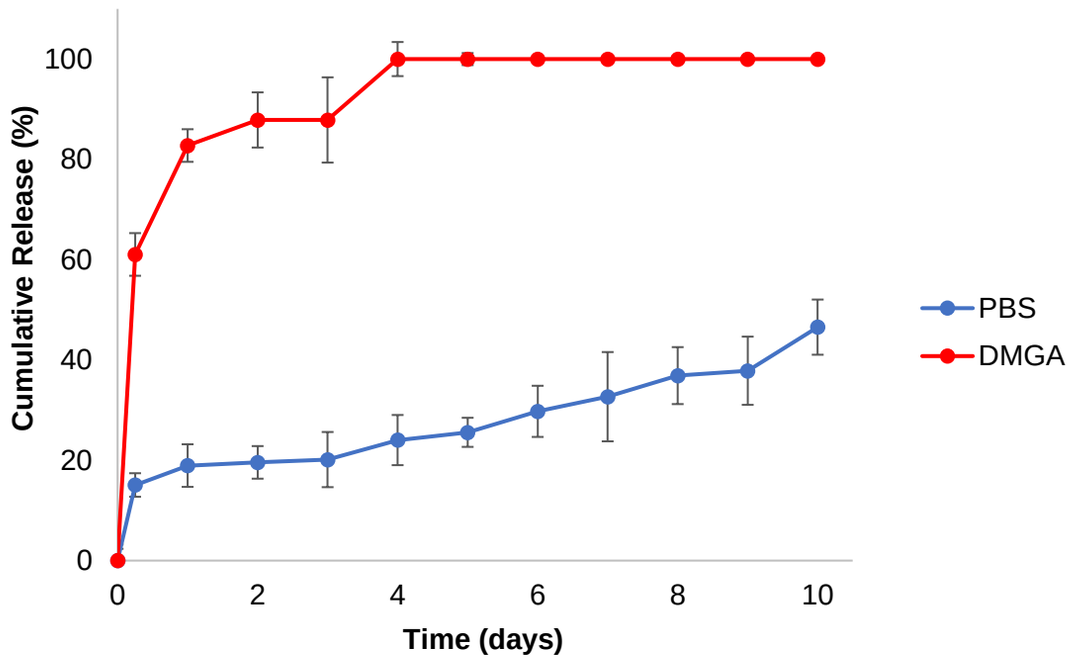

Figure 2.12. Release profile of doxorubicin-loaded PLGA NP formulated with 10% PEG-PLGA co-polymer blend at 37 °C in PBS (pH 7.4) and DMGA buffer (pH 4.5) over (A) 5 hours and (B) 10 days. Error bars represent ± SD (n=3). Statistical analysis was performed using a two-way ANOVA with Bonferroni post-hoc tests to compare individual time points between PBS and DMGA. A P value < 0.05 was considered statistically significant.

Betancourt et al. (2007) has reported similar findings on a much greater initial release of doxorubicin at pH 4.0 compared to pH 7.4. In addition to pH-induced polymer erosion, it could be postulated that the rate of drug diffusion out of the NP polymer matrix is increased at pH 4.5 due to fully ionised doxorubicin (Ayen et al., 2011), which has a pKa of 8.2 (Makkouk et al., 2015). Either of these possibilities or indeed a combination of factors are likely to cause more doxorubicin payload release at pH 4.5 compared to that observed at pH 7.4.

It is most probable that the major mechanism of drug release in PBS (pH 7.4) over this 10-day period is by drug diffusion through water-filled pores in the PLGA polymer (Fredenberg et al., 2011). This is supported by the SEM data presented in Figure 2.5, which generally indicates swelling of the NP rather than erosion in distilled water up to 10 days, at 37 °C. Furthermore, after 10 days the majority of NP are still intact, albeit as more irregular entities. The PLGA used in these studies was composed of lactic and glycolic acid units in a 50:50 ratio, however the rate of polymer degradation and subsequent payload release can be manipulated by adjusting this ratio. For example, increasing the lactic acid content of the polymer causes increased hydrophobicity due to methyl side chains and therefore less water is absorbed (Gentile et al., 2014).

Drug release data in PBS was analysed for both model drugs according to zero order, first order and Higuchi kinetics models, as shown in Table 2.10. Zero order kinetics models are used to describe drug release which is constant and linearly increases with time (Siepmann & Siepmann, 2012). First order kinetics indicates that release of drug is dependent on its concentration and is often the model used to describe the *in vivo* metabolism of most drugs (Kasperek et al., 2014). More recently, the Higuchi model has been used to describe release of water-soluble drugs from a matrix system or other type of modified release dosage form into solution (Dash et al., 2010).

Table 2.10. R-squared (R^2) values of myoglobin and doxorubicin release from PLGA NP in PBS following analysis using zero order, first order and Higuchi kinetics models.

Kinetics Model	R^2 Value Myoglobin	R^2 Value Doxorubicin
Zero order	0.857	0.862
First order	0.652	0.754
Higuchi	0.921	0.949

Table 2.10 shows the R^2 values obtained when release data of both myoglobin and doxorubicin in PBS was plotted according to the three kinetics models. The highest R^2 value and therefore the strongest correlation was obtained using the Higuchi model, the plot of which is shown in Figure 2.13 for both drugs. This supports a diffusion-based mechanism of drug release from the polymer matrix in solution (Dash et al., 2010). The R^2 values obtained from modelling release data according to zero and first order kinetics (Appendix 2) were notably lower than for the Higuchi model. This indicates that drug release is not always constant and changes in payload concentration are unlikely to have a major impact on the polymeric NP release profile.

(A)

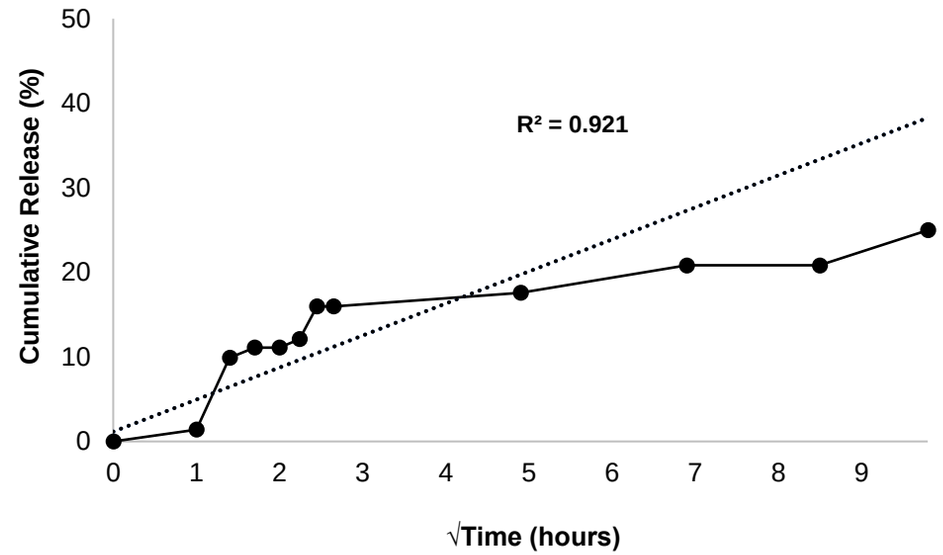

(B)

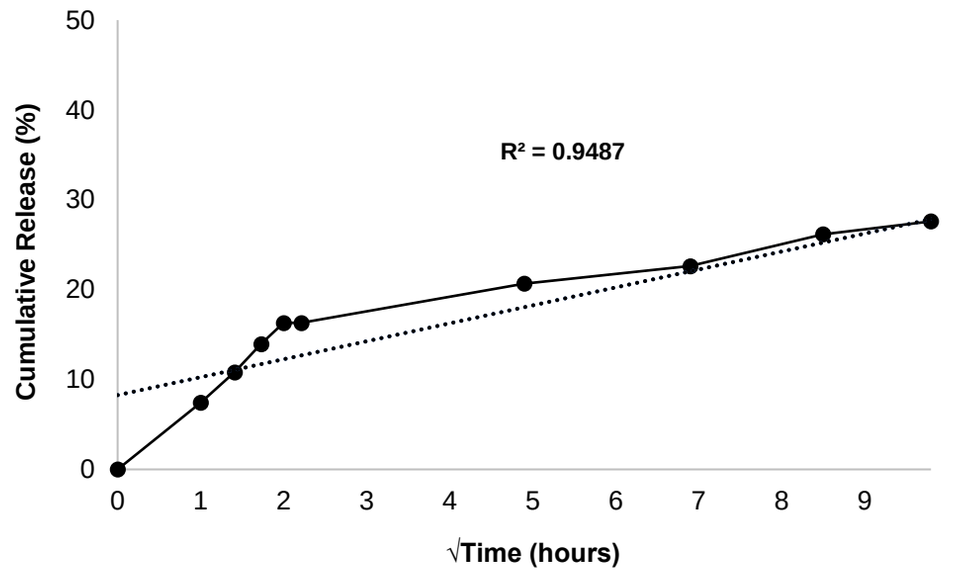

Figure 2.13. Higuchi plot showing release kinetics of (A) myoglobin and (B) doxorubicin from PLGA NP at 37°C in PBS.

Findings from all release data indicate that drug leaching in PBS at pH 7.4 and 37 °C is relatively low, however in an acidic environment, this is accelerated. Since these NP are not very leaky under normal physiological conditions, it could be hypothesised that the full NP payload will only be released inside the cell when the NP is exposed to the progressively acidified environment of the endocytic pathway (Abdul-Hammed et al., 2010). This is a very desirable property for a polymeric drug carrier, to show sustained release characteristics and release the majority of its contents at the endosomal stage. In all likelihood, it would limit the amount of drug released at unspecific locations and enhance drug accumulation at the target site in therapeutic concentrations.

2.3.5. RDP conjugation studies

RDP was attached to different PLGA NP preparations as a surface ligand via activated carboxyl groups using EDC/NHS chemistry. RDP was conjugated to all leading Dox NP preparations with a view of potentially being used for *in vitro* cell-based assays in future work. Since Myo NP have no therapeutic effect, only the Myo NP with no PEG were conjugated with RDP to assess the ability of protein-loaded NP to attach a targeting ligand. Furthermore, to preserve use of expensive peptide, CE was assessed for one sample (n=1) of each NP preparation therefore statistical analysis was not possible for results on Table 2.11.

RDP was conjugated to NP initially at 4 °C to prevent any denaturation of the peptide, however as shown in Table 2.11, conjugation efficiencies were low. As a result of this, RDP conjugation was subsequently carried out at room temperature. This greatly improved the amount of peptide which attached to NP. All Dox NP, regardless of PEG content, showed conjugation efficiencies of over 50%. RDP conjugated to Myo NP with an efficiency of 68%. This is positive for potential peptide attachment to NP loaded with bFGF or other growth factors in future work due to similarities with model drug, myoglobin. Through these studies it has been shown that biodegradable polymeric NP can be loaded with high amounts of protein payload, which show

good stability and release properties. Furthermore, these NP can be easily surface-coated with a good abundance of targeting ligand (at least 50 µg per 1 mg of NP). This drug delivery system of RDP-conjugated NP could potentially be used to target a therapeutic growth factor payload across the BBB for the treatment of Parkinson's disease. Prior to *in vivo* testing however, the ability of this nanoparticulate system to selectively target neural cells *in vitro* must be assessed.

Table 2.11. RDP conjugation efficiency (CE) to various PLGA NP preparations under different reaction conditions following addition of RDP (10% w/w) to carboxyl-activated NP.

NP Formulation	RDP CE (%) 4°C	RDP CE (%) 20°C
Blank NP	21.0	61.5
Dox NP	12.9	54.0
Dox NP (5% w/w PEG)	4.2	55.2
Dox NP (10% w/w PEG)	1.8	54.6
Myo NP	35.5	68.0

CE= peptide conjugation efficiency (%); 100 µg RDP conjugated per 1 mg NP; n=1.

In vitro cell assays studying the effect of RDP as a targeting ligand would involve comparing peptide-modified NP with an unlabelled version. Drug release or leaching from the NP should be similar for both unlabelled and peptide-conjugated NP. RDP was conjugated to Dox NP (RDP-Dox NP) and doxorubicin release was measured in PBS at 37°C. The release profile of RDP-Dox NP was compared to that of unlabelled Dox NP in Figure 2.14, to observe the effect of RDP ligand on drug release.

Doxorubicin release from RDP-Dox NP followed a similar pattern of biphasic release under physiological conditions as the unlabelled Dox NP. After 10 days, both preparations released

around 50% of payload showing no significant difference due to RDP (P value > 0.05). Release from RDP-Dox NP was significantly slower for the first five days than Dox NP (P values < 0.05), possibly due to a steric hindrance effect of the peptide on the NP surface. Alternatively, the peptide may be affecting early hydrolysis-induced degradative processes of the polymer matrix at the particle surface.

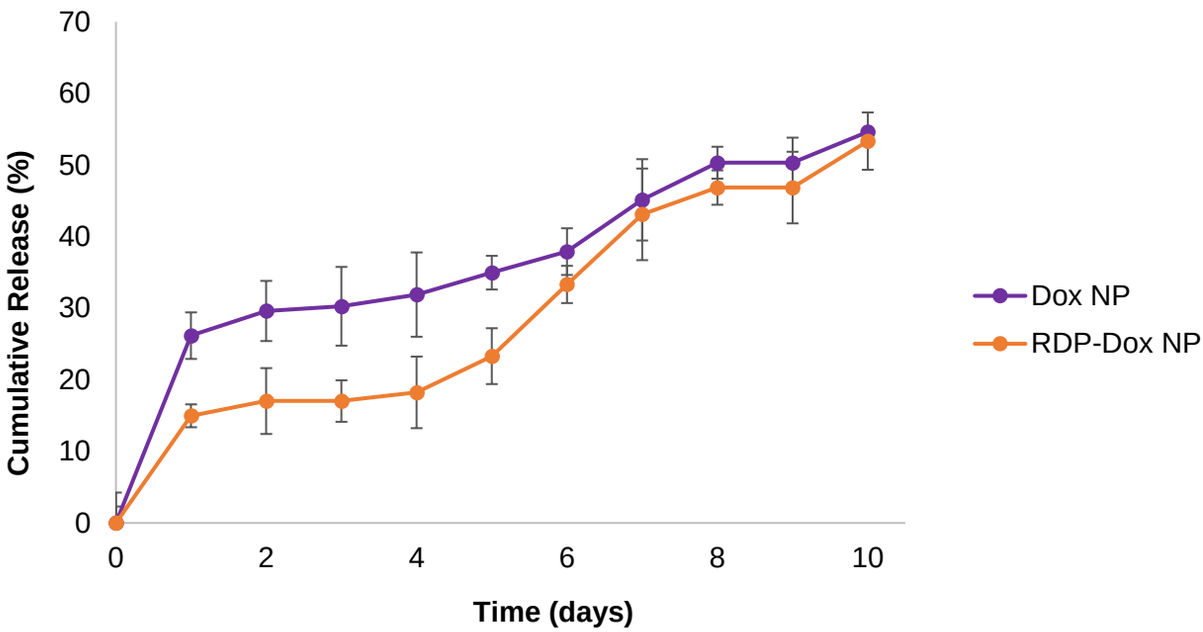

Figure 2.14. 10-day release profile of doxorubicin from unlabelled NP (Dox NP) and RDP-conjugated NP (RDP-Dox NP) at 37°C in PBS. Error bars represent ± SD (n=3). Statistical analysis was performed using a two-way ANOVA with Bonferroni post-hoc tests to compare individual time points of Dox NP v RDP-Dox NP. A P value < 0.05 was considered statistically significant.

These results show that Dox NP can be successfully conjugated with RDP targeting ligand and maintain controlled release of payload under physiological conditions (pH 7.4, 37°C). This means such NP will be suitable for *in vitro* testing on various cell types. Amoozgar & Goldberg

(2017) reported that surface protein conjugation can help prevent particle aggregation and control doxorubicin release from polymeric NP. In addition to the controlled release profile observed in the results of Figure 2.14, RDP may also confer stability to the NP suspension due an overall positive charge as a result of many arginine and lysine residues in the sequence. Similar to a good zeta potential value, this charge may prevent particle aggregation in suspension.

It could be hypothesised that NP functionalisation with RDP will ultimately be the determining factor to the success of such a targeted drug delivery system for specific neural cell internalisation and its ability to traverse an *in vitro* BBB model. Given the difficulties in drug delivery across the BBB, size and zeta potential are perhaps of less consequence (Voigt et al., 2014), especially when a functionalised surface ligand can facilitate strong interactions with a target receptor.

2.4. Conclusion

PLGA NP were successfully formulated using a double emulsion-solvent evaporation method and loaded with various model payloads. Various NP formulation parameters were investigated, resulting in modification of the original protocol to formulate NP with improved drug encapsulation whilst maintaining desirable size and zeta potential characteristics. Following the development of lead NP formulations, myoglobin and doxorubicin were incorporated as model payloads and release characteristics were analysed in different environments. Drug-loaded NP preparations showed controlled, sustained release of payload under physiological conditions (pH 7.4, 37°C) with the ability to undergo pH-induced accelerated release in an acidic environment representative of the cellular endocytosis pathway.

NP were surface-conjugated with neural cell targeting ligand, RDP, with acceptable conjugation efficiencies regardless of payload or PEG-PLGA co-polymer content. The versatility of these PLGA NP to load various drugs and attach surface ligands offers a wide scope of possibilities for future development, such as formulation of growth factor-loaded NP with surface-conjugated RDP.

Table 2.12 shows the optimal formulation parameters identified through these studies to be used in further NP investigations. Although it has been shown that PEG can be introduced into the polymer component and maintain favourable NP characteristics, PEG will be excluded from further *in vitro* cell-based work in these studies. This is to avoid any potential influence of PEG on RDP activity *in vitro.* However, this does not rule out the use of PEG in future studies beyond the scope of the work reported herein. The specific neural targeting effect of RDP, as part of a polymeric nanoparticulate system, can consequently be assessed on various cell types *in vitro* as a result of these formulation studies.

Table 2.12. Optimised NP formulation parameters selected for further *in vitro* studies on the specific targeting ability of conjugated RDP

Formulation Parameter	**Specifications**
Polymer	100 mg PLGA
Solvent	4 mL DCM
External aqueous phase (W1)	15 mL PVA (1.25%)
Internal aqueous phase (W2)	0.5 mL ddH_2O
Emulsification method	Probe sonication

Chapter 3

In vitro testing of RDP and neural cell receptor identification

This chapter reports work (with permission) from the following publications:

Huey, R., Hawthorne, S. and McCarron, P. (2017) The potential use of rabies virus glycoprotein-derived peptides to facilitate drug delivery into the central nervous system: a mini review. *Journal of drug targeting,* 25 (5), 379-385. The original article can be found in Appendix 3.

Huey, R., O'Hagan, B., McCarron, P. and Hawthorne, S. (2017) Targeted drug delivery system to neural cells utilizes the nicotinic acetylcholine receptor. *International journal of pharmaceutics,* 525 (1), 12-20. The original article can be found in Appendix 4.

3.1. Introduction

New approaches are arising for the successful delivery of therapeutics to the central nervous system (CNS). Although notoriously challenging, the delivery of drug or gene payloads specifically to neural cells may be facilitated by the use of a targeting ligand or peptide. The emergence of peptides derived from rabies virus glycoprotein (RVG) as brain targeting ligands have shown promise as an effective way of non-invasively overcoming the blood brain barrier (BBB) for targeted therapy. In recent times, derivatives of RVG, such as rabies virus-derived peptide (RDP) and RVG-29, have been successfully utilised as targeting ligands for drug delivery to the CNS. RVG is the only surface glycoprotein on the rabies virus envelope, which is responsible for the distinct neurotropism of the rabies virus infection (Yan et al., 2002). The use of RVG for specific targeting of neurotherapeutics is therefore a promising concept, which Son et al. (2011) described as a potential “magic bullet”.

RDP has shown potential as a new targeting ligand for the specific and non-invasive delivery of therapeutics to the brain, due to its ability to cross the BBB. RDP is a 39-amino acid peptide derivative of RVG residues 330-358, which has not only been successful in safely directing conjugated therapeutic payloads to the brain in mice (Fu et al. 2012; 2013a; 2013b), but also preferentially targets neural over non-neural cell types *in vitro* (Fu et al. 2013a). In a study by Gramlich et al. (2016), RDP surpassed non-specific cell penetrating peptide, TAT, and neural-specific peptides, tetanus toxin fragment C and Tet-1, in delivering a glucocerebrosidase enzyme payload to neurons for the treatment of Gaucher’s disease.

RDP has also recently been conjugated to gold NP for various purposes. Zhang & Fu (2015) observed the ability of RDP-conjugated gold nanoclusters to specifically accumulate in neural tissue *in vivo* to allow a non-invasive approach to brain screening. Xiao et al. (2017) functionalised RDP to 6-mercaptopurine-loaded gold NP to positively promote growth of neurons, without signs of toxicity. Other nanomaterials used in conjunction with RDP include curcumin-

loaded nanoliposomes, which successfully targeted intracranial glioma in a mouse model after intravenous administration (Zhao et al., 2018).

RDP-facilitated transport of a drug may improve brain bioavailability; firstly, due to a reduction in non-specific uptake in other body regions and secondly, by the ability to penetrate the specialised endothelial cells of the BBB. Moreover, sensitive and expensive therapeutics may be protected from degrading enzymes, particularly if encapsulated in a nanoparticulate delivery vehicle. This type of facilitated delivery is possible as the surface of carriers such as polymeric NP, can be easily modified (Delehanty et al., 2010). Such NP can be composed of biodegradable, biocompatible polymers with an established safety profile, such as FDA-approved poly(lactic-co-glycolic acid) (PLGA) or chitosan (Auffinger et al., 2013). Thus far, RDP has not been functionalised to polymeric NP for delivery of therapeutic cargo to the CNS.

In order to optimise the characteristics of RDP for future development as an effective drug delivery entity, it is important to know which receptor on neural cells is the target for interaction. To date, there has been conflicting evidence in the literature as to which receptor is utilised in these synthetic peptide-neural cell interactions and indeed by RVG itself. There is strong evidence of original RVG and other peptide derivatives, such as RVG-29, binding to the nicotinic acetylcholine receptor (nAChR) in a number of studies (Lentz et al., 1991; Gastka et al., 1996; Kumar et al., 2007; Sajjanar et al., 2015; Lee et al., 2017).

RVG facilitates entry of the virus specifically into neurons at the neuromuscular junction (NMJ) through interaction with neural cell receptor molecules. It was first proposed by Lentz et al. (1982), that the acetylcholine receptor is a rabies virus receptor, based on the detection of the virus at or near acetylcholine sites in cultured chick myotubes. In this study, rhodamine-labelled alpha bungarotoxin (α-BTX) was used to detect the acetylcholine receptors, as this snake venom neurotoxin competitively binds to acetylcholine binding sites. Following a pre-incubation period, α-BTX was able to significantly reduce the number of chick myotubes that became infected by rabies virus. The authors acknowledged that other molecules may be involved as infection could not be totally prevented by blocking the acetylcholine receptor. Despite this, any additional

elements must be closely associated with acetylcholine binding sites. The detection of dense clusters of acetylcholine receptors at the tips of junctional folds may serve to enhance uptake at the NMJ, allowing eventual transport into the CNS.

Lentz et al. (1991) compared a segment of RVG with the structure of a loop 2 domain of the curaremimetic neurotoxin, King Cobra Toxin b, and their subsequent interaction with the nicotinic acetylcholine receptor (nAChR). The loop 2 of snake venom neurotoxins share a few invariant amino acid residues. Interestingly, these sequences share a related homology with those found in RVG. Snake venom neurotoxin is able to bind at or near the acetylcholine binding site of nicotinic acetylcholine receptors (nAChRs) and consequently block ligand binding. It was shown by Lentz and colleagues how manipulating homologous residues of a King Cobra Toxin b derivative and a 29-residue RVG derivative decreased nAChR binding affinity. This work suggested that the homologous sequences between snake venom neurotoxins and RVG might be responsible for strong interactions with the nAChR. Furthermore, a 10-amino acid sequence of RVG-29 unrelated to the neurotoxin structure was identified as important for maintaining a high binding affinity to the nAChR.

Similar work has been carried out using King Cobra Toxin b by Zhan et al. (2010), where a short 20 residue neurotoxin-peptide was produced to facilitate drug delivery to the brain, via nAChRs, on endothelial cells of the BBB. By successfully enhancing the accumulation of coumarin-6-loaded micelles in mouse brain, it was shown that this synthetic peptide bound with similar affinity to an RVG derivative. This study inadvertently proved that an RVG derivative binds to the neuronal-type nAChR, due to its inhibitory effect on α-BTX, which binds to residues 173-204 of the alpha-1 subunit on NMJ nAChRs (Gastka et al., 1996). The aforementioned studies prove that RVG has a very strong connection with the nAChR, due to the similarities with snake venom neurotoxin residues.

Pilot work on the novel peptide, RDP, by Fu et al. (2013a) however suggested that the GABA (a) receptor subtype is most likely utilised for cellular uptake by clathrin-mediated endocytosis. In fact, Liu et al. (2009) implicated the GABA (b) receptor subtype as being responsible for the

cellular uptake of RVG-29, conflicting with the wealth of previous reports of nAChR dependence. It is possible perhaps, that different derivatives of RVG may bind different neural receptors. A lack of experimental data on RDP to date however means that the question of whether the nAChR or a GABA receptor subtype is responsible for cellular uptake cannot be answered with certainty.

The aims of this study were to:

(1) Prepare PLGA NP incorporating different model payloads to observe the effect of RDP surface-conjugation in neural and non-neural cell types. The targeting effects of RDP can be assessed following observation of NP payload effect in various cell types to determine the specificity of this ligand towards cells of neural origin only.

(2) Determine which receptor RDP binds to by blocking the nAChR, GABA(a) and GABA(b) receptors with various inhibitors in a cytotoxicity assay. Blocking the receptor responsible for RDP-facilitated effects should diminish the effect induced by the cytotoxic payload encapsulated within RDP-conjugated PLGA NP.

3.2. Materials and methods

3.2.1. Materials

Resomer® RG 502 H, Poly(D,L-lactide-*co*-glycolide)-PLGA, acid terminated **(**MW 7 000-17 000), dichloromethane (DCM), poly(vinyl) alcohol (PVA) 87-89% hydrolysed- MW 85 000-124 000, MES hydrate, 1-ethyl-3-(3-dimethylaminopropyl)**-**carbodiimide (EDC), N-hydroxysuccinimide (NHS), doxorubicin hydrochloride, fluorescein isothiocyanate–dextran (FITC-Dextran), phosphate buffered saline (PBS), Collagen (type IV), 3-[4,5-dimethylthiazol-2-yl]-2,5 diphenyl tetrazolium bromide (MTT), hexamethonium, bicuculline, saclofen and mecamylamine were all purchased from Sigma-Aldrich (UK). RDP was synthesized by GL Biochem (Shanghai) Ltd. Anti-AChRα7 rat monoclonal IgG_1 antibody (200 µg/mL) was purchased from Santa Cruz Biotechnology, Inc. (USA). Lysotracker® red DND-99 solution (1mM) and SlowFade® diamond antifade mountant were purchased from ThermoFisher Scientific.

3.2.2. Tissue culture

All tissue culture reagents and media were purchased from Gibco®/ Life Technologies. SH-SY5Y (human neuroblastoma), PC-12 (rat pheochromocytoma) and HeLa (human cervical cancer) cell lines were all cultured in RPMI 1640 medium. MDA-MB-231 (human breast cancer) cells were cultured in DMEM medium. Finally, normal and non-neural epithelial CHO (Chinese hamster ovary) cells were cultured in Ham's/F12 nutrient mixture. All tissue culture media was supplemented with 10% (v/v) foetal bovine serum and 1% (v/v) penicillin-streptomycin (5,000U mL^{-1}/5,000 µg mL^{-1}). PC-12 cells were additionally supplemented with 10% (v/v) horse serum and cultured on flasks pre-coated with 2 mL of 0.5 mg/mL type IV collagen in 0.25% (v/v) acetic acid. Cells were passaged using trypsin-EDTA 0.5%.

3.2.3. Preparation of Nanoparticles (NP)

3.2.3.1. Preparation of blank PLGA NP (Blank NP)

Acid terminated PLGA (100 mg) was dissolved in 4 mL of DCM. PVA was made up as a 1.25% (w/v) solution in distilled water (ddH_2O). The PLGA/DCM organic phase was added dropwise to 15 mL of 1.25% (w/v) PVA solution and sonicated using a Fisher Scientific FB50 sonicator probe (Pittsburgh, PA, USA) at 80% amplitude for two minutes. The resulting o/w emulsion was left to stir overnight to evaporate any solvent. The NP emulsion was then centrifuged at 18809 *g* for 30 minutes at 4 °C in a Sigma 2-16K refrigerated centrifuge (SciQuip,UK), before washing the pellet with ddH_2O for ten minutes. A 2% (w/v) sucrose solution was used to wash the NP for a second time, before a final wash with ddH_2O. The final pellet was resuspended in 5 mL ddH_2O and freeze dried using a Labconco FreeZone 4.5 plus benchtop freeze dry system on automatic mode (-40°C, 0.12 mbar) for 48 hours.

3.2.3.2. Preparation of doxorubicin-loaded NP (Dox NP)

An optimised double emulsion technique was used to encapsulate doxorubicin in PLGA NP, as previously described in chapter 2 (see Table 2.12.). Doxorubicin hydrochloride (2 mg) dissolved in 0.5 mL of ddH_2O was added dropwise to 4mL of acid terminated PLGA (100 mg) in DCM and sonicated (Fisher Scientific FB50 sonicator probe, Pittsburgh, PA, USA) for 60 seconds at 80% amplitude. The primary w/o emulsion was then added dropwise to 15 mL of 1.25% (w/v) PVA in ddH_2O and sonicated for a further 2 minutes. The resultant w/o/w emulsion was left to magnetic stir overnight to evaporate any solvent. The doxorubicin-loaded NP (Dox NP) were collected by centrifugation at 18809 *g* for 30 minutes at 4°C and washed thrice with ddH_2O. Dox NP were finally resuspended in ddH_2O and freeze dried for 48 hours as previously detailed in section 2.2.2.1. Supernatant from centrifugation was retained to determine doxorubicin entrapment efficiency (EE) using UV-Visible spectroscopy at 480 nm on a FLUOstar Omega microwell plate reader (BMG Labtech, Germany).

FITC-dextran (FITC-dex) loaded PLGA nanoparticles (FITC NP) for confocal fluorescence imaging were also prepared this way, using 4 mg of FITC-dex per 100 mg of PLGA polymer. Entrapment of FITC-dex in PLGA NP was detected using fluorescence spectroscopy (excitation 485 nm, emission 520 nm), again on a FLUOstar Omega microwell plate reader.

3.2.4. Conjugation of RDP to NP

RDP conjugation to NP was carried out according to the same method as detailed in 2.2.7. Briefly, free PLGA carboxyl groups on NP were activated by EDC/NHS chemistry and reacted overnight with RDP solution (1 mg/mL) to produce RDP-Blank NP, RDP-Dox NP and RDP-FITC NP. Supernatant from the fabrication process was collected to assess peptide conjugation efficiency (CE) using a BCA assay and UV-Vis spectrometry (562 nm). The peptide CE was calculated according to Equation 3.1.

Equation 3.1. $$CE = \frac{Mass\ of\ peptide\ conjugated\ to\ NP}{Mass\ of\ peptide\ added}\ x\ 100\%$$

3.2.5. Evaluation of NP

3.2.5.1. Dynamic Light Scattering (DLS)

Size, zeta potential (ZP) and polydispersity index (PDI) measurements were carried out using dynamic light scattering (DLS) analysis (Zetasizer, Nano-series, Malvern *Instruments*, UK). Prior to DLS analysis, 1 mg of NP were dispersed in 1 mL of ddH_2O for measuring size and PDI. For ZP measurements, NP were dispersed in 1.0 mM KCl, pH 7.5, to maintain a constant ionic strength. Results were taken as an average of six measurements (n=6).

3.2.5.2. Determination of drug entrapment efficiency (EE)

Doxorubicin and FITC-dex EE were calculated indirectly using supernatant from the formulation process, as described previously in section 2.2.3. Doxorubicin EE was again calculated from a standard UV-Vis absorption curve at 480 nm. A standard calibration curve for FITC-dex was prepared using fluorescence spectroscopy (excitation 485 nm, emission 520 nm), as shown in Figure 3.1.

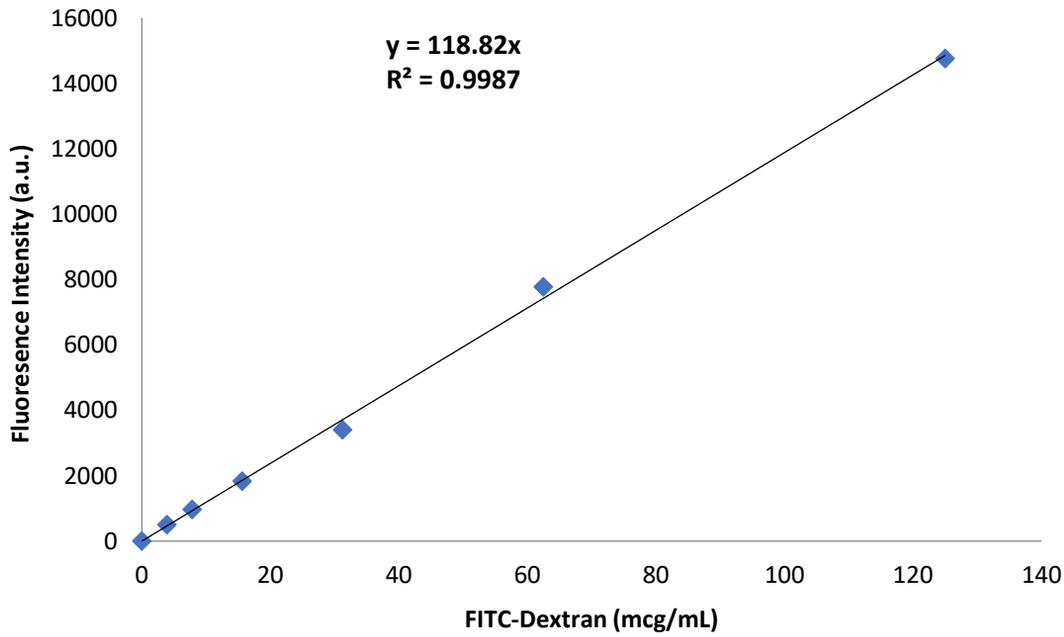

Figure 3.1. Standard calibration curve for FITC-dextran fluorescence intensity (excitation 485 nm, emission 520 nm) with increasing concentration (mcg/mL).

3.2.5.3. Determination of RDP conjugation efficiency (CE)

RDP CE to PLGA NP was determined by a BCA assay, as detailed in section 2.2.8.

3.2.5.4. FITC-dextran release from PLGA NP

Doxorubicin release from PLGA NP was described previously in section 2.2.5. To analyze FITC-dex payload release from PLGA NP under sink conditions, 3 mg of FITC-dex NP were dispersed in 1 mL of PBS and incubated at 37°C for a period of 7 days. Samples of supernatant were taken after varying amounts of time by centrifuging the NP suspension at 1680 *g* for 5 minutes and replacing each aliquot with fresh PBS. Samples were tested for fluorescence (excitation 485 nm, emission 520 nm) to detect FITC-dex release from the PLGA NP. Percentage cumulative release was expressed as a percentage of maximum FITC-dex in the NP, determined from the EE. Fluorescence values were recorded in triplicate and standard deviation calculated (n=3).

3.2.6. In vitro evaluation

3.2.6.1. Cytotoxicity study

Cells were seeded into 96 well plates at a concentration of $1x10^5$ cells/mL (200 µL per well) in the relevant culture media and incubated at 37°C and 5% CO_2 for 24 hours (Heraeus HERAcell, Thermo Fisher Scientific, UK). Dox NP and RDP-Dox NP were prepared as 200 µg/mL suspensions in serum-free media (SFM) and filter sterilised using a 450 nm filter. Blank PLGA NP with conjugated RDP (RDP-blank NP) were also prepared this way, to test for toxicity of the drug vehicle. NP treatment (200 µL) or an approximate equivalent concentration of free RDP was added to each well, with six replicates for each of the treatment groups. Control groups were treated with 200 µL of SFM only.

Initially, SH-SY5Y cells were incubated (37°C/5% CO_2) with RDP, RDP-blank NP, Dox NP and RDP-Dox NP for 1, 2, 4 or 24 hours. Following this, four different cell lines (HeLa, CHO, MDA-MB-231 and SH-SY5Y cells) were treated with the Dox NP and RDP-Dox NP formulations only for 24 hours. After the elapsed treatment time, all media was aspirated, replaced with 200 µL of complete media and incubated (37°C/5% CO_2) until an MTT assay was carried out to assess cell viability. MTT assay was carried out at 24 hours post addition of NP treatment. MTT solution

(25 µL of 5 mg/mL in sterile PBS) was added on top of the media in each well and incubated at 37°C/5% CO_2 for 2 hours. The wells were then aspirated, and purple formazan crystals dissolved by the addition of 70 µL of dimethyl sulfoxide (DMSO) per well. Absorbance was read at 570 nm (FLUOstar Omega microwell plate reader, BMG Labtech, Germany).

3.2.6.2. Confocal Microscopy

Cellular uptake of FITC NP preparations was evaluated in SH-SY5Y, PC-12 and HeLa cell lines using a Leica SP5 confocal microscope (x 63 000 magnification). Cells were seeded onto 13 mm glass coverslips at a concentration of $1x10^5$ cells/ mL (500 µL) and cultured in complete RPMI media at 37°C/5% CO_2 overnight. Cells were treated with 500 µg/mL (500 µL) of either FITC NP or RDP-FITC NP in SFM for 24 hours, whilst incubating at 37°C/5% CO_2. Controls were treated with SFM only. All treatments were subsequently aspirated, and cells were gently washed thrice with PBS to remove residual NP. Prior to imagining, all cells including controls were treated with 75 nM Lysotracker® red in SFM for 30 minutes to visualise lysosomes in cells and track potential co-localisation with NP along the cellular internalisation pathway. FITC-dex fluorescence emission was collected between 510-610 nm (excitation wavelength 488 nm). Lysotracker® emission was collected separately between 585-685 nm (excitation wavelength 543 nm).

3.2.6.3. Receptor identification study

SH-SY5Y cells were seeded onto 96 well plates, as previously described. RDP-Dox NP were prepared as 400 µg/mL suspensions in SFM. All inhibitor stock solutions were prepared in SFM to produce 200 µM bicuculline, 200 µM saclofen, 2 mM hexamethonium, 2 mM mecamylamine and a 1:50 dilution of anti-AChRα7 antibody.

SH-SY5Y cells were initially pre-treated for 30 minutes with 100 µL of either bicuculline, saclofen or hexamethonium prior to treatment with 100 µL of RDP-Dox NP suspension (400 µg/mL). Final

concentrations of inhibitors, once all treatments were added, were 100 μM for the GABA antagonists (bicuculline and saclofen), 1 mM for nAChR antagonists (hexamethonium and mecamylamine) and a 1:100 dilution of anti-AChRα7 antibody. Cells were incubated as before for 24 hours at 37 °C/5% CO_2. Control wells were treated with SFM only. After incubation, wells were aspirated, washed gently with PBS and 200 μL of fresh complete media added per well. MTT assay was subsequently carried out. This provided results for the first receptor identification assay, which was followed up by a second assay to block the nAChR only. The subsequent assay followed the same protocol, only mecamylamine and anti-AChRα7 antibody solutions were allowed to incubate with SH-SY5Y cells for 60 minutes prior to RDP-Dox NP exposure. This was to ensure adequate time for the antibody to bind any homomeric α7 nAChRs.

RDP was finally tested on PC-12 (rat pheochromocytoma) cells, a second cell line of neural origin. The effect of RDP-Dox NP in comparison to Dox NP was investigated according to the method previously described for SH-SY5Y cells. Additionally, the effect of blocking the nAChR with anti-AChRα7 antibody was explored in this cell type also.

3.2.7. Statistical analysis

All analysis carried out on cell viability values was determined using an unpaired two-tailed t-test, with P values < 0.05 indicating a statistically significant difference.

3.3. Results & Discussion

3.3.1. NP characterisation

NP were formulated according to the double emulsion method and characterised for size, ZP and PDI, the results of which are presented in Table 3.1. Using DLS analysis, it was determined that blank PLGA NP had an average particle diameter of 240.27 ± 14.72 nm, ZP of -18.4 ± 1.82 mV and PDI of 0.26 ± 0.04. Incorporation of a doxorubicin payload had no significant effect (P value > 0.05) on average NP diameter (242.73 ± 18.64 nm) however ZP increased slightly to -14.64 ± 1.32 mV, as did the PDI (0.39 ± 0.05). FITC NP had an average NP diameter of 286.50 ± 11.30 nm, which was a statistically relevant increase compared to the blank PLGA NP (P value 0.0125). FITC NP displayed a significant increase in ZP to -10.30 ± 1.00 mV in comparison to the blank PLGA NP (P value 0.0025), however the PDI (0.27 ± 0.08) remained constant (P value > 0.05). Reimold et al. (2008) prepared polymeric NP loaded with 70 kDa FITC-dex, which displayed identical ZP and PDI characteristics to the NP reported in Table 3.1.

Doxorubicin hydrochloride (579 Da) and FITC-dex (70 kDa) are both water soluble molecules, however they vary greatly in molecular weight. The high molecular weight of FITC-dex perha ps is responsible for the slightly larger NP size, however the difference observed is not crucial for this work. The larger molecule size also aids encapsulation into the PLGA NP, unlike low molecular weight doxorubicin which easily escapes into the outer aqueous phase during the double emulsion NP formulation process. A favourable entrapment efficiency (EE) of 77% (Table 3.1) was obtained for the PLGA-based FITC NP reported herein, which correlates closely with previous work at similar w/w (%) loading (Nimesh et al., 2006). Interestingly, Chiu et al. (2015) found that increasing molecular weight of FITC-dex corresponds with higher EE in polymeric NP.

All NP formulations were successfully conjugated to RDP with efficiencies of over 50%. Conjugation efficiency (CE) of RDP to FITC NP (73%) was considerably better in comparison to both doxorubicin-loaded (54%) and unloaded NP (55%). The presence of FITC-dex molecules

encapsulated in the PLGA NP potentially aids surface binding of RDP, through somehow influencing NP surface characteristics or availability of free, activated carboxyl groups for RDP to react with.

Table 3.1. Characterisation parameters of blank PLGA NP, Dox NP and FITC NP prepared by a double emulsion method.

NP Sample	Size (nm)	ZP[a] (mV)	PDI[b]	DC[c] (µg/mg)	RDP[d] (µg/mg)
Blank NP	240.27 ± 14.72	-18.40 ± 1.82	0.26 ± 0.04	-	55.00
Dox NP	242.73 ± 18.64	-14.60 ± 1.32	0.39 ± 0.05	12.80	54.00
FITC NP	286.50 ± 11.30	-10.30 ± 1.00	0.27 ± 0.08	30.80	73.00

[a] Zeta potential (mV), [b] polydispersity index, [c] DC= drug content per 1 mg of NP based on entrapment efficiencies of 64% (Dox) and 77% (FITC-dex); [d] RDP content per 1 mg of NP based on conjugation efficiencies of 55.0% (blank NP), 54% (Dox NP) and 73.0% (FITC NP). Size, ZP and PDI as measured by DLS are expressed as average ± standard deviation (n=6). A student's unpaired T-test was used for statistical analysis; a two-tailed P-value was considered statistically significant if < 0.05.

3.3.2. In vitro release of FITC NP in PBS

FITC-dex release from PLGA NP, shown in Figure 3.2, was measured *in vitro* for 7 days under physiological conditions (37°C, pH 7.4). After 7 days of incubation, up to 42% of the payload was released from the NP, as detected by FITC fluorescence emission. Nimesh et al. (2006) reported a similar release profile for a polymeric NP formulation loaded with FITC-dex, in which release of around 50% was observed after 7 days in PBS (pH 7.4). In Figure 3.2, the rate of payload release retarded following an initial burst phase, in which 25% of the payload was released in the first 24 hours. This showed that the FITC-dex payload was able to escape from

the NP matrix in a controlled manner, which is favourable for both *in vitro* testing and *in vivo* drug delivery.

It Is essential that the payload can release from the NP during *in vitro* testing, however very leaky NP are of no value as free drug will affect results associated with tissue culture work. Like the Dox NP which were analysed in chapter 2, the FITC NP described here are also suitable for cellular uptake studies to observe the effect of RDP conjugation. The small fraction of payload released within 24 hours is unlikely to affect cellular uptake studies, particularly as FITC-dextran is too large and hydrophilic to be passively taken up into cells at such low concentrations.

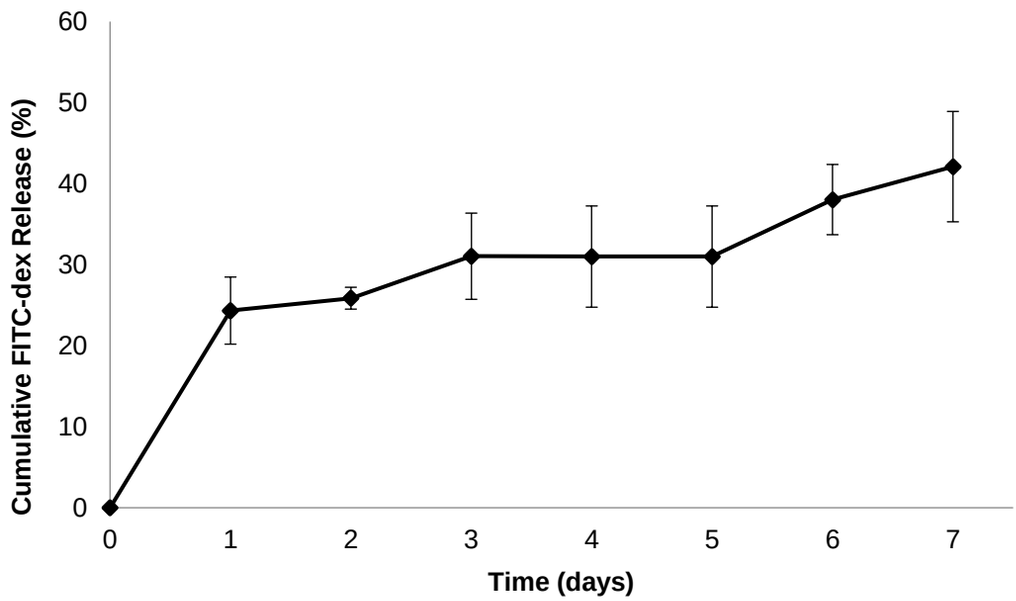

Figure 3.2. *In vitro* 7-day release of FITC-dextran from PLGA NP in PBS at 37°C, as measured by fluorescence spectroscopy. Error bars ± standard deviation (n= 3).

3.3.3. In vitro evaluation

3.3.3.1. Cytotoxicity study

SH-SY5Y neuroblastoma cells were treated with RDP, RDP-Blank NP, Dox NP and RDP-Dox NP to assess cytotoxic effects over varying exposure times (Figure 3.3). RDP alone or conjugated to blank PLGA NP (RDP-Blank NP) showed no significant cytotoxicity over the experimental period, as average cell viability remained at 95% or above (no significant difference) compared to control, even after 24 hours of NP exposure. Additionally, it is clear that any significant cell death observed in Figure 3.3 was due to release of the cytotoxic NP payload, doxorubicin. This result showed that RDP can be used as a non-toxic targeting ligand *in vitro* and was in accordance with the *in vivo* findings by Fu et al. (2012; 2013a; 2013b) on the lack of RDP adverse effects. In fact, Fu et al. (2013a; 2013b) reported no toxic reactions to RDP over experimental periods of three weeks following repeated systemic administration in mice. Moreover, these results confirm that the PLGA NP drug vehicle is also not toxic.

Dox NP imparted 13% cytotoxicity on SH-SY5Y cells following up to 2 hours of exposure time, leading to a significantly lower cell viability of 87.0% compared to control (P value <0.05). After 24 hours, there was a small increase in cytotoxicity causing cell viability to decrease to 82.7% after Dox NP treatment. This toxicity could be expected due to an initial release of cell permeable doxorubicin from the NP, according to the release data previously detailed in chapter 2. Alternatively, it is possible that some non-specific NP uptake has occurred through absorptive processes, particularly after 24 hours.

Results from Figure 3.3 show that incubation of SH-SY5Y neuroblastoma cells with RDP-Dox NP resulted in a significant decrease in cell viability to 67.0% compared to control after 24 hours. The cytotoxicity caused by RDP-Dox NP (33%) was almost double that of Dox NP (17.3%) at 24 hours, also causing a statistically significant difference (P value <0.05). In fact, RDP-Dox NP were significantly more cytotoxic than Dox NP at all treatment times observed. This is perhaps

not surprising, as it was first reported by Fu et al. (2012) that RDP activity was detectable within 15 minutes of administration *in vivo*.

Due to the fact that RDP itself does not appear toxic, this enhancement of cytotoxicity must be due to an increased accumulation of doxorubicin inside the cell. It can therefore be deduced from the results in Figure 3.3, that RDP conjugation is responsible for facilitating enhanced cellular NP uptake, in comparison to an unlabelled formulation.

The pilot *in vitro* study on SH-SY5Y cell viability (Figure 3.3) showed minimal difference between different NP exposure times, particularly for RDP-Dox NP treatment, for which there might be various explanations. RDP-facilitated NP uptake could be limited by an initial rapid saturation of receptor sites within the first hour. This would cause a temporary delay in further RDP-cell interactions, preventing further NP uptake until the ligand-receptor complexes are internalised and degraded or recycled back to the cell surface again. Receptor recycling can occur over time periods ranging from a few hours to several days, depending on the ligand-receptor interaction (Bruneau et al., 2005).

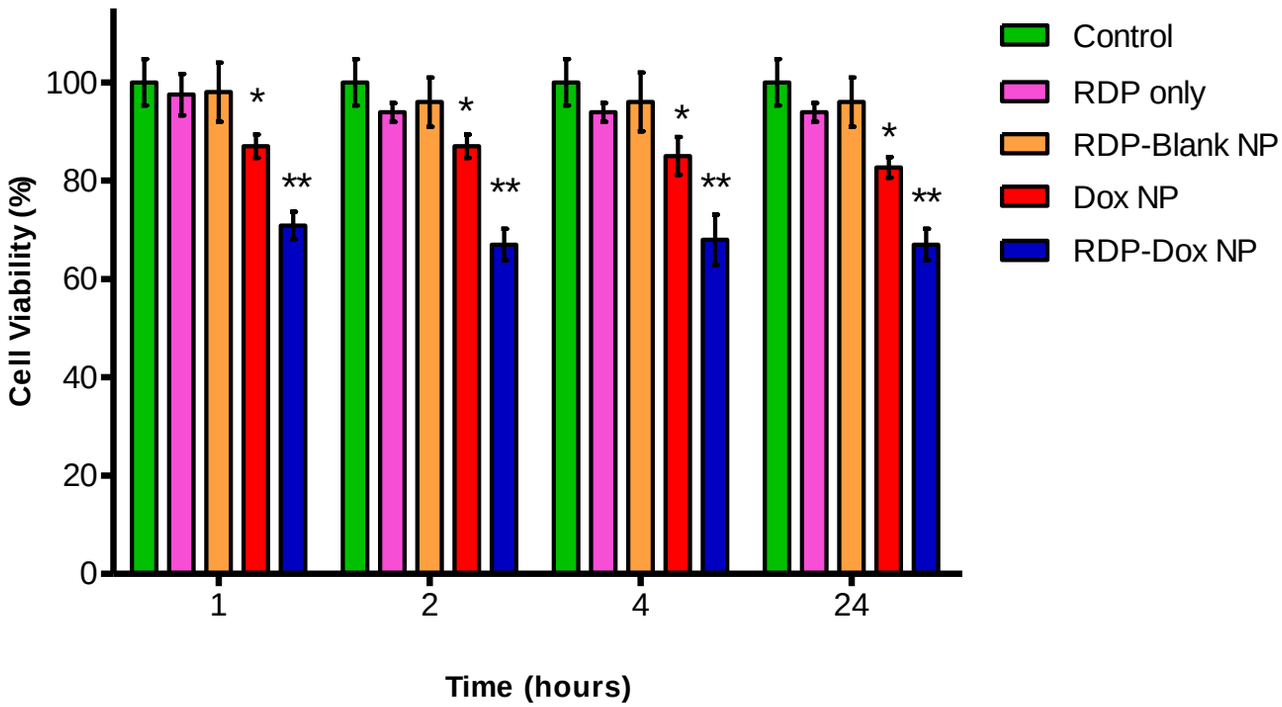

Figure 3.3. Percentage cell viability of SH-SY5Y neuroblastoma cells following treatment with either serum free media (control), RDP, RDP-Blank NP, Dox NP or RDP-Dox NP over varying exposure times. Error bars represent ± standard deviation (n= 6). * Statistically significant difference compared to control; ** statistically significant difference compared to control and Dox NP group (P value < 0.05).

It is possible that observations beyond 24 hours might show further RDP-Dox NP enhanced cytotoxicity, however this is neither ideal nor necessary for further *in vitro* studies. The effect of RDP is observed within 24 hours which is sufficient for many cell-based assays, as times beyond this may result in non-specific cell death from over-confluency. Considering this, it was decided that for further work, NP would be incubated with cells for 24 hours. This would give cells sufficient time to undergo potential NP internalisation processes such as endocytosis, which might be occurring during treatment. It is also true that the consistency and effectiveness of

gentle cell washing after a given period of time cannot be guaranteed, leading to inaccuracies in amount of NP exposed to cells prior to MTT assay. Furthermore, the amount of time NP are in contact with cells cannot be selected during *in vivo* studies and for these reasons, 24 hours treatment time was determined to be most appropriate for *in vitro* studies.

RDP has been previously shown to preferentially target neural cells, both *in vitro* and *in vivo* (Fu et al., 2012; 2013a; 2013b). Results from Figure 3.4 show that RDP conjugation significantly enhanced the cytotoxicity of the Dox NP treatment in the SH-SY5Y neural cell type as opposed to three other non-neural cell types (CHO, MDA-MB-231 & HeLa). In Figure 3.4, cell viabilities for the non-neural cell types- MDA-MB-231, CHO and HeLa, remained similar following treatment with either NP formulation. The MDA-MB-231 and HeLa cell lines (non-neural) were not significantly affected by either NP treatment, although some toxicity was certainly observed compared to control. MDA-MB-231 cell line retained a cell viability of 91.9% after Dox-NP treatment and 92.6% following RDP-Dox NP treatment. For the HeLa cell group, cell viability reduced to 91.0% following Dox-NP exposure and to 87.1% after RDP-Dox NP treatment (not significant). RDP, therefore, had no significant effect on the cytotoxicity of the Dox-NP formulation within these non-neural cell types.

The normal, non-neural CHO cell line displayed cell viabilities of 83.4% and 86.7% following treatment with Dox-NP and RDP-Dox NP, respectively. Both of these values marginally turned out to have a statistically significant P value (< 0.05) compared to control, but not to each other. This means that RDP labelling did not have an effect on the toxicity of Dox-NP within the CHO cell line. This was not the case for the SH-SY5Y neuroblastoma cells, which had a significantly lower cell viability of 65.9%, when treated with the RDP-Dox NP compared to 78.3% when treated with the unlabelled Dox NP. The difference between these two treatment groups was approximately 13% and shown to be significant ($P < 0.05$), indicating alteration in cell viability due to RDP labelling.

It is clear from these findings that RDP enhanced cellular uptake of an attached nanocarrier within the neural cells exclusively. It has already been conclusively shown by Fu et al. (2012;

2013a) that RDP conjugates enter neural cells by energy-dependent means. If free doxorubicin was only causing effects through NP leakage, results for Dox NP and RDP-Dox NP treatments would be similar for SH-SY5Y cells, as was seen with the CHO, MDA-MB-231 and HeLa cell lines. To this end, it would appear that when attached to a polymeric NP, RDP retains the neurotropism of the parent glycoprotein, RVG.

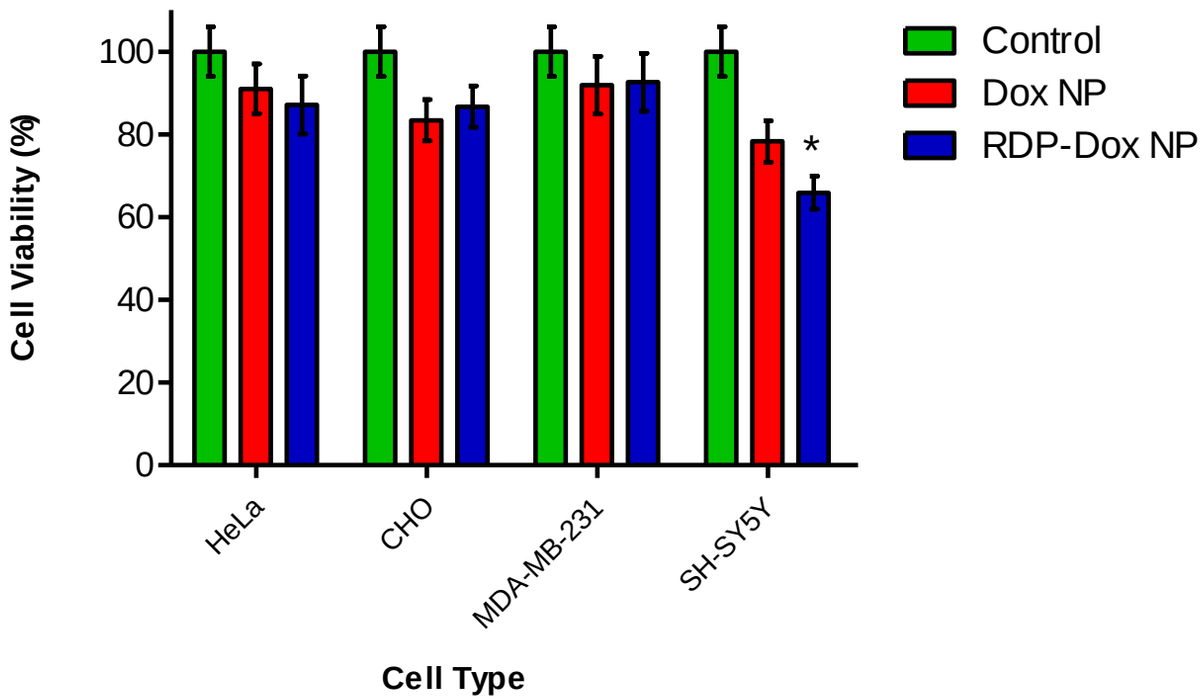

Figure 3.4. Percentage cell viability of MDA-MB-231, CHO, HeLa and SH-SY5Y cells following treatment with either serum free media (control), Dox NP or RDP-Dox NP. SH-SY5Y cells of neural origin, are the only cell line to show a statistically significant difference in cell viability between the Dox NP group and RDP-Dox NP group (P value= 0.028, <0.05). Error bars ± standard deviation (n= 6). * Statistically significant difference compared to Dox NP treatment.

3.3.3.2. Confocal microscopy

Visualisation of FITC-NP uptake by confocal fluorescence microscopy (Figure 3.5) demonstrates the ability of RDP to preferentially target SH-SY5Y neuroblastoma (Figure 3.5A) and PC-12 (pheochromocytoma) neural cells (Figure 3.5B), promoting visibly greater cellular uptake compared to the unlabelled FITC NP. In contrast, fluorescence signal detected in Hela cells of Figure 3.5C was low. No notable difference in HeLa cell uptake was visualised between all formulations, indicating that RDP is not effective as a targeting peptide in this non-neural cell line, supporting the findings from Figure 3.4.

St. Pierre et al. (2011) detected association of original RVG with the endocytic pathway in a mouse neuroblastoma cell line, concluding that RVG is most likely internalised by a receptor-mediated endocytosis mechanism. The signal pattern detected by Lysotracker® red indicates that there may be co-localisation of lysosomes and internalised FITC-NP in SH-SY5Y and PC-12 cells. It was first suggested by Fu et al. (2013a), that the cellular uptake mechanism of RDP may involve energy-dependent internalisation pathways, such as clathrin-dependent endocytosis. It was later shown by Zhang & Fu (2015), that RDP-gold NP conjugates were detected in SH-SY5Y cell endosomes and cytoplasm by transmission electron microscopy. This uptake was greatly reduced in an ATP-depleted environment, implicating the dependence of RDP on energy-mediated uptake mechanisms, rather than passive. Indeed, observations of potential co-localisation between RDP conjugates and lysosomes in Figure 3.5 support this idea.

No evidence of free FITC-dex entering cells could be detected after 24 hours of incubation, meaning concerns of free drug leaching from NP to affect uptake studies could be disregarded, probably due to the size and hydrophilic nature of the FITC-dex molecule. If free drug were interfering with results, greater fluorescence would be seen with the unlabelled NP preparation. However, this was not the case, with minimal fluorescence from FITC NP detected in all of the cell lines studied.

SH-SY5Y cells are commonly employed for studying drug delivery to neural cells and are often used as a dopaminergic model for PD research (Forster et al., 2016; Xicoy et al., 2017). PC-12

cells were introduced as an additional cell line of neural origin to provide further insight into the neural-specific targeting capability of RDP. The uptake of RDP-conjugated cargo, as detected by various microscope imaging techniques, has been most commonly studied in SH-SY5Y cells. For example, Wu et al. (2016) detected RDP-p53 fusion protein by confocal imaging in SH-SY5Y cells, but not in HepG-2 hepatocellular carcinoma cells. Although using a different RVG derivative, Son et al. (2011) showed that an RVG-29-targeted gene delivery vector was detected by confocal fluorescence imaging in Neuro-2a cells, but not in non-neural HeLa cells. Findings from this confocal study, as presented in Figure 3.5B, are the first reported images of RDP action in PC-12 cells and thus providing further support for the neural cell-specific permeability of this peptide.

(A)

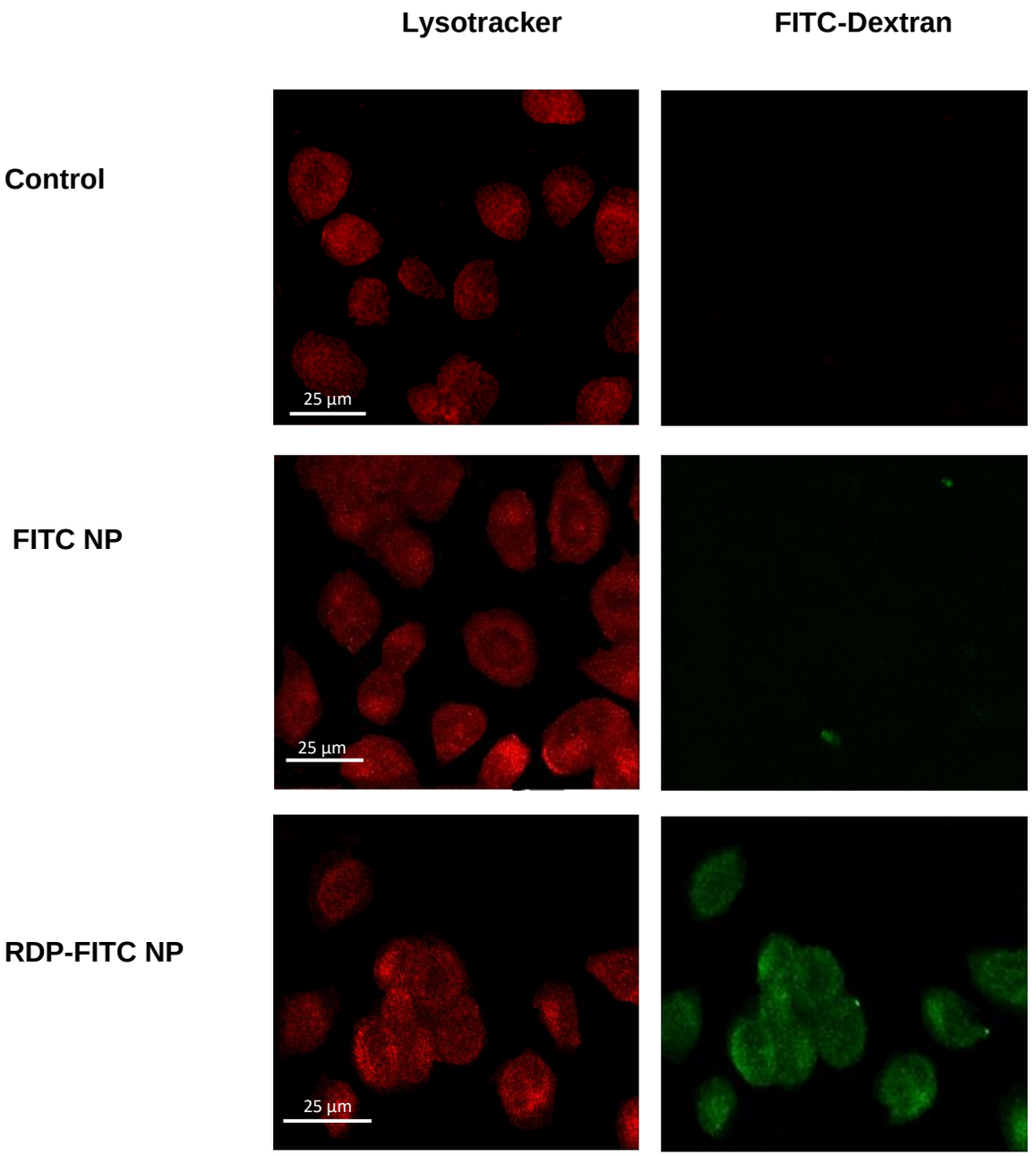
Lysotracker
FITC-Dextran
Control
FITC NP
RDP-FITC NP
25 µm
25 µm
25 µm

(B)

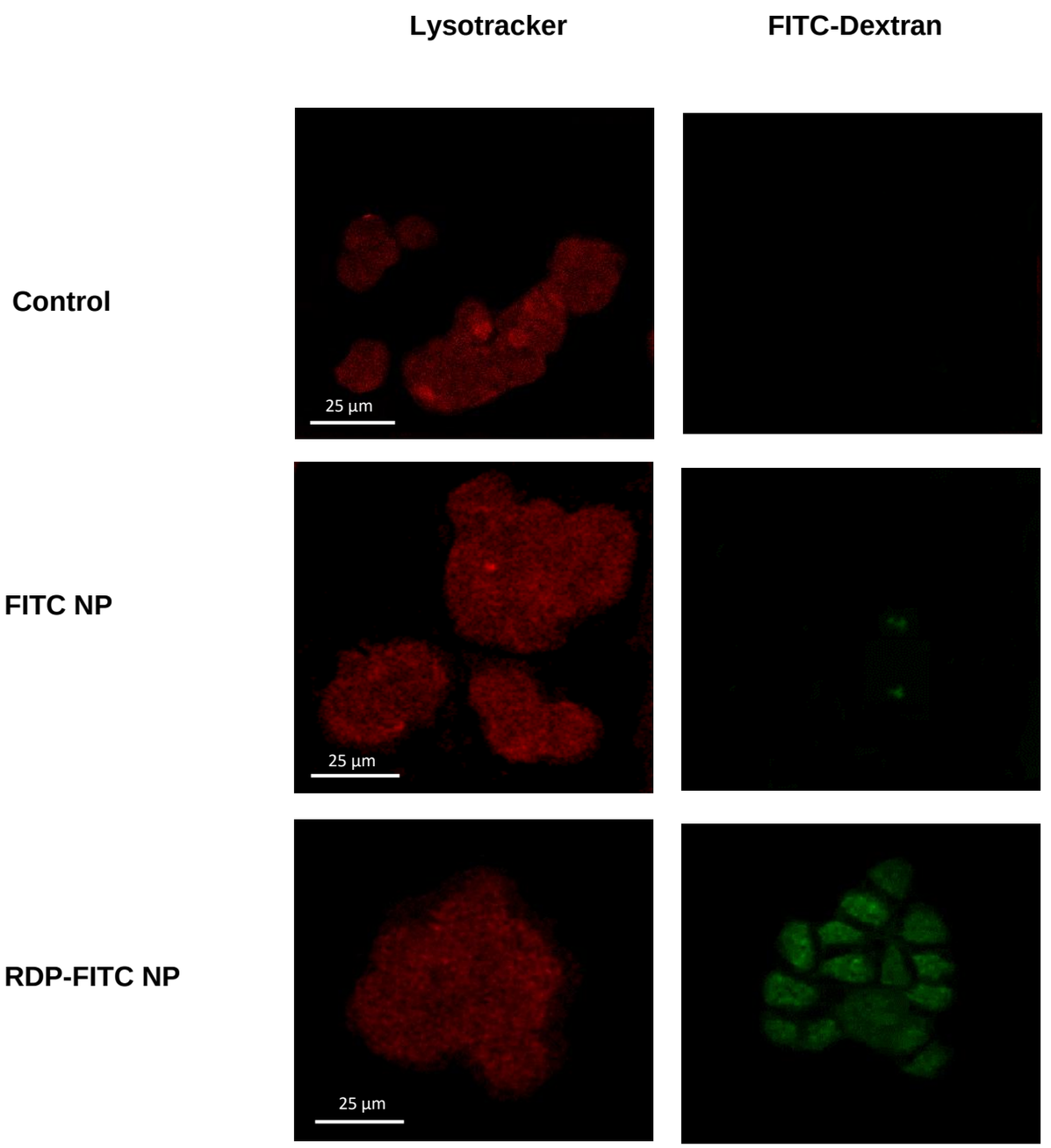
Lysotracker
FITC-Dextran
Control
FITC NP
RDP-FITC NP
25 µm
25 µm
25 µm

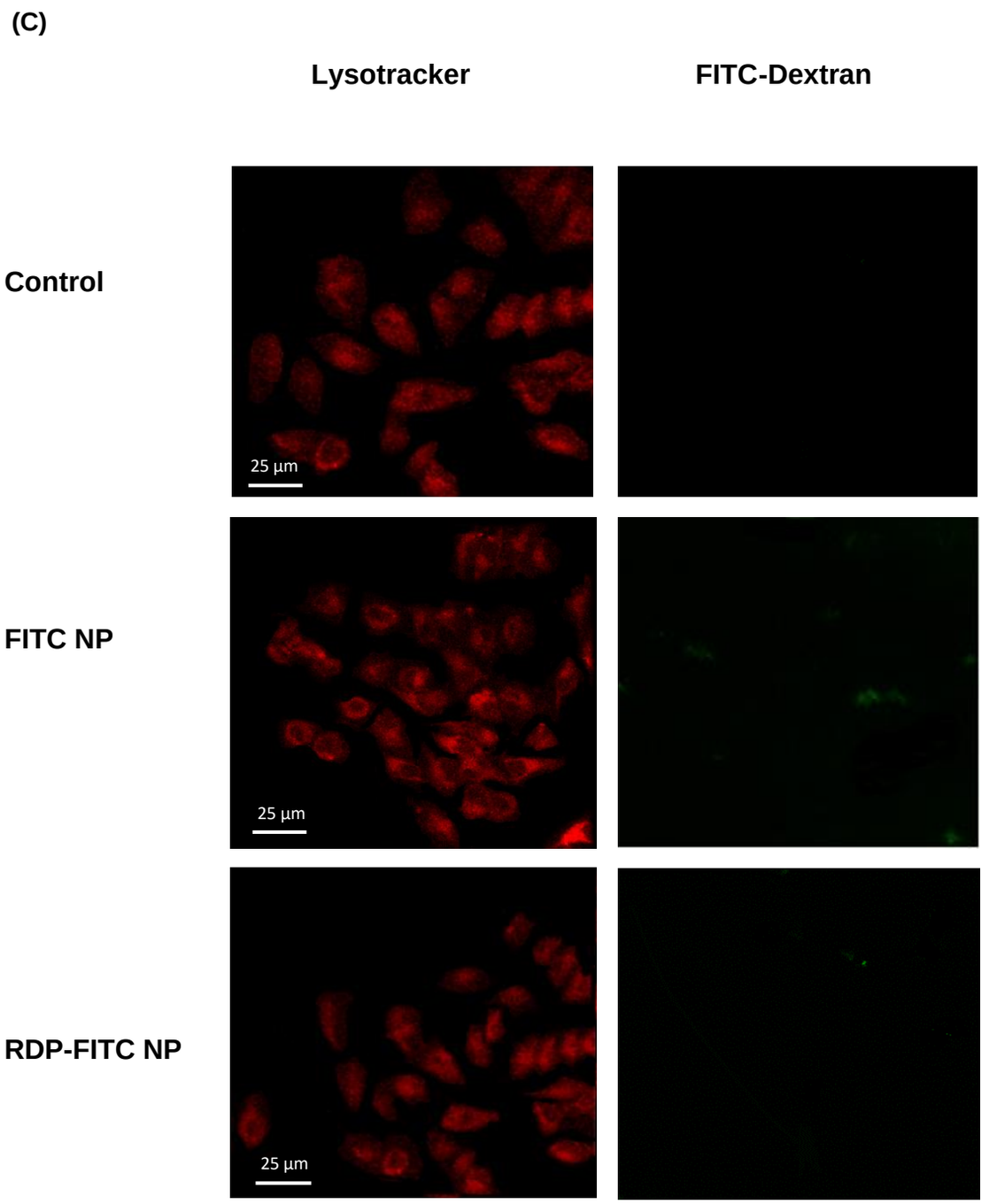

Figure 3.5. Confocal images showing location of intracellular lysosomes (red) and the effect of RDP labelling on the cellular uptake of FITC-NP (green) in (A) SH-SY5Y (B) PC-12 and (C) HeLa cells.

3.3.4. Receptor identification study

Receptor mediated endocytosis is the proposed mechanism of RDP cellular uptake (Fu et al., 2013a) and indeed for most NP modified with targeting ligands (Danhier et al., 2012). In order to determine which receptor is responsible for cellular interaction with RDP, SH-SY5Y neuroblastoma cells were used alongside various inhibitors of the main neural receptor types, namely the GABA receptor and the nicotinic acetylcholine receptor (nAChR).

Results from Figures 3.4 & 3.5 provided evidence that RDP enhanced the cytotoxic effect of Dox NP on these cells specifically. SH-SY5Y cells were therefore an appropriate selection for receptor identification. Different antagonists of the nAChR, GABA(a) and GABA(b) receptors were utilised to test the effect on RDP-Dox NP treatment of SH-SY5Y cells. Cells were pre-treated with either bicuculline or saclofen (competitive antagonists of the GABA receptor A and B subtypes, respectively) or hexamethonium (competitive antagonist of the nAChR). Results displayed in Figure 3.6 show that the hexamethonium pre-treated group was the only one to maintain a cell viability of 99.3%, compared to control. The GABA inhibitors bicuculline and saclofen were unable to prevent a significant decrease in cell viability, as RDP-Dox NP treatment caused cell viability to decrease to 84.8% ($P < 0.05$ compared to control) for both groups. This suggested that RDP did not depend on either GABA receptor subtype for gaining cell entry, conflicting with the findings of Fu et al. (2013a).

Treatment with hexamethonium, saclofen or bicuculline alone did not cause any cell death and so any decreases in cell viability was due to RDP-Dox NP treatment. The SH-SY5Y cell viability of the RDP-Dox NP treated cells with no prior treatment with a receptor inhibitor was 80.5%. This level of cell death was similar to the bicuculline and saclofen pre-treated groups, where there was approximately 16% cell death. In contrast, the hexamethonium pre-treated cells were significantly different to those with no prior inhibitor treatment ($P < 0.05$).

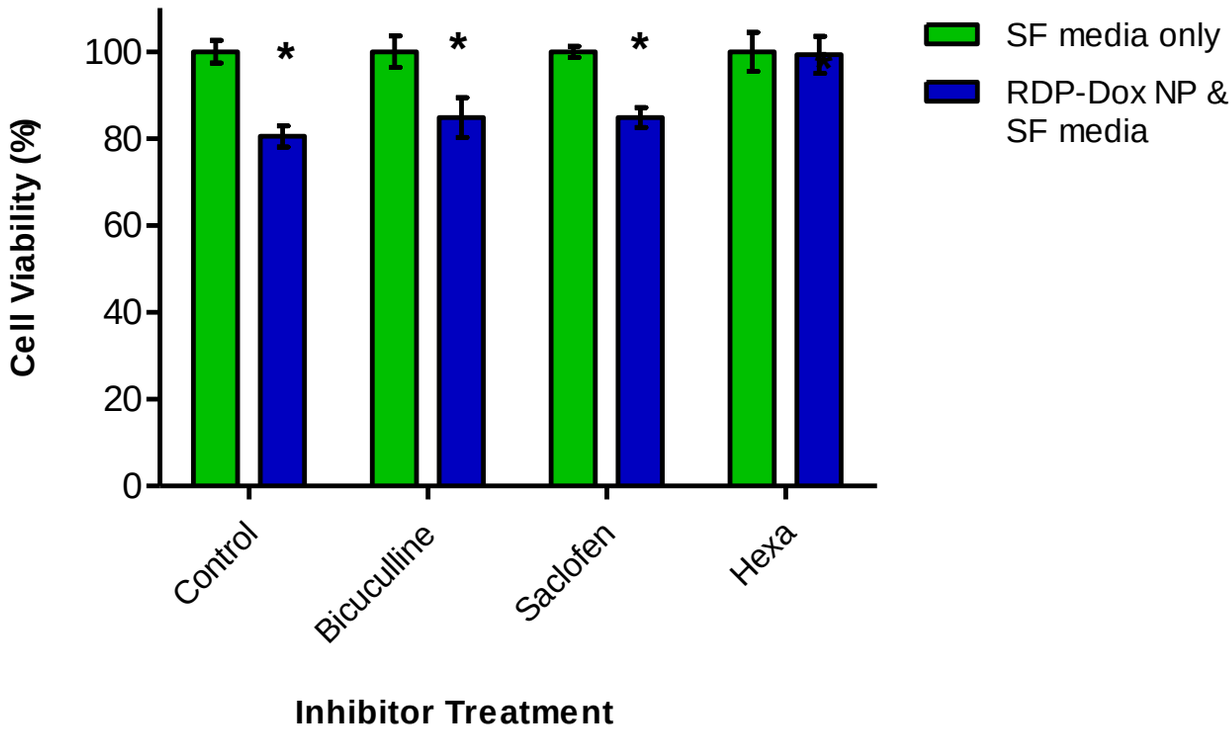

Figure 3.6. Percentage cell viability of SH-SY5Y neuroblastoma cells following treatment with RDP-Dox NP for 24 hours to assess the effect of 30 minutes pre-treatment with different receptor inhibitors on RDP-facilitated NP uptake. Hexamethonium (Hexa), the competitive nAChR antagonist, was the only inhibitor able to block the effect of NP treatment. Error bars represent ± standard deviation (n= 6). *Statistically significant difference compared with control; Two-tailed T-test P value <0.05.

Figure 3.7 shows that pre-treatment of SH-SY5Y cells with either anti-AChRα7 antibody or the non-competitive nAChR antagonist, mecamylamine, prevented RDP-Dox NP-induced SH-SY5Y cell death as viability remained comparable to control. None of the inhibitors used in the experiments of both Figures 3.6 & 3.7 are cell permeable, but rather bind to extracellular receptors. The lack of effect caused by RDP-Dox NP over 24 hours in the presence of hexamethonium, mecamylamine and anti-AChRα7 antibody indicated a receptor-dependent mechanism of RDP cellular uptake.

Results from Figure 3.6 and Figure 3.7 revealed that the nAChR is necessary for RDP-Dox NP to have any significant effect on SH-SY5Y cell viability. A competitive nAChR antagonist (hexamethonium), a non-competitive nAChR antagonist (mecamylamine) and a specific antibody of the nAChR all prevented RDP-facilitated effects on SH-SY5Y cells. Conversely, blocking either GABA(a) or GABA(b) receptor subtypes had no effect in preventing a significant decrease in SH-SY5Y cell viability (Figure 3.6). It can, therefore, be concluded from this work that the nAChR most definitely plays an important role in cellular interaction with RDP. It is most likely that via this receptor, RDP facilitates the internalisation of a conjugated payload, leading to the specific effects observed in SH-SY5Y cells.

These findings conflict with Fu et al. (2013a), who reported that GABA itself prevented cellular uptake of RDP. It is possible that high concentrations of GABA causes desensitisation of the nAChR through negative feedback mechanisms which control acetylcholine-mediated GABA release (McClure-Begley et al., 2014). If this were the case, it would falsely appear as though GABA is preventing RDP uptake via a GABA receptor rather than the desensitising effect on the nAChR. In this instance, the nAChR may not be able to bind RDP and consequently undergo receptor-mediated endocytosis. This, however, does not explain why Fu et al. (2013a) found that nicotine was unable to prevent RDP uptake, unless RDP was able to outcompete the nicotinic agonist in a concentration-dependent manner.

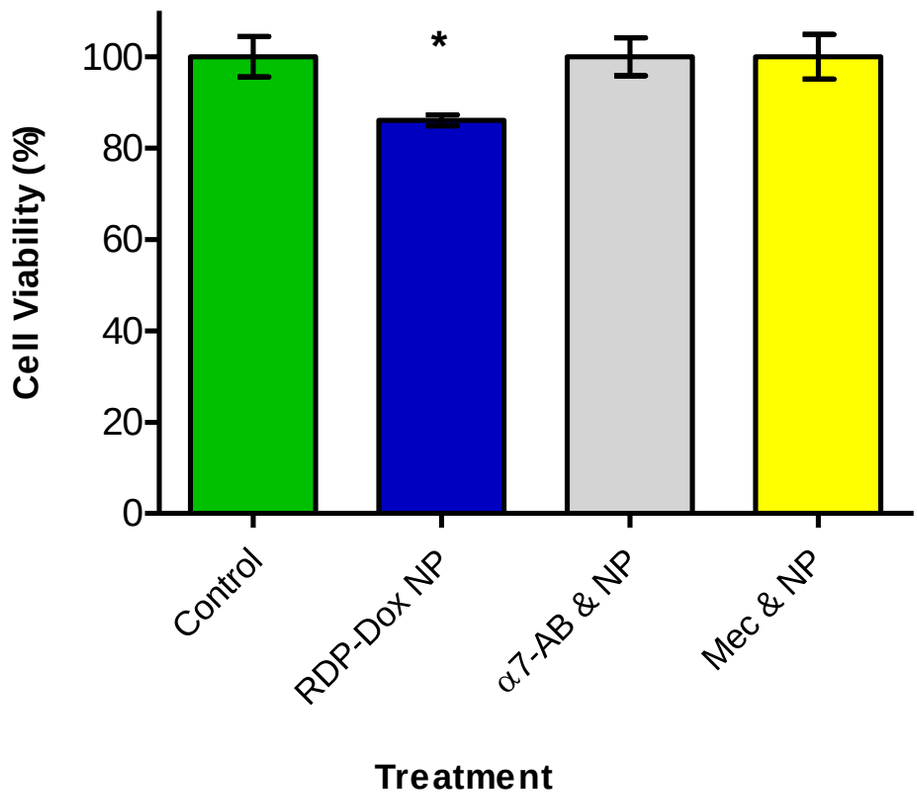

Figure 3.7. Percentage cell viability of SH-SY5Y neuroblastoma cells following pre-treatment with different nAChR inhibitors and exposure to RDP-Dox NP. Mecamylamine (Mec) and anti-AChRα7 antibody (AB) both blocked the effect of RDP-Dox NP. Error bars represent ± standard deviation (n= 6). * Cell Viability = 86.1%; statistically significant difference compared to control (P value= 0.027, <0.05). "NP" represents RDP-Dox NP treatment.

Following the confocal study of Figure 3.5, it was shown that RDP is active in both SH-SY5Y and PC-12 cells. To further verify that RDP function is dependent on interaction with the nAChR, the specific AChRα7 antibody was tested for its effect on RDP-Dox NP action in PC-12 cells. Results from Figure 3.8 showed that similar to SH-SY5Y cells, PC-12 cells were susceptible to the effects of RDP-enhanced uptake of Dox NP. Treatment with RDP-Dox NP was significantly more cytotoxic than the unlabelled Dox NP preparation, however this difference was negated by pre-incubation of PC-12 cells with anti-AChRα7 antibody. Blocking this receptor caused cell viability

to remain higher (91%) after RDP-Dox NP treatment, in comparison to cell viability when the receptor was uninhibited (79%). These findings substantiate the conclusions drawn from Figures 3.6 & 3.7, that the nAChR is majorly involved in neural cell association with RDP.

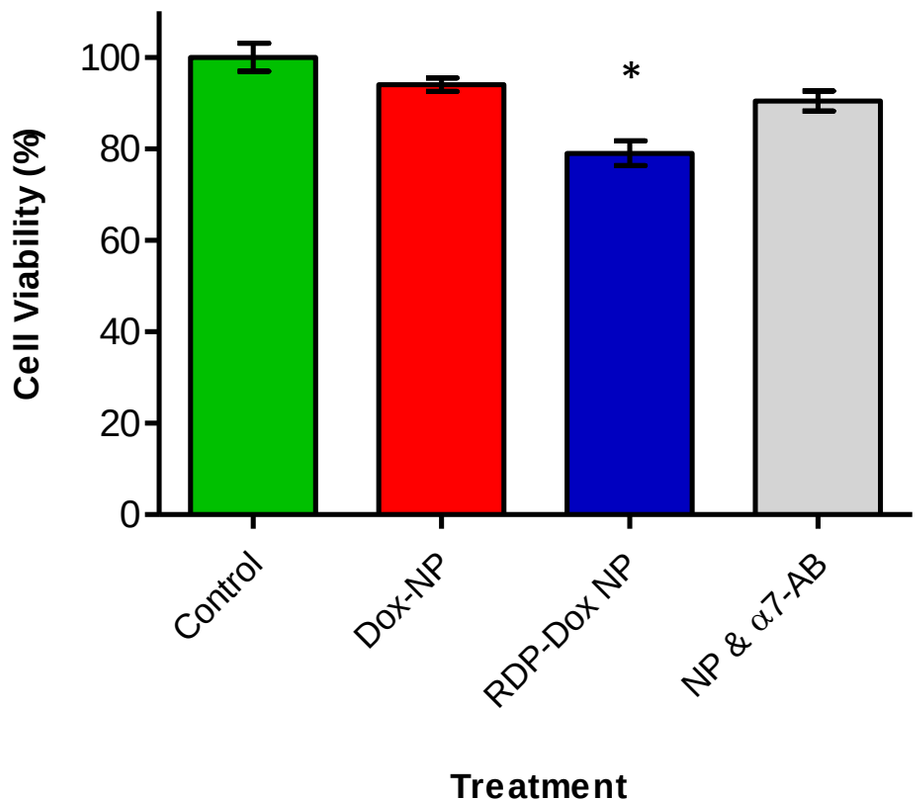

Figure 3.8. PC-12 cell viability in response to treatment with different NP preparations. The effect of blocking the α7-nAChR on RDP-facilitated NP uptake was investigated by blocking the receptor with a specific antibody. Error bars ± standard deviation (n=6). * cell viability= 79%; statistically significant difference compared to Dox NP (P value <0.05). "NP & α7-AB" represents RDP-Dox NP treatment in combination with anti-AChRα7 antibody.

There are two principal subtypes of acetylcholine receptor in the human body, the metabotropic muscarinic acetylcholine receptor and the ionotropic nicotinic acetylcholine receptor (nAChR). Both of these groups are activated by the endogenous ligand, acetylcholine, at neuronal and non-neuronal sites. The muscarinic subtype has been distinguished by its typical activation by

muscarine, the mushroom toxin from *Amanita muscaria,* whereas the nicotinic subclass is prominently activated by the exogenous ligand, nicotine. nAChRs are a family of cationic channels and along with the muscarinic subtype, 5-Hydroxytryptamine (serotonin) receptors and γ-aminobutyric acid (GABA) $_{A/C}$ receptors, they form part of the Cys-loop gene superfamily commonly known as ligand-gated ion channels (Gotti & Clementi, 2004; Dunckley & Lukas, 2006). They nAChR subfamily has classically been further subdivided into neuronal-type and muscle-type.

Neuronal-type nAChRs exist as homopentameric or heteropentameric subtypes. This means they are typically composed of 5 subunits surrounding a central pore, as depicted in Figure 3.9. Thus far, the subunits which have been identified in mammalian neuronal-type nAChRs are nine α (α1-α9) and three β (β2-β4) subunits. (Hadaddian et al. 2008; Quik & Wanacott, 2011). The homopentameric arrangement (Figure 3.9A), also known as α-Bungarotoxin sensitive, is composed of five identical α7 subunits and therefore five identical agonist binding sites. In the human central and peripheral nervous systems, α7 homomeric receptors are one of the most commonly found, particularly in neurons of hippocampal origin. It is possible that α8 and α9 subunits also compose these homomeric receptors, but so far, the α8 subunit has not been identified in humans and the α9 subunit has presently not been isolated in neurons (Gotti & Clementi, 2004).

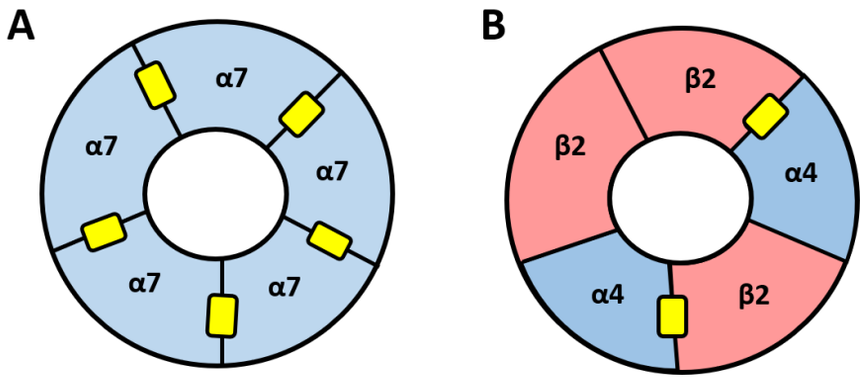

Figure 3.9. A representation of the neuronal-type nicotinic acetylcholine receptor subunit composition for the common (A) α7 homopentameric and (B) α4β2* heteropentameric subtypes. The ligand binding sites (yellow) are situated between alpha subunits (homopentameric) or alpha and beta subunits (heteropentameric).

The heteropentameric arrangement (Figure 3.9B) is generally in the stoichiometry arrangement of 2α3β*; where * signifies the possibility of a different additional α subunit in the complex (Paterson & Nordberg, 2000). These receptors will have two agonist binding sites, between α and β units, both of which must be occupied for activation of the receptor. These are also known as α-Bungarotoxin insensitive but show a higher affinity in agonist binding compared to their homomeric counterparts. Although the α2, α3, α4, α6, β2 and β4 subunits play a role in binding and may be co-expressed by a particular neuron, only a few combinations may actually be formed. This led to the conclusion that α5 and β3 subunits merely play a supportive role rather than being involved in agonist binding (Gotti & Clementi, 2006).

The major nAChR subtypes in the mammalian central nervous system are α4β2* and α7*, comprising approximately 90%. The structure of both these receptor subtypes and their respective binding sites are shown in Figure 3.9. In the CNS, nAChRs are widely expressed, as they form a major part of the cholinergic transmission pathways in the brain and peripheral ganglia (Table 3.2). Their role in pre-synaptic neurotransmitter release and post-synaptic

transmission means that central innervation gives rise to many different functions. These include cognition, reward, pain processing, arousal and motor activity (Gotti & Clementi, 2006). These functions of the nAChR depend on brain location and indeed subunit composition. Table 3.2 details nAChR subunits found throughout different areas of the nervous system.

At the interface between the central nervous system and the blood circulation, there has been detection of nAChR subunits on brain endothelial cells of the BBB. These cells specifically express the α3, α5, α7, β2 and β3 subunits, as reported by Abbruscato et al. (2002) in an immunoreactivity assay. If RDP can enter neural cells and cross the BBB *in vivo* via nAChR-dependent means, it must be able to bind to one or more nAChR subtypes expressed on brain endothelial cells.

Table 3.2. Evidence of neuronal-type nAChR subunit detection and composition in different areas throughout the brain and at the NMJ.

Organ/system	Location	Neuronal-type nicotinic acetylcholine receptor subunits
Brain	Unspecified	α3, α4, α5, α6, α7, β2, β3 & β4 (Maus et al., 1998)
	Hippocampus	Mainly α7 (Court et al., 2000)
	Cerebellum	α3, α4, α7 & β2 (Court et al., 2000)
	Striatum	α3, α4, α7 & β2 (Court et al., 2000)
	Substantia Nigra	α3, α4, α7 & β2 (Court et al., 2000)
	Cortex	α3, α4*, α7 & β2(Court et al., 2000)
	Microglia	α7 (De Simone et al., 2005)
Blood Brain Barrier	Brain Endothelial Cells	α3, α5, α7, β2 & β3 (Abbruscato et al., 2002)
Muscle	Muscle Fibre (rat)	α7 (Fischer et al., 1999)

It has been established that RVG can bind to residues 173-204 of the α1 subunit of muscle-type nAChRs present at the NMJ, hence leading to rabies virus infection (Lentz et al. 1990; Gastka et al. 1996). In early studies by Lentz et al. (1990), it was concluded that the rabies virus shares

a binding site with α-BTX (a competitive inhibitor of acetylcholine) at the α1 subunit. Lentz and colleagues also found that that the virus was able to bind to the α3 subunit, confirming that the rabies virus does in fact bind to neuronal-type nAChRs as well as muscle-type. Evidence of neuronal-type nAChR subunits such as α7 have been detected in muscle (Fischer et al. 1999), meaning that additional subunits at the NMJ are very likely to play a role in RVG binding and explain the ability of the rabies virus to traverse the CNS so readily.

Other molecules have been thought to be associated with rabies virus infectivity of the CNS. The involvement of neural cell adhesion molecule (NCAM) in cell attachment and uptake of the rabies virus is somewhat ambiguous and subsequently passed over in comparison to the nAChR. Also known as CD56, it is a glycoprotein from the immunoglobulin (Ig) superfamily with functions in cell adhesion and signalling (Paratcha et al., 2003). NCAM plays a role in nervous system development by influencing cell migration, adhesion, neurite outgrowth and synaptic plasticity (Hubschmann et al., 2005). There has also been evidence to suggest that NCAM is required to maintain normal synaptic function at the NMJ, particularly following injury (Chipman et al, 2010).

Thoulouze et al. (1998) attempted to determine the role of NCAM in rabies virus infection, using NCAM-positive and NCAM-negative cells. It emerged that NCAM-negative cells transfected with the NCAM gene, showed enhanced susceptibility to the rabies virus infection and that blocking NCAM with a specific antibody and a heparin ligand reduced susceptibility. The authors believed this evidence would indicate that NCAM is a receptor for the rabies virus, certainly at the very least, it would suggest that NCAM plays a role in infection. Thoulouze et al. (1998) considered that the nicotinic receptor and NCAM may both be closely involved or even synergistic in nature. The independence of NCAM from the acetylcholine receptor is questionable, as the *in vivo* work from this same study showed that the brains of NCAM deficient mice were still infected by rabies virus and equally so in the hippocampus, albeit far less efficiently than in the NCAM-positive wild-type mice. Furthermore, NCAM deficiency does not prevent rabies-induced death in mice but only delays it. The fact that NCAM is not essential for infectivity means that although it seems to play an important role, it cannot be classified as a main receptor. Given the expression of

NCAM throughout the central and peripheral nervous system in astrocytes, neurons and non-myelinating Schwann cells, it is quite possible that NCAM forms part of a receptor complex which is responsible for the neurotropism of RVG at the NMJ (Lafon, 2005).

Hislop et al. (2014) described how RVG associated with three types of receptor *in vitro.* These were the aforementioned nAChR, NCAM and the low-affinity nerve-growth factor/neurotrophin ($P75^{NTR}$) receptor. $P75^{NTR}$ is from the tumour necrosis factor (TNF) family of receptors and although it is responsible for neurotrophin signalling pathways, it has also been implicated in neurodegenerative processes. It was proposed by Tuffereau et al. (1998) that $P75^{NTR}$ could be a receptor for the rabies virus, after detecting association with RVG in infected cell lines *in vitro*. Almost a decade later, following doubts over association *in vivo,* Tuffereau et al. (2007) revisited this work and concluded that $P75^{NTR}$ was not essential for rabies virus infection. It was also detailed that $P75^{NTR}$ expression alone was not sufficient enough to infect cells *in vivo* and other factors were almost certainly implicated.

It should be noted that the interaction of RVG with $P75^{NTR}$ as accounted by Hislop et al. (2014), was in a mouse hybrid cell line of neuroblastoma and spinal cord cells. This model was not representative of the *in vivo* NMJ and there appears to be no *in vivo* evidence of $P75^{NTR}$ presence at the NMJ (Lafon, 2005). Whether or not NCAM and $P75^{NTR}$ play a key role *in vivo* or merely an accessory role in the neurotropism of RVG remains unclear, as conclusions drawn from *in vitro* results have deviated from *in vivo* behaviour.

Prior to this work, the major receptor responsible for RDP cellular uptake had not been elucidated for certain. It has been well established however, that an energy-dependent endocytosis mechanism is responsible, a theoretical representation of which is shown in Figure 3.10.

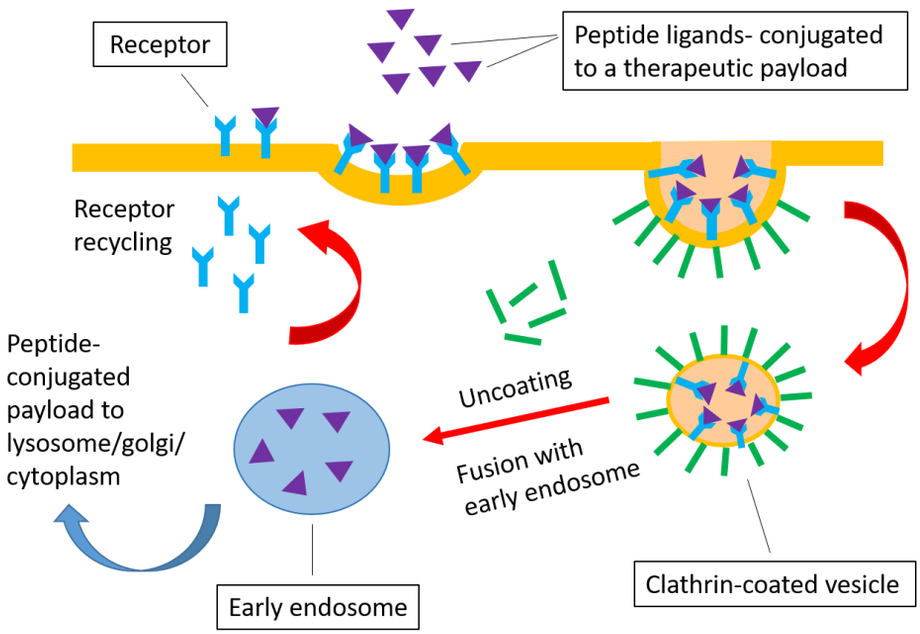

Figure 3.10. Hypothetical route of uptake of rabies virus-derived peptide (RDP) via clathrin-dependent receptor-mediated endocytosis.

Given the results from Figures 3.6-3.8, it is clear that the nAChR is responsible to a considerable extent for the effects of RDP as a targeting ligand in two different neural cell types, SH-SY5Y and PC-12. Like BBB endothelial cells, SH-SY5Y and PC-12 cells are known to express α3 and α7 nAChR subunits (Madhok et al., 1995; Drisdel et al., 2004; Dunckley & Lukas, 2006). This commonality between cell types certainly supports the conclusions drawn from this work, that like the original virus glycoprotein, RDP most likely interacts with at least one or more nAChR subtypes to facilitate internalisation of an attached payload. The mutual expression of the α7-nAChR subtype particularly amongst potential CNS entry points at the BBB and NMJ, presents a viable avenue for future receptor-ligand studies.

3.4. Conclusion

In order for RDP to be advanced as a therapeutic CNS targeting ligand, it is necessary to know which neural surface receptor the peptide targets. This study aimed to determine which receptor RDP binds to on neural cells following conjugation to a doxorubicin-loaded NP vehicle. In agreement with work by others on RDP-conjugates, it was shown that RDP-Dox NP and RDP-FITC NP selectively enhanced uptake of payload in two neural cell lines, SH-SY5Y and PC-12, compared to unlabelled preparations. This preferential targeting ability was not observed in various non-neural cell types. This study also showed neither RDP alone nor the PLGA vehicle are toxic *in vitro*.

Various receptor inhibitors were used in attempt to block RDP activity in SH-SY5Y cells, which resulted in the nAChR being identified as necessary for RDP-facilitated uptake of Dox NP. This was confirmed when RDP-enhanced cytotoxicity in PC-12 cells diminished upon blocking the homomeric α7 nAChR. In identifying the nAChR as necessary for RDP uptake, progression can be made in the development of this ligand for use in targeted drug delivery systems.

Early success and the attractive properties of this novel peptide for targeting neural cells can be attributed to inheritance of the strong neurotropism displayed by the parent glycoprotein, RVG. Mazarakis et al. (2001) proposed that viral envelope glycoproteins such as RVG, may be utilised for treating neurodegenerative disorders such as Parkinson's, Alzheimer's and Motor-Neuron diseases. Taking advantage of the neurotrophic properties of RDP *in vivo* and the ubiquitous nature of the nAChR in the CNS may provide the basis for new brain targeting mechanisms, such as the work already mentioned by Fu et al. (2012 & 2013) and Zhang & Fu (2015) on RDP-conjugates. The use of RDP within polymeric drug carrier formulations may provide a safe and valuable approach to neural cell-targeting, protecting sensitive therapeutics from enzymatic degradation whilst enabling BBB passage.

Further investigation of RDP properties may highlight the need to optimise this large, hydrophilic peptide for future *in vivo* success. RDP is relatively sizeable for a targeting ligand, presenting opportunity for enzymatic degradation by serum proteases following *in vivo* administration. Despite the early *in vivo* success of RDP, it remains to be seen how resistant RDP itself is to serum degradation and if this can be modified through sequence development. It is certainly most desirable to achieve optimum stability whilst retaining targeting efficacy, to make advances in the pursuit for a viable brain-targeting ligand for neurodegenerative treatment.

Chapter 4

Development of an optimised RDP sequence- evaluation of stability and *in vitro* efficacy.

This chapter reports work (with permission) from the following in press publication:

Huey, R., Rathbone, D., McCarron, P and Hawthorne, S. (In Press). Design, Stability and Efficacy of a New Targeting Peptide for Nanoparticulate Drug Delivery to SH-SY5Y Neuroblastoma Cells. *Journal of drug targeting.* The original article can be found in Appendix 3.

4.1. Introduction

Specific targeting of therapeutics is a growing area of research for a number of different disease states. The benefits of this over conventional drug delivery are numerous, including better bioavailability of the drug at the target organ, reduction of unwanted side effects and smaller dosages required for therapeutic effect. Cell penetrating peptides (CPPs) can greatly enhance the intracellular uptake of conjugated cargo across biological membranes in a non-invasive, non-disruptive manner. However, due to lack of tissue specificity, CPPs such as TAT (transactivating transcriptional activator) peptide, penetratin and polyarginine are not as efficient when aiming to deliver expensive or toxic drugs (Malhotra & Prakash, 2011). A certain area of the body where it is particularly difficult to achieve efficient drug accumulation, due to the natural biological barrier, is the brain. Active targeting of therapeutics to the central nervous system (CNS) is becoming essential, as many developed drugs for neurological disorders are unable to passively cross the blood brain barrier (BBB). The difficulties in achieving drug delivery across the BBB due to its unique structure of brain endothelial cells, tight junctions and glial cells has been extensively reviewed in the literature (Teixido & Giralt, 2008; Alyautdin et al., 2014; Banks, 2016; Saraiva et al., 2016).

CNS-specific peptide targeting ligands have been explored in the past decade to deliver therapeutic agents to the brain in animal studies with success (Kumar et al., 2007; Kwon et al., 2010; Zhang et al., 2013; Gao et al., 2014; Soddu et al., 2015;). Many promising CNS-targeting peptides take advantage of native receptors, transporters or enzymes to deliver therapeutic cargo across the BBB. Derivatives from natural neurotoxic agents have been utilised due to their highly efficient transport abilities across the CNS. These include tetanus toxin fragment C (Toivonen et al., 2010), neurotropic virus glycoproteins and fragments of snake, scorpion and bee venoms (Soddu et al., 2015). Thus far, promising results with these ligands are still surrounded with concerns of immune reactions and true specificity for neural cells only. Kumar et al. (2007) first showed that a derivative of RVG, RVG-29, utilised nicotinic acetylcholine

receptor (nAChR) transport to safely and non-invasively deliver siRNA to the CNS. Following this success, derivatives of RVG have since been utilised to take advantage of this property for drug delivery to the CNS to treat a range of brain disorders (Liu et al., 2009; Chen et al., 2011; Son et al., 2011).

Rabies virus-derived peptide (RDP) has shown early success as a neural cell-targeting ligand both *in vitro* and *in vivo* (Fu et al., 2012, 2013a, 2013b; Wu et al., 2016). It was shown previously (Chapter 3) that RDP is dependent upon interaction with the nAChR and activity was considerably inhibited by blocking the homomeric α7 subtype of this receptor, commonly found throughout the CNS. An obstacle in the development of many peptide targeting ligands is the issue of serum instability due to proteolysis, hence breakdown of the peptide upon systemic administration.

Rapid degradation and clearance of therapeutic peptides is common, necessitating administration via intravenous, intramuscular or subcutaneous routes due to poor oral bioavailability (Uhlig et al., 2014). Despite proven efficacy *in vivo*, substantial proteolysis post-administration can limit the progression of peptide-linked therapeutics as serious drug candidates. For many peptide-based drug delivery systems, prolonging blood plasma residence time is often a pre-requisite of clinical development (Werle & Bernkop-Schnurch, 2006). Degraded peptide often results in loss of receptor binding ability, meaning the need for higher drug concentrations and more frequent dosing. Consequently, patient safety is jeopardised due to higher risk of side effects and associated costs accelerate.

The human body comprises at least 569 proteolytic enzymes (López-Otín & Matrisian, 2007), a multitude of which exist in the blood plasma. Other enzymes, such as the cytochrome P450 family, also contribute to *in vivo* drug metabolism. Exopeptidases and endopeptidases favour degradation of large and flexible amino acid sequences (Rader et al., 2018). BBB cerebrovascular endothelial cells are also enriched with numerous peptidases such as dipeptidyl aminopeptidase, endopeptidase and angiotensin-converting enzyme to name but a few, which carry out metabolism of blood-borne proteins (Witt et al., 2001). Basic amino acid residues such

as lysine and arginine are especially prone to enzymatic cleavage, particularly by serine proteases, which are chiefly involved in blood coagulation (Boettger et al., 2017). RDP (KSVRTWNEIIPSKGCLRVGGRCHPHVNGGGRRRRRRRRR) is enriched with potential cleavage sites and considering its relatively large 39-amino acid sequence, may be susceptible to high enzymatic degradation and stability issues in future studies.

Enzymatic degradation is one pitfall in the development of peptide targeting ligands. Other factors which affect bioavailability are the ability to cross biological barriers, receptor affinity and susceptibility to efflux mechanisms, particularly at the BBB. Serum degradation is perhaps the simplest factor to assess through *in vitro* studies. Indeed, for RDP, the need to improve receptor affinity or membrane permeability is not necessary at this stage in its development, due to the *in vivo* efficacy already reported. Fu et al. (2012) found that RDP can cross the BBB in mice within fifteen minutes of intravenous injection, however the approximate *in vivo* half-life of RDP-fusion protein is only one hour. Additionally, Fu and colleagues reported an RDP-DNA complex was stable in mouse serum for up to 8 hours *in vitro* (Fu et al., 2013b). The stability of RDP ligand alone in human serum however, has not yet been reported in detail.

In vitro testing of peptide stability in blood can be analysed using plasma or serum. Blood plasma, composed of serum and clotting factors, is prevented from coagulating *in vitro* by addition of an anticoagulant, such as heparin or EDTA (Thavasu et al., 1992). These anticoagulants inactivate enzymes, mainly serine proteases, which are involved in the coagulation cascade (Tanaka et al., 2009). However, this inhibition also reduces non-specific proteolysis of peptides. Proteolytic activity is greater in serum than plasma, as enzyme inhibition is not required due to absence of clotting factors (Falciani et al., 2007). As a result, analysis of peptide stability in serum is more likely to resemble *in vivo* conditions, due to a higher level of active proteases.

The somatostatin analogue, octreotide, is a well-known drug used for symptomatic relief in patients with gastroentero-pancreatic tumours. It was optimised from the original somatostatin sequence for clinical use by enhancing stability in blood plasma, through reduction of sequence

size and substitutions with D-amino acids (Harris, 1994). Changing the biodegradation of a therapeutic peptide may be achieved by methods such as N-methylation, polymer conjugation, pegylation and conformational/structural modifications for example, head-to-tail cyclisation and D-amino acid substitutions (Fominaya et al., 2015; Fosgeran & Hoffmann, 2015; Räder et al., 2015). Potential disadvantages exist for each method, commonly concerning non-specific peptide activity, plasma protein binding, lower receptor affinity and high production costs (Witt et al., 2001). It is therefore necessary to select a feasible approach for improving stability, whilst balancing therapeutic efficacy.

The aims of the work herein were to:

(1) Analyse the stability of RDP in human serum.

(2) Design a new peptide sequence based upon RDP interactions with the nAChR. Following the assessment of RDP stability in human serum, attempts to improve proteolytic resistance will stem from the identification of important RDP residues involved in interactions at the receptor site.

(3) Evaluate the *in vitro* targeting activity of the newly-derived RDP sequence in neural and non-neural cell types. Stability studies and cell-based assays previously carried out for RDP in Chapter 3 will be repeated for a new targeting ligand to assess resistance to degradation and neural-specific targeting capability.

4.2. Materials and Methods

4.2.1. Materials

Trichloroacetic acid (TCA), human serum from male AB plasma (USA origin) and α-cyano-4-hydroxycinnamic acid (CHCA) matrix were all purchased from Sigma-Aldrich (UK). RDP, DAS and scrambled DAS (sc-DAS) peptides were synthesised by GL Biochem (Shanghai) Ltd. All other materials used and cell culture conditions are as listed in section 3.2.1.

4.2.2. Molecular modelling studies

Potential interactions between RDP and the α7 homomeric nAChR were explored, using α-subunit residues 173-204 as a starting point in this study. Original rabies virus glycoprotein is reported to bind to these residues of the α1 nAChR subunit found at the neuromuscular junction (NMJ), hence facilitating the entry of the rabies virus into the nervous system (Lentz, 1990; Gastka et al., 1996). The residues of RDP which are responsible for interaction with the α7 homomeric nAChR were identified by Dr Dan Rathbone (Aston University, Birmingham, UK) through *in silico* molecular modelling studies.

Briefly, protein-ligand docking was carried out after obtaining the coordinates of the neuronal nAChR α7 subunit and acetylcholine-binding protein from the Protein Databank entry 3SQ6, chain A (Li et al., 2011). This was imported into CACHe Worksystem Pro (version 7.5.0.85; Fujitsu Ltd). The 30-mer of RDP, KSVRTWNEIIPSKGCLRVGGRCHPHVNGGG, was divided into all possible contiguous ten amino acid fragments (residues 1-10; 2-11; 3-12 etc.) and each docked four times, using CACHe Worksystem Pro, into the prepared protein structure from 3SQ6 where the potential active site was defined as residues 173–204. Molecular dynamics simulations of the docked protein-ligand complexes were prepared using version 14 of the AMBER Tools package (Case et al., 2005; Goetz et al., 2012; Le Grand et al., 2013; Salomon-

Ferrer et al., 2013). 5 residues of interest from RDP (GCLRV) were identified from this work and subsequently were incorporated into the design of a new peptide.

4.2.3. Design of novel targeting peptide

A widely used flexible linking sequence -GGGGS- was subsequently added to the -GCLRV- sequence as a spacer in the design of a new peptide (Chen et al., 2013), to allow freedom of movement once conjugated to PLGA NP. A similar linking sequence was used by Fan et al. (2016) to limit steric hinderance of a newly developed tumour-targeting peptide, GE11, upon conjugation to phospholipid micelles. Two glycine residues followed by an arginine tail consisting of 6 alternating L- and D- arginine residues –GGRrRrRr- were also added to the sequence for enhanced stability and resistance to metabolic processes (Wender et al., 2008). The new D-arginine-containing 18-amino acid sequence, termed DAS, was NH_2-GGGGSGCLRVGGRrRrRr-COOH.

4.2.4. Serum stability of RDP and DAS peptides

Peptide stability testing in human serum was carried out according to a previously detailed method (Nguyen et al., 2010). Briefly, human serum was diluted to 25% (v/v) with phosphate buffered saline (PBS) and subsequently centrifuged at 18809 *g* for 10 minutes to remove lipids, before incubating at 37°C. RDP and newly derived peptide, DAS, were prepared so that final serum peptide concentration was 10 µM prior to incubation at 37°C. A 200 µL aliquot was removed from each serum-peptide mixture at various time points and reacted with 40 µL of 15% (v/v) TCA for 15 minutes at 4°C to remove larger serum proteins. The collected samples were centrifuged at 18809 *g* to remove precipitated serum proteins for 10 minutes and supernatant collected for storage at -20°C. Samples were analysed by MALDI-TOF mass spectrometry (PerSeptive Biosystems Voyager-DE Biospectrometer, Herefordshire UK). A 10 µL aliquot of

serum sample was mixed with 10 µL of CHCA matrix (10 mg/mL fully dissolved), 1.5 µL of which was used for analysis. The mass/charge ratio (m/z) was plotted against relative abundance. Peptide stability was also assessed in double distilled water over 24 hours. At various time points, samples were taken and subsequently analysed by MALDI-TOF mass spectrometry.

4.2.5. Preparation of nanoparticles and conjugation of peptide to NP

Doxorubicin-loaded PLGA nanoparticles (Dox NP) and FITC-Dextran-loaded PLGA nanoparticles (FITC NP) were prepared by a double emulsion technique and characterised according to methods previously described (sections 3.2.3-3.2.5). DAS or a scrambled version of DAS peptide (scDAS) were conjugated to nanoparticles (NP) according to the method previously described for RDP. The amount of DAS or scDAS added per 5 mg of carboxyl-activated PLGA NP was 250 mcg.

4.2.6. In vitro cellular uptake study

Cellular uptake of FITC-NP preparations were evaluated in SH-SY5Y, PC-12 and HeLa cell lines using a Leica SP5 confocal microscope (x 63 000 magnification) as detailed in section 3.2.6.2. In summary, cells were cultured on 13 mm glass coverslips overnight in complete media, which was aspirated prior to treatment. Cells were treated with 1 mg/mL (500 µL) of either FITC NP or DAS-FITC NP in serum-free media (SFM) for 24 hours whilst incubating at 37°C/5% CO_2. Prior to imaging, all cells were treated with 75 nM Lysotracker® red in SFM for 30 minutes as before, to visualise lysosomes within cells. FITC fluorescence emission was collected between 510- 550 nm (excitation wavelength 490 nm). Lysotracker® emission was collected separately between 590-650 nm (excitation wavelength 580 nm).

4.2.7. In vitro cytotoxicity study in neural and non-neural cells types

An initial study was carried out to determine the effect of DAS-Dox NP over various concentrations. SH-SY5Y cells were plated out at a concentration of $1x10^5$ cells/mL in complete RPMI medium and incubated at 37°C/5% CO_2 for 16 hours. All existing media was aspirated before addition of DAS-Dox NP or Dox NP to cells at various concentrations ranging from 0.5-3.0 mg/mL in SFM. Control groups were treated with SFM only. Cell viability was assessed after incubating for 24 hours (37°C/5% CO_2), using an MTT assay. To calculate cell viability, 25 µL of MTT (5 mg/ml) in sterile PBS was added to each well on top of media and incubated at 37°C/5% CO_2 for 2 hours. After this, all media was aspirated and cells solubilised with 70 µL of DMSO per well. UV-Vis absorbance was read at 570 nm and cell viability calculated.

The cytotoxic effect of a scrambled version of DAS (NH_2-RVGGCSGGGGGLRrRrRr-COOH) conjugated to Dox NP (scDAS-Dox NP) was also assessed in SH-SY5Y cells, according to the method described above. Briefly, cells were treated with 160 µL of NP suspension (1.5 mg/mL) in SFM and incubated for 24 hours (37°C/5% CO_2). The cytotoxicity of free DAS was also evaluated by treating SH-SY5Y cells with a concentration of free peptide equivalent to maximum NP content, as determined by conjugation efficiency. To further assess targeting specificity to neural cells, NP treatment was also added to neural PC-12 cells and non-neural cell lines CHO, HeLa and MDA-MB-231 according to the same protocol.

It was demonstrated previously that RDP function could be blocked with nAChR inhibitors (Chapter 3, section 3.3.4). To determine whether nAChR antagonists would affect the activity of DAS, SH-SY5Y cells were preincubated for 30 minutes with 100 µL of either 2 mM hexamethonium (competitive) or 2 mM mecamylamine (non-competitive) in SFM, prior to addition of 100 µL Dox NP or DAS-Dox NP (3 mg/mL), using the method described above. SH-SY5Y and PC-12 cell types were also preincubated for 60 minutes with 100 µL of anti-AChRα7 antibody (1:50 dilution) before addition of NP treatment (final concentration 1.5 mg/mL) for 24 hours as before.

4.2.8. Statistical Analysis

All results reported were statistically analysed using an unpaired two-tailed t-test. A P-value of < 0.05 was considered statistically significant.

4.3. Results & Discussion

4.3.1. Interaction between RDP segment GCLRV and α7-nAChR identified through molecular modelling

RDP is a 39-residue peptide, with an overall positive charge due to arginine and lysine residues in the sequence. The large size of RDP potentially increases the likelihood of proteolysis and so a smaller derivative, retaining any part of the sequence essential for binding to the nAChR, would be an ideal starting point for remodelling. It was previously reported in section 3.3 (Chapter 3) that RDP requires the nAChR for function, a receptor first reported by Lentz et al. (1982) as being responsible for rabies virus infection.

A model of the receptor was built using the X-ray crystal structure coordinates from the Protein Databank, entry 3SQ6, chain A (Li et al, 2011). For the purposes of the docking experiments the active site was defined as residues 173 – 204. The 30-mer KSVRTWNEIIPSKGCLRVGGRCHPHVNGGG was divided into all possible contiguous ten amino acid fragments (residues 1-10; 2-11; 3-12 etc.) and docked into the receptor. A 10-mer fragment comprising residues 9-18 (IIPSKGCLRV) was identified to contain potentially active residues through formation of a relatively stable conformation on the receptor. Consequently, this 10-mer fragment -IIPSKGCLRV- was cut down to a version containing residues 14-18 (GCLRV), where hydrogen bonding and hydrophobic interactions were observed with the receptor surface via the leucine and valine residues in the fragment. A representation of the

receptor-GCLRV molecular dynamic simulation is shown in Figure 4.1. A new peptide (DAS), incorporating the GCLRV fragment from RDP was designed accordingly, consisting of 18 amino acids (GGGGSGCLRVGGRrRrRr) as described in section 4.2.3.

A common feature of many successful CPPs is the presence of guanidium-rich groups, such as arginine. CPPs however, are non-specific and prone to degradation by peptidases (Kristensen et al., 2016). The original RDP sequence ending with octa-arginine (R8) is an important component to aid rapid cell penetration and promote high water solubility. The most frequently used polyarginines in targeting peptides are octa-arginine (R8) and nona-arginine (R9), however it has been shown that as little as six arginine residues confer highly effective cell penetrating properties to a conjugated cargo whilst prolonging circulation time (Liu et al., 2017b; Wender et al., 2008). Purkayastha et al. (2013) found that having 6 consecutive L-Arginine (Arg) residues in a peptide sequence leads to better cell penetrating properties. The number of arginine residues in the new RDP-derived sequence were subsequently reduced to six, which would reduce the overall positive charge of the peptide. In doing this, the whole peptide would be less vulnerable to negatively charged plasma proteins, an effect which Liu et al. (2017) reported as similar to pegylation.

It has been reported that D-amino acids improve serum stability and cellular uptake characteristics of a peptide (Molhoek et al., 2011). The mix and positioning of L- and D- amino acids in the sequence can affect the cell uptake rate as well as modulating the peptide half-life (Purkayastha et al., 2013). For example, if a sequence was composed of all D-amino acids, not only would this be more expensive, but it would be too stable (> 7 days) and perhaps accumulate extensively over time *in vivo*. Due to this, alternating L- and D- Arg residues were incorporated into the design of DAS.

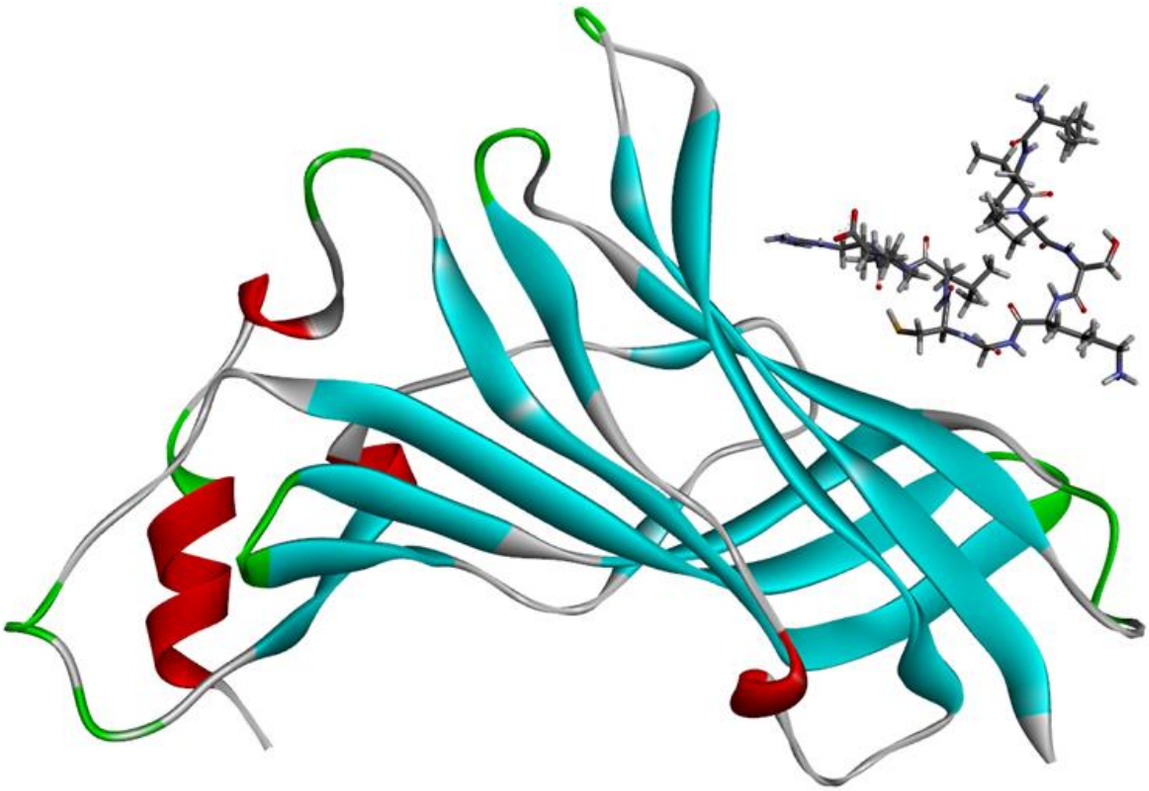

Figure 4.1. Molecular dynamics simulation of fragment IIPSKGCLRV (stick form) with the nicotinic acetylcholine receptor (ribbon form). Residues IIPS are not in contact with the receptor surface and thus were not included in the design of the new RDP derivative.

4.3.2. Characterisation of NP preparations

PLGA NP were successfully loaded with either cytotoxic doxorubicin or FITC-dex and characterised as previously detailed in section 3.3.1 of Chapter 3. NP characteristics such size, zeta potential and PDI are summarised in Table 4.1. DAS ligand was successfully attached to Dox NP and FITC NP by EDC/NHS chemistry, in an identical method as described for RDP. Conjugation efficiency of DAS to FITC NP was particularly high at 88.0%, in comparison to Dox NP (58.0%), meaning the FITC NP had almost twice as much surface-conjugated DAS (µg/mg). This is consistent with findings for RDP conjugation to FITC NP (section 3.3.1), where NP surface characteristics might affect the EDC/NHS-enabled attachment of peptide to PLGA carboxyl

groups. Such a peptide-decorated nanoparticulate drug vehicle is developed with a view of encapsulating payloads such as growth factors, for treatment of neurodegenerative processes. These larger, protein-based payloads are more likely to resemble model drugs such as myoglobin and FITC-dex, rather than small molecules such as doxorubicin. Given the favourable conjugation of peptide to NP encapsulating the model payloads previously described, it is probable that a similar amount of peptide would be successfully added to growth factor-loaded NP, whether it is RDP or DAS. For the purpose of this work, the difference in amount of surface-conjugated peptide between different NP preparations is not a concern, so long as there is evidence of substantial conjugation. Future studies however, may provide insight into how this may affect NP targeting.

Table 4.1. Characterisation parameters of drug-loaded PLGA nanoparticles conjugated to newly-derived DAS ligand.

NP Sample	Size (nm)	ZP[a] (mV)	PDI[b]	DC[c] (µg/mg)	DAS[d] (µg/mg)
Dox NP	242.73 ± 18.64	-14.60 ± 1.32	0.39 ± 0.05	12.80	23.20
FITC NP	286.50 ± 11.30	-10.30 ± 1.00	0.27 ± 0.08	30.80	43.90

[a]Zeta potential (mV), [b] polydispersity index, [c] DC= drug content per 1 mg of NP based on entrapment efficiencies of 64% (Dox) and 77% (FITC-dex); [d] DAS content per 1 mg of NP based on conjugation efficiencies of 58.0% (Dox NP) and 88.0% (FITC NP). Size, ZP and PDI as measured by DLS are expressed as average ± standard deviation (n=6).

4.3.3. Stability of RDP & newly-derived peptide, DAS, in distilled water and human serum at 37°C

RDP was incubated both in water (Figure 4.2) and 25% human serum (Figure 4.3) at 37°C and then analysed by MALDI-TOF mass spectrometry to determine stability. RDP was firstly analysed in water to determine how prone RDP might be to hydrolysis, without the presence of enzymes. It can be seen from Figure 4.2, that RDP does not break down and is stable over 24 hours at 37°C, as mass-spectrometry traces are identical from time zero (Figure 4.2B) up to 24 hours (Figure 4.2F). Figure 4.2A shows the background signal detected due to the CHCA matrix in which the sample was prepared.

The same time points were used, with the addition of a sample at 2 hours when RDP was incubated in serum. RDP in serum (T=0) (Figure 4.3C) gave rise to a peak (4.6 kDa) consistent with its molecular weight. The background trace due to serum is shown in Figure 4.3B. Upon incubation in serum for 1 hour, the signal for intact RDP at 4.6 kDa was no longer detectable (Figure 4.2D). New peaks detected between 2.7-3.2 kDa in Figure 4.2D, most likely represent RDP breakdown fragments. These signals gradually lessened following 4 and 8 hours of incubation in Figures 4.3 (F)-(G). A minimal trace of RDP-related fragments remained in Figure 4.2H, suggesting RDP and its degradation products had continued to degrade over 24 hours.

The recent success of RDP as a neural cell-specific targeting ligand both *in vitro* and *in vivo* has been a promising step towards facilitating delivery of therapeutics to neural cells. It has not been explored as of yet whether this sequence may be optimised further, taking human serum stability into account. Previously, Fu et al. (2013b) reported on the 8-hour stability of an RDP-plasmid complex in mouse serum, however this study has shown that RDP breaks down when incubated with human serum (37°C) within an hour (Figure 4.3). The aforementioned work by Fu and colleagues described how the secondary conformational structure of RDP changed upon plasmid DNA binding, possibly making it more stable than it otherwise would be alone. This means potential use of RDP with other types of therapeutic conjugates may not be so successful, hence

it would be preferable to optimise the peptide sequence to make it less prone to enzymatic degradation in serum.

Palm et al. (2007) indicated that membrane bound proteases are also responsible for extracellular degradation of targeting peptides. This is dependent on cell type and density, however it augments the need to minimise the risk of peptide degradation prior to cellular uptake, as intact targeting peptide on the NP is essential for delivery of therapeutic cargo. If serum half-life is longer, then potential dosing would be lower and less frequent, which is preferable when conjugating to expensive or toxic therapeutics. It is desirable however, that targeting peptides are eventually degraded intracellularly for cargo release and reduction of toxicity risk. Consequently, the newly-designed peptide (DAS) was investigated to establish the effect of D-amino acid substitutions and sequence shortening on serum stability.

(A) CHCA matrix (500-8000 Da)

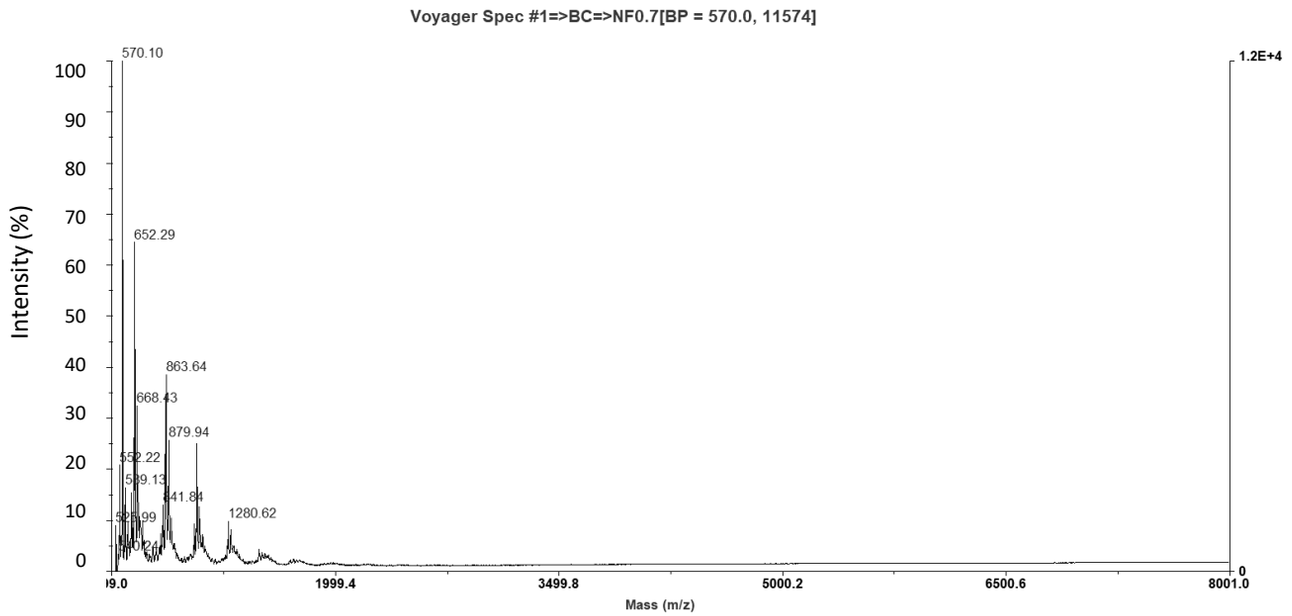

(B) RDP- T=0

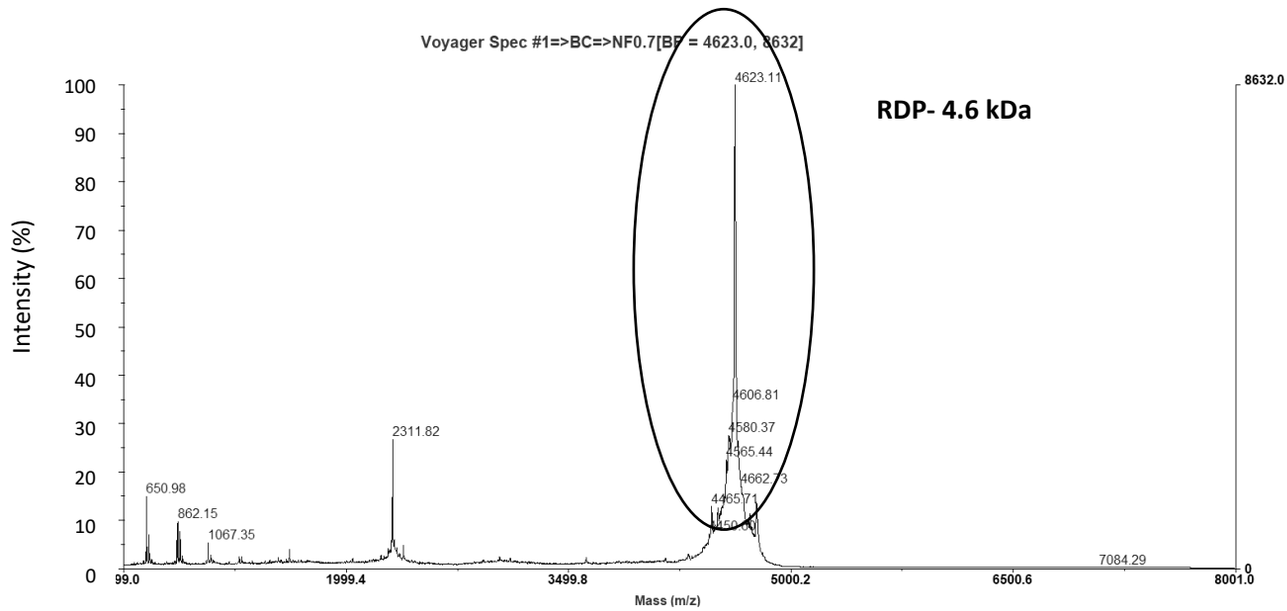

(C) RDP- T=1h

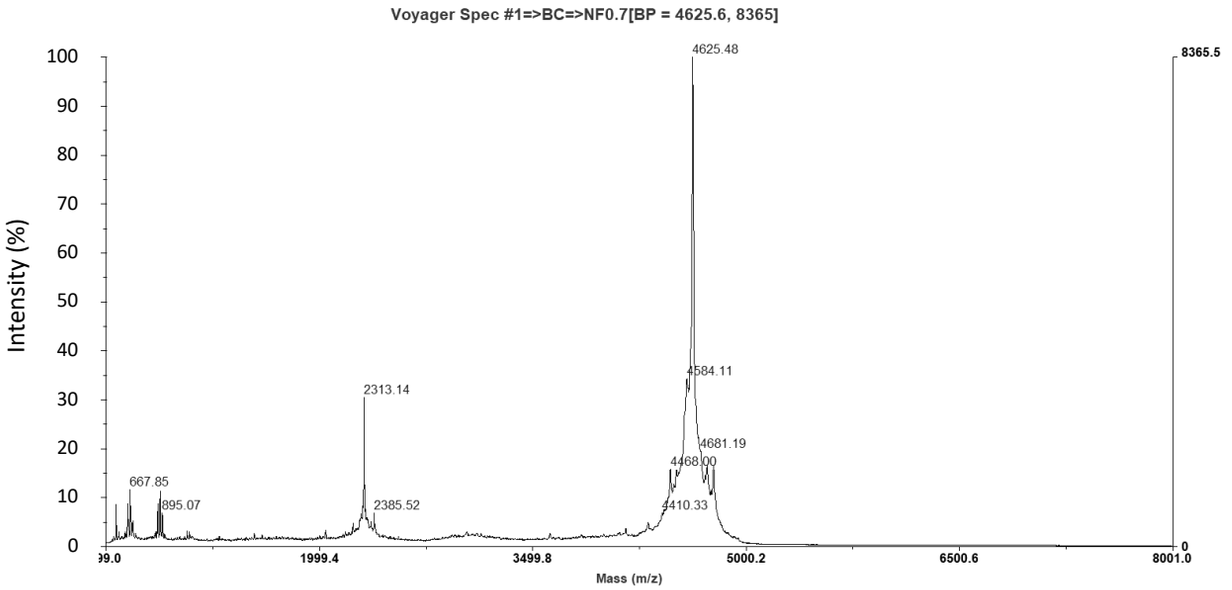

(D) RDP- T=4h

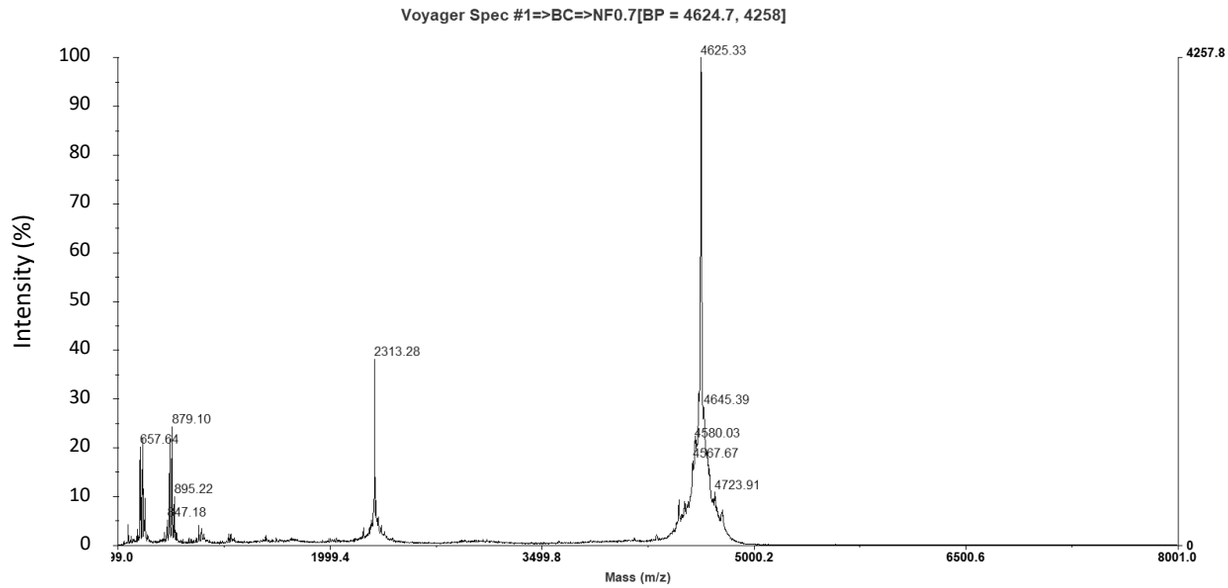

(E) RDP- T=8h

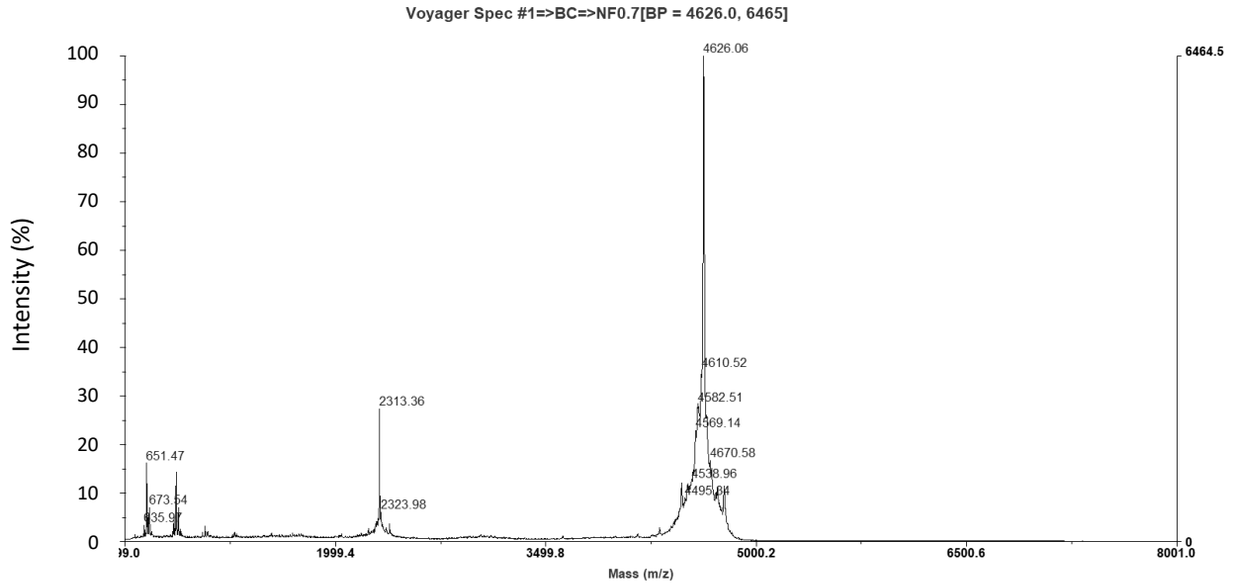

(F) RDP- T=24h

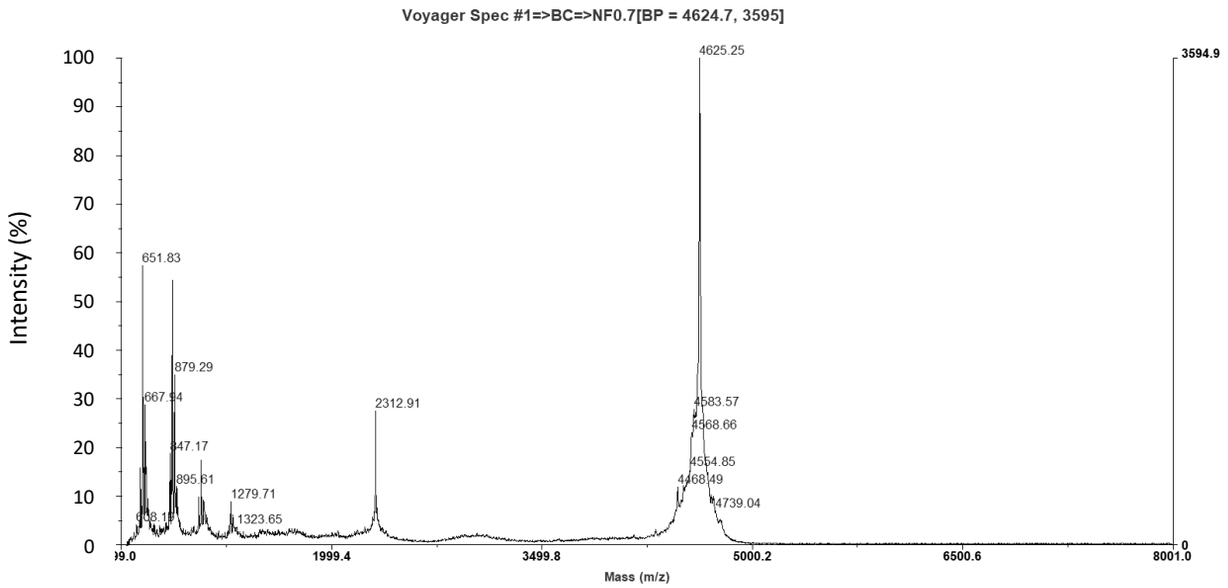

Figure 4.2. MALDI-TOF mass spectrometry analysis of (A) CHCA matrix and (B)-(F) RDP following incubation at 37°C in double distilled water for varying lengths of time. Peak for intact RDP is indicated in (B).

(A) CHCA matrix (500-8000 Da)

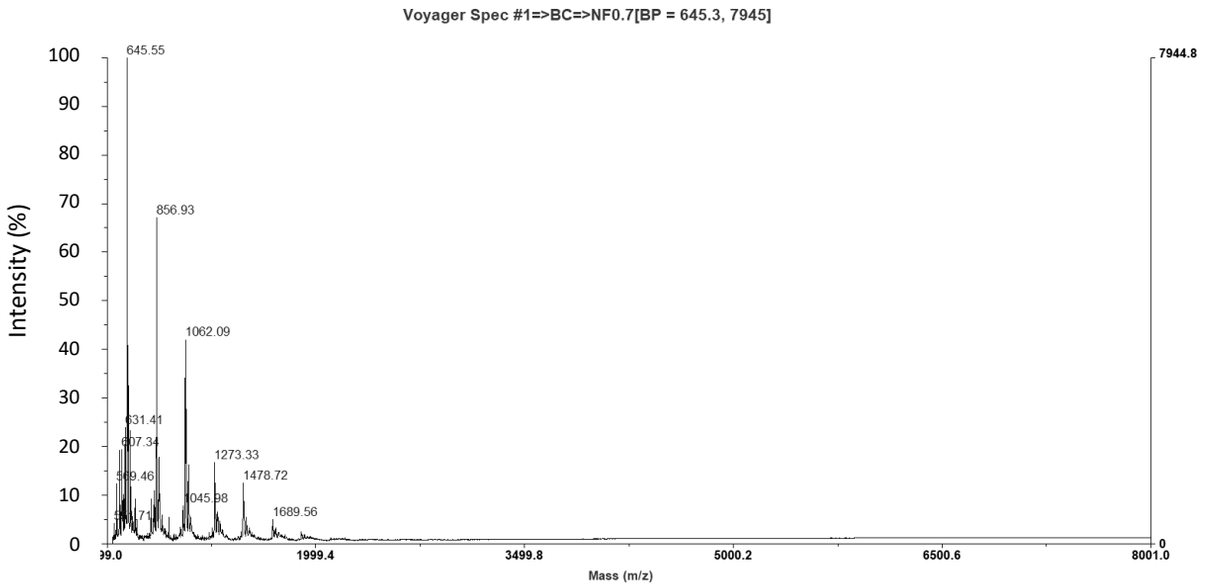

(B) Serum

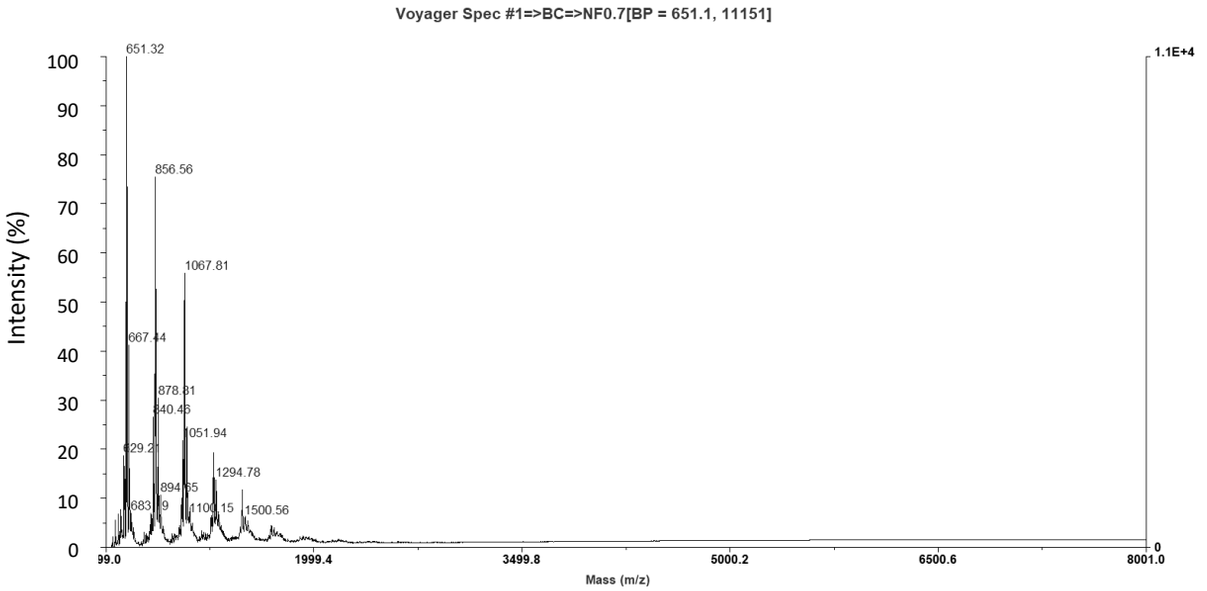

(C) RDP- T=0

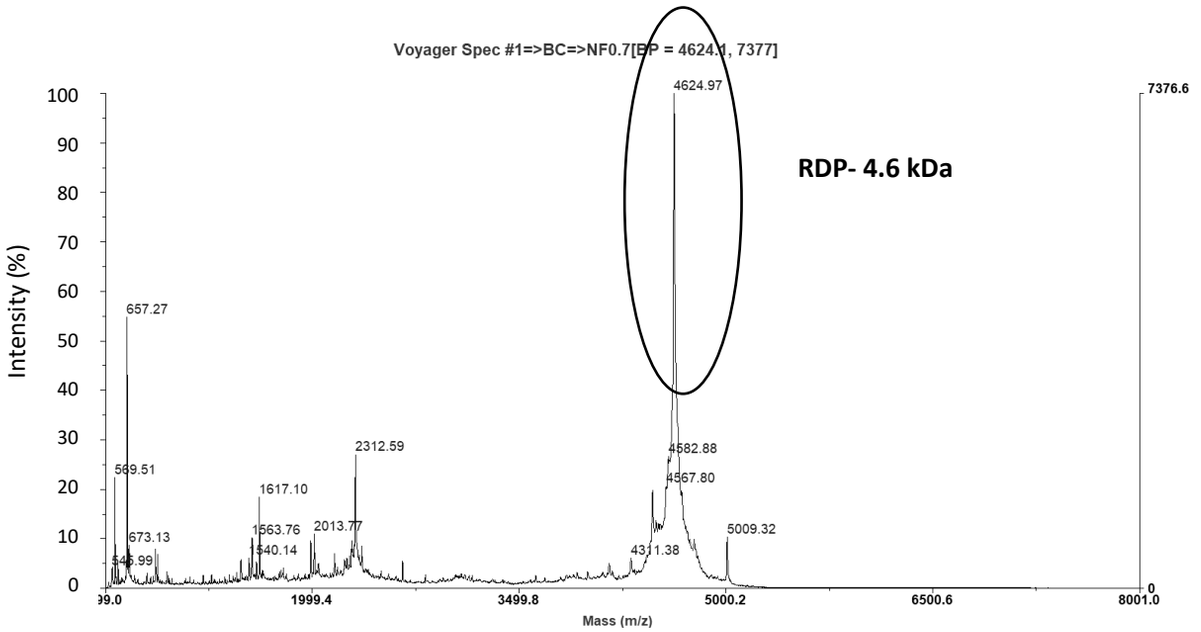

(D) RDP- T=1h

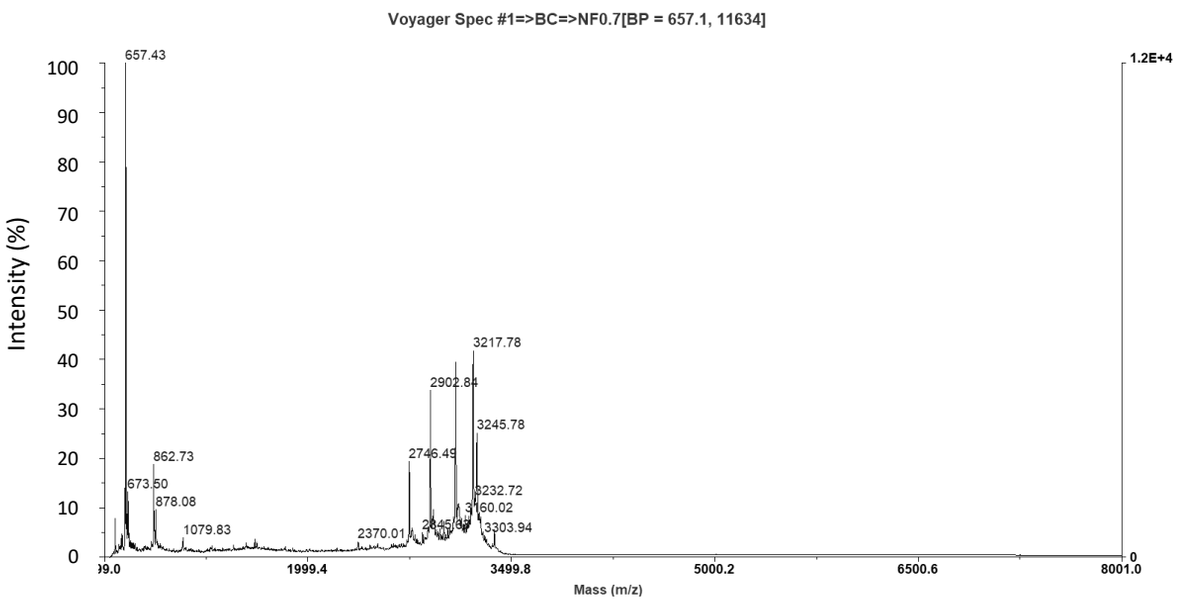

(E) RDP- T=2h

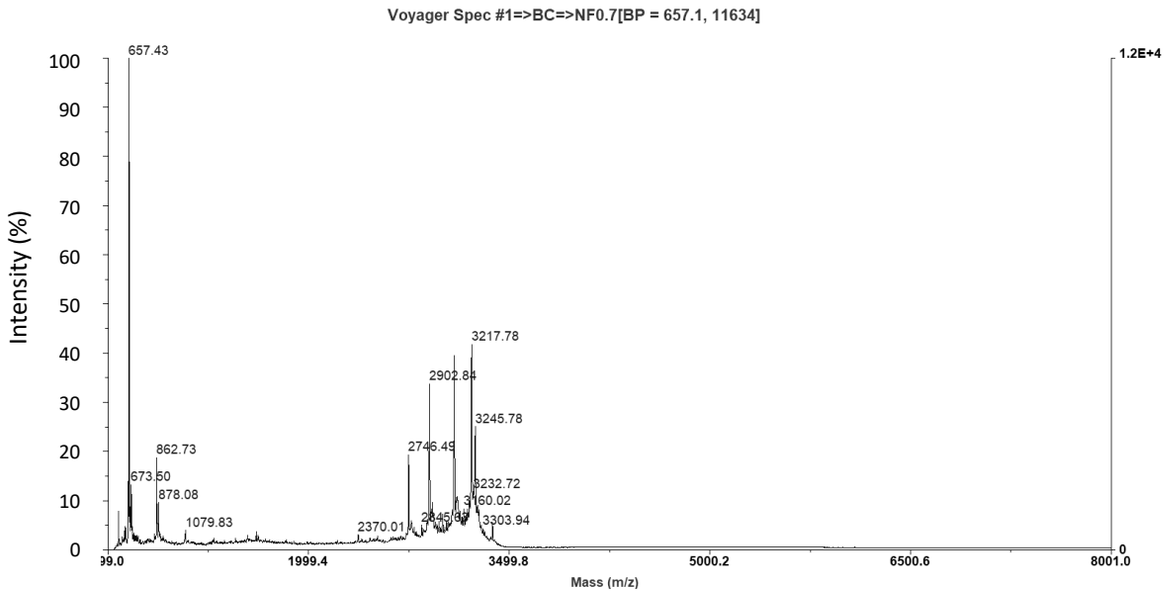

(F) RDP- T=4h

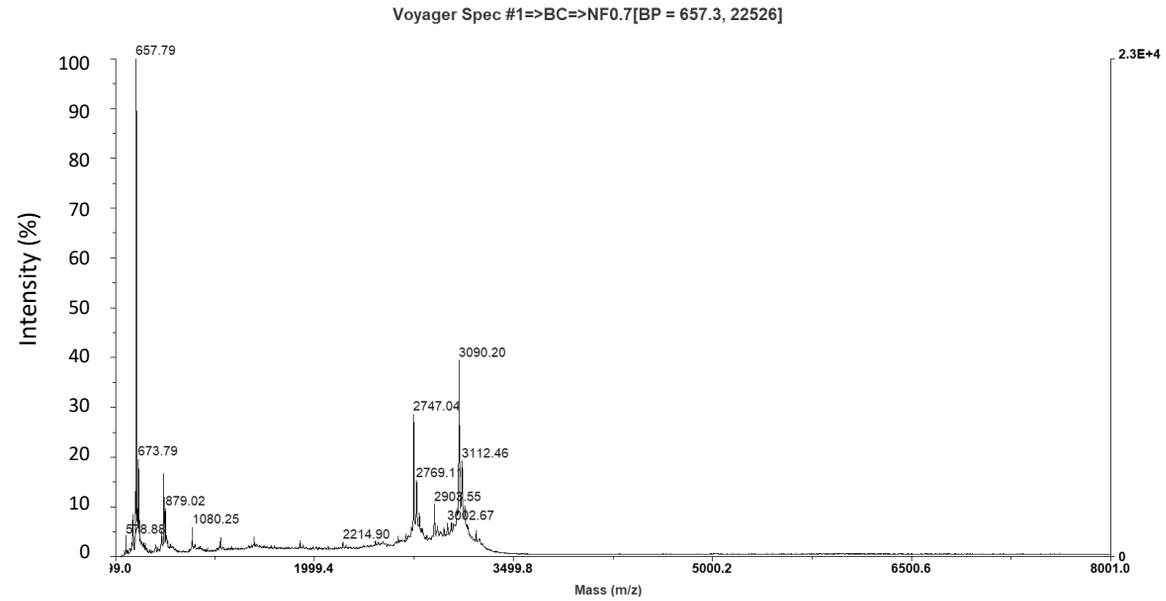

(G) RDP- T=8h

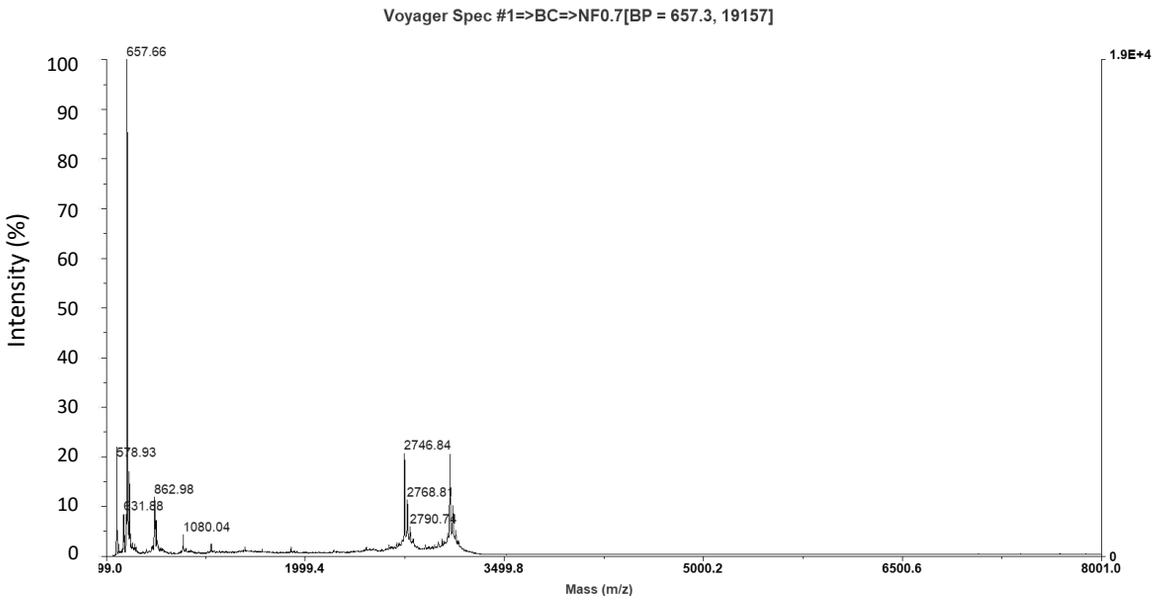

(H) RDP- T=24h

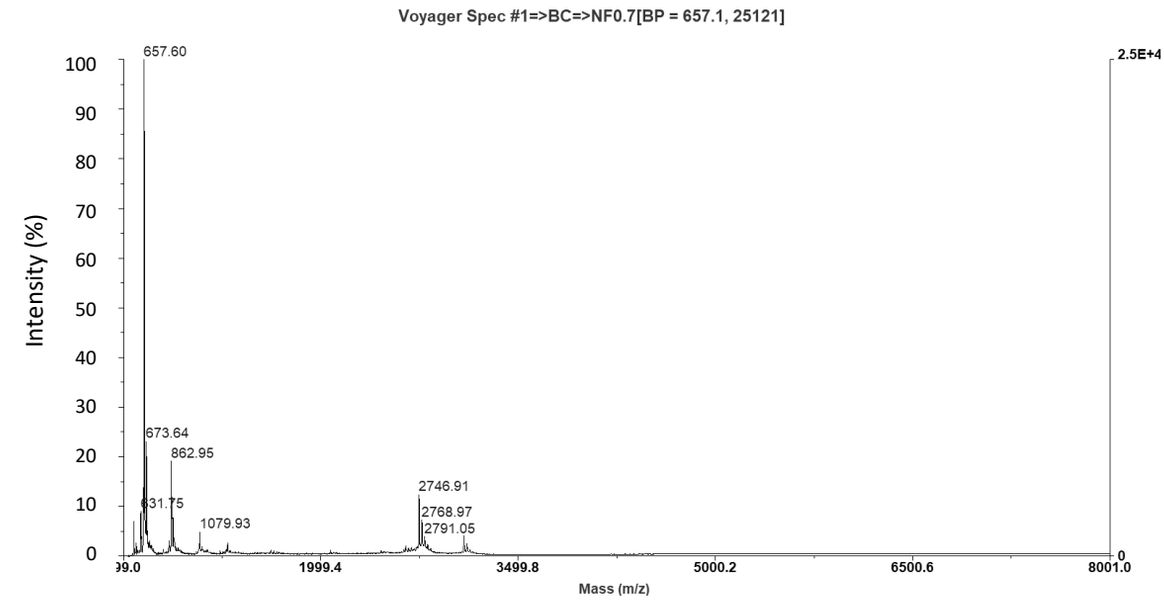

Figure 4.3. MALDI-TOF mass spectrometry analysis of RDP stability in 25% human serum at 37°C for various periods of time. (A) CHCA matrix and (B) Human serum with no peptide. (C)-(H) Mass spectrometry profile detected for RDP (MW approx. 4.6 kDa) in serum up to 24 hours of incubation. Peaks for intact peptide are indicated on the intensity/mass traces.

In water, a strong peak was detected for DAS at the expected molecular weight of 1.9 kDa at all time points observed. This meant that like RDP, DAS was completely stable for 24 hours under these conditions as no evidence of breakdown could be detected (Figure 4.4). The serum stability of DAS was subsequently assessed at the same time points as for RDP previously. Fully intact DAS in serum (time zero) expectedly gave rise to a peak at around 1.9 kDa indicated in Figure 4.5B, prior to incubation at 37°C. After 1 and 2 hours of incubation, peaks approximately 50% the size of the original (Figure 4.5B) are detected in Figures 4.5 (C) and (D). After 4 hours in serum, a peak approximately one third the size of the original at time zero was detected, signalling a small amount of intact DAS remained at this time (Figure 4.5E). The DAS signal was again detected at 8 hours, despite now being approximately 10-20% of that detected in Figure 4.5B. Finally, DAS was no longer detected at 24 hours, indicating total degradation of the 18-mer sequence (Figure 4.5G).

Over the time course observed, the new peptide, DAS, was more resistant to degradation by serum proteases than RDP. Mass spectrometry analysis detected intact DAS peptide up to 8 hours after incubation in human serum at 37°C, suggesting improvement in stability characteristics compared to RDP, which degraded within 1 hour. D-amino acids like the D-arginine residues incorporated into DAS, have been used to improve the proteolytic resistance of peptides successfully within the area of drug delivery due to their ability to avoid quick metabolism (Wender et al., 2008; Purkayastha et al., 2013; Meng et al., 2017).

There have been many successful findings on the use of D- amino acid substitutions to promote serum stability of targeting peptides, with no significant toxicity concerns *in vitro* and *in vivo.* Di Grazia et al. (2015) reported improved human serum stability and activity when frog skin-derived antimicrobial peptide, esculentin-1a(1-21)-NH_2, was substituted with two D-amino acids at potential cleavage sites. Wang et al. (2013) also successfully developed a targeting ligand, YSA, to target prostate cancer *in vivo* by taking advantage of EphA2 receptor (tyrosine kinase family) overexpression. Wang and colleagues wanted to improve the efficacy and other pharmacological properties of YSA when conjugated to a therapeutic payload. Two non-natural

amino acids were substituted in place of methionine and N-terminus tyrosine to produce newly optimised peptide, dYNH. This new derivative was more stable in mouse serum after 24 hours whilst retaining selectivity for targeting EphA2 receptor-positive cells by receptor mediated uptake of payload into lysosomal pathways.

The development of a peptide such as DAS, offers a more stable neural cell-targeting ligand than RDP, a property most essential for efficient drug delivery *in vivo*. A 10-amino acid peptide for targeting of breast cancer cells showed instability against serum proteases in work by Soudy et al. (2011), limiting bioavailability *in vivo*. Two L- to D- amino acid substitutions in the sequence of a new analogue improved resistance to protease-induced degradation in human serum, much like observations made for DAS from Figure 4.5. Furthermore, the improvement in peptide stability displayed higher uptake into breast cancer cell lines compared to the parent peptide. Ngambenjawong et al. (2016) identified a lead analogue of macrophage targeting peptide, M2pep, through cyclisation of the sequence. This new version of the peptide was more stable to serum degradation and displayed better *in vivo* accumulation at tumour sites. Cyclisation of RDP is another avenue which could be explored in prospective studies, in addition to D-amino acid substitutions.

(A) DAS- T=0

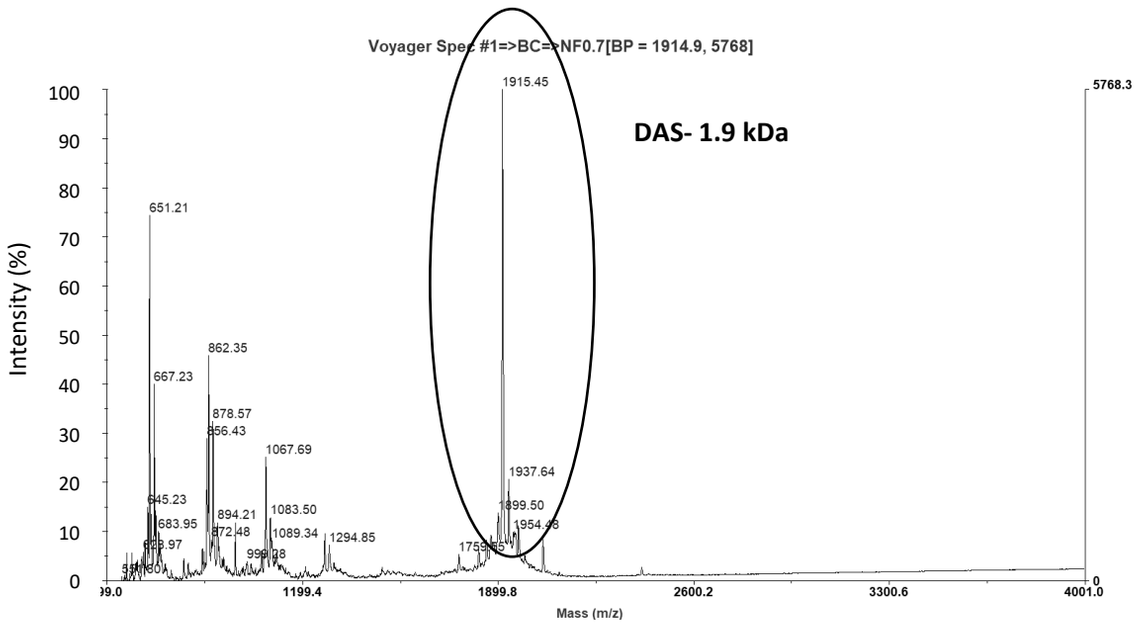

(B) DAS- T=1h

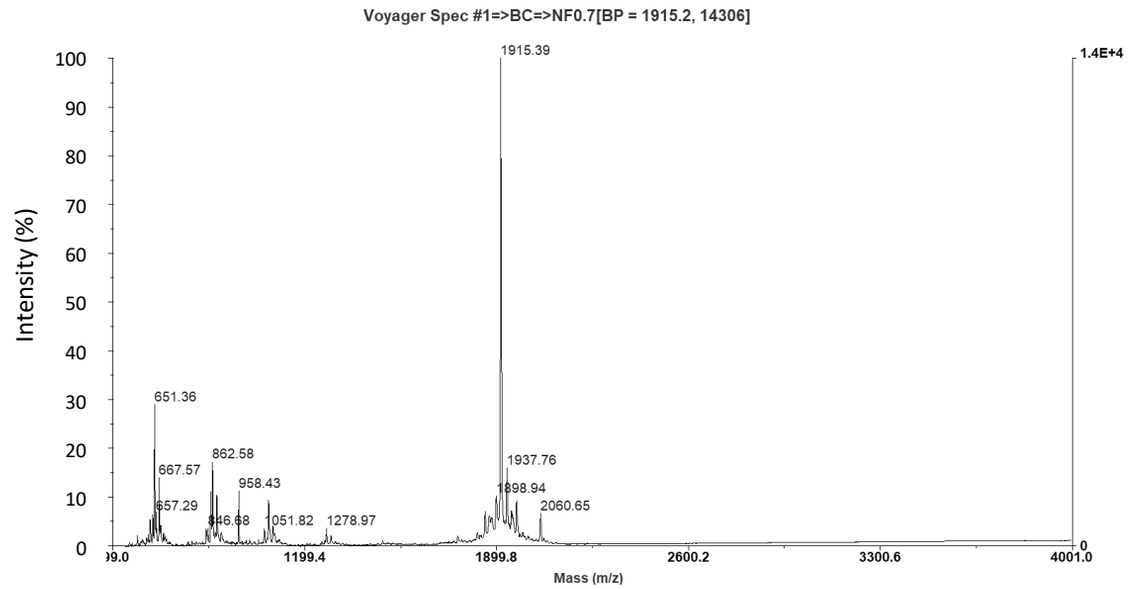

(C) DAS- T=4h

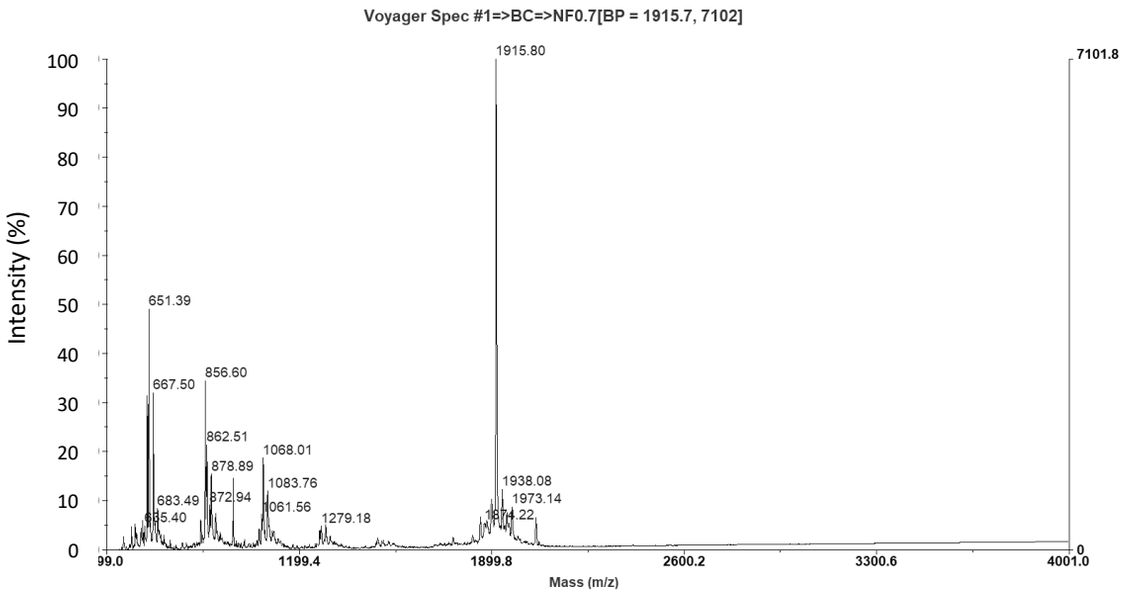

(D) DAS- T=8h

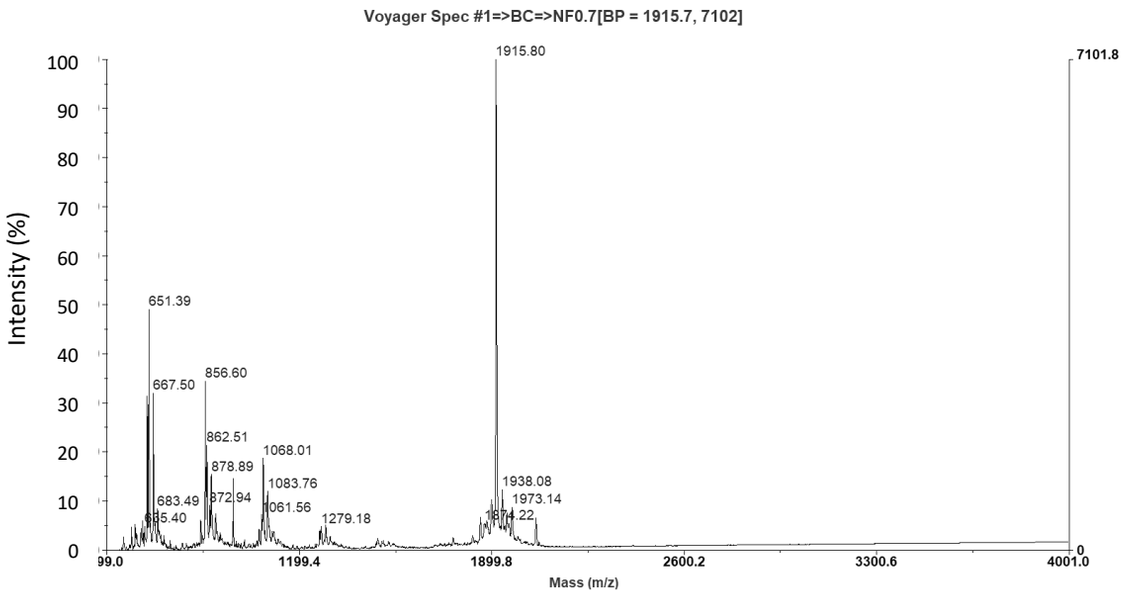

(E) DAS- T= 24h

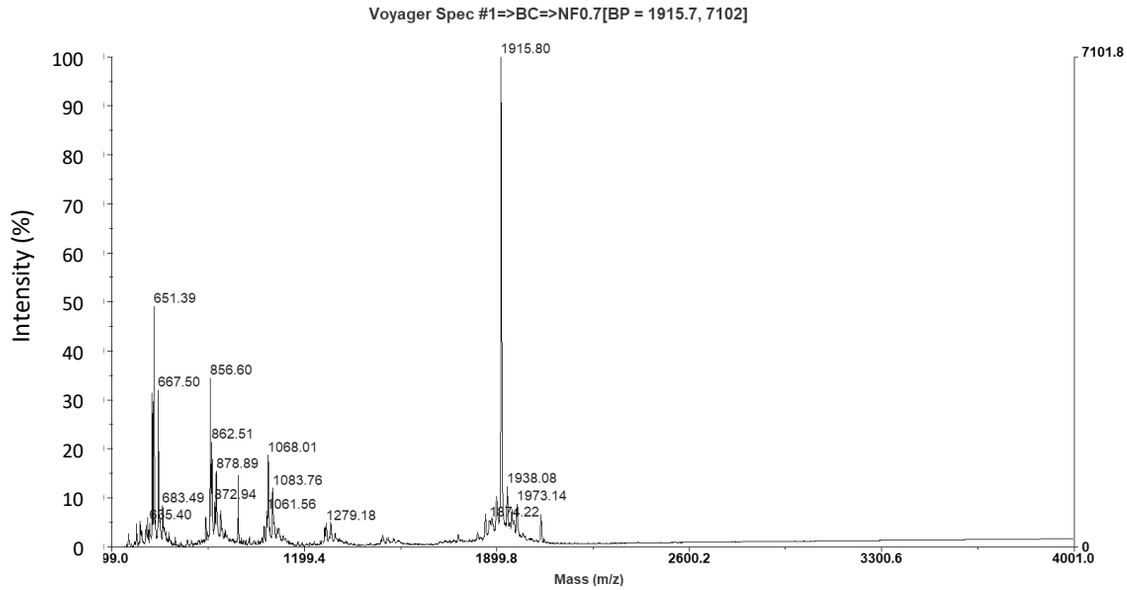

Figure 4.4. (A)-(E) MALDI-TOF mass spectrometry analysis of DAS following incubation at 37°C in double distilled water for varying lengths of time. The peak for intact peptide is indicated in (A).

(A) Serum

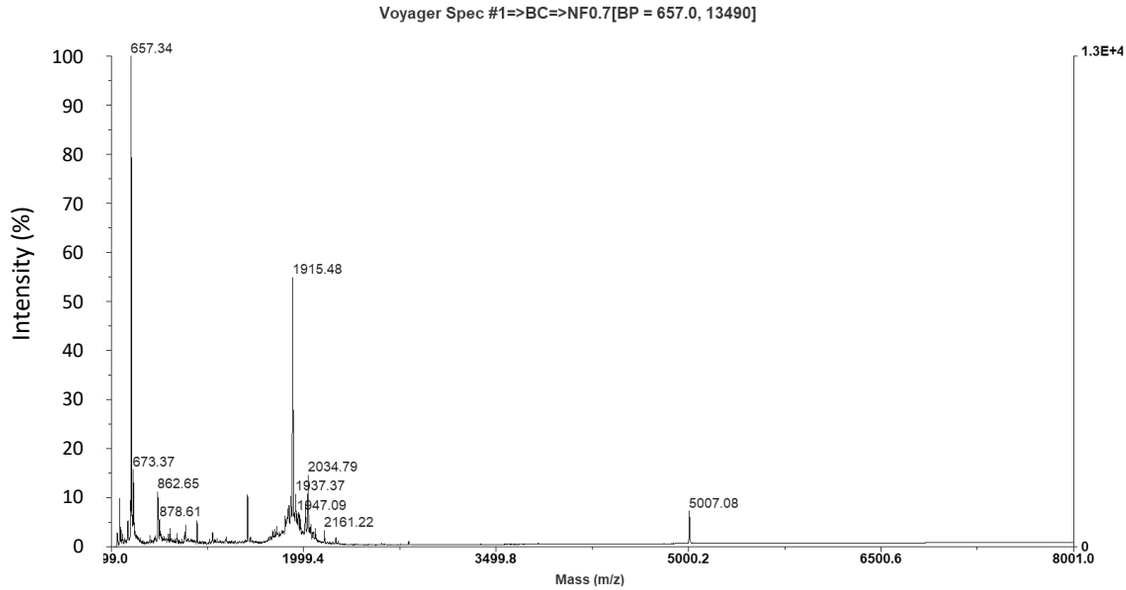

(B) DAS- T=0

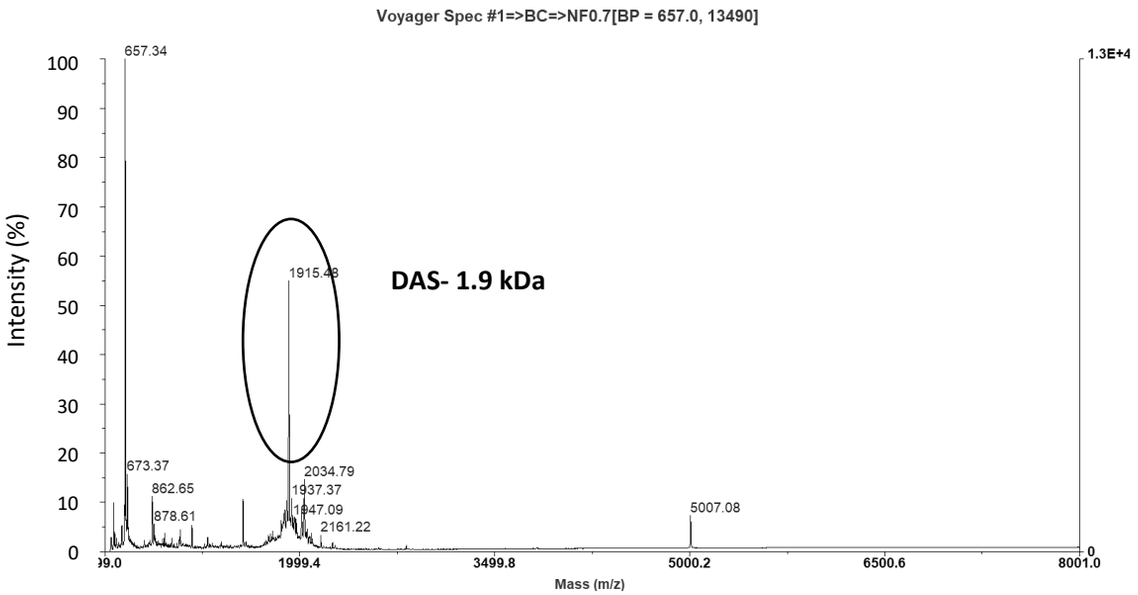

(C) DAS- T=1h

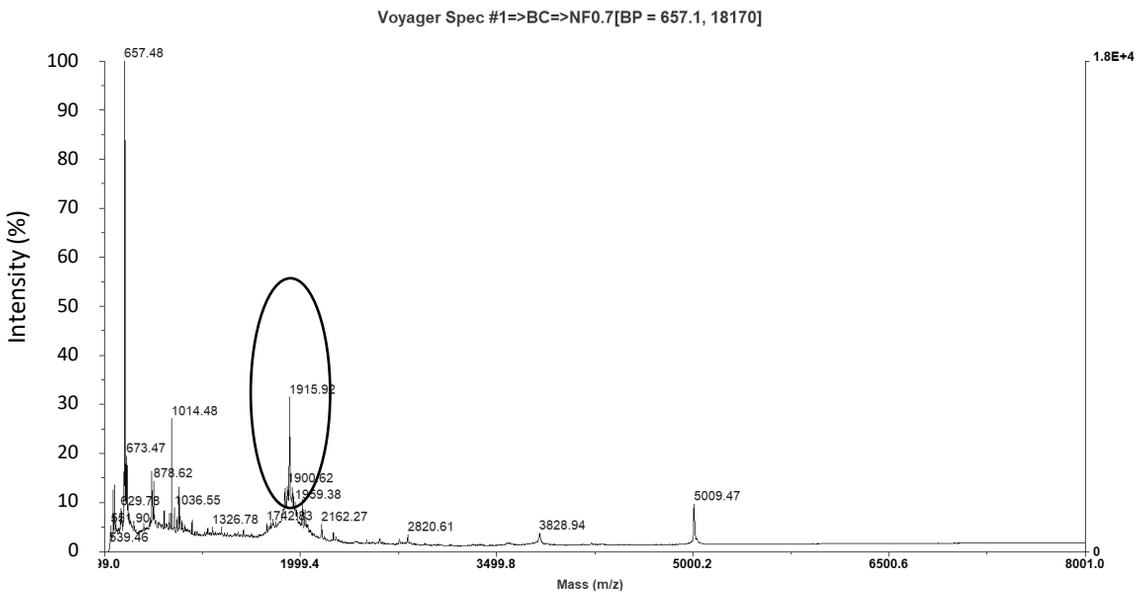

(D) DAS- T=2h

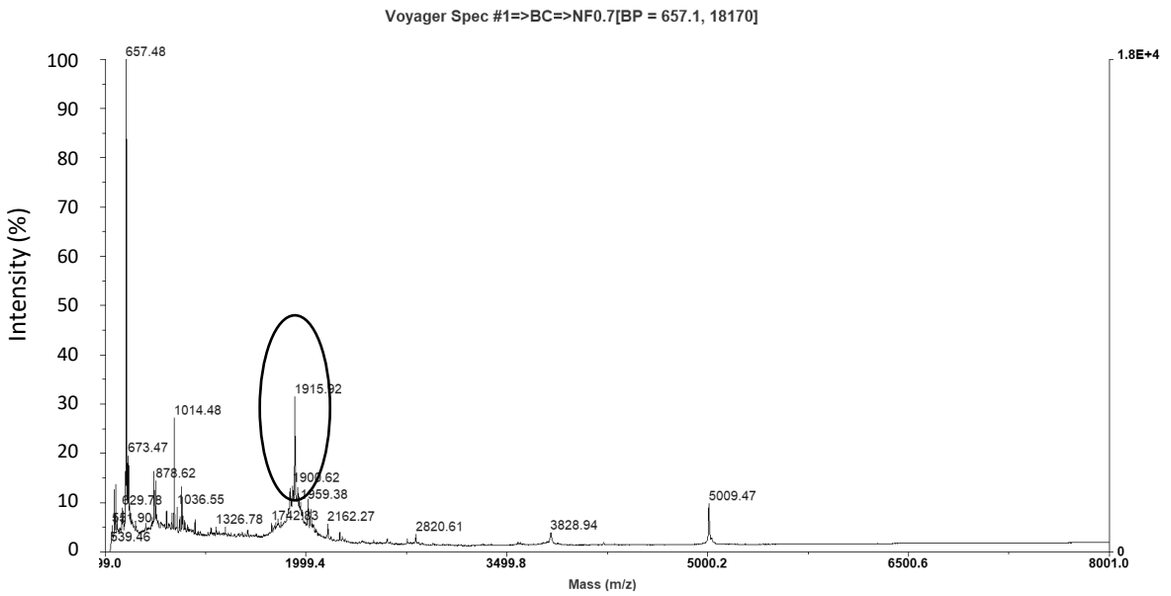

(E) DAS- T=4h

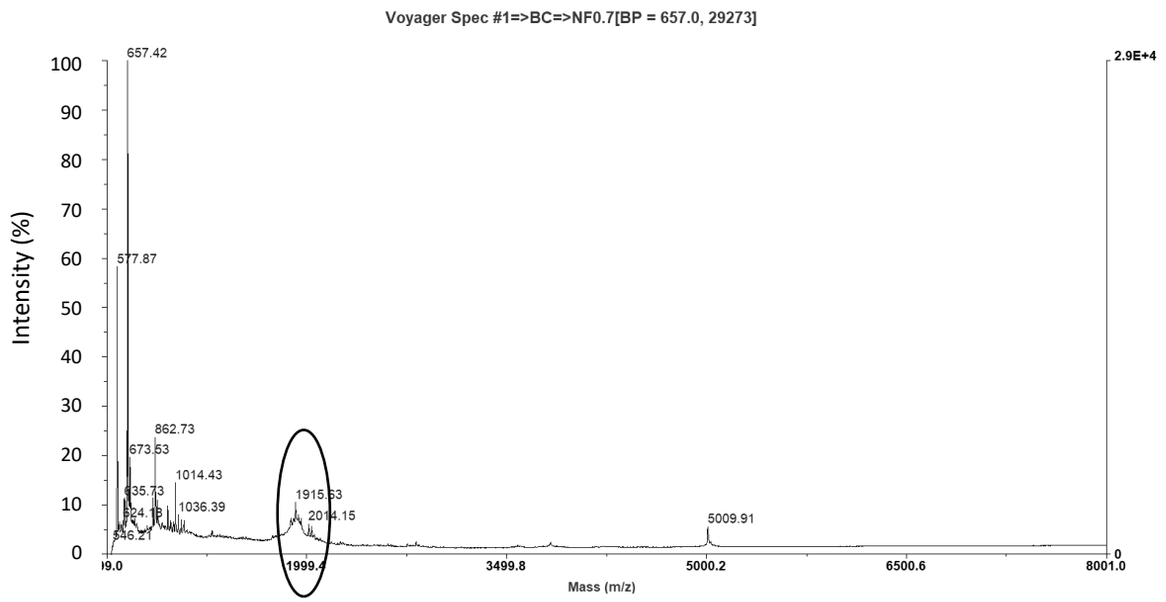

(F) DAS- T=8h

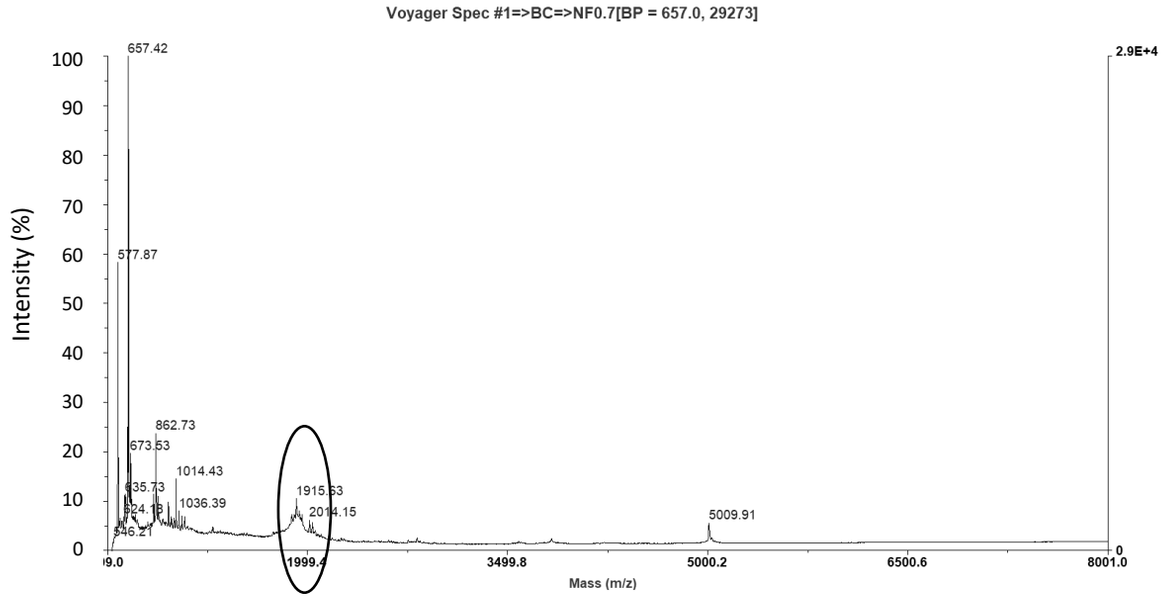

(G) DAS- T=24h

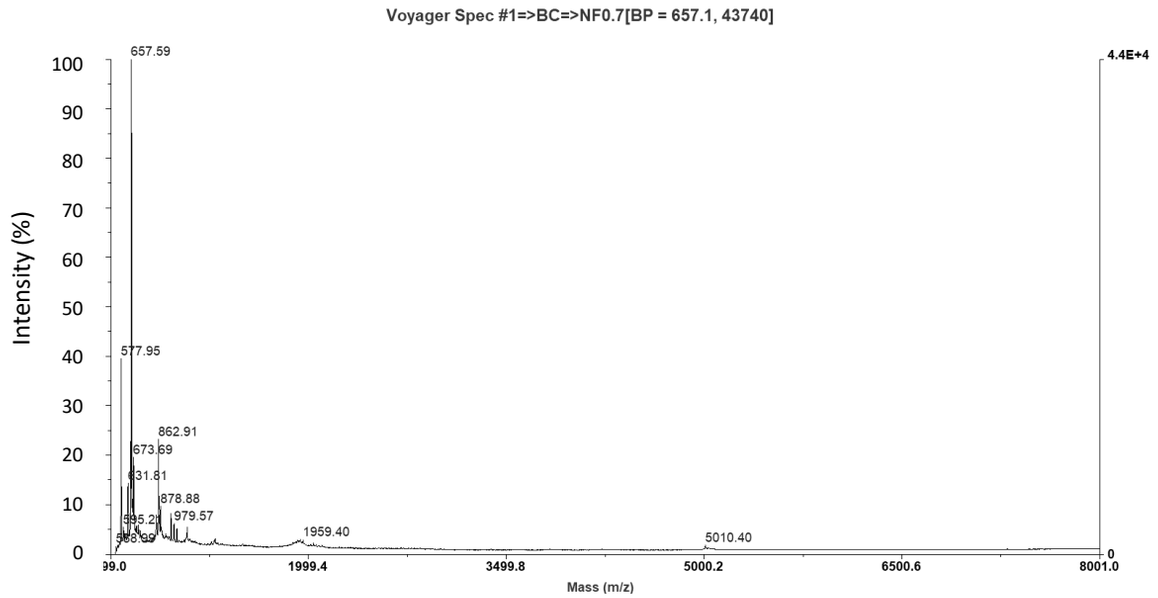

Figure 4.5. MALDI-TOF mass spectrometry analysis of DAS stability in 25% human serum at 37°C for various periods of time. (A) Human serum with no peptide. (B)-(G) Mass spectrometry profile detected for DAS (MW approx. 1.9 kDa) in human serum up to 24 hours of incubation. DAS signal in indicated by encircled peaks.

4.3.4. Confocal imaging of DAS-facilitated NP uptake in vitro

Visualisation of DAS-FITC NP cellular uptake by confocal fluorescence microscopy (Figure 4.6) was carried out as for RDP-FITC NP previously reported in section 3.3 (Chapter 3). It was demonstrated in Figure 4.6 that DAS preferentially promotes cellular uptake of NP in SH-SY5Y (Figure 4.6A) and PC-12 (Figure 4.6B) neural cells when compared to the untargeted FITC NP. In contrast, detected fluorescence signal was low in Hela cells (Figure 4.6C) and no notable difference in cellular uptake was observed between all formulations, indicating that like RDP, DAS is not effective as a targeting peptide in this non-neural cell line. Lysotracker® red was used to visualise cell lysosomes and compare to any emission pattern of FITC within the cell. Similarities in signal detected from Lysotracker® emission and that of FITC would indicate that there may be co-localisation of lysosomes and internalised FITC NP. Indeed, there was evidence of co-localisation in SH-SY5Y cells and also in PC-12 cells between lysosomes and internalised FITC.

In Chapter 3, it was shown how RDP can enhance the uptake of a conjugated payload to induce cytotoxic effects in neural cells and this was supported by confocal fluorescence imaging. Results from Figure 4.6 suggest that DAS has retained the neural-specific targeting ability of RDP, as NP uptake was visibly greater in neural cells than the non-neural cell type. It has been suggested by Fu et al. (2013a), that the cellular uptake mechanism of RDP may involve energy-dependent internalisation pathways such as clathrin-dependent endocytosis. Indeed, observations of co-localisation between RDP (Figure 3.5, Chapter 3) and DAS conjugates with lysosomes in this work (Figure 4.6) support this idea.

Clathrin-dependent endocytosis accounts for the majority of receptor-mediated internalisation of NP, however intracellular trafficking routes are generally not well characterised for nanoparticulate transport (Yameen et al., 2014). Non-targeted NP can be internalised by pinocytosis mechanisms such as clathrin- and caveolae-mediated endocytosis. The mechanism of non-specific NP uptake is dependent on attributes such as size, zeta potential and shape, in

addition to cell type (Beddoes et al., 2015). Most endocytosed NP will eventually end up in late endosomes or lysosomes where pH-induced degradation results in intracellular payload release (Iverson et al., 2011).

Caveolae-mediated endocytosis is generally for small NP (<100 nm) and can sometimes be unpredictable, as internalised NP can evade lysosomal trafficking via this route (Yameen et al., 2014). The use of larger NP (200-300 nm), as in this study, limits non-specific uptake and attachment of a targeting ligand facilitates cellular uptake towards more predicable pathways. It is essential for therapeutic affect that internalised NP are trafficked towards degradative pathways, to ensure payload release. Non-specific uptake via endocytic mechanisms is most likely responsible for the low level of FITC NP and DAS-FITC NP uptake observed in HeLa cells, which do not express a neuronal-type nAChR (Figure 4.6C).

Early endosomes are known as the sorting stations in which intracellular cargo is processed through either recycling or degradative pathways (Hu et al., 2015). Late endosomes eventually fuse with lysosomes which contain degradative enzymes at low pH 4.5. Endogenous acetylcholine receptors undergo cell surface internalisation and lysosomal degradation for regulation of synaptic plasticity in excitable cells. This response in the natural turnover of cell surface receptors is also replicated upon binding with agonists such as nicotine (St John & Gordon, 2001). Kumari et al. (2008) found that binding of alpha-bungarotoxin at the nAChR caused ligand-receptor complex internalisation along an energy-dependent endocytic pathway into late endosomes. The ligand-receptor complex was found to be co-localised with late endosomal markers such as LAMP-1 (lysosomal-associated membrane protein 1). It is possible that both RDP and DAS binding at the nAChR in neural cell types induces a similar response, which results in NP localised in areas highlighted by Lysotracker®.

(A)

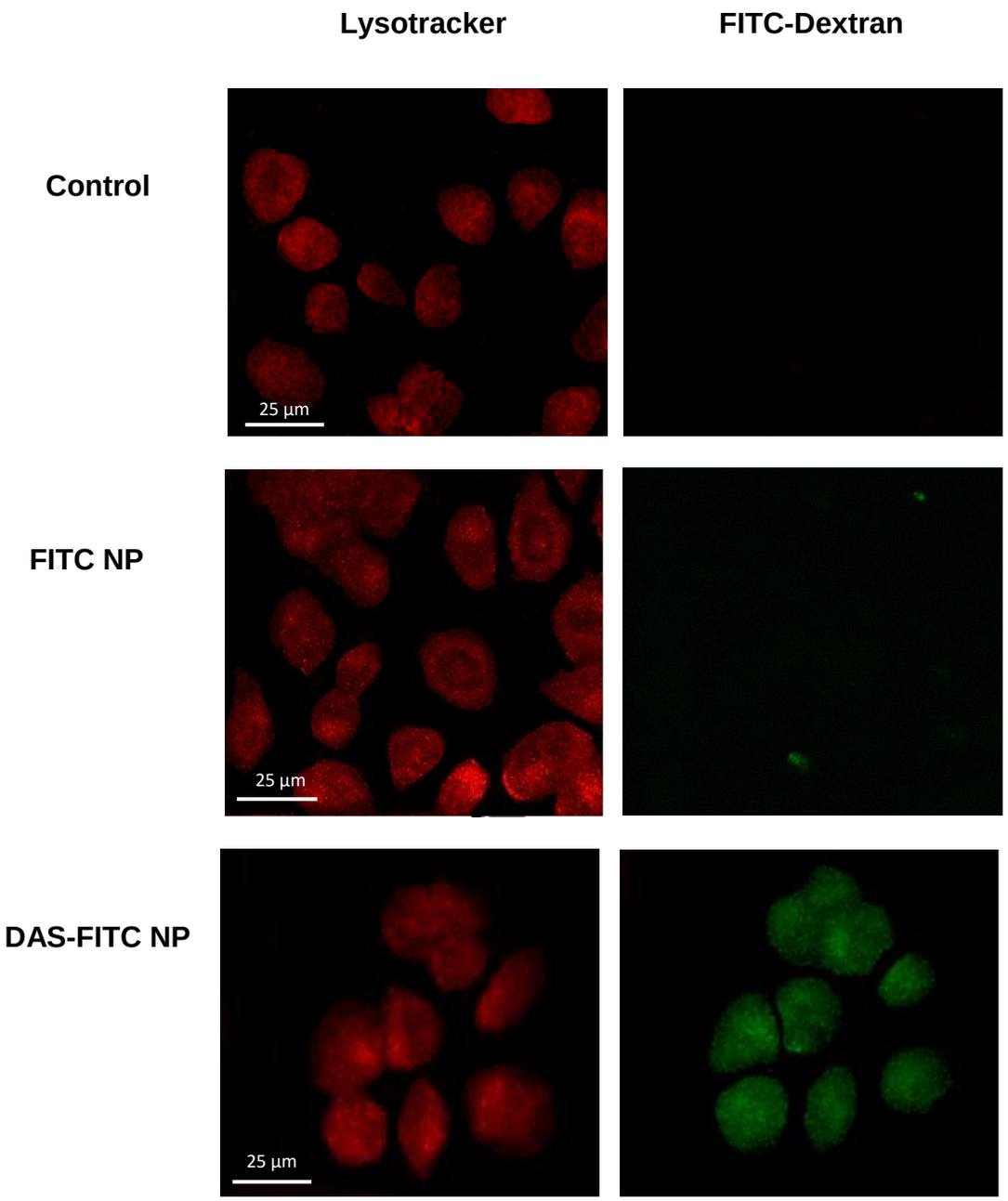
Lysotracker
FITC-Dextran
Control
FITC NP
DAS-FITC NP
25 µm
25 µm
25 µm

(B)

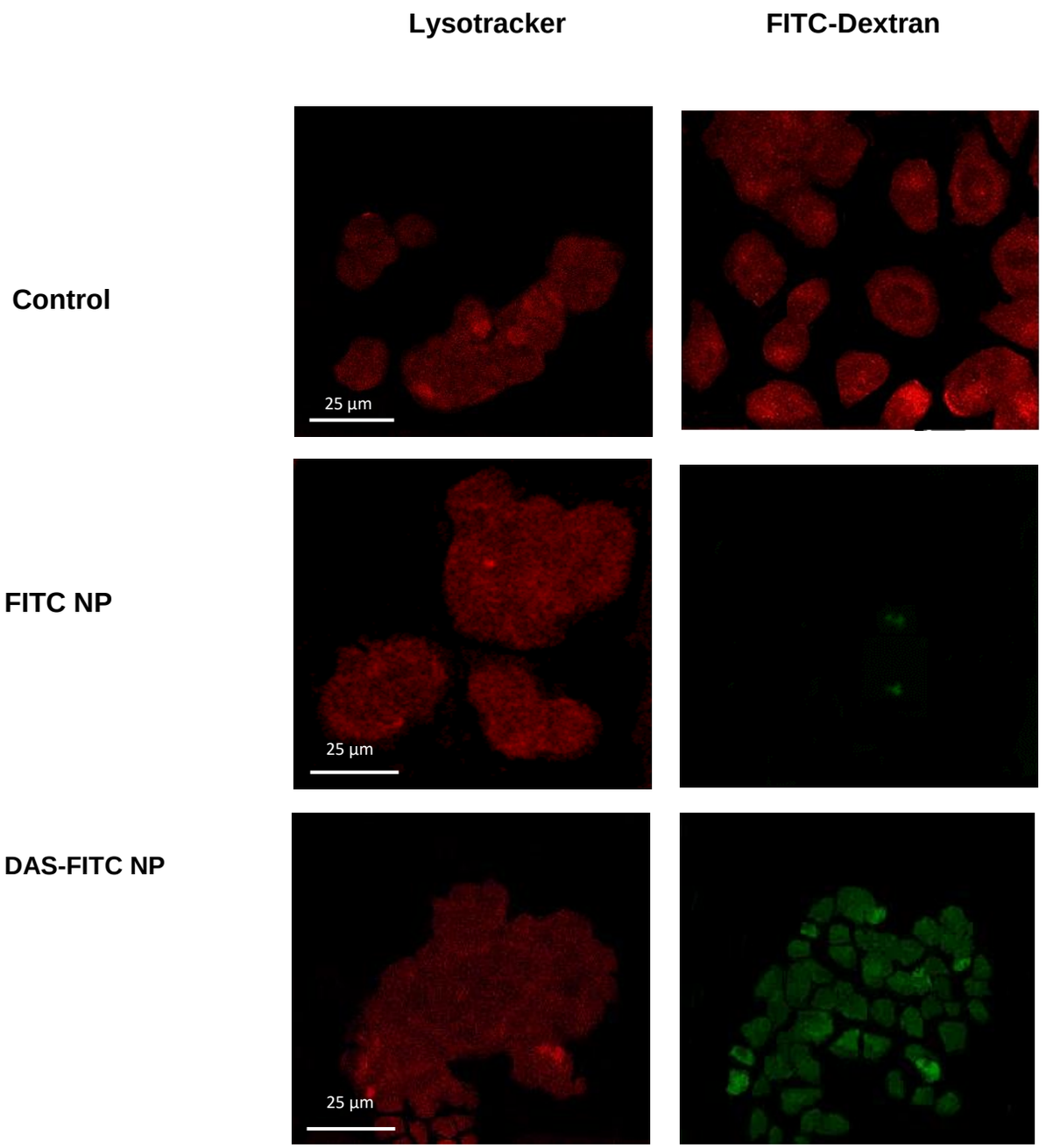
Lysotracker
FITC-Dextran
Control
FITC NP
DAS-FITC NP
25 µm
25 µm
25 µm

(C)

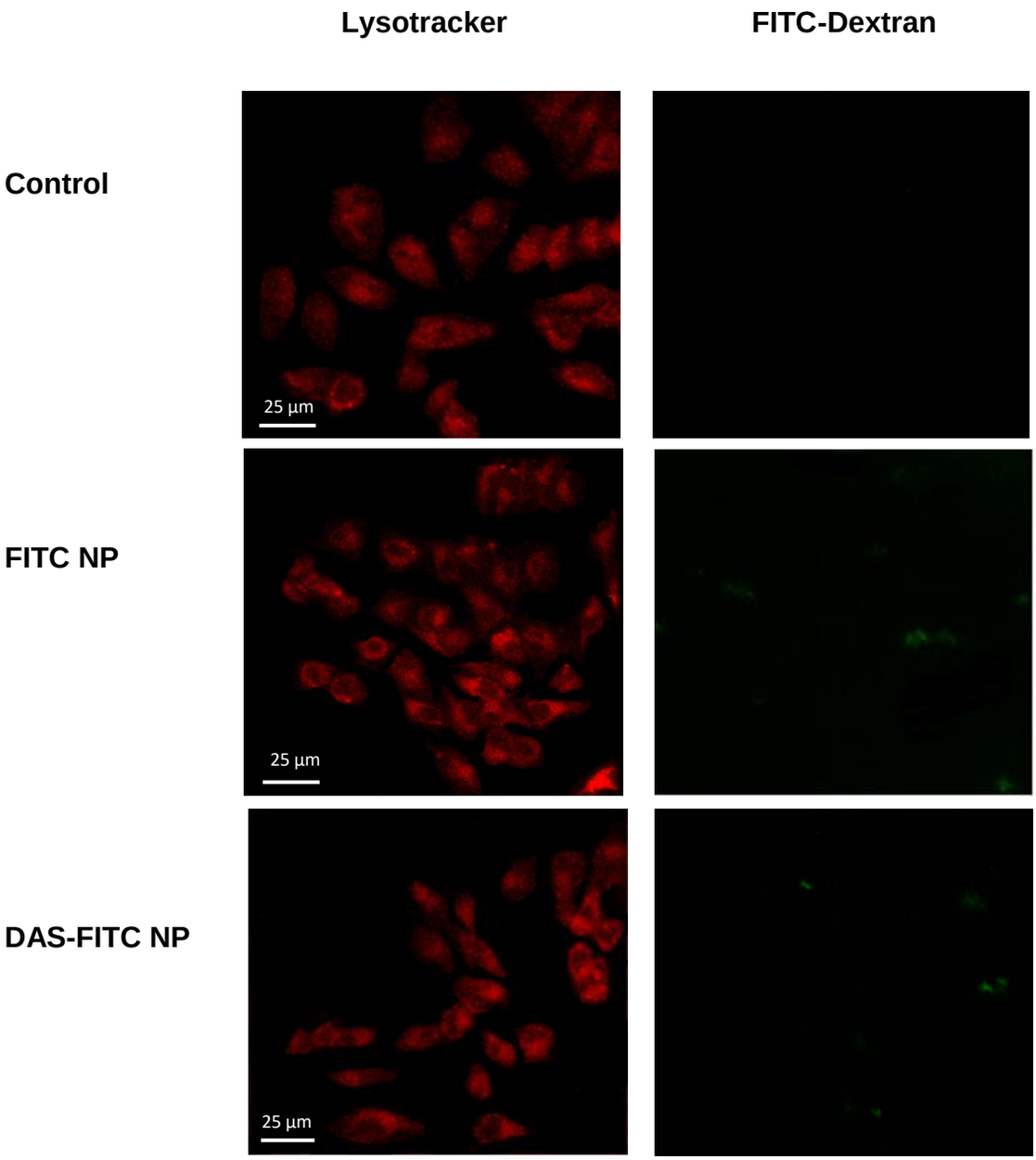

Figure 4.6. Confocal images of intracellular fluorescence emission from Lysotracker® (red) and FITC (green) in (A) SH-SY5Y, (B) PC-12 and (C) HeLa cells to assess the *in vitro* effect of targeting ligand, DAS. Lysotracker® accumulates in acidic lysosomes, vesicles containing hydrolytic enzymes which are involved in the late-stage endocytosis uptake pathway within cells. FITC fluorescence emission is due to uptake of FITC-dextran payload within polymeric NP.

4.3.5. In vitro cytotoxicity

Figure 4.7 shows the cytotoxic effect of DAS conjugation to Dox NP in SH-SY5Y human neuroblastoma cells over 24 hours using a range of concentrations. DAS significantly enhanced cytotoxicity of the nanoparticulate payload in comparison to the unlabelled Dox NP at concentrations between 1.0- 2.0 mg/mL. The IC_{50} of DAS-Dox NP was 0.9 mg/mL in comparison to 1.35 mg/mL for Dox NP. This supports the findings from confocal microscopy images in Figure 4.6 and indeed suggests that DAS has retained the preferential targeting ability of RDP to neural cell types. Concentrations above 2.0 mg/mL nullified the targeting effect of DAS in this study. This is possibly because extracellular doxorubicin leaching from both NP preparations at such concentrations over 24 hours imparted cytotoxicity beyond NP-induced effects. Based on these observations, it was decided to use NP at 1.5 mg/mL for further cell-based *in vitro* assays.

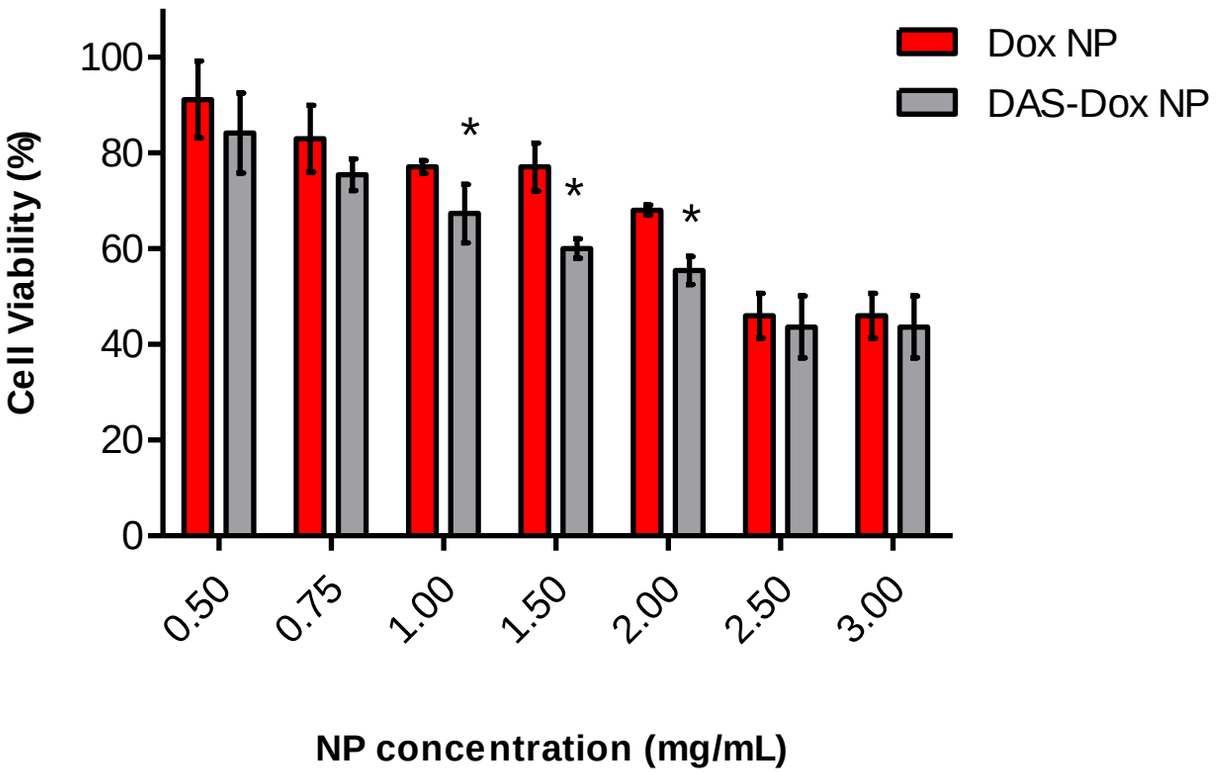

Figure 4.7. Cell viability of SH-SY5Y cells following exposure to varying concentrations of doxorubicin-loaded NP either unlabelled (Dox NP) or conjugated to peptide ligand, DAS (DAS-Dox NP). *Statistically significant difference compared to Dox NP (P value <0.05, n=6).

DAS peptide alone did not cause any detectable toxicity to cells over the time course observed in Figure 4.8, giving early indication that this ligand may also be safely used as part of a drug delivery system. Treatment with DAS-Dox NP caused a significant enhancement in SH-SY5Y cytotoxicity, as cell viability decreased to 60.0% (± 7.0% SD) compared with 75.0% (± 5.0% SD) when treated with untargeted Dox NP.

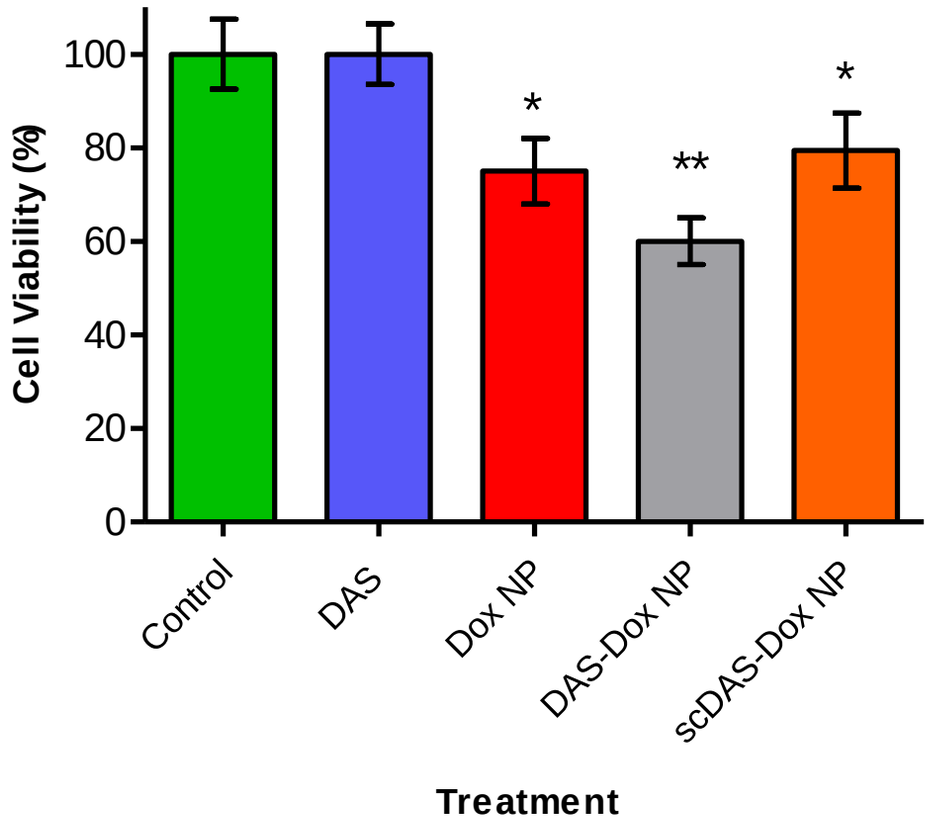

Figure 4.8. SH-SY5Y neuroblastoma cell viability determined by MTT assay following treatment with either serum-free medium (control), DAS ligand or different cytotoxic NP formulations for 24 hours. Statistically significant difference to; *control, ** Dox NP (P value <0.05, n=6). ScDAS= scrambled version of DAS peptide.

To test the significance of the -GCLRV- fragment for neural cell interaction of DAS, a scrambled version of the peptide (scDAS) was conjugated to Dox NP and exposed to SH-SY5Y cells as for DAS-Dox NP. Results from Figure 4.8 show that scDAS was ineffective at promoting enhanced cellular uptake of cytotoxic NP compared to the untargeted formulation. Cell viability following scDAS-Dox NP treatment decreased to 79.4% (± 8.0% SD), which was similar to Dox NP and almost 20% higher than DAS-Dox NP. This result confirms that the -GCLRV- sequence, as identified through molecular modelling of RDP, is essential for the inherent neurotropism of DAS.

The effects of DAS-Dox NP on the non-neural cell lines HeLa, MDA-MB-231 and CHO are presented in Figure 4.9. Cell viabilities for the non-neural, normal CHO cells and the cancer cell lines, HeLa and MDA-MB-231, showed no significant difference between Dox NP and DAS-Dox NP treatments. In the neural SH-SY5Y cell line however, DAS promoted susceptibility of the cells to the cytotoxic effects of Dox NP, causing a statistically significant decrease in cell viability to 62.0% (± 9.8% SD) for DAS-Dox NP compared to 75.0% (± 7.1% SD) for the untargeted Dox NP. Both NP treatments caused a certain amount of cytotoxicity to non-neural CHO, HeLa and MDA-MB-231 cells possibly be due to some extracellular doxorubicin leaching from NP over the 24-hour experimental period. It is clear however, that when the NP are targeted with DAS, there is a significant change within the neural cell type only.

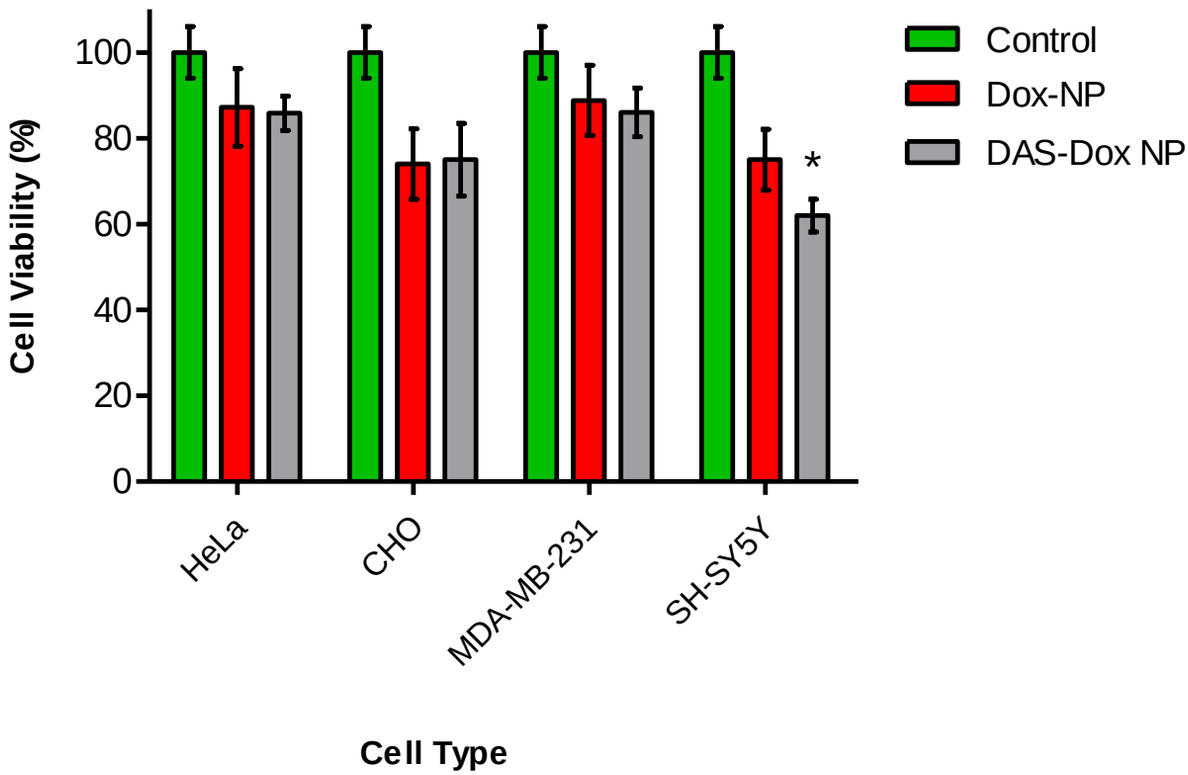

Figure 4.9. Effect of peptide targeting ligand, DAS, on doxorubicin-loaded NP toxicity towards non-neural cell lines HeLa, CHO and MDA-MB-231 compared to SH-SY5Y neural cells. Control groups were treated with serum-free media only. Error bars represent mean ± standard deviation (n=6). * Statistically significant difference compared to Dox NP (P value <0.05).

Given DAS was modelled upon RDP interactions with the nAChR, it was investigated whether blocking this receptor would affect targeting activity of the peptide. Figure 4.10 shows the effect of preincubating SH-SY5Y cells with the nAChR antagonists hexamethonium, mecamylamine and anti-AChRα7 antibody. In hexamethonium-treated cells, viable cell count remained at 82.0% (± 9.7% SD) of control when exposed to DAS-Dox NP compared to 72.0% (± 5.5% SD) with untargeted Dox-NP. This is in distinct contrast to the cell viability of 63.4% (± 6.7% SD) obtained upon DAS-Dox NP exposure when there was no prior inhibition of the nAChR and this receptor was available for interaction. Mecamylamine-treated cells produced an almost identical result,

with DAS-Dox NP causing cell viability to drop to just 85.0% (± 4.0% SD) compared to 62.0% (± 7.0% SD) with no prior inhibitory treatment.

Pretreatment with all of the antagonists inhibited SH-SY5Y cell susceptibility to the amplified cytotoxic effects of DAS conjugated Dox NP. In fact, DAS-Dox NP treatment in the presence of nAChR inhibitors is less toxic than the unlabelled preparation. This is possibly due to a steric hinderance effect caused by peptide on the NP surface, making the peptide-conjugated NP too bulky for non-specific membrane absorption and subsequent internalisation. The unlabelled NP formulation however, may have particles small enough to undergo cellular uptake by non-specific endocytic routes over a 24-hour period.

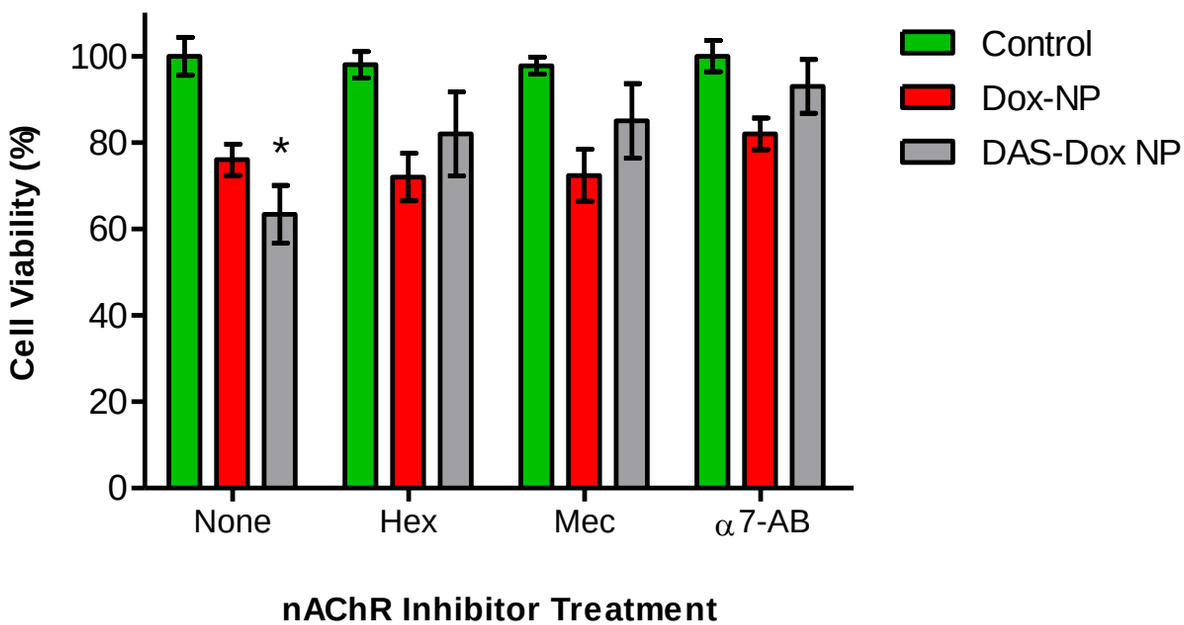

Figure 4.10. Effect of nAChR antagonists hexamethonium (Hex), mecamylamine (Mec) and anti-AChRα7 antibody (α7-AB) on DAS ligand activity following NP treatment on SH-SY5Y neural cells. Control groups were treated with SFM only. Error bars represent mean ± standard deviation (n=6) * Statistically significant difference compared to Dox NP (two-tailed T-test P value <0.05).

An anti-AChRα7 antibody was once again employed to block the α7-nAChR to observe the effects on DAS-Dox NP cytotoxicity. Results show that DAS did not promote more cytotoxicity than unlabelled Dox NP when this receptor subtype was blocked and thus the targeting effect of DAS was cancelled out in SH-SY5Y cells. Gan et al. (2018) also used a competing antibody, cetuximab, to evidence the targeting ability of a newly identified peptide towards the epidermal growth factor receptor. Ultimately, these results suggest that DAS is facilitating uptake of cytotoxic NP through mechanisms involving the nAChR, namely the α7-nAChR subtype, in these particular neuroblastoma cells. At this early stage in the development of new peptide ligand, DAS, it can be postulated that the additional 13 amino acids added to the -GCLRV- sequence had no adverse effect on the neurotrophic properties of the ligand or affected its ability to interact with the nAChR.

DAS was again tested on PC-12 (rat adrenal pheochromocytoma) cells, also of neural origin, to support the hypothesis that the new peptide preferentially targets neural cells (Figure 4.11). After 24 hours of DAS-Dox NP treatment, cell viability decreased to 71.6% (± 8.4% SD). This was statistically significant (P value < 0.05) compared to the cells which were treated with untargeted Dox NP, where cell viability was 94.0% (± 3.0% SD). Interestingly, DAS appeared slightly more effective in promoting NP uptake in PC-12 (Figure 4.11) than SH-SY5Y cells (Figures 4.7 & 4.8). Indeed, this could be due to the known varying expression of nAChR subtypes between neural cells (Court et al., 2000; Abbruscato et al., 2002; Gotti et al., 2006) and affinity of targeting peptide to them.

It was established form Figure 4.10 that DAS is dependent upon the α7-nAChR for activity in SH-SY5Y cells. It was therefore investigated whether this anti-AChRα7 antibody would also block DAS activity in PC-12 cells (Figure 4.11). Surprisingly, DAS-Dox NP still exhibited significantly more cytotoxic activity (77% cell viability) than unlabelled Dox NP. Although anti-AChRα7 antibody marginally inhibited the effect of DAS-Dox NP, it is possible that DAS does not solely function via the α7-nAChR in these cells. The 28.4% cytotoxicity observed in PC-12 cells

following DAS-Dox NP treatment may be due to DAS interactions with other nAChR subtypes preferentially expressed by PC-12 cells. This would require further investigation into receptor binding of the DAS ligand in future studies. Alternatively, PC-12 cells may express a higher number of α7-nAChR than SH-SY5Y cells and thus a higher concentration of antibody would be required to completely block receptor interactions with DAS.

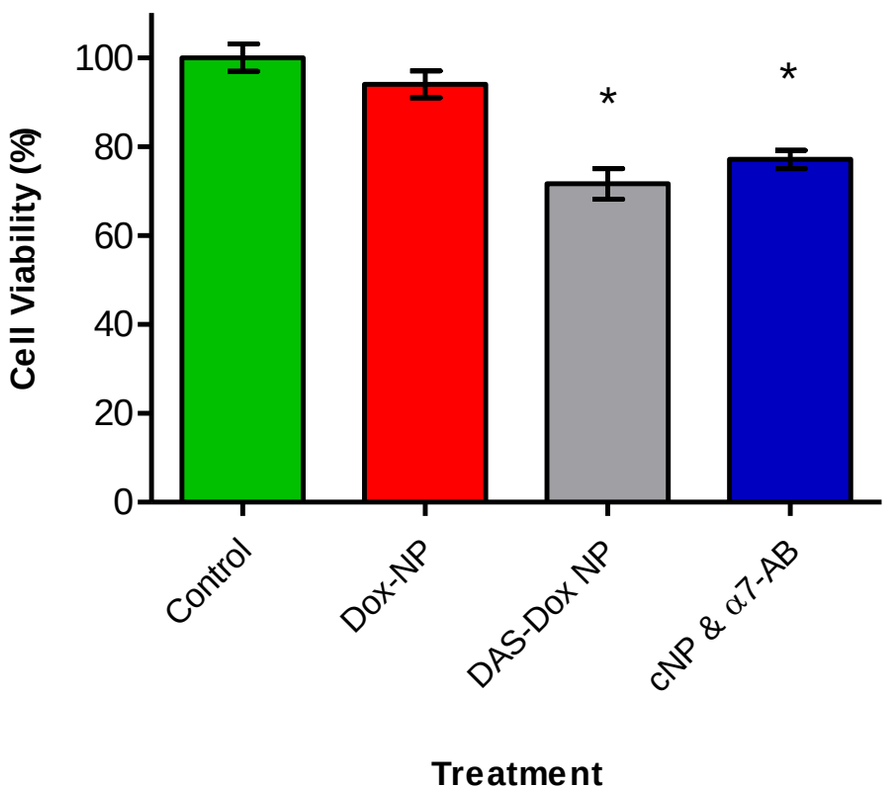

Figure 4.11. PC-12 cell viability following different cytotoxic NP treatments. The effect of DAS targeting peptide conjugation to NP is compared to untargeted Dox NP and also pre-incubation with anti-AChRα7 antibody (α7-AB). * Statistically significant difference compared to Dox NP (P value <0.05, n=6). cNP= conjugated NP (DAS-Dox NP).

It was first hypothesised by Kumar et al. (2007) that RVG derivative, RVG-29, might utilise the α7-nAChR to traverse the BBB and facilitate delivery of siRNA to the brain *in vivo* due to widespread expression of this receptor throughout the nervous system. In this study, it has been shown that RDP and DAS target two different neural cell types, SH-SY5Y and PC-12. Additionally, Hwang et al. (2011) used nAChR-positive neuro-2a cells to show the neural-specific targeting properties of an RVG derivative in comparison to non-neural HeLa cells. Many nAChR ligands have different specificities towards various nAChR subtypes (Resende et al., 2009) and to this end, it is possible that DAS may show higher targeting affinity to nAChR subunits expressed on PC-12 cells, than on SH-SY5Y. Indeed, as with many nAChR ligands, it is possible that DAS might bind to more than one nAChR subtype, rather than the α7 subunit exclusively.

4.4. Conclusion

In silico modelling for interactions between RDP and the α7-nAChR uncovered a 5-amino acid section of the RDP sequence, 'GCLRV', as a potential target sequence. This 5-mer was therefore incorporated into a newly developed sequence, termed DAS. A flexible linking sequence allowed successful conjugation of DAS to a polymeric PLGA nanoparticulate drug delivery vehicle. Increased resistance to degradation by serum proteases was achieved by addition of alternating artificial D-Arginine residues at the end of the sequence. The final 18-mer peptide ligand showed enhanced resistance to degradation in serum over 8 hours than RDP, which degraded within an hour.

In vitro testing of DAS revealed that the new ligand retained the neural cell targeting selectivity of the parent molecule, RDP. DAS specifically enhanced uptake of two different drug-loaded NP preparations in SH-SY5Y and PC-12 neural cells, but not in non-neural cell types. Furthermore,

it was demonstrated that DAS ligand alone was non-toxic to cells over the experimental period observed.

It was previously shown that RDP relies upon nAChR interactions for uptake into neural cells. Since DAS was modelled upon interactions of RDP with the nAChR, it was investigated whether inhibiting this receptor with different antagonists would affect DAS activity in SH-SY5Y cells. Results showed that DAS does require nAChR function, more specifically of the α7-nAChR subtype, for uptake activity in SH-SY5Y cells. This confirmed that DAS exhibits *in vitro* activity at the receptor upon which it was originally modelled. It was subsequently explored whether this would also be the case for DAS targeting in PC-12 cells. Studies revealed that DAS may in fact utilise more than one nAChR subtype in PC-12 cells, as inhibition of the α7-nAChR only fractionally affected cytotoxicity of DAS-Dox NP. This is supported by the fact that DAS appeared more effective as a targeting ligand in PC-12 cells than SH-SY5Y cells. Indeed, if a targeting ligand can bind more than one subtype of major neural receptor, it is likely to be beneficial *in vivo* and increase affinity for specific drug delivery to the brain.

The promising results from the pilot work reported herein warrants further exploration into DAS as a neural cell-specific targeting ligand. DAS was shown to be as effective as RDP in two neural cell lines and hence the ability of DAS to traverse an *in vitro* model of the BBB should be investigated. The use of an *in vitro* BBB model as a pre-requisite to *in vivo* work is beneficial to allow observations of how efficiently DAS can target a conjugated payload across multiple cell layers in the presence of tight junction proteins, which characteristically make drug transport across brain endothelial cells challenging.

Chapter 5

Modelling of an *in vitro* blood brain barrier model for the evaluation of RDP derivative, DAS, as targeting ligand.

5.1. Introduction

In vitro BBB models are useful for the assessment of targeted drug transport studies as a precursor to *in vivo* work. This is due to lower costs, the ability to directly quantify compounds and gain information on their mechanism of action. It is also beneficial to detect potential cytotoxicity at an early stage in development before commencing animal studies (Bicker et al., 2014). Different types of *in vitro* cell-based BBB models have been developed over recent years ranging from monoculture models to those including multiple cell types from the neurovascular unit (NVU). Diverse sources of endothelial cells have been sought to create *in vitro* BBB models such as primary brain tissue, immortalised brain microvascular endothelial cells and stem cells (Toth et al., 2011). Each source offers different advantages and drawbacks, however the TEER value and expression of BBB markers such as tight junction (TJ) proteins ultimately determine whether a model is robust enough for drug transport studies (Wilhelm et al., 2011).

To assess the integrity of a BBB model, the trans-endothelial electrical resistance (TEER) across the endothelial monolayer is measured (Reichel et al., 2003). The higher the TEER, the more restrictive the barrier to endothelial trans- and para-cellular transport. The distinguishing characteristics of the BBB, which make CNS drug delivery so difficult, are typified by an *in vivo* TEER in excess of 1000 Ωcm^2. For *in vitro* BBB systems however, it is generally accepted that a minimum TEER of 150 Ωcm^2 is sufficient for drug transport studies (Deli et al., 2005).

Fluctuations in TEER can reflect disruption to the endothelial monolayer, as a decrease in barrier integrity leads to increased permeability. In the development of *in vitro* BBB models, TEER measurement is important as it not only reflects the integrity of the barrier but can also indicate how experimental materials might affect endothelial monolayer integrity over time. This is useful as an early predictor of *in vivo* toxicity for new brain-targeted drug formulations. Traditionally, TEER is measured by AC systems such as the commercially available EVOM2 voltmeter and expressed as the product of the resistance measured (Ω) and the area (cm^2) of the endothelial

membrane surface (Watson et al., 2013). TEER values can also be calculated by impedance spectroscopy, which can consider the contribution from TJ proteins to the total resistance between and through cells (Srinivasan et al., 2015). Additionally, impedance spectroscopy allows continuous monitoring during cell growth without causing damage (Benson et al., 2013).

Cell-based *in vitro* BBB models can be derived from the same species (isogenic) or be composed of cell layers from different species (transgenic). Cells of porcine, bovine, rat, mouse and human origin have all been utilised to make such models (Mukhtar & Pomerantz, 2000). Immortalised endothelial cells of human (Duvar et al., 2000; Poller et al., 2008; Daniels et al., 2013), rat (Regina et al., 1999; Roux & Couraud, 2005) and mouse origin (Omidi et al., 2003; Watanabe et al., 2013) have all been used to construct *in vitro* BBB models. Despite this, TEER values are usually lower than desired for drug transport studies in comparison to primary cell lines. This is due to loss of BBB phenotype through decreased expression of TJ proteins, transporters and enzymes. Immortalised cell lines therefore, may only be useful for mechanistic studies where a tight barrier is not necessary (Reichel et al., 2003), for example when analysing NP endo-lysosomal trafficking (Ye et al., 2013). Primary cells generally exhibit better TEER values, however the main drawback of their use is the difficulty in obtaining them and loss of BBB phenotype with high passage number. Regardless, primary cells of human origin remain the ideal for gaining invaluable information on pathophysiology and other physiological mechanisms in the brain (Reichel, 2006). Most recently, stem cells have been used with much success to produce human *in vitro* BBB models which exhibit desirable TEER values and markers of BBB characteristics (Cecchelli et al., 2014; Appelt-Menzel et al., 2017; Canfield et al., 2017). The use of stem cells however, is difficult due to controversial ethical issues and higher cost to culture.

Cells used for constructing BBB models are usually seeded onto a microporous membrane which separates two compartments of culture medium, the apical (blood) side and the basolateral (brain) side. Tissue culture wells with inserts containing the membrane allow cells to be seeded on either side, permitting bidirectional exchange of soluble components. If a third cell type is introduced, it can be seeded in the bottom of the well creating a co-culture system. Many brain

endothelial monolayer models have been created for looking at various aspects of drug transport, including peptide targeting studies (Dan et al., 2013; Zhao et al., 2016). It has been shown however, that introducing other cells of the NVU to produce either double or triple co-culture models are superior to monocultures (Nakagawa et al., 2007, 2009; Veszelka et al., 2018) and thus more accurately represent a selectively permeable barrier.

Co-culture models of the BBB can comprise any of the cells of the NVU, such as astrocytes, pericytes, neurons and macrophages. Astrocytes are most commonly used in co-culture with endothelial cells in BBB models due to a wealth of evidence that they improve TEER values and enhance endothelial expression of the BBB phenotype (Abbott et al., 2006; Li et al., 2010; Shayan et al., 2011). Triple cultures including astrocytes and pericytes have more recently been utilised in drug transport studies due to further improvements in BBB characteristics (Nakagawa et al., 2007,2009; Wisniewska-Kruk et al., 2012; Thomsen et al., 2015; Dos Santos Rodrigues et al., 2018). The optimal arrangement of cells within these models however, has been reported with varying results. Nakagawa et al. (2009) found that pericytes were better seeded on the underside of the microporous membrane, in direct contact with the endothelial cells seeded on top. Conversely, Wisniewska-Kruk et al. (2012) found that optimal barrier tightness resulted when astrocytes were seeded directly below the endothelial cells. Nevertheless, a functional *in vitro* BBB model can be useful to assess targeting efficacy and safety of neuro-pharmaceuticals prior to *in vivo* testing.

Various features of nanoparticulate drug delivery including toxicity (Xu et al., 2015), transport pathways (Ragnaill et al., 2011) and size-dependence (Hanada et al., 2014) have been studied using such models. The efficacy of peptides as brain targeting ligands for different therapeutics has also been studied, for example Song et al. (2017) described how lactoferrin-conjugated NP could cross the endothelial layer of a triple culture BBB model *in vitro*. Similarly, Zhao et al. (2016) demonstrated how TAT-labelled magnetic NP could penetrate BBB endothelial cells to target basolateral glioma cells. Size-dependent studies by Hanada et al. (2014) showed that NP with sizes around 400 nm were barely able to pass through a co-culture *in vitro* BBB model by

non-targeted means. These recent advances are encouraging in the field of drug delivery, as the utility of nanoparticulate systems in delivering therapeutics across a selectively-permeable barrier can be assessed at an earlier stage of development.

New RDP derivative, DAS, has shown the ability to specifically target neural cells, however it is not yet known if DAS can facilitate the uptake and subsequent passage of an attached payload across the BBB. *In vivo* results previously reported in the literature suggests that RDP can target the brain. Before *in vivo* work is carried out on a suitable animal model, it would be appropriate to assess the targeting ability and safety of DAS ligand on an *in vitro* BBB model when conjugated to a NP payload. This would provide valuable information on how well DAS, as a neural-specific targeting ligand, can traverse a tight endothelial layer in comparison to RDP. Additionally, the effect of DAS and RDP on barrier integrity *in vitro* could be monitored, as well as potential mechanism of action.

The aims of the work reported herein were therefore to:

(1) Develop an *in vitro* BBB model using primary human cell lines, investigating the optimal arrangement of cells based on TEER measurements and expression of TJ proteins. To construct BBB models, major neurovascular unit cellular components such as brain microvascular endothelial cells, astrocytes and pericytes are cultured on multi-layer microwell inserts under specific protocols.

(2) Use the leading BBB model to study the effect of RDP and DAS as targeting ligands when conjugated to polymeric NP with different drug payloads. The appropriate BBB model should express sufficient barrier characteristics so that passive permeability to polymeric NP is restricted, thus allowing the effect of targeting ligand to be observed.

5.2. Materials and Methods

5.2.1. Materials

The following materials were purchased from Sigma-Aldrich (UK) unless otherwise stated. Goat anti-mouse alkaline phosphatase secondary polyclonal antibody, goat anti-rabbit alkaline phosphatase secondary polyclonal antibody, fibronectin from bovine plasma, hydrocortisone 0.05 mM aqueous solution, heparin sodium salt from porcine intestinal mucosa, human basic fibroblast growth factor (bFGF), BCIP®/NBT solution, Corning Transwell® 0.4 µm pore polycarbonate membrane cell culture inserts, 1% eosin solution, 0.1% haematoxylin solution (Mayer's), fluorescein isothiocyanate–dextran (FITC-dex) average MW 70 000 and indocyanine green (ICG).

Primary human brain microvascular endothelial cells (HBMVEC), human pericytes and human astrocytes were all purchased from iXcells Biotechnologies (USA). Poly-L-lysine solution was purchased from Millipore (UK). Anti-claudin-5 and anti-actin antibodies were purchased from Santa Cruz biotechnology (USA). Anti-TJP1 (tight junction protein 1) (ZO-1) antibody was purchased from Abbexa, (UK). Invitrogen NuPAGE 4-12% bis-tris gels, nitrocellulose/filter paper sandwich (0.45 µm pore size) 8.5 cm x 13.5 cm, DMEM culture medium, DMEM/F12 and insulin-transferrin-selenium (ITS) 100x solution were all purchased from ThermoFisher Scientific (UK).

5.2.2. NP formulation

High molecular weight (70 kDa) FITC-dex PLGA NP were synthesised according to the method described previously in section 3.2.3.2 of Chapter 3. Indocyanine green (ICG) NP were similarly prepared by this method. 2 mg of ICG (MW 774.96) was dissolved in 0.5 mL of double distilled water (ddH_2O) and loaded with 100 mg of PLGA polymer. Following centrifugation of the

resulting ICG NP, supernatant was collected to quantify entrapment efficiency using UV-Vis spectrometry at 800 nm.

5.2.3. NP Characterisation

NP were characterised for size, zeta potential and polydispersity index by DLS as described in section 2.2.4 (Chapter 2). To calculate drug entrapment efficiency, supernatant following centrifugation of NP was collected and analysed using fluorescence spectrometry for FITC-dextran (see section 3.2.5.2 of Chapter 3) and UV-Vis spectrometry for ICG. A calibration graph for ICG absorption at 800 nm was generated to produce an equation for approximate ICG content expressed as µg/mL (Figure 5.1). To measure release, 5 mg of ICG NP were dispersed in 1 mL of ddH_2O and incubated at 37 °C for 7 days. ICG is poorly soluble in PBS, therefore this was not used as the release medium. At various time points, the ICG NP suspension was centrifuged at 1680 *g* for 5 minutes and a sample of release medium was removed. ICG content was measured using UV-Vis absorbance at 800 nm (n=3) and aliquots were replaced with fresh ddH_2O.

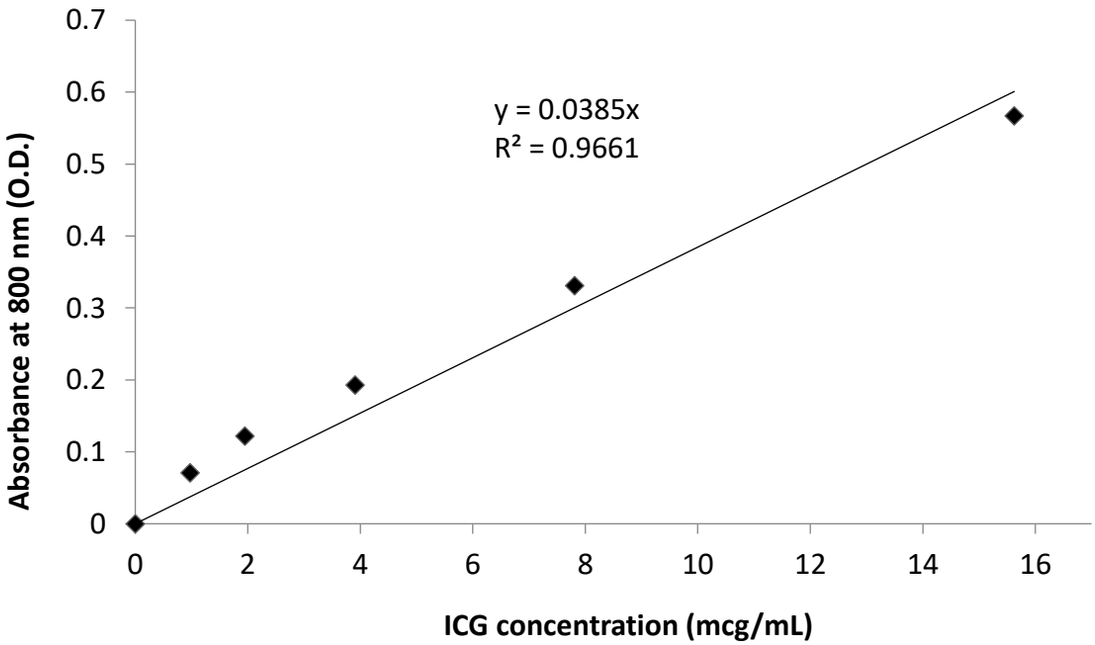

Figure 5.1. Calibration curve of indocyanine green (ICG) absorption at 800 nm in double distilled water.

5.2.4. Peptide Conjugation

The protocol for attachment of both RDP and DAS to drug-loaded NP by EDC/NHS chemistry and subsequent assessment of conjugation efficiency by BCA assay are detailed in previous chapters (2-4). 250 µg of DAS or 750 µg of RDP were reacted per 5 mg of ICG NP.

5.2.5. BBB model construction

Tissue culture vessels for all three BBB cell types were pre-coated overnight with 2.5 mL of poly-L-lysine solution (0.01%) and washed thrice with sterile PBS before air drying under sterile conditions. HBMVEC were cultured in DMEM/F12 medium supplemented with 1% PS, 10% FBS, 2.5 mL insulin-transferrin-sodium selenite (ITS) solution, 1.5 ng/mL basic fibroblast growth

factor (bFGF) and heparin sodium (100 IU/mL). Both astrocytes and pericytes were cultured in DMEM supplemented with 1% PS and 10% FBS.

BBB models were constructed according to methods described by Nakagawa et al. (2007, 2009) and Wisniewska-Kruk et al. (2012). Corning Transwell polycarbonate membrane 0.33 cm^2 tissue culture inserts (0.4 µm pore size) were pre-coated overnight on both sides with 50 µL of 0.1% poly-L-lysine solution prior to seeding of cells. Firstly, on the underside of the inserts, 20 000 pericytes or astrocytes in a volume of 40 µL were seeded and incubated for 2 hours (37°C/5% CO_2). After this, the inserts were placed in a well containing 600 µL of complete DMEM medium and incubated at 37°C/5% CO_2 for 24 hours. Subsequently, 600 µL of astrocytes or pericytes ($1x10^5$ cells/mL) were then seeded in separate wells of the plate, also pre-coated with 0.1% poly-L-lysine (300 µL). Following a further 24 hours of incubation (37°C/5% CO_2), HBMVEC were seeded onto the upper side of the Transwell insert at a density of $1.5x10^5$ cells/cm^2 in 100 µL of complete DMEM/F12 and the insert placed in the well containing pericytes/astrocytes. The assembled Transwell plate was incubated overnight (37°C/5% CO_2), at which point all media was aspirated and replaced with complete DMEM/F12 as previously described, with the addition of 500 nM hydrocortisone solution. Medium was changed every two days and transendothelial electrical resistance (TEER) was measured daily from day 2 of culturing onwards to determine the optimum combination of cell layers in the BBB model.

TEER was measured by impedance spectroscopy using a Flocel TEER Measurement Unit (Flocel Inc. Ohio, USA) with STX-2 chopstick electrodes (World Precision Instruments, Florida, USA). TEER values were expressed as Ωcm^2. A blank surface-coated well was used as a control and subtracted from all TEER values obtained prior to reporting.

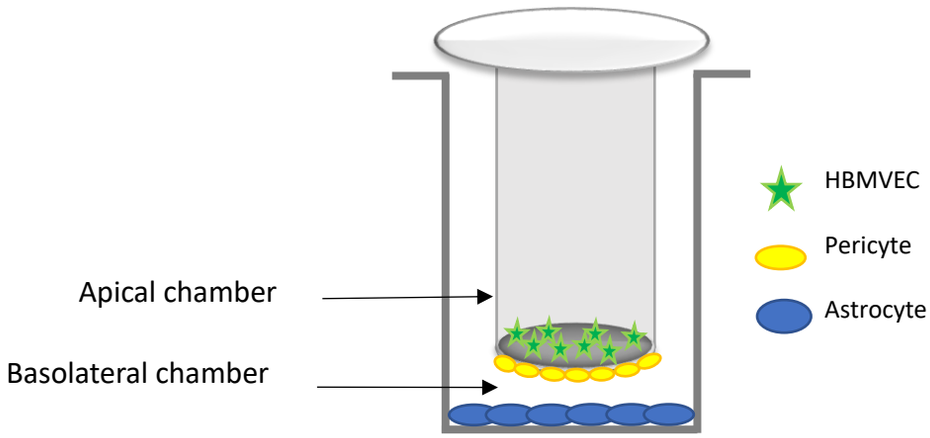

Figure 5.2. Diagrammatic representation of a triple culture *in vitro* BBB model, including human brain microvascular endothelial cells (HBMVEC), pericytes and astrocytes.

To ensure adherence of cells to the polycarbonate membrane of the Transwell insert, membranes with either cultured pericytes, astrocytes or HBMVEC were stained to visualise under a light microscope. Inserts were soaked in 100% ethanol for 5 minutes, stained with 1% eosin solution for 1 minute, washed and then stained again with 0.1% haematoxylin solution for 5 minutes. Membranes were then washed, cut from the insert and mounted onto a glass slide to be visualised at x 20 000 magnification.

5.2.6. Western blot detection of Claudin-5 and ZO-1 levels in HBMVEC

After 5 days of culture in Transwell vessels, HBMVEC were harvested from the polycarbonate inserts with lysis buffer and adjusted to an approximate equal concentration of protein for each sample using a BCA assay, to ensure fair sample concentrations of cells. Any samples found to have an abnormally higher protein content were diluted with lysis buffer.

Briefly, cells were scraped into 50 µL of cold lysis buffer and left on ice for 20 minutes. Samples were then centrifuged at 150*g* for 5 minutes, after which supernatant was removed and frozen until ready for analysis.

Western blotting was used to detect levels of Claudin-5 (MW 23 kDa) and ZO-1 (MW 195 kDa), important tight junction proteins which indicate the formation of tight junctions within the endothelial cell layer of the BBB. Cell lysates were prepared for SDS-PAGE by boiling 30 µL with 6 µL of 5x Laemmli sample treatment buffer for ten minutes. Cell proteins were separated by gel electrophoresis using a 4-12% NuPage bis-tris gel and MES running buffer prior to western blotting. The western blot was first blocked with a 5% BSA solution in tris-buffered saline (TBS) for one hour and then washed thrice with TBS for 5 minutes. Anti-claudin-5 mouse monoclonal antibody (200 µg/mL) or anti-ZO-1 rabbit polyclonal IgG antibody (200 µg/mL) were diluted 1:400 in TBS before incubating with the nitrocellulose for 90 minutes at room temperature with gentle shaking. The nitrocellulose was then washed as before, prior to incubation with either a goat anti-mouse (for Claudin-5) or goat anti-rabbit (for ZO-1) alkaline phosphatase secondary antibody (1:30 000 dilution) for a further 90 minutes at room temperature. After washing for a final time, the western blot was developed by addition of alkaline phosphatase substrate BCIP®/NBT solution until protein bands were visible.

To provide a further control for cell concentration in each sample, western blots were stripped for 10 minutes with stripping buffer and subsequently re-probed for actin (MW 42kDa), a common and abundant cell protein. Anti-actin mouse monoclonal IgG antibody (200 µg/mL) was diluted 1:400 in TBS and the process was repeated as for Claudin-5 and ZO-1 detection. Each band was quantified by densitometry on a G:Box chemi XRQ imaging system (Syngene, Cambridge, UK) using Genetools and Genesys software.

5.2.7. Effect of targeting peptides RDP and DAS on NP uptake across a BBB model

The optimum BBB model selected for uptake studies was determined by the work carried out in section 5.2.5. The Transwell culture vessels were prepared as a triple culture of astrocytes, pericytes and HBMVEC according to the protocol previously described, however the poly-L-lysine coating on the upper surface of the inserts was changed to 0.1 mg/mL fibronectin, in attempt to maintain better barrier integrity in NP treatment assays. The BBB model was cultured until day 4 after assembly (37°C/5% CO_2), at which point the TEER was measured in each well. Only wells with TEER measurements of at least 150 Ωcm^2 were selected to commence NP uptake studies on day 4.

5.2.7.1. Analysis of FITC NP uptake in BBB model

FITC-loaded NP (FITC NP), RDP-conjugated FITC NP (RDP-FITC NP) and DAS-conjugated FITC NP (DAS-FITC NP) were diluted from stock suspensions of 10 mg/mL in PBS to 0.5 mg/mL in serum-free DMEM/F12. Existing culture medium was removed from the apical (upper) compartment of the BBB model and replaced with 100 µL of NP treatment. Cells were incubated at 37°C/5% CO_2 and samples of 300 µL were taken at 2 hours and 24 hours post treatment from the basolateral (bottom) compartment and replaced with fresh BBB medium. TEER was measured before each sample was taken to monitor barrier integrity in response to the treatment. Following 24 hours, all inserts and media were removed from the plate. The astrocytes remaining in the bottom wells were subsequently washed twice with sterile PBS and then lysed. Ice cold lysis buffer (300 µL) was added to cells for 20 minutes before mixing and centrifuging at 150*g* for 5 minutes. The supernatant from lysed astrocytes was transferred to a Corning Costar microtiter plate and assessed for FITC fluorescence emission on an Omega FLUOstar plate reader (excitation 485 nm, emission 520 nm).

5.2.7.2. Analysis of ICG NP uptake in BBB model

ICG-loaded NP (ICG NP), RDP-conjugated ICG NP (RDP-ICG NP) and DAS-conjugated ICG NP (DAS-ICG NP) were diluted from stock suspensions of 10 mg/mL in PBS to 1 mg/mL in serum-free DMEM/F12. To observe the effect of RDP and DAS on NP movement across the BBB model, RDP-ICG NP and DAS-ICG NP would also be incubated with the respective free peptide to provide competition for receptor binding. An approximate equivalent concentration of free RDP (50 mcg/mL) or DAS (44 mcg/mL) were added to the BBB model and incubated at 37°C/5% CO_2 for 20 minutes prior addition of NP treatment.

TEER was monitored and samples of BBB media were taken as described in section 5.2.7.1 (Chapter 4) at 2 hours and 24 hours post treatment. Following 24 hours of incubation (37°C/5% CO_2), all media was aspirated to allow gentle washing of individual inserts and wells with PBS. Following washing, astrocytes in the bottom of the well and pericytes on the underside of the inserts were imaged for ICG fluorescence (excitation 780 nm, emission 820 nm) *in situ* using a VivoVision IVIS Lumina imaging system (Xenogen, California, USA) with Living Image 3.2 software. The BBB media samples collected were also analysed after addition to a 96 well plate. Regions of interest on fluorescence images were quantified in photons/second/cm^2/steradian (p/sec/cm^2/sr).

5.2.8. Statistical analysis

All results reported were statistically analysed using either an unpaired two-tailed t-test or a two-way ANOVA with post-hoc tests. A P-value of < 0.05 was considered statistically significant.

5.3. Results and Discussion

5.3.1. Development of an in vitro BBB model

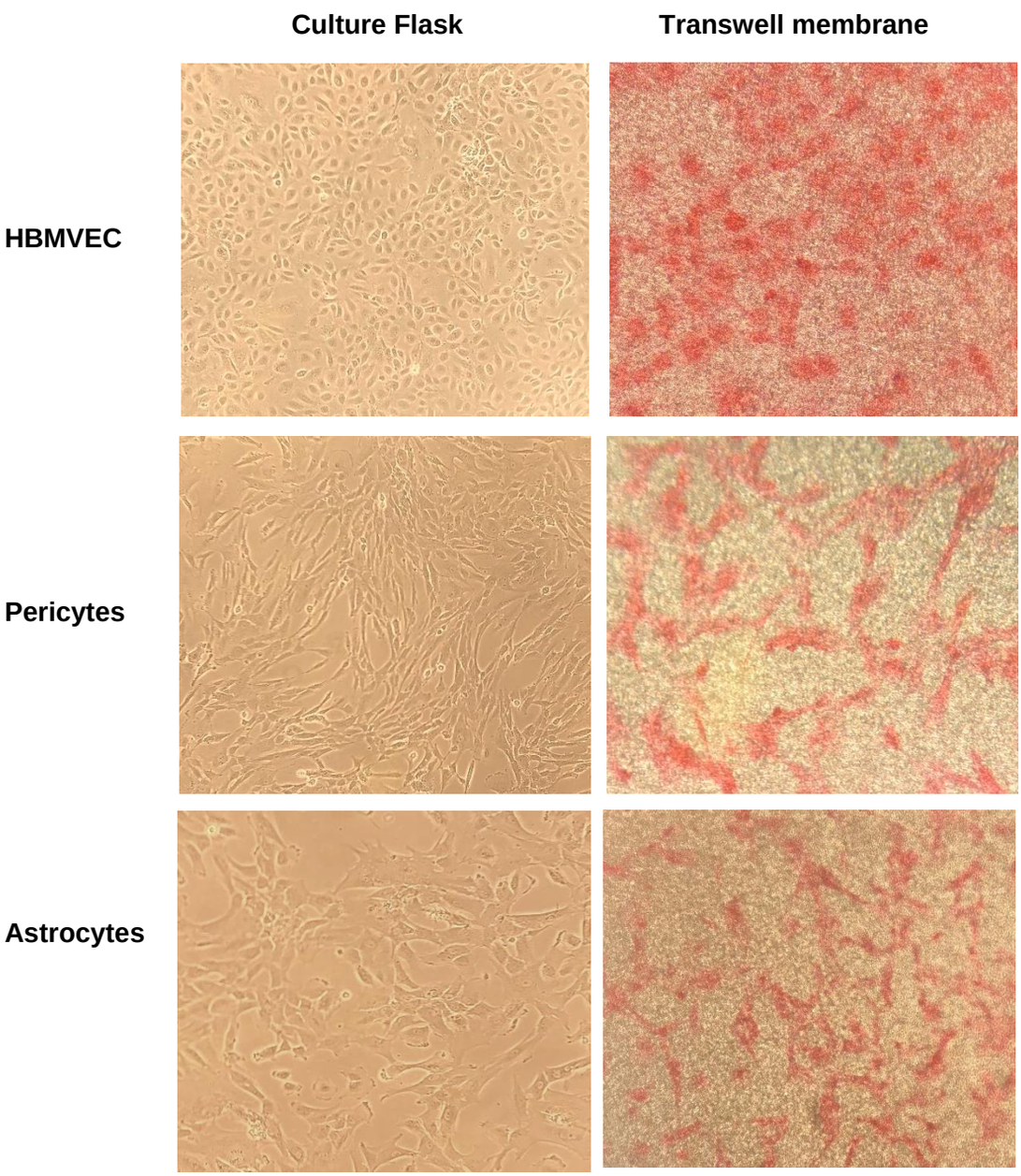

Figure 5.3. Images of BBB cells in culture (left column) and following staining to confirm adherence to the Transwell membrane (right column). Images are shown at x 20 000 magnification.

HBMVEC were cultured in Transwell inserts with different combinations of microglial BBB astrocytes and pericytes, integral components of the human BBB. All three cell types used could successfully adhere to the Transwell membrane and proliferate under culture conditions, observed from the images displayed in Figure 5.3. Seven different BBB models were constructed to investigate the optimal conditions for induction of endothelial barrier properties, as illustrated in Figure 5.4. TEER values of all constructs were monitored over 6 days and showed a steady increase starting from day 2 until day 5. After peaking at day 5, TEER values appeared to decrease for all combinations of cells on day 6. It was therefore determined that 5 days of culture produced the optimal TEER value (Figure 5.5).

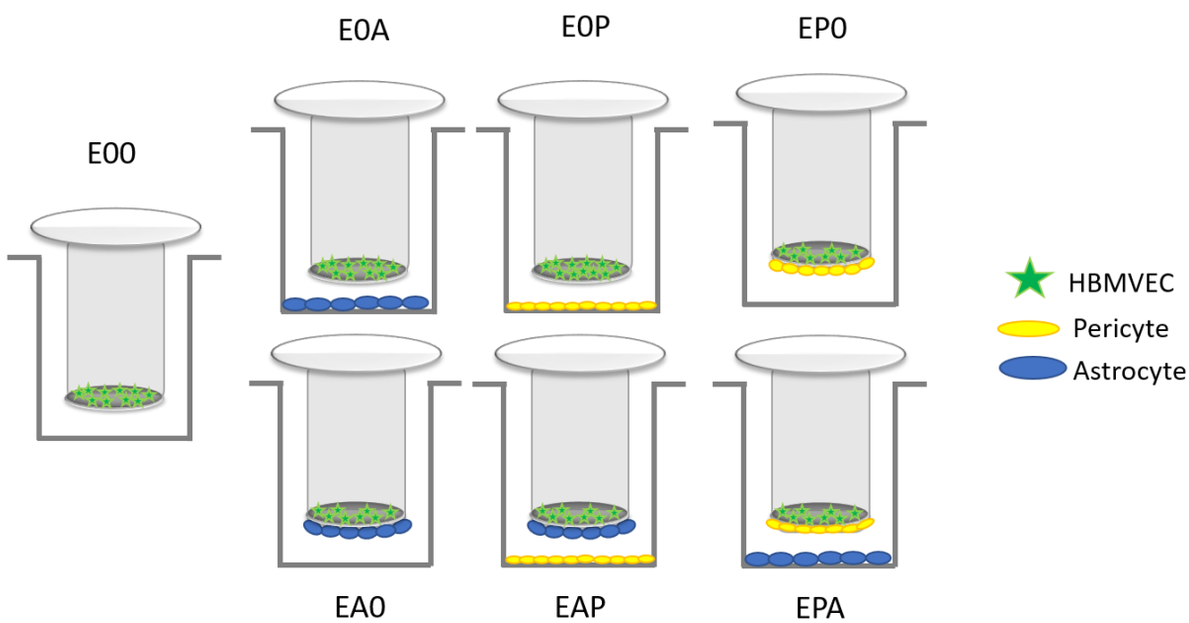

Figure 5.4. Diagrammatic representation of *in vitro* human BBB model constructs using human brain microvascular endothelial cells (HBMVEC) as the apical layer, with different combinations of astrocytes and pericytes in the basolateral chamber. A monoculture model of HBMVEC only (E00) was developed alongside double (E0A, E0P, EA0 & EP0) and triple culture (EAP & EPA) models to determine the optimal composition of cells for induction of barrier properties. E= HBMVEC, P= human pericytes, A= human astrocytes and 0= no cells.

The TEER of the E00 monoculture model containing only HBMVEC peaked at 95 Ωcm^2 after 5 days of incubation. It was evident from the results displayed in Figure 5.5 that both triple culture BBB models (EAP and EPA) consisting of HBMVEC, astrocytes and pericytes provided the highest TEER values. Only the EPA model however, had significantly higher TEER values (P value <0.01) than the monoculture E00 model at days 4 and 5. A maximum TEER value of 184 Ωcm^2 was reached in the EPA model after 5 days, shown in Figure 5.5A, where pericytes were in direct physical contact with the membrane and HBMVEC on the upper surface. In Figure 5.5B, the EAP model had a maximum TEER of 120 Ωcm^2. In the literature, there is evidence that primary cell-based triple culture systems (Nakagawa et al., 2007; 2009; Wisniewska-Kruk et al., 2012) develop better overall barrier-like properties and TEER values in comparison to monocultures, co-cultures and immortalised cell lines (Li et al., 2010).

Similar to findings reported by Banks et al. (2018), there was no significant improvement in TEER observed with any of the double co-culture models compared to the monoculture E00 model. The addition of both astrocytes and pericytes to the *in vitro* BBB model was therefore required for optimal barrier conditions. It was determined from these results that the most promising *in vitro* BBB model was the EPA triple culture, as it not only reached a TEER of above 150 Ωcm^2, but the organisation of cellular layers had significantly higher resistance across the *in vitro* membrane than the EAP model.

(A)

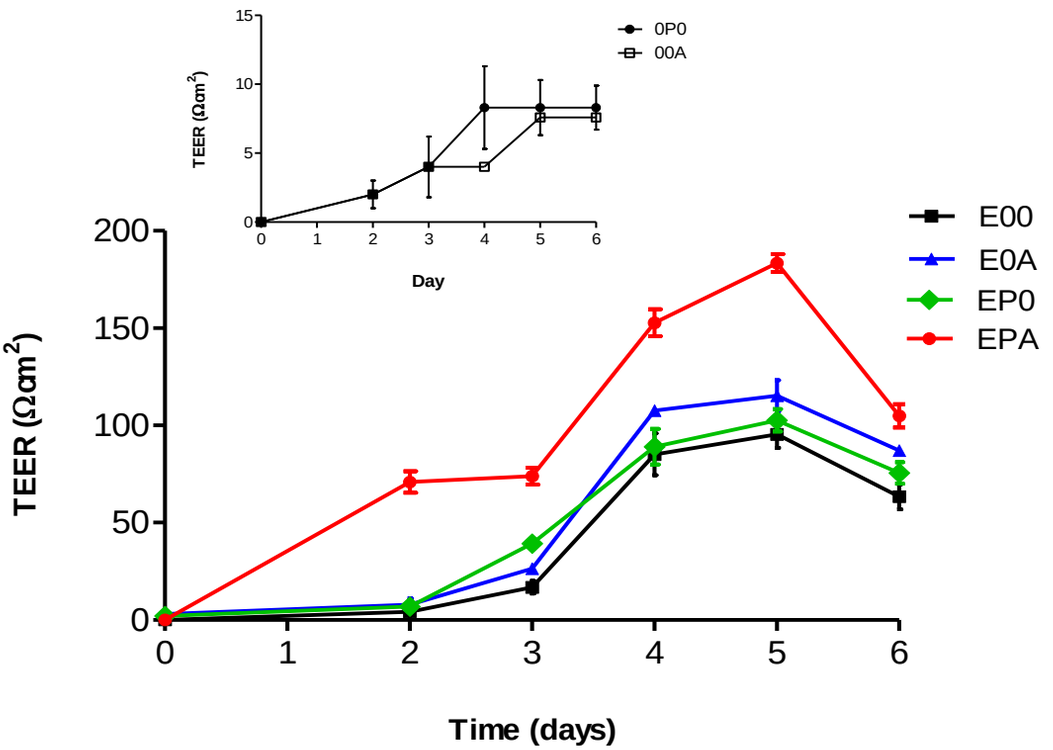

(B)

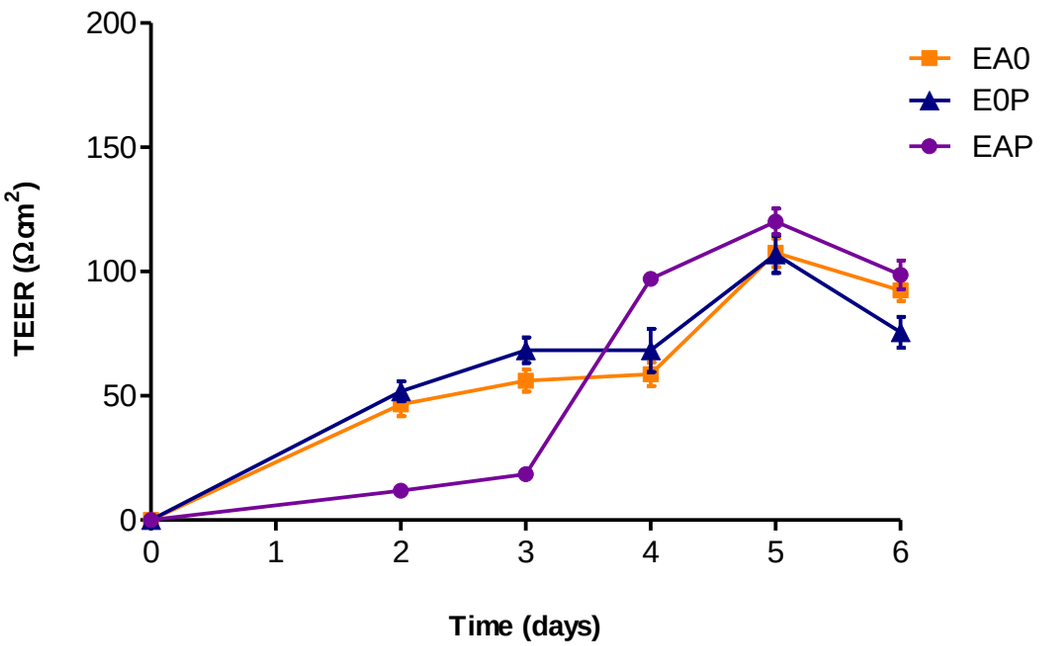

Figure 5.5. Transendothelial electrical resistance (TEER) values of different BBB models over 6 days. The organisation of cellular layers within the *in vitro* BBB models were investigated for optimal arrangement with either no cells, (A) pericytes or (B) astrocytes in direct contact with the endothelial layer. All measurements were recorded in triplicate ± standard deviation (n=3). Statistics were carried out using a two-way ANOVA with post-hoc analysis.

It is generally accepted that for drug transport studies, *in vitro* cell-based BBB models should have a restrictive paracellular barrier with a TEER measuring at least 150 Ωcm^2 (Gaillard & de Boer, 2000). *In vivo*, pericytes are in direct contact with up to 70% of the abluminal endothelial surface, all of which is then overlaid with astrocyte end-feet (Giannoni et al., 2018). Cell architecture should also be as realistic to *in vivo* conditions as possible (Gumbleton & Audus, 2001), further supporting the use of the EPA model.

Pericytes are key in the establishment of the BBB from embryogenesis (Daneman et al., 2010). They are associated with tight junction formation, differentiation of endothelial cells, regulation of microvascular permeability and provide structural support from the early stages of development (Balabanov & Dore-Duffy, 1998; Armulik et al., 2010). Astrocytes, produced at a later stage, are believed to have a complex role in barrier maintenance and regulation of endothelial cell physiology and permeability via chemical signalling (Abbott, 2002). It is the cross-communication between these cells and others of the NVU, such as neurons and microglia (Banks et al., 2018), which induce the unique characteristics of BBB endothelial cells (Hawkins & Davis, 2005). Chemo-modulators such as cytokines and prostaglandins have been identified *in vitro* as mediators of NVU communication (Kovac et al., 2011), the highest levels of which have been found in triple culture *in vitro* models (Banks et al., 2018). Indeed, the generation of a functional BBB *in vivo* is dependent on multi-cellular interactions, which has been reflected by *in vitro* investigations.

Only endothelial cells can adopt barrier-like properties and this was shown in Figure 5.5A when a monoculture of pericytes or astrocytes alone failed to show any considerable development of resistance across the membrane. After 6 days of culture, TEER values reached between 5-10 Ωcm^2 for both cell types, however this can probably be attributed to an over-confluent cell layer rather than any true resistance.

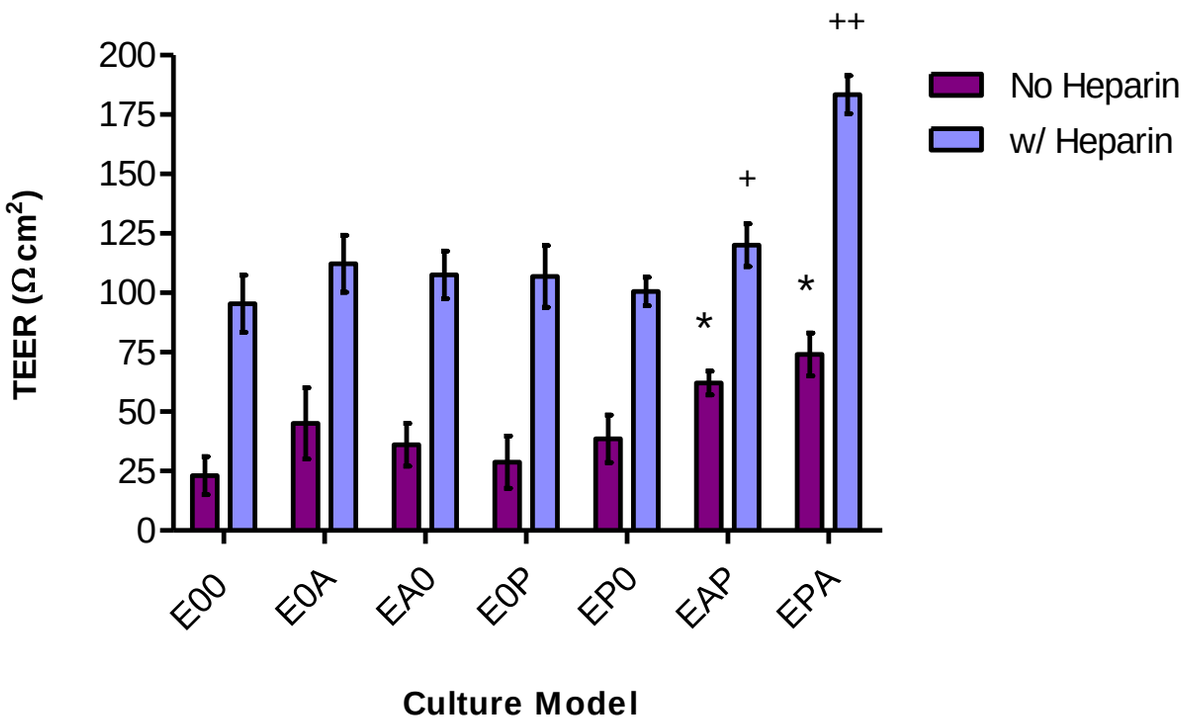

Figure 5.6. Graph showing peak TEER values of BBB models on day 5 of culture, with and without the addition of heparin to the culture medium. All measurements were recorded in triplicate ± standard deviation (n=3). P values from two-way ANOVA with post-hoc analysis considered statistically significant if < 0.05. */ $^{+}$ Statistically significant difference compared to respective monoculture (E00) model. $^{++}$ Statistically significant difference compared to EAP model (with heparin).

Figure 5.6 also shows the difference in TEER values obtained at peak day 5 when heparin is not included in the culture medium. In the monoculture BBB model of HBMVEC (E00), TEER increased almost 4-fold from 23.8 Ωcm^2 to 95.37 Ωcm^2 when cultured in medium containing heparin (P value < 0.001). Caldwell et al. (2004) previously reported that inclusion of heparin in culture medium greatly improves the *in vitro* stability of the mitogen, basic fibroblast growth factor (bFGF), improving receptor binding and hence cell growth. The use of heparin as part of the BBB medium proved to be essential in obtaining a satisfactory TEER for drug transport studies, as it induced a more resistant endothelial layer in the EPA model to above the threshold value

of 150 Ωcm^2. In all cases, the use of heparin significantly increased the TEER value of each BBB model (P values < 0.001) and therefore it was included in further studies.

5.3.2. Detection of tight junction proteins Claudin-5 and ZO-1

HBMVEC were harvested from BBB models after 5 days of culture and tested for expression of claudin-5 and ZO-1 proteins using western blotting, results of which are shown in Figure 5.7. It is evident from Figure 5.7A, that the most visible bands for claudin-5 and ZO-1 were detected in the triple culture models EPA and EAP. There appears to be a greater amount of claudin-5 detected in HBMVEC when they are in direct contact with astrocytes (EA0) in the double culture model, compared to pericytes (EP0). In contrast, ZO-1 levels are higher in the double culture when pericytes are in direct contact with the HBMVEC layer. Astrocytes and pericytes may have different roles in the formation of tight junctions at the BBB endothelium. It is clear from these results, that expression of tight junction proteins in HBMVEC is promoted when in direct contact with astrocytes or pericytes, and even more so when both cell types are included in the culture.

Relative to E00, the EPA and EAP models showed significantly higher levels of claudin-5, 1.58 and 1.47 respectively, as detected by densitometry (Figure 5.7B). The relative levels of ZO-1 in the triple culture models compared to the E00 model were even greater. Relative expression of ZO-1 in the EAP model was 1.80 and for the EPA model was 2.16. It can also be observed from the western blot images in Figure 5.7A that actin levels were consistent, meaning that variations in claudin-5 or ZO-1 were not due to unfair differences in protein loaded onto the blot. To further support this, actin bands were quantified using densitometry and subsequently tight junction protein results were normalised for ratio of actin compared to the E00 model.

(A)

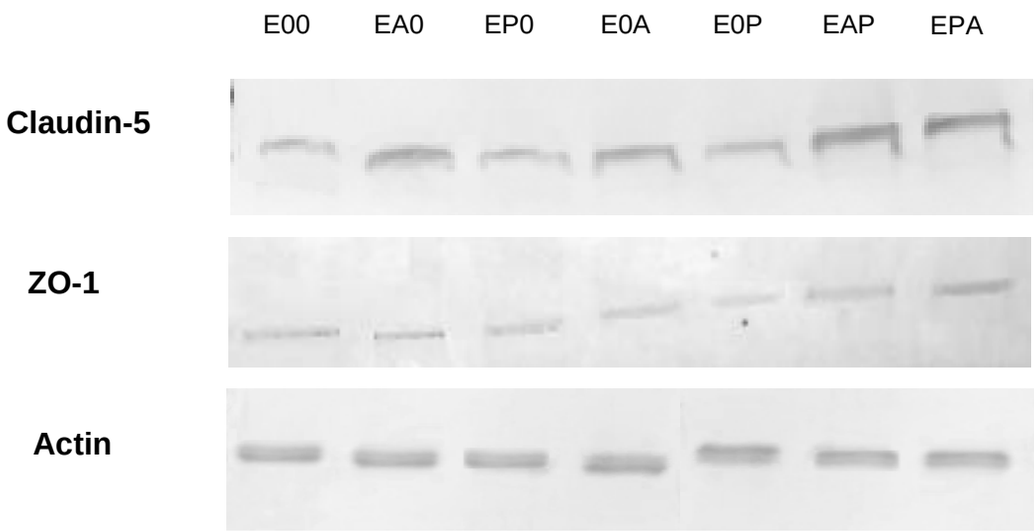

(B)

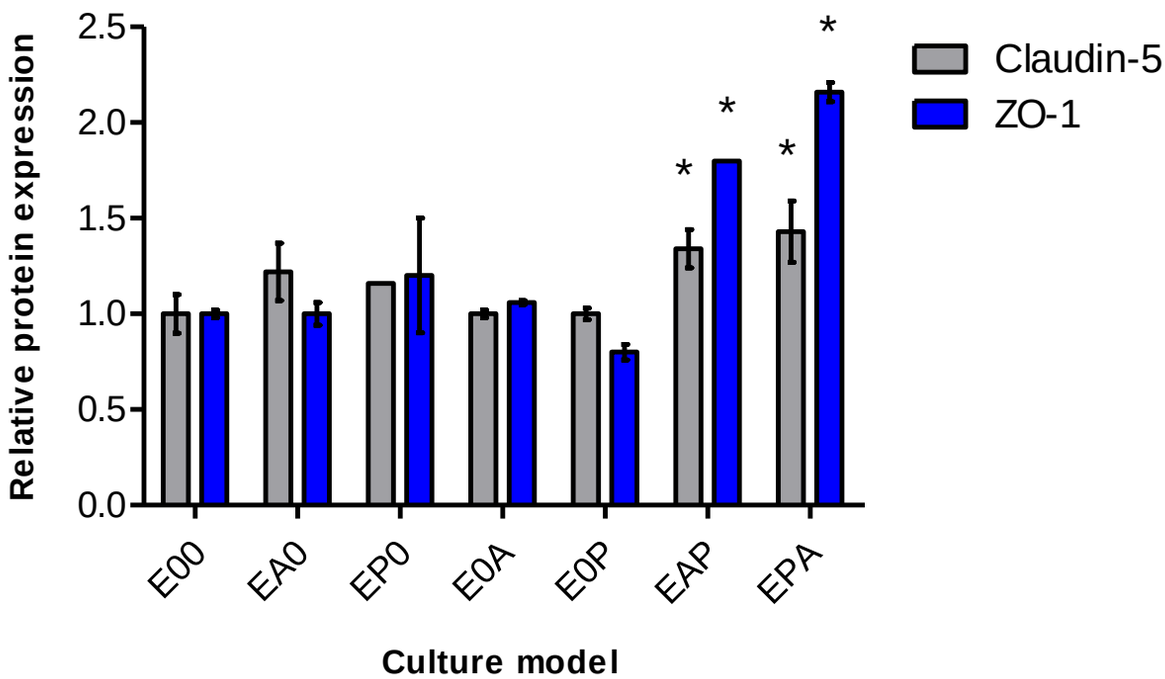

Figure 5.7. (A) Western blot showing detection of tight junction proteins claudin-5 and ZO-1 alongside actin in human brain microvascular endothelial cells (HBMVEC) after 5 days of culture in different blood brain barrier (BBB) models. HBMVEC were either cultured alone (E00), in double culture with either astrocytes and pericytes (E0A, EA0, E0P & EP0) or triple culture with both astrocytes and pericytes (EAP & EPA). **(**B**)** Graph showing the relative expression of claudin-5 and ZO-1 in different BBB models detected by densitometry of the western blot. * Statistically significant difference compared to respective E00 model (two-tailed T-test P value <0.05). Error bars ± standard deviation (n=3).

Claudin is a fundamental constituent of intercellular tight junctions (Chiba et al., 2008). Claudin-5, occludin and junctional adhesion molecule (JAM-1) are three TJ-specific transmembrane proteins which have been found co-localised with peripheral zonula occludens protein (ZO-1) in human brain microvasculature (Vorbrodt & Dobrogowska, 2004). Claudin-5 and ZO-1 expression are therefore key markers for detecting the induction of barrier characteristics in endothelial cells of *in vitro* BBB models. It has been found that the combination of pericytes and astrocytes in triple cultures induce expression of more tight junction proteins at the inter-endothelial cell surface (Banks et al., 2018), rather than in the cytoplasm, as has been observed for monocultures (Stamatovic et al., 2005). This contributes to tight junction formation, inhibition of paracellular transport and increase in barrier resistance. The EPA model reported herein generated the highest TEER and expression of tight junction proteins claudin-5 and ZO-1, comparable to the rat-based *in vitro* model described by Nakagawa et al. (2009).

5.3.3. Effect of neural cell targeting peptides, RDP and DAS, on in vitro BBB model

PLGA NP were successfully prepared incorporating either ICG or FITC-dextran as a payload. Characterisation properties, including release profile of FITC-dextran NP, are previously reported in sections 3.3.1- 3.3.2 (Chapter 3). Properties of ICG-loaded NP (ICG NP) are detailed in Table 5.1, which shows an average NP size of 293.50 nm (± 1.70 SD) which is consistent with sizes measured previously when loaded PLGA NP are prepared by this method (chapters 2-4). Other parameters such as PDI (0.36 ± 0.09 SD) and zeta potential (-7.50 mV ± 0.2 SD) also remained similar to results previously obtained. Water-soluble ICG (MW 774.96) had an entrapment efficiency of 40% when loaded into PLGA NP (2% loading) by the double emulsion method, comparable to doxorubicin (MW 543.52) in section 2.3 (Chapter 2). Both peptides were surface conjugated to ICG NP with coupling efficiencies of 66.9% and 87.6% for RDP and DAS respectively. Both FITC-dextran and ICG-loaded NP to be tested in the BBB model were of a very similar size and zeta potential.

Table 5.1. Characterisation of polymeric PLGA nanoparticles loaded with small molecule cyanine dye ICG (MW 774.96).

Characterisation Parameter	ICG NP
Size (d.nm)	293.50 ± 1.70
Zeta potential (mV)	-7.50 ± 0.20
Polydispersity Index (PDI)	0.36 ± 0.09
ICG content (µg/mg)	7.92 (40.0% EE)
RDP conjugation (µg/mg)	50.15 (66.9% CE)
DAS conjugation (µg/mg)	43.82 (87.6% CE)

The release profile of ICG (Figure 5.8) shows that in distilled water at 37°C, a controlled release is displayed under sink conditions over 7 days, at which point around 30% of the maximum payload is released. The peripheral attachment of RDP or DAS to the NP surface slowed down ICG release which was significant in comparison to the unlabelled ICG NP by day 7 (P values < 0.05). This is possibly due to steric hinderance, especially as release from RDP-ICG NP is lower than those surface-coated with the smaller peptide, DAS, over the first three days of incubation. Importantly, no ICG release could be detected from RDP-ICG NP and only 1% from DAS-ICG NP after 24 hours. This was desirable to ensure free drug interference with BBB assay results was as limited as possible, as unlike FITC-dextran, ICG is freely cell permeable.

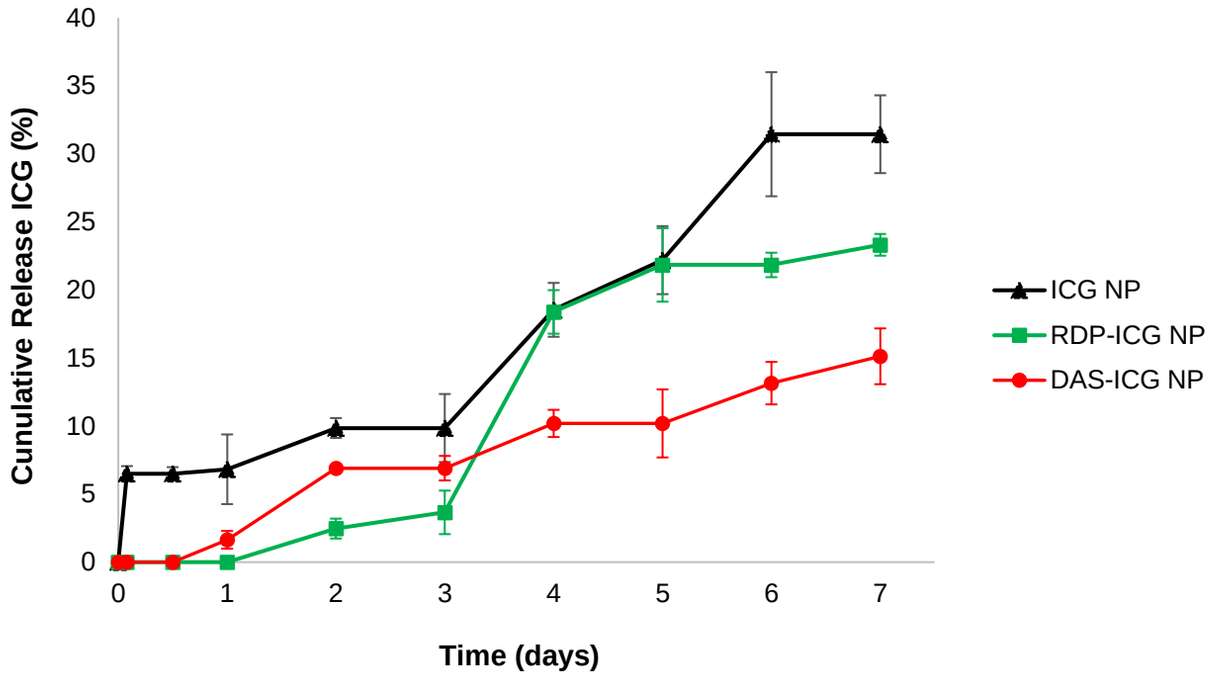

Figure 5.8. Graphs showing the release of ICG from PLGA nanoparticles (NP) at 37°C in double distilled water over a period of 7 days ± standard deviation (n=3). The effect of RDP and DAS surface attachment on the release profile is shown. Statistical analysis was performed using a two-way ANOVA with post-hoc analysis.

Figure 5.9 shows the result of different FITC NP treatments on the triple culture *in vitro* BBB model after 24 hours of exposure at 37°C. Upon sampling the media in the bottom or basolateral compartment of the BBB model wells after 2 and 24 hours (Figure 5.9A), significantly more FITC fluorescence was detected in those samples treated with DAS-FITC NP than when treated with unlabelled FITC NP (P value <0.05). At the 24-hour time point, this was also the case for RDP-FITC NP.

Astrocytes, the lowest cellular layer of the BBB model, were harvested and tested for fluorescence signal of FITC after 24 hours (Figure 5.9B). Again, significantly higher emission

was detected in those treated with both RDP- and DAS-conjugated NP compared to FITC NP-treated cells, where no fluorescence was detected.

The decrease in fluorescence detected in BBB medium from 2 hours to 24 hours is probably due to FITC NP uptake from the medium into the astrocytes for the RDP-FITC NP and DAS-FITC NP treatment groups. The detection of fluorescence after FITC NP treatment in the basolateral media at 2 hours incubation, but little after 24 hours and none in the astrocytes, is possibly due to free FITC-dextran, which perhaps leached from the NP across the barrier and then was removed upon sampling. Other explanations of this anomalous result are that unlabelled NP may have been taken up by endothelial cells and free FITC-dextran released across the membrane. Alternatively, despite the consistent TEER values, there may have been an intercellular gap in the endothelial layer which allowed passage of FITC NP from upper to lower compartment. Any of these possibilities may explain why fluorescence was observed in the medium at an early stage but not in the astrocytes after unlabelled NP treatment.

(A)

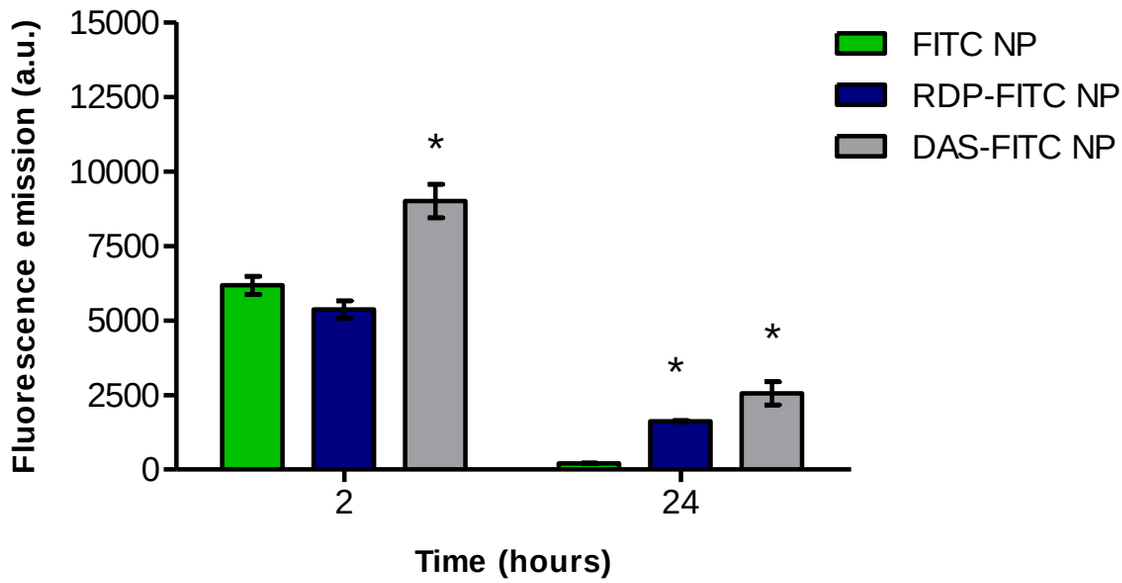

(B)

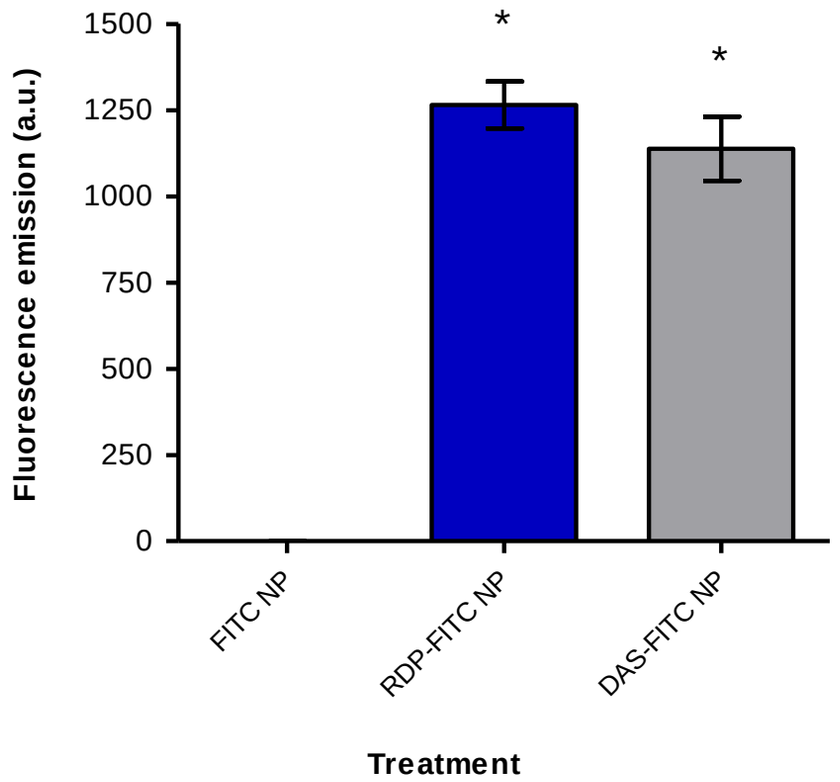

Figure 5.9. (A) FITC-dextran fluorescence detected in the basolateral media (bottom chamber) of the BBB model at 2 and 24 hours post addition of different NP preparations and (B) lysate from the astrocyte layer of cells of the BBB model triple culture (EPA). * Statistically significant difference compared to unlabelled FITC NP (two-tailed T-test P value <0.05, n=3).

FITC-dextran of high molecular weight (70 kDa) is largely considered cell impermeable due its size and presence of many hydroxyl groups. FITC conjugates are commonly used for drug transport and uptake studies (Agyare et al., 2008; Gil et al., 2012; McCarthy et al., 2015). If free drug is present in the cell medium it cannot be passively taken up into cells, especially over short periods of time. If the FITC NP with no attached peptide remained intact and crossed the endothelial layer and pericytes via cell mediated transport, it is likely that fluorescence would have also been observed in the lowest BBB layer of astrocytes as with the two targeted NP preparations. It is therefore more likely, that the fluorescence detected in the BBB media at 2 hours (Figure 5.9A) is due to a small gap in the barrier or free FITC-dextran release. It could be postulated that peptide conjugation somewhat protects the NP from intracellular degradation and hence a proportion of intact NP with targeting peptide can effectively pass two cellular layers (HBMVEC and pericytes) to accumulate in the final layer (astrocytes). Unlabelled NP of course can be taken up by cells, however the difference in cellular targeting ability over 24 hours is evident. The results demonstrate that peptide attachment to the NP is facilitating an accumulation of drug payload in the target cells, in comparison to the untargeted delivery vehicle.

The BBB retained integrity after addition of NP as TEER values were measured at 2 and 24 hours post treatment (Figure 5.10). The triple culture (EPA) BBB model showed not only maintenance, but improvement in TEER after 24 hours with all values greater than 200 Ωcm^2 irrespective of treatment group (P values < 0.001). The observed increase in TEER 4 to 5 days post preparation of the triple culture, is typical of an untreated BBB model, as was shown in Figure 5.5A. The addition of NP treatment therefore had no adverse effect on the integrity of this BBB model (P values > 0.05 comparing treatment groups to control at all time points) and endorses both RDP and DAS as active facilitators of safe NP transport across neural cell layers. Freese et al. (2013) also reported an increase in TEER after surface-modified NP treatment in a porcine *in vitro* BBB model. Freese and colleagues attributed this to the use of primary cells, which express more favourable barrier properties than immortalised cell lines as previously mentioned.

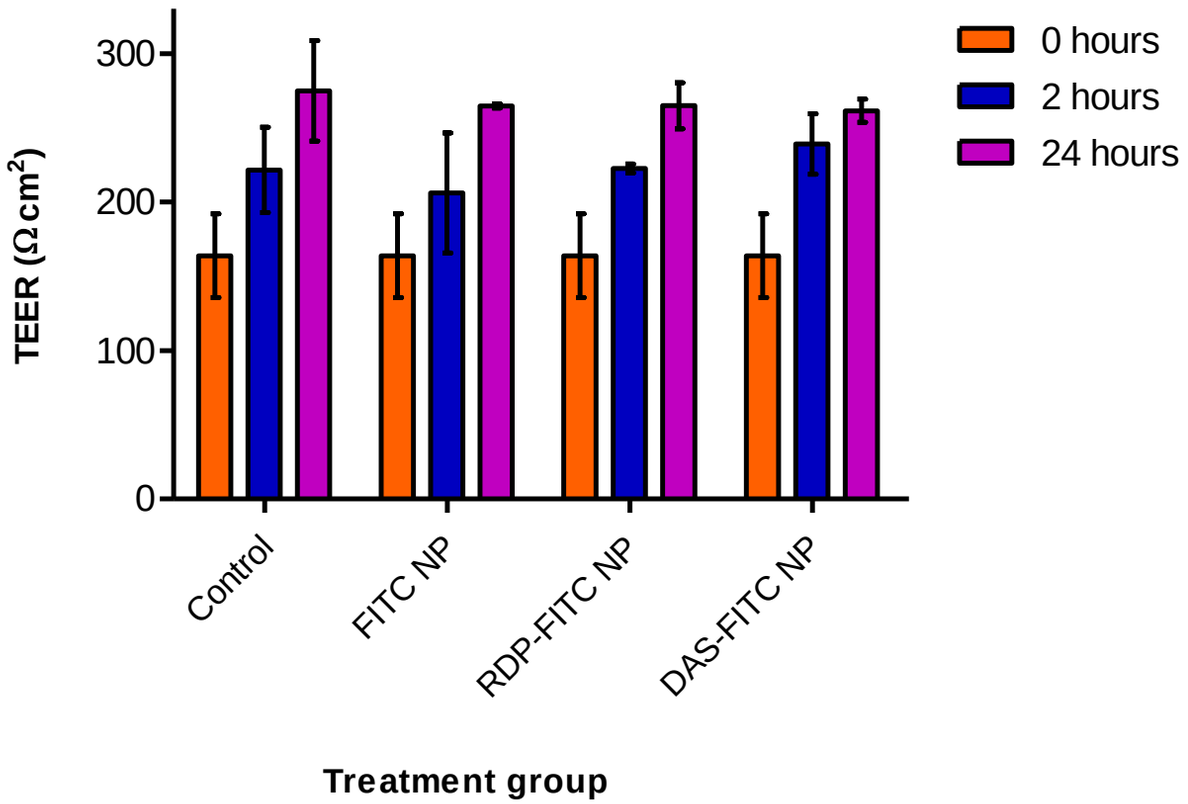

Figure 5.10. Graph showing monitored TEER values of *in vitro* BBB model before addition of NP followed by 2 and 24 hours post NP treatment. Measurements were recorded in triplicate (n=3) and reported as average TEER with error bars representing ± standard deviation. Statistical analysis was performed using a two-way ANOVA with post-hoc tests.

A similar assay to Figures 5.9 & 5.10 was carried out using ICG as the NP payload instead of FITC-dextran, the results of which are shown in Figures 5.11-5.14. This time, ICG fluorescence was measured semi-quantitatively in the middle pericyte layer, the basolateral BBB medium and the astrocytes at the same time points as for the FITC NP BBB assay. Additionally, the two peptide-conjugated NP preparations were co-incubated with corresponding free peptide to assess the effect, if any, on NP transport across the *in vitro* BBB model.

Due to the capability of the instrumentation to image BBB model cell layers *in situ*, ICG fluorescence emission was detected in the middle pericyte layer on the bottom of the Transwell insert (Figure 5.11). Images in Figure 5.11A and subsequent quantification of signal intensity in Figure 5.11B show that more ICG is present following treatment with RDP-ICG NP and DAS-ICG NP than untargeted ICG NP. It was demonstrated that the use of free peptide alongside peptide-targeted ICG NP has a profound negative effect on the amount of NP payload detected in cells. The signal pattern imaged for the ICG NP group in Figure 5.11A is suggestive of non-specific uptake into pericytes around the circumference of the Transwell membrane. The endothelial layer may be susceptible to gaps where the membrane attaches to the inserts, leading to leakage of NP through the membrane, as little fluorescence is seen in the centre of the well.

Assessment of BBB media at 2 hours post addition of NP treatment (Figure 5.12) show significantly higher detection of ICG fluorescence in the RDP-ICG NP and DAS-ICG NP groups than untargeted ICG NP. The amount of ICG fluorescence however, again significantly reduced on co-incubation with free peptide. At 24 hours, no significant ICG fluorescence could be detected in the media for any group (results not shown).

Figure 5.13 shows ICG fluorescence detected from astrocytes in the bottom of the BBB model well after 24 hours of incubation at 37°C. Upon imaging of these cells, there was considerably more ICG detected in astrocytes when NP were conjugated to new peptide, DAS, even compared with RDP. No ICG could be detected in the unlabelled NP treatment group (ICG NP), supporting the findings from Figure 5.9B. This was also the case for RDP-ICG NP when incubated with free RDP. Although there was still some evidence of ICG uptake in astrocytes when DAS-ICG NP were co-incubated with free DAS, the signal intensity was significantly diminished. The use of free peptide to compete with peptide-conjugated NP at potential binding sites displayed substantial inhibition of NP movement through the BBB model and hence the importance of RDP and DAS as targeting moieties is evident.

(A)

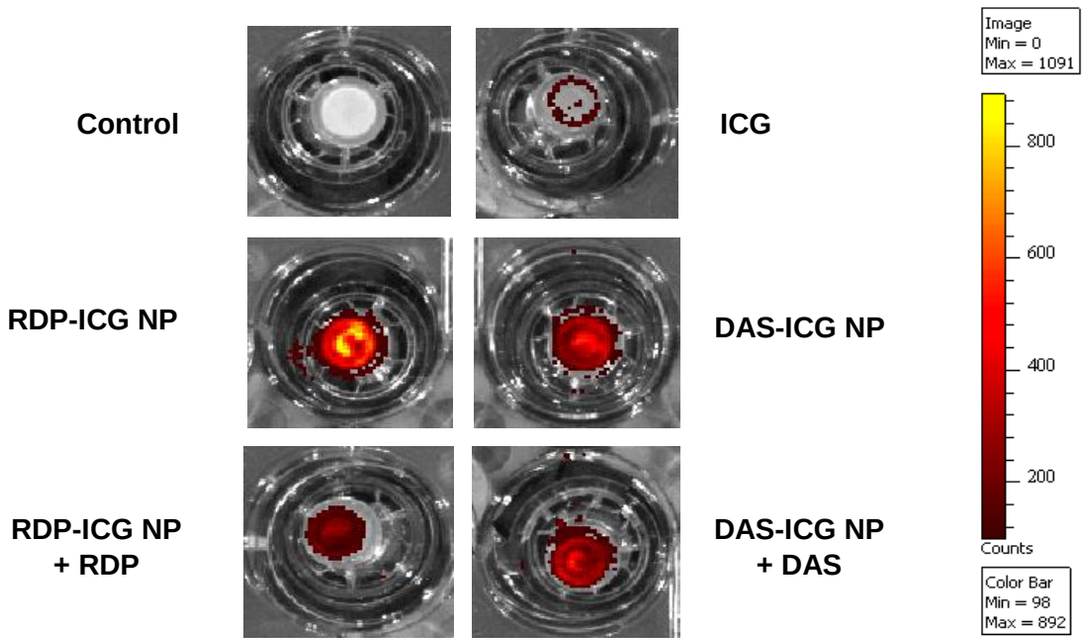

(B)

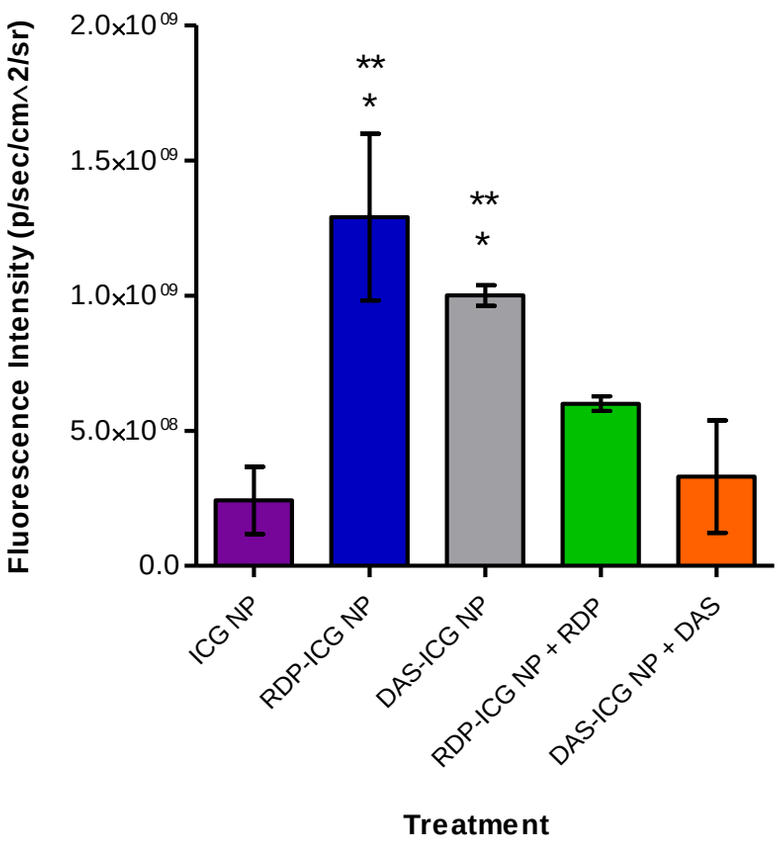

Figure 5.11. (A) Images and (B) graph showing ICG fluorescence detected from pericytes on the underside of Transwell inserts 24 hours post exposure to different NP treatments. *Statistically significant increase in fluorescence compared to all other treatment groups except DAS-ICG NP. $^{\alpha}$ Statistically significant increase in fluorescence compared to all other treatment groups except RDP-ICG NP. Two-tailed P value < 0.05 (n=3 ± SD).

(A)

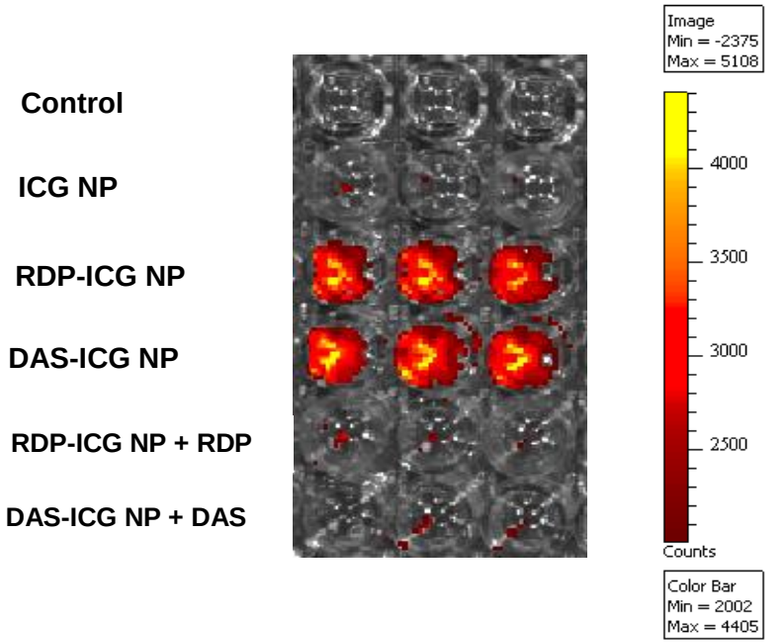

(B)

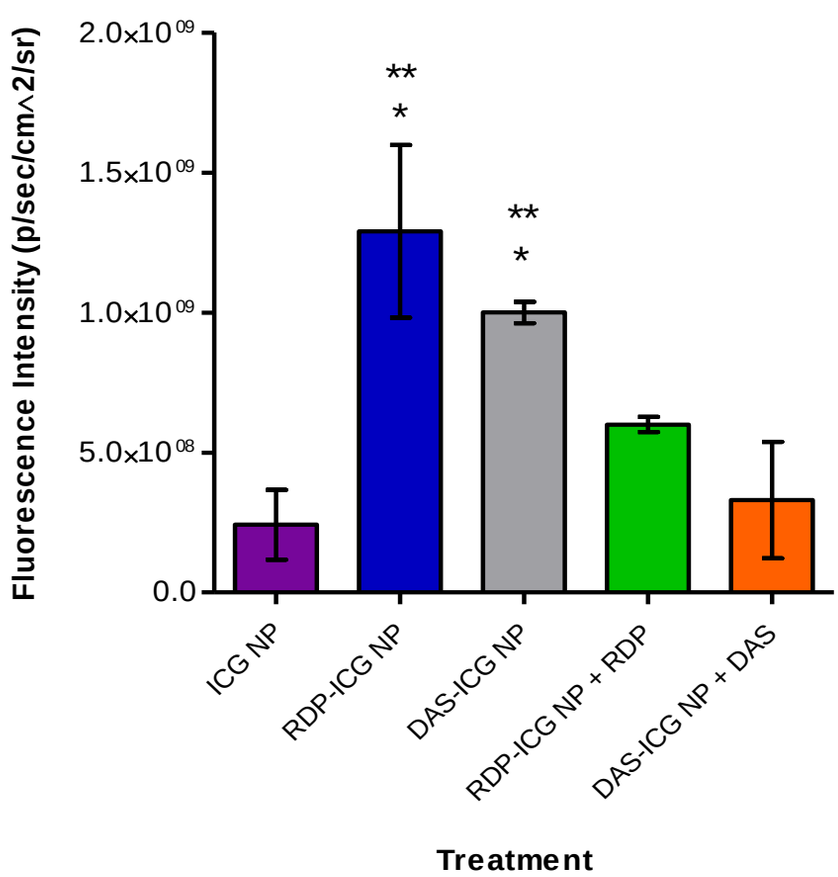

Figure 5.12. (A) Images and (B) graph of ICG fluorescence signal detected in the BBB model basolateral chamber media 2 hours post addition of different NP preparations to the Transwell insert (apical chamber). *Statistically significant increase in fluorescence compared to all other treatment groups except DAS-ICG NP. ** Statistically significant increase in fluorescence compared to all other treatment groups. Two-tailed P value < 0.05 (n=3 ± SD).

(A)

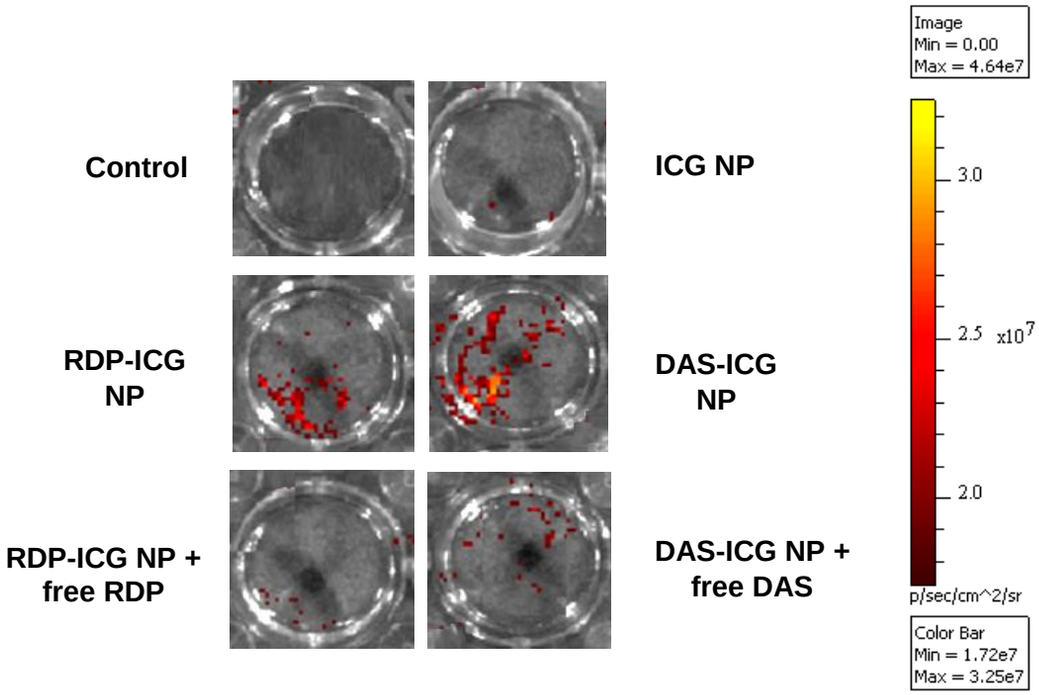

(B)

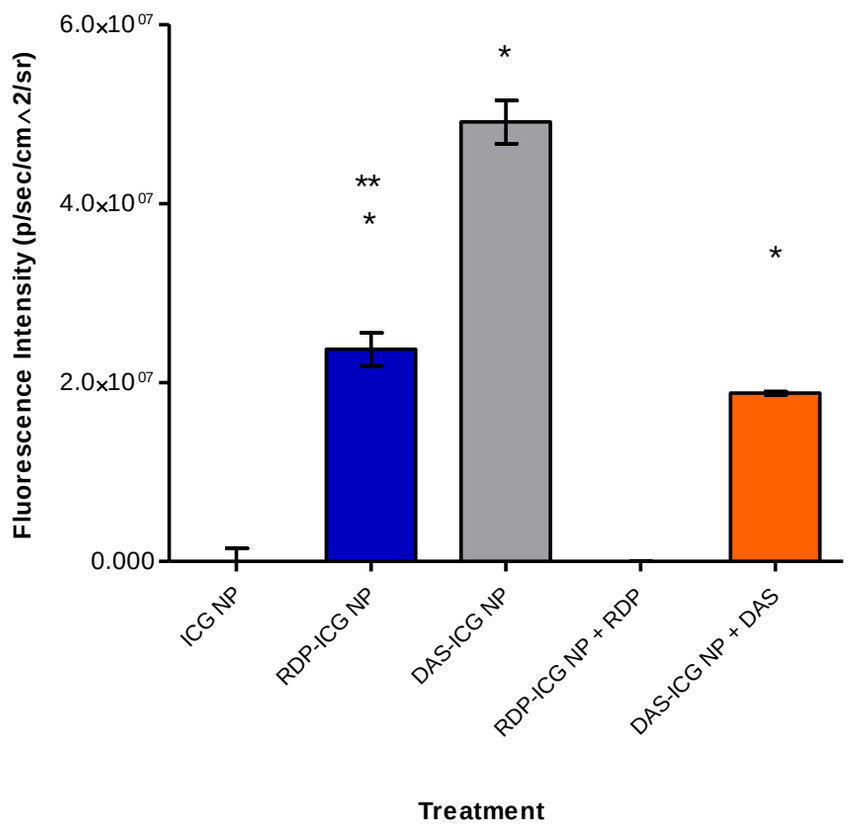

Figure 5.13. (A) Images and (B) graph of ICG fluorescence signal detected in astrocytes, the bottom layer of cells in the BBB model 24 hours post NP exposure. *Statistically significant increase in fluorescence compared to all other treatment groups except DAS-ICG NP. ** Statistically significant increase in fluorescence compared to all other treatment groups. Two-tailed P value < 0.05 (n=3 ± SD).

Table 5.2. Representation of ICG fluorescence detected in pericytes and astrocytes of *in vitro* BBB model after 24 hours of NP treatment.

Treatment	Apical to basolateral direction: Pericytes → Astrocytes
ICG NP	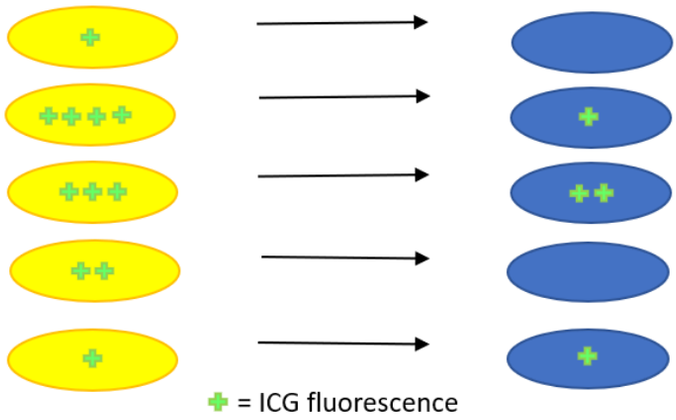
RDP-ICG NP	
DAS-ICG NP	
RDP-ICG NP + RDP	
DAS-ICG NP + DAS	

It appears that DAS may facilitate NP transport through the BBB model more effectively than RDP, due to higher levels of ICG being detected in the astrocyte layer when DAS is the targeting ligand. This is generally summarised in Table 5.2, which shows the location of ICG payload after 24 hours of NP treatment. Interestingly, no ICG fluorescence detected in the basolateral medium after 24 hours, suggests that the targeted NP preferentially accumulate in cells rather than in the medium. This could be a positive effect for prospective *in vivo* studies, as the peptide ligand might confer the ability of the payload to enter cells rather than remain in interstitial fluid. It could be postulated that further studies observing a period of time longer than 24 hours, might show a shift in accumulated payload from predominantly pericytes to astrocytes.

The fact there is no ICG detected in the astrocytes following ICG NP exposure, confirms the findings from Figure 5.8 that the NP do not leach payload over the time course observed. Furthermore, both peptides effectively facilitate NP transport in these neural cell types, most

likely by receptor-mediated mechanisms, due to the inhibition caused by competing free peptides. Song et al. (2017) reported on a triple culture rat brain-derived model of comparable TEER (200 Ωcm^2), where lactoferrin-targeted fluorescent payload was detected in the bottom cell layer. Similar to results from Figures 5.11-5.13, free ligand out-competed the conjugate leading Song and colleagues to propose a receptor-mediated endocytosis mechanism of transport.

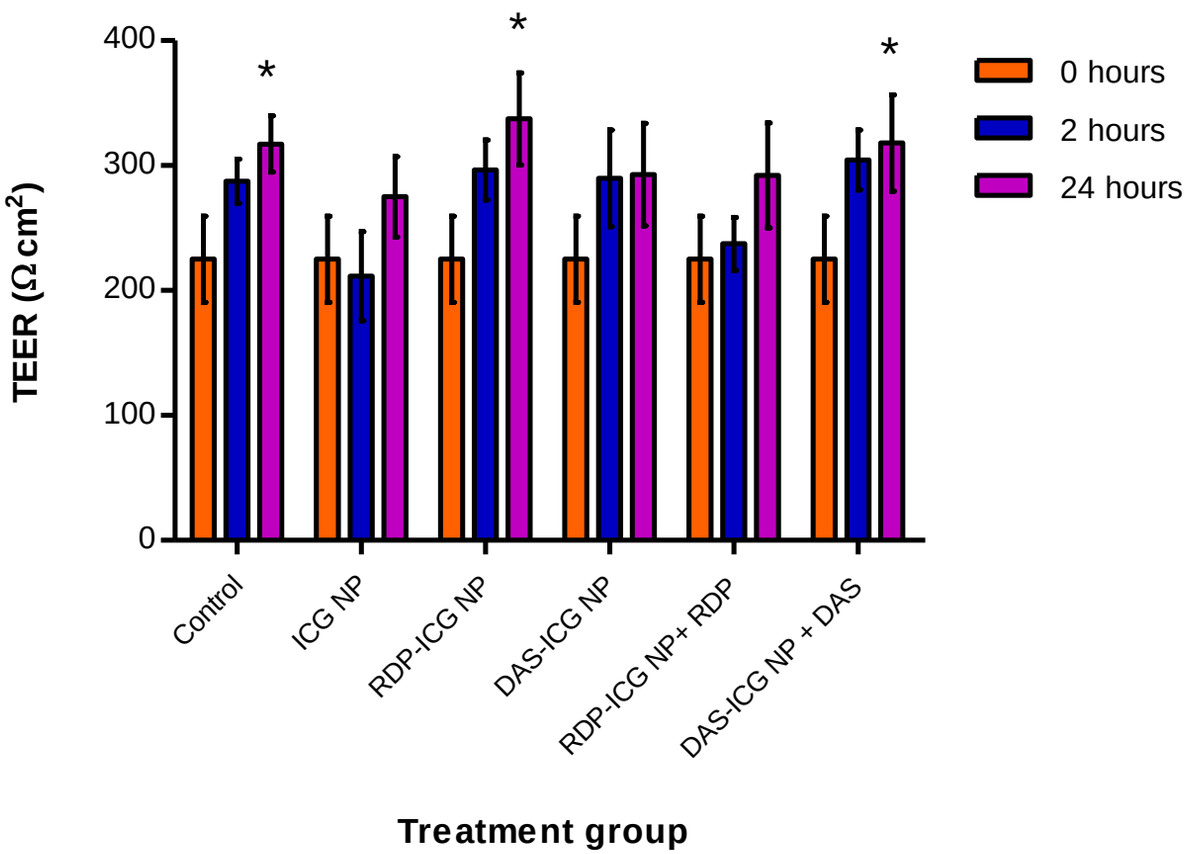

Figure 5.14. TEER values of BBB triple culture model (EPA) before, then at both 2 and 24 hours after addition of various ICG-loaded NP treatments. Measurements were recorded in triplicate (n=3) and reported as average TEER with error bars representing ± standard deviation. Statistical analysis was performed using a two-way ANOVA with post-hoc tests. * P- value < 0.001 compared to 0 hours.

The integrity of the *in vitro* BBB model remained unaffected by the addition of NP as TEER was higher by the end of the 24-hour period, than the beginning, for every treatment group (Figure 5.14). Addition of a fibronectin coating to the Transwell insert upper surface prior to seeding of HBMVEC improved TEER values in comparison to poly-L-lysine, which was used as a coating up until this point. It can be seen in Figure 5.14, that 24 hours after treatment (day 5 after assembly of the BBB model) some TEER values reach 300 Ωcm^2. This is a 66.7% increase in the maximum TEER value (180 Ωcm^2) recorded for the EPA model at day 5 in the initial work carried out in Figure 5.5.

Fibronectin is an essential component of the BBB basal membrane alongside collagen, laminin and proteoglycans (Krizbai et al., 2011). Mainly adhesive in function, fibronectin assists in adherence of brain endothelial cells to each other and to the basement membrane. The basement membrane is a special extracellular matrix which is important for proper barrier formation at the blood-brain interface. This is due to the self-association of matrix proteins which form a scaffold to allow cellular interactions promoting adhesion, differentiation and proliferation of endothelial cells (Daneman and Prat, 2015). In fact, cultured brain endothelial cells show an elevated TEER when grown on any of the extracellular matrix proteins; fibronectin, collagen or laminin (Tilling et al., 2002).

Many *in vitro* BBB models have been constructed over the past two decades either containing a single monolayer of endothelial cells (Franke et al., 2000; Qiao et al., 2012; Clark & Davis, 2015; Yang et al., 2018) or in co-culture with glial cells (Megard et al., 2002; Omidi et al., 2003; Veszelka et al., 2007; Hutamekalin et al., 2008; Xu et al., 2008). These models, derived from varying species, display a range of TEER values (30-800 Ωcm^2) and do not contain pericytes, which are important in the arrangement of *in vivo* BBB cells. Multi-cellular models, like the EPA model described in this work, are necessary for considering the complex dynamic of NVU cross-talk and thus drawing strong conclusions about nano-carrier transport across multiple cell layers (Gidwani & Singh, 2013). Furthermore, the model described herein is of human origin, an attractive property for a biomimetic system given the potential differences in the BBB amongst

species (Modarres et al., 2018). Indeed, the commercially available PharmaCo-Cell model by Nakagawa et al. (2009) was based on primary rat tissue, which is known to naturally express higher levels of Claudin-5 (Hoshi et al., 2013).

Finally, it is evident from the results that DAS is at least equally as effective as RDP in targeting a NP payload across an *in vitro* BBB model and subsequently is superior to untargeted NP in neural cell-targeting.

5.4. Conclusion

In conclusion, an *in vitro* human BBB model was developed from a triple culture of HBMVEC, pericytes and astrocytes which produced acceptable TEER values (>150 Ωcm^2) and expression of TJ protein for drug transport studies. Using this model, it was demonstrated that RDP and the new derivative, DAS, could successfully facilitate the passage of two different NP payloads across the endothelial-pericyte membrane after 24 hours. Unlabelled NP did not exhibit this targeting ability; therefore, it can be concluded that the effect observed was due to the action of RDP and DAS ligands. Finally, the TEER value of the *in vitro* BBB model was not adversely affected by NP treatment, providing useful insight firstly into the safety of the delivery vehicles, and secondly, the ability of the BBB model to retain a strong TEER value over an experimental period.

To this end, the findings communicated from this work support the continued development of DAS and potentially other RDP derivatives, which can be easily screened *in vitro* for potential BBB targeting properties.

Chapter 6

Concluding remarks and future work

6.1. General conclusion

In this work it was shown that the effective brain targeting ligand RDP, derived from the rabies virus, preferentially interacts with neural cell types via the neuronal nicotinic acetylcholine receptor. The expression of this receptor at the BBB and throughout the CNS presents a relatively specific endogenous target that can be exploited for the delivery of promising PD therapeutics such as neurotrophic factors. This thesis described the optimisation of RDP to a more proteolytically resistant ligand termed DAS, which maintained neural-specific activity when conjugated to drug-loaded polymeric NP. DAS, like RDP, did not show any significant targeting effect in non-neural cell types.

A triple culture *in vitro* BBB model was developed from human-derived cell types which displayed fundamental barrier characteristics for transport studies. Both RDP and DAS ligands facilitated the transport of loaded NP through this BBB model more efficiently than unlabelled NP. Neither ligand had an adverse impact on barrier properties nor caused significant cytotoxicity, suggesting RDP and DAS would be safe for future i*n vivo* investigations.

6.2. Study limitations

The residual solvent remaining in PLGA NP following formulation was not tested during these studies. In chapter 2, it was discussed how washing may reduce residual DCM in NP to below the acceptable limit of 600 ppm set by the International Committee for Harmonisation. Despite this, it would be preferable to test the level of residual solvent remaining in NP using headspace gas chromatography, especially for future *in vivo* work.

An MTT assay was used to assess cell viability in these studies, which is a metabolic test measuring cell respiration. Metabolic rate may vary amongst cells types and also will depend on the cellular environment. MTT assay as the sole measurement of cell viability therefore may not be the most accurate reflection of cell death, requiring a second non-metabolic test such as dye exclusion to provide robust results for i*n vitro* cell assays.

Confocal studies in Chapters 3 & 4 were able to show preferential peptide-facilitated uptake of a fluorescent payload in neural cells; however, this was not quantified. Furthermore, peptide conjugation studies throughout the thesis were limited in sample number due to the expense of the peptide. Statistical analysis was therefore not possible in these studies.

Finally, although SH-SY5Y cells are a commonly used cell type in PD research and other neural drug delivery studies, they were not differentiated to their neuronal phenotype in this work. Further studies using RDP and DAS on differentiated cells expressing neuronal characteristics would be appropriate for assessing the targeting ability of these peptides amongst neuronal populations for PD treatment. Despite this limitation, the nAChRs required for peptide uptake are still present on undifferentiated SH-SY5Y cells.

6.3. Future impact

Progress in PD research has been slow over recent decades due to the difficulties presented by the BBB and the lack of understanding surrounding PD pathology. Many promising drug candidates have failed to achieve success in preclinical and clinical trials for varying reasons, however the inability to achieve effective drug delivery to the brain remains the biggest obstacle. Ongoing studies contributing to our knowledge and understanding of PD will undoubtedly give rise to more therapeutic agents with the potential to target the cascade of detrimental oxidative stress within dopaminergic neurons, in addition to neurorestorative approaches with the use of neurotrophic growth factors. The role of peptides such as RDP and

DAS within a drug delivery system to target the brain may crucially enhance the possibility of clinical success for new therapeutic agents.

The derivation of DAS from RDP creates a neural-specific targeting ligand which can be easily incorporated into nanoparticulate drug delivery systems, affording a higher level of serum stability than the parent peptide. Additionally, the development of an *in vitro* human-derived BBB model as presented in these studies, is useful for the early assessment of the targeting potential of such peptide-conjugated systems prior to *in vivo* testing. This model is advantageous because, unlike the commercially available Pharmaco-Cell model from Nakagawa et al. (2009), it is isogenic in nature comprised only of non-immortalised human cell lines. Although inter-species models have been successfully used in drug transport studies, it is advantageous to have an all human-derived model. The differences between interspecies BBB cells is not well known, however use of human cells may more accurately predict human *in vivo* responses to drugs and their delivery vehicles.

RDP or derivatives such as DAS may prove beneficial in the pursuit of effective regenerative treatments for PD, providing a means of delivery for new therapeutics with curative potential. The *in situ* regeneration of dopaminergic neurons in the SNpc of the brain through non-invasive means is an attractive prospect for the treatment of PD. To slow or indeed reverse the disease process would delay the gradual worsening of symptoms which patients endure during progression of the disease, improving the quality of life of those affected Furthermore, these targeting ligands may also be useful in other brain-related disorders, as they ultimately provide a means of overcoming the restrictions of the BBB.

6.4. Future work

DAS is only one derivative from RDP which was shown to be effective from the results reported in this thesis. In continued molecular modelling studies of RDP and DAS at the nicotinic acetylcholine receptor, identification of different RDP analogues and further optimisation of DAS may be possible. Given the apparent safety and efficacy of DAS *in vitro*, progression to *in vivo* studies in an appropriate animal model is the next rational stage in the development of this ligand. Firstly, assessment of the BBB transport efficacy of DAS *in vivo* using easily visualised NP payloads such as fluorescent dyes, would be necessary before commencing work in a PD model rodent. Following satisfactory results from this work, DAS or other newly designed analogues of RDP could then be analysed for utility within neurotrophic factor-loaded nanoparticulate systems in PD model rodents. NP loaded with therapeutic agents such as basic fibroblast growth factor could be functionalised with RDP-derived peptide ligands for delivery to Parkinsonian brain models *in vivo.*

The *in vitro* BBB model developed in this work could also be optimised further, including detailed transport studies and expression of key BBB markers such as efflux transporters and other tight junction proteins from the claudin and occludin families.

Chapter 7

References

Abbott, N., Ronnback, L. and Hansson, E. (2006) Astrocyte-endothelial interactions at the blood-brain barrier. *Nature Reviews Neuroscience,* 7 (1), 41-53.

Abbott, N.J. (2002) Astrocyte-endothelial interactions and blood-brain barrier permeability. *Journal of anatomy,* 200 (6), 629-638.

Abbruscato, T.J., Lopez, S.P., Mark, K.S., Hawkins, B.T. and Davis, T.P. (2002) Nicotine and cotinine modulate cerebral microvascular permeability and protein expression of ZO-1 through nicotinic acetylcholine receptors expressed on brain endothelial cells. *Journal of pharmaceutical sciences,* 91 (12), 2525-2538.

Abdul-Hammed, M., Breiden, B., Adebayo, M.A., Babalola, J.O., Schwarzmann, G. and Sandhoff, K. (2010) Role of endosomal membrane lipids and NPC2 in cholesterol transfer and membrane fusion. *Journal of lipid research,* 51 (7), 1747-1760.

Abe, K. and Saitoh, H. (2001) Effects of basic fibroblast growth factor on central nervous system functions. *Pharmacological Research,* 43 (4), 307-312.

Agyare, E.K., Curran, G.L., Ramakrishnan, M., Yu, C.C., Poduslo, J.F. and Kandimalla, K.K. (2008) Development of a smart nano-vehicle to target cerebrovascular amyloid deposits and brain parenchymal plaques observed in Alzheimer's disease and cerebral amyloid angiopathy. *Pharmaceutical research,* 25 (11), 2674-2684.

Aktas, Y., Yemisci, M., Andrieux, K., Gursoy, R., Alonso, M., Fernandez-Megia, E., Novoa-Carballal, R., Quinoa, E., Riguera, R., Sargon, M., Celik, H., Demir, A., Hincal, A., Dalkara, T., Capan, Y. and Couvreur, P. (2005) Development and brain delivery of chitosan-PEG nanoparticles functionalized with the monoclonal antibody OX26. *Bioconjugate chemistry,* 16 (6), 1503-1511.

Alyautdin, R., Khalin, I., Nafeeza, M.I., Haron, M.H. and Kuznetsov, D. (2014) Nanoscale drug delivery systems and the blood-brain barrier. *International Journal of Nanomedicine,* 9 795-811.

Ammayappan, A., Peng, K. and Russell, S.J. (2013) Characteristics of Oncolytic Vesicular Stomatitis Virus Displaying Tumor-Targeting Ligands. *Journal of virology,* 87 (24), 13543-13555.

Amoozgar, Z. and Yeo, Y. (2012) Recent advances in stealth coating of nanoparticle drug delivery systems. *Wiley Interdisciplinary Reviews-Nanomedicine and Nanobiotechnology,* 4 (2), 219-233.

Anderson, J.M. and Shive, M.S. (1997) Biodegradation and biocompatibility of PLA and PLGA microspheres. *Advanced Drug Delivery Reviews,* 28 (1), 5-24.

Appelt-Menzel, A., Cubukova, A., Guenther, K., Edenhofer, F., Piontek, J., Krause, G., Stueber, T., Walles, H., Neuhaus, W. and Metzger, M. (2017) Establishment of a Human Blood-Brain Barrier Co-culture Model Mimicking the Neurovascular Unit Using Induced Pluri- and Multipotent Stem Cells. *Stem Cell Reports,* 8 (4), 894-906.

Apple, D.M., Solano-Fonseca, R. and Kokovay, E. (2017) Neurogenesis in the aging brain. *Biochemical Pharmacology,* 141 77-85.

Applerot, G., Lellouche, J., Lipovsky, A., Nitzan, Y., Lubart, R., Gedanken, A. and Banin, E. (2012) Understanding the Antibacterial Mechanism of CuO Nanoparticles: Revealing the Route of Induced Oxidative Stress. *Small,* 8 (21), 3326-3337.

Armulik, A., Genove, G., Mae, M., Nisancioglu, M.H., Wallgard, E., Niaudet, C., He, L., Norlin, J., Lindblom, P., Strittmatter, K., Johansson, B.R. and Betsholtz, C. (2010) Pericytes regulate the blood-brain barrier. *Nature,* 468 (7323), 557-U231.

Aron, L. and Klein, R. (2011) Repairing the parkinsonian brain with neurotrophic factors. *Trends in neurosciences,* 34 (2), 88-100.

Arvidsson, A., Collin, T., Kirik, D., Kokaia, Z. and Lindvall, O. (2002) Neuronal replacement from endogenous precursors in the adult brain after stroke. *Nature medicine,* 8 (9), 963-970.

Ascherio, A., Chen, H., Weisskopf, M.G., O'Reilly, E., McCullough, M.L., Calle, E.E., Schwarzschild, M.A. and Thun, M.J. (2006) Pesticide exposure and risk for Parkinson's disease. *Annals of Neurology,* 60 (2), 197-203.

Auffinger, B., Morshed, R., Tobias, A., Cheng, Y., Ahmed, A.U. and Lesniak, M.S. (2013) Drug-loaded nanoparticle systems and adult stem cells: a potential marriage for the treatment of malignant glioma? *Oncotarget,* 4(3), 378-396.

Auluck, P., Meulener, M. and Bonini, N. (2005) Mechanisms of suppression of alpha-synuclein neurotoxicity by geldanamycin in Drosophila. *Journal of Biological Chemistry,* 280 (4), 2873-2878.

Ayen, W.Y., Garkhal, K. and Kumar, N. (2011) Doxorubicin-Loaded (PEG)(3)-PLA Nanopolymersomes: Effect of Solvents and Process Parameters on Formulation Development and In Vitro Study. *Molecular Pharmaceutics,* 8 (2), 466-478.

Baez-Mendoza, R. and Schultz, W. (2013) The role of the striatum in social behaviour. *Frontiers in Neuroscience,* 7 233.

Balabanov, R. and Dore-Duffy, P. (1998) Role of the CNS microvascular pericyte in the blood-brain barrier. *Journal of neuroscience research,* 53 (6), 637-644.

Banik, M., Patra, M., Dutta, D., Mukherjee, R. and Basu, T. (2018) A simple robust method of synthesis of copper-silver core-shell nano-particle: evaluation of its structural and chemical properties with anticancer potency. *Nanotechnology,* 29 (32), 325102.

Banks, W.A. (2016) From blood-brain barrier to blood-brain interface: new opportunities for CNS drug delivery. *Nature Reviews Drug Discovery,* 15 (4), 275-292.

Banks, W.A., Kovac, A. and Morofuji, Y. (2018) Neurovascular unit crosstalk: Pericytes and astrocytes modify cytokine secretion patterns of brain endothelial cells. *Journal of Cerebral Blood Flow and Metabolism,* 38 (6), 1104-1118.

Bartus, R.T., Baumann, T.L., Brown, L., Kruegel, B.R., Ostrove, J.M. and Herzog, C.D. (2013) Advancing neurotrophic factors as treatments for age-related neurodegenerative diseases: developing and demonstrating “clinical proof-of-concept” for AAV-neurturin (CERE-120) in Parkinson's disease. *Neurobiology of aging,* 34 (1), 35-61.

Bartus, R.T., Brown, L., Wilson, A., Kruegel, B., Siffert, J., Johnson, E.M., Jr., Kordower, J.H. and Herzog, C.D. (2011) Properly scaled and targeted AAV2-NRTN (neurturin) to the substantia nigra is safe, effective and causes no weight loss: Support for nigral targeting in Parkinson's disease. *Neurobiology of disease,* 44 (1), 38-52.

Barua, S., Banerjee, P.P., Sadhu, A., Sengupta, A., Chatterjee, S., Sarkar, S., Barman, S., Chattopadhyay, A., Bhattacharya, S., Mondal, N.C. and Karak, N. (2017) Silver Nanoparticles as Antibacterial and Anticancer Materials Against Human Breast, Cervical and Oral Cancer Cells. *Journal of Nanoscience and Nanotechnology,* 17 (2), 968-976.

Beach, T.G., Sue, L.I., Walker, D.G., Lue, L.F., Connor, D.J., Caviness, J.N., Sabbagh, M.N. and Adler, C.H. (2007) Marked microglial reaction in normal aging human substantia nigra: correlation with extraneuronal neuromelanin pigment deposits. *Acta Neuropathologica,* 114 (4), 419-424.

Beck, K.D., Valverde, J., Alexi, T., Poulsen, K., Moffat, B., Vandlen, R.A., Rosenthal, A. and Hefti, F. (1995) Mesencephalic Dopaminergic-Neurons Protected by Gdnf from Axotomy-Induced Degeneration in the Adult Brain. *Nature,* 373 (6512), 339-341.

Beddoes, C.M., Case, C.P. and Briscoe, W.H. (2015) Understanding nanoparticle cellular entry: A physicochemical perspective. *Advances in Colloid and Interface Science,* 218 48-68.

Benson, K., Cramer, S. and Galla, H. (2013) Impedance-based cell monitoring: barrier properties and beyond. *Fluids and barriers of the CNS,* 10 (1), 5.

Betancourt, T., Brown, B. and Brannon-Peppas, L. (2007) Doxorubicin-loaded PLGA nanoparticles by nanoprecipitation: preparation, characterization and in vitro evaluation. *Nanomedicine,* 2 (2), 219-232.

Bhatt, P.C., Verma, A., Al-Abbasi, F.A., Anwar, F., Kumar, V. and Panda, B.P. (2017) Development of surface-engineered PLGA nanoparticulate-delivery system of Tet 1-conjugated nattokinase enzyme for inhibition of A beta(40) plaques in Alzheimer's disease. *International Journal of Nanomedicine,* 12 8749-8768.

Bi, M., Jiao, Q., Du, X. and Jiang, H. (2018) Glut9-mediated Urate Uptake Is Responsible for Its Protective Effects on Dopaminergic Neurons in Parkinson's Disease Models. *Frontiers in Molecular Neuroscience,* 11 21.

Bicker, J., Alves, G., Fortuna, A. and Falcao, A. (2014) Blood-brain barrier models and their relevance for a successful development of CNS drug delivery systems: A review. *European Journal of Pharmaceutics and Biopharmaceutics,* 87 (3), 409-432.

Bilati, U., Allemann, E. and Doelker, E. (2005a) Poly(D,L-lactide-co-glycolide) protein-loaded nanoparticles prepared by the double emulsion method-processing and formulation issues for enhanced entrapment efficiency. *Journal of microencapsulation,* 22 (2), 205-214.

Bilati, U., Allemann, E. and Doelker, E. (2005b) Nanoprecipitation versus emulsion-based techniques for the encapsulation of proteins into biodegradable nanoparticles and process-related stability issues. *Aaps Pharmscitech,* 6 (4),

Blanco, E., Shen, H. and Ferrari, M. (2015) Principles of nanoparticle design for overcoming biological barriers to drug delivery. *Nature biotechnology,* 33 (9), 941-951.

Blesa, J., Trigo-Damas, I., Quiroga-Varela, A. and Jackson-Lewis, V.R. (2015) Oxidative stress and Parkinson's disease. *Frontiers in Neuroanatomy,* 9 91.

Boettger, R., Hoffmann, R. and Knappe, D. (2017) Differential stability of therapeutic peptides with different proteolytic cleavage sites in blood, plasma and serum. *Plos One,* 12 (6), e0178943.

Bonuccelli, U. and Pavese, N. (2006) Dopamine agonists in the treatment of Parkinson's disease. *Expert review of neurotherapeutics,* 6 (1), 81-89.

Booth, H.D.E., Hirst, W.D. and Wade-Martins, R. (2017) The role of astrocyte dysfunction in Parkinson's disease pathogenesis. *Trends in Neurosciences,* 40 (6), 358-370.

Bowenkamp, K.E., Hoffman, A.F., Gerhardt, G.A., Henry, M.A., Biddle, P.T., Hoffer, B.J. and Granholm, A.C.E. (1995) Glial-Cell Line-Derived Neurotrophic Factor Supports Survival of Injured Midbrain Dopaminergic-Neurons. *Journal of Comparative Neurology,* 355 (4), 479-489.

Brouwer, M., Huss, A., van der Mark, M., Nijssen, P.C.G., Mulleners, W.M., Sas, A.M.G., van Laar, T., de Snoo, G.R., Kromhout, H. and Vermeulen, R.C.H. (2017) Environmental exposure to pesticides and the risk of Parkinson's disease in the Netherlands. *Environment international,* 107 100-110.

Bruneau, E., Sutter, D., Hume, R. and Akaaboune, M. (2005) Identification of nicotinic acetylcholine receptor recycling and its role in maintaining receptor density at the neuromuscular junction in vivo. *Journal of Neuroscience,* 25 (43), 9949-9959.

Burbulla, L.F., Song, P., Mazzulli, J.R., Zampese, E., Wong, Y.C., Jeon, S., Santos, D.P., Blanz, J., Obermaier, C.D., Strojny, C., Savas, J.N., Kiskinis, E., Zhuang, X., Kruger, R., Surmeier, D.J. and Krainc, D. (2017) Dopamine oxidation mediates mitochondrial and lysosomal dysfunction in Parkinson's disease. *Science,* 357 (6357), 1255-+.

Burg, K.J.L., Porter, S. and Kellam, J.F. (2000) Biomaterial developments for bone tissue engineering. *Biomaterials,* 21 (23), 2347-2359.

Byeon, H.J., Thao, L.Q., Lee, S., Min, S.Y., Lee, E.S., Shin, B.S., Choi, H. and Youn, Y.S. (2016) Doxorubicin-loaded nanoparticles consisted of cationic- and mannose-modified-albumins for dual-targeting in brain tumors. *Journal of Controlled Release,* 225 301-313.

Caldwell, M.A., Garcion, E., terBorg, M.G., He, X.L. and Svendsen, C.N. (2004) Heparin stabilizes FGF-2 and modulates striatal precursor cell behavior in response to EGF. *Experimental neurology,* 188 (2), 408-420.

Canfield, S.G., Stebbins, M.J., Morales, B.S., Asai, S.W., Vatine, G.D., Svendsen, C.N., Palecek, S.P. and Shusta, E.V. (2017) An isogenic blood-brain barrier model comprising brain endothelial cells, astrocytes, and neurons derived from human induced pluripotent stem cells. *Journal of neurochemistry,* 140 (6), 874-888.

Carrillo-Mora, P., Silva-Adaya, D. and Villaseñor-Aguayo, K. (2013) Glutamate in Parkinson's disease: Role of antiglutamatergic drugs. *Basal Ganglia,* 3 (3), 147-157.

Case, D., Cheatham, T., Darden, T., Gohlke, H., Luo, R., Merz, K., Onufriev, A., Simmerling, C., Wang, B. and Woods, R. (2005) The Amber biomolecular simulation programs. *Journal of Computational Chemistry,* 26 (16), 1668-1688.

Catiker, E., Gumusderelioglu, M. and Guner, A. (2000) Degradation of PLA, PLGA homo- and copolymers in the presence of serum albumin: a spectroscopic investigation. *Polymer International,* 49 (7), 728-734.

Cecchelli, R., Aday, S., Sevin, E., Almeida, C., Culot, M., Dehouck, L., Coisne, C., Engelhardt, B., Dehouck, M. and Ferreira, L. (2014) A Stable and Reproducible Human Blood-Brain Barrier Model Derived from Hematopoietic Stem Cells. *Plos One,* 9 (6), e99733.

Chang, K., Cheng, M., Chiang, M. and Chen, C. (2018) Lipophilic antioxidants in neurodegenerative diseases. *Clinica Chimica Acta,* 485 79-87.

Chaudhuri, K.R. and Logishetty, K. (2009) Dopamine receptor agonists and sleep disturbances in Parkinson's disease. *Parkinsonism & related disorders,* 15 Suppl 4 S101-4.

Chen, W., Zhan, C., Gu, B., Meng, Q., Wang, H., Lu, W. and Hou, H. (2011a) Targeted brain delivery of itraconazole via RVG29 anchored nanoparticles. *Journal of drug targeting,* 19 (3), 228-234.

Chen, C., Geng, J., Pu, F., Yang, X., Ren, J. and Qu, X. (2011b) Polyvalent Nucleic Acid/Mesoporous Silica Nanoparticle Conjugates: Dual Stimuli-Responsive Vehicles for Intracellular Drug Delivery. *Angewandte Chemie International Edition,* 50 (4), 882-886.

Chen, X., Zaro, J.L. and Shen, W. (2013) Fusion protein linkers: Property, design and functionality. *Advanced Drug Delivery Reviews,* 65 (10), 1357-1369.

Chen, Y., Wang, F. and Benson, H.A.E. (2008) Effect of formulation factors on incorporation of the hydrophilic peptide dalargin into PLGA and mPEG-PLGA nanoparticles. *Biopolymers,* 90 (5), 644-650.

Cheng, H. C., Ulane, C. M., & Burke, R. E. (2010). Clinical progression in Parkinson disease and the neurobiology of axons. *Annals of neurology*, *67*(6), 715–725.

Cheng, J., Teply, B.A., Sherifi, I., Sung, J., Luther, G., Gu, F.X., Levy-Nissenbaum, E., Radovic-Moreno, A.F., Langer, R. and Farokhzad, O.C. (2007) Formulation of functionalized PLGA-PEG nanoparticles for in vivo targeted drug delivery. *Biomaterials,* 28 (5), 869-876.

Cheng, R., Meng, F., Deng, C., Klok, H. and Zhong, Z. (2013) Dual and multi-stimuli responsive polymeric nanoparticles for programmed site-specific drug delivery. *Biomaterials,* 34 (14), 3647-3657.

Cheng, Y., He, G., Mu, X., Zhang, T., Li, X., Hu, J., Xu, B. and Du, G. (2008) Neuroprotective effect of baicalein against MPTP neurotoxicity: Behavioural, biochemical and immunohistochemical profile. *Neuroscience Letters,* 441 (1), 16-20.

Cherian, S. Singh, R. Anjaneya. Singh (2015) Rabies Glycoprotein: A Benefit to the Virus, us or both? *Journal of Vetinary Sciences,* 1 (1), 1-2-9.

Chiba, H., Osanai, M., Murata, M., Kojima, T. and Sawada, N. (2008) Transmembrane proteins of tight junctions. *Biochimica Et Biophysica Acta-Biomembranes,* 1778 (3), 588-600.

Chipman, P.H., Franz, C.K., Nelson, A., Schachner, M. and Rafuse, V.F. (2010) Neural cell adhesion molecule is required for stability of reinnervated neuromuscular junctions. *European Journal of Neuroscience,* 31(2), 238-249.

Chiu, J.Z.S., Tucker, I.G., McLeod, B.J. and McDowell, A. (2015) Arginine-tagging of polymeric nanoparticles via histidine to improve cellular uptake. *European Journal of Pharmaceutics and Biopharmaceutics,* 89 48-55.

Choi, K.Y., Min, K.H., Yoon, H.Y., Kim, K., Park, J.H., Kwon, I.C., Choi, K. and Jeong, S.Y. (2011) PEGylation of hyaluronic acid nanoparticles improves tumor targetability in vivo. *Biomaterials,* 32 (7), 1880-1889.

Chu, C., Li, G., Janowski, M., Bulte, J.W.M., Li, S., Pearl, M. and Walczak, P. (2018) Real-Time MRI Guidance for Reproducible Hyperosmolar Opening of the Blood-Brain Barrier in Mice. *Frontiers in Neurology,* 9 921.

Clark, A.J. and Davis, M.E. (2015) Increased brain uptake of targeted nanoparticles by adding an acid-cleavable linkage between transferrin and the nanoparticle core. *Proceedings of the National Academy of Sciences of the United States of America,* 112 (40), 12486-12491.

Claus, P., Werner, S., Timmer, M. and Grothe, C. (2004) Expression of the fibroblast growth factor-2 isoforms and the FGF receptor 1-4 transcripts in the rat model system of Parkinson's disease. *Neuroscience letters,* 360 (3), 117-120.

Clogston, J.D. and Patri, A.K. (2011) Zeta potential measurement. *Methods in molecular biology (Clifton, N.J.),* 697 63-70.

Cooper, J.M., Wiklander, P.B.O., Nordin, J.Z., Al-Shawi, R., Wood, M.J., Vithlani, M., Schapira, A.H.V., Simons, J.P., El-Andaloussi, S. and Alvarez-Erviti, L. (2014) Systemic Exosomal siRNA Delivery Reduced Alpha-Synuclein Aggregates in Brains of Transgenic Mice. *Movement Disorders,* 29 (12), 1476-1485.

Cordero-Llana, O., Houghton, B.C., Rinaldi, F., Taylor, H., Yanez-Munoz, R.J., Uney, J.B., Wong, L. and Caldwell, M.A. (2015) Enhanced Efficacy of the CDNF/MANF Family by Combined Intranigral Overexpression in the 6-OHDA Rat Model of Parkinson's Disease. *Molecular Therapy,* 23 (2), 244-254.

Cortese, M., Riise, T., Engeland, A., Ascherio, A. and Bjornevik, K. (2018) Urate and the risk of Parkinson's disease in men and women. *Parkinsonism & related disorders,* 52 76-82.

Costa, P.M., Cardoso, A.L., Mendonca, L.S., Serani, A., Custodia, C., Conceicao, M., Simoes, S., Moreira, J.N., de Almeida, L.P. and Pedroso de Lima, M.C. (2013) Tumor-targeted Chlorotoxin-coupled Nanoparticles for Nucleic Acid Delivery to Glioblastoma Cells: A Promising System for Glioblastoma Treatment. *Molecular Therapy-Nucleic Acids,* 2 e100.

Court, J.A., Martin-Ruiz, C., Graham, A. and Perry, E. (2000) Nicotinic receptors in human brain: topography and pathology. *Journal of chemical neuroanatomy,* 20 (3–4), 281-298.

Cronin, A. and Grealy, M. (2017) Neuroprotective and Neuro-restorative Effects of Minocycline and Rasagiline in a Zebrafish 6-Hydroxydopamine Model of Parkinson's Disease. *Neuroscience,* 367 34-46.

Dan, M., Cochran, D.B., Yokel, R.A. and Dziubla, T.D. (2013) Binding, Transcytosis and Biodistribution of Anti-PECAM-1 Iron Oxide Nanoparticles for Brain-Targeted Delivery. *Plos One,* 8 (11), e81051.

Daneman, R. and Prat, A. (2015) The Blood-Brain Barrier. *Cold Spring Harbor Perspectives in Biology,* 7 (1), a020412.

Daneman, R., Zhou, L., Kebede, A.A. and Barres, B.A. (2010) Pericytes are required for blood-brain barrier integrity during embryogenesis. *Nature,* 468 (7323), 562-U238.

Danhier, F., Ansorena, E., Silva, J.M., Coco, R., Le Breton, A. and Preat, V. (2012) PLGA-based nanoparticles: An overview of biomedical applications. *Journal of Controlled Release,* 161(2), 505-522.

Daniels, B.P., Cruz-Orengo, L., Pasieka, T.J., Couraud, P., Romero, I.A., Weksler, B., Cooper, J.A., Doering, T.L. and Klein, R.S. (2013) Immortalized human cerebral microvascular endothelial cells maintain the properties of primary cells in an in vitro model of immune migration across the blood brain barrier. *Journal of neuroscience methods,* 212 (1), 173-179.

Dash, S., Murthy, P.N., Nath, L. and Chowdhury, P. (2010) Kinetic Modeling on Drug Release from Controlled Drug Delivery Systems. *Acta Poloniae Pharmaceutica,* 67 (3), 217-223.

Davidson, T., Harel, S., Arboleda, V., Prunell, G., Shelanski, M., Greene, L. and Troy, C. (2004) Highly efficient small interfering RNA delivery to primary mammalian neurons induces MicroRNA-like effects before mRNA degradation. *Journal of Neuroscience,* 24 (45), 10040-10046.

De Simone, R., Ajmone-Cat, M.A., Carnevale, D. and Minghetti, L. (2005) Activation of alpha 7 nicotinic acetylcholine receptor by nicotine selectively up-regulates cyclooxygenase-2 and prostaglandin E-2 in rat microglial cultures. *Journal of Neuroinflammation,* 2 4.

Decimo, I., Bifari, F., Krampera, M. and Fumagalli, G. (2012) Neural Stem Cell Niches in Health and Diseases. *Current pharmaceutical design,* 18 (13), 1755-1783.

Delehanty, J.B., Boeneman, K., Bradburne, C.E., Robertson, K., Bongard, J.E. and Medintz, I.L. (2010) Peptides for specific intracellular delivery and targeting of nanoparticles: implications for developing nanoparticle-mediated drug delivery. *Therapeutic Delivery,* 1(3), 411-33.

Deli, M., Abraham, C., Kataoka, Y. and Niwa, M. (2005) Permeability studies on in vitro blood-brain barrier models: Physiology, pathology, and pharmacology. *Cellular and molecular neurobiology,* 25 (1), 59-127.

Deng, H., Wang, P. and Jankovic, J. (2018) The genetics of Parkinson disease. *Ageing Research Reviews,* 42 72-85.

Deng, X., Wang, Y., Zhang, F., Yin, Z., Hu, Q., Xiao, X., Zhou, Z., Wu, Y., Sheng, W. and Zeng, Y. (2016) Acidic pH-induced charge-reversal nanoparticles for accelerated endosomal escape and enhanced microRNA modulation in cancer cells. *Chemical Communications,* 52 (15), 3243-3246.

Di Grazia, A., Cappiello, F., Cohen, H., Casciaro, B., Luca, V., Pini, A., Di, Y.P., Shai, Y. and Mangoni, M.L. (2015) D-Amino acids incorporation in the frog skin-derived peptide esculentin-1a(1-21)NH2 is beneficial for its multiple functions. *Amino acids,* 47 (12), 2505-2519.

Dos Santos Rodrigues, B., Oue, H., Banerjee, A., Kanekiyo, T. and Singh, J. (2018) Dual functionalized liposome-mediated gene delivery across triple co-culture blood brain barrier model and specific in vivo neuronal transfection. *Journal of controlled release: official journal of the Controlled Release Society,* 286 264-278.

Drisdel, R., Manzana, E. and Green, W. (2004) The role of palmitoylation in functional expression of nicotinic alpha 7 receptors. *Journal of Neuroscience,* 24 (46), 10502-10510.

Dunckley, T. and Lukas, R.J. (2006) Nicotinic modulation of gene expression in SH-SY5Y neuroblastoma cells. *Brain research,* 1116 39-49.

Duvar, S., Suzuki, M., Muruganandam, A. and Yu, R. (2000) Glycosphingolipid composition of a new immortalized human cerebromicrovascular endothelial cell line. *Journal of neurochemistry,* 75 (5), 1970-1976.

Edmundson, M.C., Capeness, M. and Horsfall, L. (2014) Exploring the potential of metallic nanoparticles within synthetic biology. *New Biotechnology,* 31 (6), 572-578.

Elbaz, A., Clavel, J., Rathouz, P.J., Moisan, F., Galanaud, J., Delemotte, B., Alperovitch, A. and Tzourio, C. (2009) Professional Exposure to Pesticides and Parkinson Disease. *Annals of Neurology,* 66 (4), 494-504.

Elgadir, M.A., Uddin, M.S., Ferdosh, S., Adam, A., Chowdhury, A.J.K. and Sarker, M.Z.I. (2015) Impact of chitosan composites and chitosan nanoparticle composites on various drug delivery systems: A review. *Journal of Food and Drug Analysis,* 23 (4), 619-629.

Elmer, L.W. and Bertoni, J.M. (2008) The increasing role of monoamine oxidase type B inhibitors in Parkinson's disease therapy. *Expert opinion on pharmacotherapy,* 9 (16), 2759-2772.

El-Sayed, I.H., Huang, X.H. and El-Sayed, M.A. (2005) Surface plasmon resonance scattering and absorption of anti-EGFR antibody conjugated gold nanoparticles in cancer diagnostics: Applications in oral cancer. *Nano Letters,* 5 (5), 829-834.

Emborg, M.E., Moirano, J., Raschke, J., Bondarenko, V., Zufferey, R., Peng, S., Ebert, A.D., Joers, V., Roitberg, B., Holden, J.E., Koprich, J., Lipton, J., Kordower, J.H. and Aebischer, P. (2009) Response of aged parkinsonian monkeys to in vivo gene transfer of GDNF. *Neurobiology of disease,* 36 (2), 303-311.

Ernst, A., Alkass, K., Bernard, S., Salehpour, M., Perl, S., Tisdale, J., Possnert, G., Druid, H. and Frisen, J. (2014) Neurogenesis in the Striatum of the Adult Human Brain. *Cell,* 156 (5), 1072-1083.

Fahn, S. (1992) A Pilot Trial of High-Dose Alpha-Tocopherol and Ascorbate in Early Parkinsons-Disease. *Annals of Neurology,* 32 S128-S132.

Falciani, C., Lozzi, L., Pini, A., Corti, F., Fabbrini, M., Bernini, A., Lelli, B., Niccolai, N. and Bracci, L. (2007) Molecular basis of branched peptides resistance to enzyme proteolysis. *Chemical Biology & Drug Design,* 69 (3), 216-221.

Fan, M., Liang, X., Yang, D., Pan, X., Li, Z., Wang, H. and Shi, B. (2016) Epidermal growth factor receptor-targeted peptide conjugated phospholipid micelles for doxorubicin delivery. *Journal of drug targeting,* 24 (2), 111-119.

Farzanehfar, P. (2018) Comparative review of adult midbrain and striatum neurogenesis with classical neurogenesis. *Neuroscience Research,* 134, 1-9.

Feczkó, T., Tóth, J., Dósa, G. and Gyenis, J. (2011) Influence of process conditions on the mean size of PLGA nanoparticles. *Chemical Engineering and Processing: Process Intensification,* 50 (8), 846-853.

Fereshtehnejad, S. and Postuma, R.B. (2017) Subtypes of Parkinson's Disease: What Do They Tell Us About Disease Progression? *Current Neurology and Neuroscience Reports,* 17 (4), 34.

Fischer, U., Reinhardt, S., Albuquerque, E.X. and Maelicke, A. (1999) Expression of functional alpha 7 nicotinic acetylcholine receptor during mammalian muscle development and denervation. *European Journal of Neuroscience,* 11 (8), 2856-2864.

Fominaya, J., Bravo, J., Decaudin, D., Brossa, J.Y., Nemati, F. and Rebollo, A. (2015) Enhanced serum proteolysis resistance of cell-penetrating peptides. *Therapeutic Delivery,* 6 (2), 139-147.

Fonseca, C., Simoes, S. and Gaspar, R. (2002) Paclitaxel-loaded PLGA nanoparticles: preparation, physicochemical characterization and in vitro anti-tumoral activity. *Journal of Controlled Release,* 83 (2), 273-286.

Forster, J.I., Koglsberger, S., Trefois, C., Boyd, O., Baumuratov, A.S., Buck, L., Balling, R. and Antony, P.M.A. (2016) Characterization of Differentiated SH-SY5Y as Neuronal Screening Model Reveals Increased Oxidative Vulnerability. *Journal of Biomolecular Screening,* 21 (5), 496-509.

Fosgerau, K. and Hoffmann, T. (2015) Peptide therapeutics: current status and future directions. *Drug Discovery Today*, 20(1), 122-128.

Fox, C.M., Gash, D.M., Smoot, M.K. and Cass, W.A. (2001) Neuroprotective effects of GDNF against 6-OHDA in young and aged rats. *Brain research,* 896 (1-2), 56-63.

Fox, S.H. and Lang, A.E. (2008) Levodopa-related motor complications - Phenomenology. *Movement Disorders,* 23 S509-S514.

Franke, H., Galla, H. and Beuckmann, C. (2000) Primary cultures of brain microvessel endothelial cells: a valid and flexible model to study drug transport through the blood-brain barrier in vitro. *Brain Research Protocols,* 5 (3), 248-256.

Fredenberg, S., Wahlgren, M., Reslow, M. and Axelsson, A. (2011) The mechanisms of drug release in poly(lactic-co-glycolic acid)-based drug delivery systems-A review. *International journal of pharmaceutics,* 415 (1-2), 34-52.

Freese, C., Unger, R.E., Deller, R.C., Gibson, M.I., Brochhausen, C., Klok, H. and Kirkpatrick, C.J. (2013) Uptake of poly(2-hydroxypropylmethacrylamide)-coated gold nanoparticles in microvascular endothelial cells and transport across the blood-brain barrier. *Biomaterials Science,* 1 (8), 824-833.

Friedman, J.H. and Factor, S.A. (2000) Atypical antipsychotics in the treatment of drug-induced psychosis in Parkinson's disease. *Movement Disorders,* 15 (2), 201-211.

Froehlich, E. (2012) The role of surface charge in cellular uptake and cytotoxicity of medical nanoparticles. *International Journal of Nanomedicine,* 7 5577-5591.

Fu, A., Zhang, M., Gao, F., Xu, X. and Chen, Z. (2013b) A novel peptide delivers plasmids across blood-brain barrier into neuronal cells as a single-component transfer vector. *Plos One,* 8(3), e59642.

Fu, A.L., Wang, Y.L., Zhan, L.P. and Zhou, R.M. (2012) Targeted delivery of proteins into the central nervous system mediated by rabies virus glycoprotein-derived peptide. *Pharmaceutical Research,* 29(6), 1562-1569.

Fu, A.L., Zhao, Z.Z., Gao, F.Y. and Zhang, M.M. (2013a) Cellular uptake mechanism and therapeutic utility of a novel peptide in targeted-delivery of proteins into neuronal cells. *Pharmaceutical Research,* 30(8), 2108-2117.

Fu, C., Xiang, Y., Li, X. and Fu, A. (2018) Targeted transport of nanocarriers into brain for theranosis with rabies virus glycoprotein-derived peptide. *Materials Science and Engineering: C,* 87 155-166.

Fukae, J., Mizuno, Y. and Hattori, N. (2007) Mitochondrial dysfunction in Parkinson’s disease. *Mitochondrion,* 7 (1), 58-62.

Furno, F., Morley, K.S., Wong, B., Sharp, B.L., Arnold, P.L., Howdle, S.M., Bayston, R., Brown, P.D., Winship, P.D. and Reid, H.J. (2004) Silver nanoparticles and polymeric medical devices: a new approach to prevention of infection? *Journal of Antimicrobial Chemotherapy,* 54 (6), 1019-1024.

Gaillard, P.J. and de Boer, A.G. (2000) Relationship between permeability status of the blood-brain barrier and in vitro permeability coefficient of a drug. *European Journal of Pharmaceutical Sciences,* 12 (2), 95-102.

Gan, B.K., Yong, C.Y., Ho, K.L., Omar, A.R., Alitheen, N.B. and Tan, W.S. (2018) Targeted Delivery of Cell Penetrating Peptide Virus-like Nanoparticles to Skin Cancer Cells. *Scientific Reports,* 8

Ganta, S., Devalapally, H., Shahiwala, A. and Amiji, M. (2008) A review of stimuli-responsive nanocarriers for drug and gene delivery. *Journal of Controlled Release,* 126 (3), 187-204.

Gao, X., Chen, H., Choi, H.K., Curhan, G., Schwarzschild, M.A. and Ascherio, A. (2008) Diet, urate, and Parkinson's disease risk in men. *American Journal of Epidemiology,* 167 (7), 831-838.

Gao, Y., Wang, Z., Zhang, J., Zhang, Y., Huo, H., Wang, T., Jiang, T. and Wang, S. (2014) RVG-Peptide-Linked Trimethylated Chitosan for Delivery of siRNA to the Brain. *Biomacromolecules,* 15 (3), 1010-1018.

Gastka, M., Horvath, J. and Lentz, T.L. (1996) Rabies virus binding to the nicotinic acetylcholine receptor alpha subunit demonstrated by virus overlay protein binding assay. *Journal of General Virology,* 77 2437-2440.

Geldenhuys, W., Wehrung, D., Groshev, A., Hirani, A. and Sutariya, V. (2015) Brain-targeted delivery of doxorubicin using glutathione-coated nanoparticles for brain cancers. *Pharmaceutical development and technology,* 20 (4), 497-506.

Gelperina, S., Khalansky, A., Skidan, I., Smirnova, Z., Bobruskin, A., Severin, S., Turowski, B., Zanella, F. and Kreuter, J. (2002) Toxicological studies of doxorubicin bound to polysorbate 80-coated poly(butyl cyanoacrylate) nanoparticles in healthy rats and rats with intracranial glioblastoma. *Toxicology letters,* 126 (2), 131-141.

Gentile, P., Chiono, V., Carmagnola, I., & Hatton, P. V. (2014) An overview of poly(lactic-co-glycolic) acid (PLGA)-based biomaterials for bone tissue engineering. *International journal of molecular sciences*, 15(3), 3640–3659.

Giannoni, P., Badaut, J., Dargazanli, C., De Maudave, A.F., Klement, W., Costalat, V. and Marchi, N. (2018) The pericyte-glia interface at the blood-brain barrier. *Clinical science,* 132 (3), 361-374.

Gidwani, M. and Singh, A.V. (2013) Nanoparticle Enabled Drug Delivery Across the Blood Brain Barrier: in vivo and in vitro Models, Opportunities and Challenges. *Current Pharmaceutical Biotechnology,* 14 (14), 1201-1212.

Gil, E.S., Wu, L., Xu, L. and Lowe, T.L. (2012) beta-Cyclodextrin-poly(beta-Amino Ester) Nanoparticles for Sustained Drug Delivery across the Blood-Brain Barrier. *Biomacromolecules,* 13 (11), 3533-3541.

Gilgun-Sherki, Y., Melamed, E. and Offen, D. (2001) Oxidative stress induced-neurodegenerative diseases: the need for antioxidants that penetrate the blood brain barrier. *Neuropharmacology,* 40 (8), 959-975.

Gladkova, C., Maslen, S.L., Skehel, J.M. and Komander, D. (2018) Mechanism of parkin activation by PINK1. *Nature,* 559 (7714), 411.

Goetz, A.W., Williamson, M.J., Xu, D., Poole, D., Le Grand, S. and Walker, R.C. (2012) Routine Microsecond Molecular Dynamics Simulations with AMBER on GPUs. 1. Generalized Born. *Journal of Chemical Theory and Computation,* 8 (5), 1542-1555.

Gooding, M., Malhotra, M., McCarthy, D.J., Godinho, B.M.D.C., Cryan, J.F., Darcy, R. and O'Driscoll, C.M. (2015) Synthesis and characterization of rabies virus glycoprotein-tagged amphiphilic cyclodextrins for siRNA delivery in human glioblastoma cells: In vitro analysis. *European Journal of Pharmaceutical Sciences,* 71 80-92.

Gotti, C. and Clementi, F. (2004) Neuronal nicotinic receptors: from structure to pathology. *Progress in neurobiology,* 74 (6), 363-396.

Gotti, C., Zoli, M. and Clementi, F. (2006) Brain nicotinic acetylcholine receptors: native subtypes and their relevance. *Trends in pharmacological sciences,* 27 (9), 482-491.

Gramlich, P.A., Westbroek, W., Feldman, R.A., Awad, O., Mello, N., Remington, M.P., Sun, Y., Zhang, W., Sidransky, E., Betenbaugh, M.J. and Fishman, P.S. (2016) A peptide-linked recombinant glucocerebrosidase for targeted neuronal delivery: Design, production, and assessment. *Journal of Biotechnology,* 221 1-12.

Gray, R., Ives, N., Rick, C., Patel, S., Gray, A., Jenkinson, C., McIntosh, E., Wheatley, K., Williams, A. and PD MED Collaborative Grp (2014) Long-term effectiveness of dopamine agonists and monoamine oxidase B inhibitors compared with levodopa as initial treatment for Parkinson's disease (PD MED): a large, open-label, pragmatic randomised trial. *Lancet,* 384 (9949), 1196-1205.

Grothe, C. and Timmer, M. (2007) The physiological and pharmacological role of basic fibroblast growth factor in the dopaminergic nigrostriatal system. *Brain Research Reviews,* 54 (1), 80-91.

Guarnieri, D., Falanga, A., Muscetti, O., Tarallo, R., Fusco, S., Galdiero, M., Galdiero, S. and Netti, P.A. (2013) Shuttle-Mediated Nanoparticle Delivery to the Blood-Brain Barrier. *Small,* 9 (6), 853-862.

Guerrero-Cázares, H., Tzeng, S.Y., Young, N.P., Abutaleb, A.O., Quiñones-Hinojosa, A. and Green, J.J. (2014) Biodegradable polymeric nanoparticles show high efficacy and specificity at DNA delivery to human glioblastoma in vitro and in vivo. *ACS Nano,* 8 (5), 5141-5153.

Gulyaev, A., Gelperina, S., Skidan, I., Antropov, A., Kivman, G. and Kreuter, J. (1999) Significant transport of doxorubicin into the brain with polysorbate 80-coated nanoparticles. *Pharmaceutical research,* 16 (10), 1564-1569.

Gumbleton, M. and Audus, K.L. (2001) Progress and limitations in the use of in vitro cell cultures to serve as a permeability screen for the blood-brain barrier. *Journal of pharmaceutical sciences,* 90 (11), 1681-1698.

Gupta, A.K. and Curtis, A.S.G. (2004) Surface modified superparamagnetic nanoparticles for drug delivery: Interaction studies with human fibroblasts in culture. *Journal of Materials Science-Materials in Medicine,* 15 (4), 493-496.

Gupta, A.K. and Gupta, M. (2005) Synthesis and surface engineering of iron oxide nanoparticles for biomedical applications. *Biomaterials,* 26 (18), 3995-4021.

Haddadian, E.J., Cheng, M.H., Coalson, R.D., Xu, Y. and Tang, P. (2008) In Silico Models for the Human alpha 4 beta 2 Nicotinic Acetylcholine Receptor. *Journal of Physical Chemistry B,* 112 (44), 13981-13990.

Hamoudeh, M., Diab, R., Fessi, H., Dumontet, C. and Cuchet, D. (2008) Paclitaxel-loaded microparticles for intratumoral administration via the TMT technique: Preparation, characterization, and preliminary antitumoral evaluation. *Drug development and industrial pharmacy,* 34 (7), 698-707.

Hanada, S., Fujioka, K., Inoue, Y., Kanaya, F., Manome, Y. and Yamamoto, K. (2014) Cell-Based in Vitro Blood-Brain Barrier Model Can Rapidly Evaluate Nanoparticles' Brain Permeability in Association with Particle Size and Surface Modification. *International Journal of Molecular Sciences,* 15 (2), 1812-1825.

Harris, A. (1994) Somatostatin and Somatostatin Analogs - Pharmacokinetics and Pharmacodynamic Effects. *Gut,* 35 S1-S4.

Hauser, D.N. and Hastings, T.G. (2013) Mitochondrial dysfunction and oxidative stress in Parkinson's disease and monogenic parkinsonism. *Neurobiology of disease,* 51 35-42.

Hawkins, B. and Davis, T. (2005) The blood-brain barrier/neurovascular unit in health and disease. *Pharmacological reviews,* 57 (2), 173-185.

He, C., Hu, Y., Yin, L., Tang, C. and Yin, C. (2010) Effects of particle size and surface charge on cellular uptake and biodistribution of polymeric nanoparticles. *Biomaterials,* 31 (13), 3657-3666.

Hegarty, S.V., O'Keeffe, G.W. and Sullivan, A.M. (2014) Neurotrophic factors: from neurodevelopmental regulators to novel therapies for Parkinson's disease. *Neural Regeneration Research,* 9 (19), 1708-1711.

Herman, A. and Herman, A.P. (2014) Nanoparticles as Antimicrobial Agents: Their Toxicity and Mechanisms of Action. *Journal of Nanoscience and Nanotechnology,* 14 (1), 946-957.

Herran, E., Requejo, C., Angel Ruiz-Ortega, J., Aristieta, A., Igartua, M., Bengoetxea, H., Ugedo, L., Luis Pedraz, J., Vicente Lafuente, J. and Maria Hernandez, R. (2014) Increased antiparkinson efficacy of the combined administration of VEGF- and GDNF-loaded nanospheres in a partial lesion model of Parkinson's disease. *International Journal of Nanomedicine,* 9 2677-2687.

Herzog, C.D., Brown, L., Kruegel, B.R., Wilson, A., Tansey, M.G., Gage, F.H., Johnson, E.M.,Jr. and Bartus, R.T. (2013) Enhanced neurotrophic distribution, cell signaling and neuroprotection following substantia nigral versus striatal delivery of AAV2-NRTN (CERE-120). *Neurobiology of disease,* 58 38-48.

Hislop, J.N., Islam, T.A., Eleftheriadou, I., Carpentier, D.C.J., Trabalza, A., Parkinson, M., Schiavo, G. and Mazarakis, N.D. (2014) Rabies Virus Envelope Glycoprotein Targets Lentiviral Vectors to the Axonal Retrograde Pathway in Motor Neurons. *Journal of Biological Chemistry,* 289 (23), 16148-16163.

Höbel, S., Appeldoorn, C. C., Gaillard, P. J., & Aigner, A. (2011). Targeted CRM197-PEG-PEI/siRNA Complexes for Therapeutic RNAi in Glioblastoma. *Pharmaceuticals*, 4(12), 1591-1606.

Honary, S. and Zahir, F. (2013) Effect of Zeta Potential on the Properties of Nano-Drug Delivery Systems - A Review (Part 1). *Tropical Journal of Pharmaceutical Research,* 12 (2), 255-264.

Hoshi, Y., Uchida, Y., Tachikawa, M., Inoue, T., Ohtsuki, S. and Terasaki, T. (2013) Quantitative Atlas of Blood-Brain Barrier Transporters, Receptors, and Tight Junction Proteins in Rats and Common Marmoset. *Journal of pharmaceutical sciences,* 102 (9), 3343-3355.

Hu, C. and Liu, Y.K. (2011) Quality Control in Pharmaceuticals: Residual Solvents Testing and Analysis. *In:* Akyar, I., ed. *Wide Spectra of Quality Control* 183--209.

Hu, F., Zhang, Y., Du, Y. and Yuan, H. (2008) Nimodipine loaded lipid nanospheres prepared by solvent diffusion method in a drug saturated aqueous system. *International Journal of Pharmaceutics,* 348 (1), 146-152.

Hu, K., Li, J., Shen, Y., Lu, W., Gao, X., Zhang, Q. and Jiang, X. (2009) Lactoferrin-conjugated PEG-PLA nanoparticles with improved brain delivery: In vitro and in vivo evaluations. *Journal of Controlled Release,* 134 (1), 55-61.

Hu, Y., Dammer, E.B., Ren, R. and Wang, G. (2015) The endosomal-lysosomal system: from acidification and cargo sorting to neurodegeneration. *Translational Neurodegeneration,* 4 UNSP 18.

Huang, R., Ke, W., Liu, Y., Wu, D., Feng, L., Jiang, C. and Pei, Y. (2010a) Gene therapy using lactoferrin-modified nanoparticles in a rotenone-induced chronic Parkinson model. *Journal of the Neurological Sciences,* 290 (1), 123-130.

Huang, X., El-Sayed, I.H. and El-Sayed, M.A. (2010b) Applications of gold nanorods for cancer imaging and photothermal therapy. *Methods in molecular biology (Clifton, N.J.),* 624 343-57.

Huang, Y., Liu, W., Gao, F., Fang, X. and Chen, Y. (2016) c(RGDyK)-decorated Pluronic micelles for enhanced doxorubicin and paclitaxel delivery to brain glioma. *International Journal of Nanomedicine,* 11 1629-1641.

Hubschmann, M.V., Skladchikova, G., Bock, E. and Berezin, V. (2005) Neural cell adhesion molecule function is regulated by metalloproteinase-mediated ectodomain release. *Journal of Neuroscience Research,* 80(6), 826-837.

Hussein, A.S., Abdullah, N. and Ahmadun, F. (2013) In vitro degradation of poly (D, L-lactide-co-glycolide) nanoparticles loaded with linamarin. *Iet Nanobiotechnology,* 7 (2), 33-41.

Hutamekalin, P., Farkas, A.E., Orbok, A., Wilhelm, I., Nagyoszi, P., Veszelka, S., Deli, M.A., Buzas, K., Hunyadi-Gulyas, E., Medzihradszky, K.F., Meksuriyen, D. and Krizbai, I.A. (2008) Effect of nicotine and polyaromtic hydrocarbons on cerebral endothelial cells. *Cell biology international,* 32 (2), 198-209.

Hwang, D.W., Son, S., Jang, J., Youn, H., Lee, S., Lee, D., Lee, Y., Jeong, J.M., Kim, W.J. and Lee, D.S. (2011) A brain-targeted rabies virus glycoprotein-disulfide linked PEI nanocarrier for delivery of neurogenic microRNA. *Biomaterials,* 32 (21), 4968-4975.

Iversen, T., Skotland, T. and Sandvig, K. (2011) Endocytosis and intracellular transport of nanoparticles: Present knowledge and need for future studies. *Nano Today,* 6 (2), 176-185.

Jackson, A.C. (2013) Current and future approaches to the therapy of human rabies. *Antiviral Research,* 99 (1), 61-67.

Jain, R.A. (2000) The manufacturing techniques of various drug loaded biodegradable poly(lactide-co-glycolide) (PLGA) devices. *Biomaterials,* 21 (23), 2475-2490.

Jana, U., Mohanty, A.K., Pal, S.L., Manna, P.K. and Mohanta, G.P. (2014) Felodipine loaded PLGA nanoparticles: preparation, physicochemical characterization and *in vivo* toxicity study. *Nano Convergence,* 1 (31),

Jankovic, J. (2005) Motor fluctuations and dyskinesias in Parkinson's disease: clinical manifestations. *Movement Disorders,* 20 S11-S16.

Jiang, W., Kim, B.Y.S., Rutka, J.T. and Chan, W.C.W. (2008) Nanoparticle-mediated cellular response is size-dependent. *Nature Nanotechnology,* 3 (3), 145-150.

Jokerst, J.V., Lobovkina, T., Zare, R.N. and Gambhir, S.S. (2011) Nanoparticle PEGylation for imaging and therapy. *Nanomedicine,* 6 (4), 715-728.

Joshi, S., Cooke, J.R.N., Ellis, J.A., Emala, C.W. and Bruce, J.N. (2017) Targeting brain tumors by intra-arterial delivery of cell-penetrating peptides: a novel approach for primary and metastatic brain malignancy. *Journal of neuro-oncology,* 135 (3), 497-506.

Jungnickel, J., Haase, K., Konitzer, J., Timmer, M. and Grothe, C. (2006) Faster nerve regeneration after sciatic nerve injury in mice over-expressing basic fibroblast growth factor. *Journal of neurobiology,* 66 (9), 940-948.

Kalaria, D.R., Sharma, G., Beniwal, V. and Kumar, M.N.V.R. (2009) Design of Biodegradable Nanoparticles for Oral Delivery of Doxorubicin: In vivo Pharmacokinetics and Toxicity Studies in Rats. *Pharmaceutical research,* 26 (3), 492-501.

Kalia, L.V. and Lang, A.E. (2015) Parkinson's disease. *Lancet,* 386 (9996), 896-912.

Kang, C., Yuan, X., Zhong, Y., Pu, P., Guo, Y., Albadany, A., Yu, S., Zhang, Z., Li, Y., Chang, J. and Sheng, J. (2009) Growth Inhibition Against Intracranial C6 Glioma Cells by Stereotactic Delivery of BCNU by Controlled Release from poly(D,L-lactic acid) Nanoparticles. *Technology in Cancer Research & Treatment,* 8 (1), 61-70.

Kasperek, R., Trebacz, H., Zimmer, L. and Poleszak, E. (2014) The Effect of Excipients on the Release Kinetics of Diclofenac Sodium and Papaverine Hydrochloride from Composed Tablets. *Acta Poloniae Pharmaceutica,* 71 (3), 439-449.

Kelly, M.J., O'Keeffe, G.W. and Sullivan, A.M. (2015) Viral vector delivery of neurotrophic factors for Parkinson's disease therapy. *Expert Reviews in Molecular Medicine,* 17 e8.

Khor, S. and Hsu, A. (2007) The pharmacokinetics and pharmacodynamics of levodopa in the treatment of Parkinson's disease. *Current clinical pharmacology,* 2 (3), 234-43.

Kim, H.J., Jeon, B.S. and Jenner, P. (2017) Chapter Eleven - Hallmarks of Treatment Aspects: Parkinson's Disease Throughout Centuries Including l-Dopa. *In:* Bhatia, K.P., Chaudhuri, K.R. and Stamelou, M., eds. *Parkinson's Disease.* Academic Press, 295-343.

Kini, R.M. and Doley, R. (2010) Structure, function and evolution of three-finger toxins: Mini proteins with multiple targets. *Toxicon,* 56 (6), 855-867.

Klein, C. and Westenberger, A. (2012) Genetics of Parkinson's Disease. *Cold Spring Harbor Perspectives in Medicine,* 2 (1), a008888.

Kovac, A., Erickson, M.A. and Banks, W.A. (2011) Brain microvascular pericytes are immunoactive in culture: cytokine, chemokine, nitric oxide, and LRP-1 expression in response to lipopolysaccharide. *Journal of Neuroinflammation,* 8 139.

Kreuter, J., Alyautdin, R.N., Kharkevich, D.A. and Ivanov, A.A. (1995) Passage of peptides through the blood-brain barrier with colloidal polymer particles (nanoparticles). *Brain Research,* 674 (1), 171-174.

Kristensen, M., Birch, D. and Nielsen, H.M. (2016) Applications and Challenges for Use of Cell-Penetrating Peptides as Delivery Vectors for Peptide and Protein Cargos. *International Journal of Molecular Sciences,* 17 (2), 185.

Krizbai, I., Fazakas, C., Nagyoszi, P., Farkas, A., Hasko, J., Molnar, J., Vegh, G., Varo, G. and Wilhelm, I. (2011) The role of the blood-brain barrier in the formation of brain metastases. *Pharmacological Reports,* 63 (5), 1275-1275.

Kuan, W., Poole, E., Fletcher, M., Karniely, S., Tyers, P., Wills, M., Barker, R.A. and Sinclair, J.H. (2012) A novel neuroprotective therapy for Parkinson's disease using a viral noncoding RNA that protects mitochondrial Complex I activity. *Journal of Experimental Medicine,* 209 (1), 1-10.

Kulkarni, S.A. and Feng, S. (2011) Effects of surface modification on delivery efficiency of biodegradable nanoparticles across the blood-brain barrier. *Nanomedicine,* 6 (2), 377-394.

Kumar, P., Ban, H., Kim, S., Wu, H., Pearson, T., Greiner, D.L., Laouar, A., Yao, J., Haridas, V., Habiro, K., Yang, Y., Jeong, J., Lee, K., Kim, Y., Kim, S.W., Peipp, M., Fey, G.H., Manjunath, N., Shultz, L.D., Lee, S. and Shankar, P. (2008) T cell-specific siRNA delivery suppresses HIV-1 infection in humanized mice. *Cell,* 134 (4), 577-586.

Kumar, P., Wu, H., McBride, J.L., Jung, K., Kim, M.H., Davidson, B.L., Lee, S.K., Shankar, P. and Manjunath, N. (2007) Transvascular delivery of small interfering RNA to the central nervous system. *Nature,* 448 (7149), 39-43.

Kumari, A., Yadav, S.K. and Yadav, S.C. (2010) Biodegradable polymeric nanoparticles-based drug delivery systems. *Colloids and Surfaces B: Biointerfaces,* 75 (1), 1-18.

Kumari, S., Borroni, V., Chaudhry, A., Chanda, B., Massol, R., Mayor, S. and Barrantes, F.J. (2008) Nicotinic acetylcholine receptor is internalized via a Rac-dependent, dynamin-independent endocytic pathway. *Journal of Cell Biology,* 181 (7), 1179-1193.

Kurakhmaeva, K.B., Djindjikhashvili, I.A., Petrov, V.E., Balabanyan, V.U., Voronina, T.A., Trofimov, S.S., Kreuter, J., Gelperina, S., Begley, D. and Alyautdin, R.N. (2009) Brain targeting of nerve growth factor using poly(butyl cyanoacrylate) nanoparticles. *Journal of drug targeting,* 17 (8), 564-574.

Kwon, E.J., Lasiene, J., Jacobson, B.E., Park, I., Horner, P.J. and Pun, S.H. (2010) Targeted nonviral delivery vehicles to neural progenitor cells in the mouse subventricular zone. *Biomaterials,* 31 (8), 2417-2424.

Lafon, M. (2005) Rabies virus receptors. *Journal of NeuroVirology,* 11(1), 82-87.

Larsen, K.E., Benn, S.C., Ay, I., Chian, R., Celia, S.A., Remington, M.P., Bejarano, M., Liu, M., Ross, J., Carmillo, P., Sah, D., Phillips, K.A., Sulzer, D., Pepinsky, R.B., Fishman, P.S., Brown, R.H., Jr. and Francis, J.W. (2006) A glial cell line-derived neurotrophic factor (GDNF): tetanus toxin fragment C protein conjugate improves delivery of GDNF to spinal cord motor neurons in mice. *Brain research,* 1120 1-12.

Laurent, S., Forge, D., Port, M., Roch, A., Robic, C., Elst, L.V. and Muller, R.N. (2008) Magnetic iron oxide nanoparticles: Synthesis, stabilization, vectorization, physicochemical characterizations, and biological applications. *Chemical reviews,* 108 (6), 2064-2110.

Le Grand, S., Goetz, A.W. and Walker, R.C. (2013) SPFP: Speed without compromise-A mixed precision model for GPU accelerated molecular dynamics simulations. *Computer Physics Communications,* 184 (2), 374-380.

Le Ouay, B. and Stellacci, F. (2015) Antibacterial activity of silver nanoparticles: A surface science insight. *Nano Today,* 10 (3), 339-354.

Lee, C., Hwang, H.S., Lee, S., Kim, B., Kim, J.O., Oh, K.T., Lee, E.S., Choi, H. and Youn, Y.S. (2017) Rabies Virus-Inspired Silica-Coated Gold Nanorods as a Photothermal Therapeutic Platform for Treating Brain Tumors. *Advanced Materials,* 29 (13), 1605563.

Lee, E., Park, H.R., Ji, S.T., Lee, Y. and Lee, J. (2014) Baicalein Attenuates Astroglial Activation in the 1-Methyl-4-Phenyl-1,2,3, 4-Tetrahydropyridine-Induced Parkinson's Disease Model by Downregulating the Activations of Nuclear Factor-kappa B, ERK, and JNK. *Journal of neuroscience research,* 92 (1), 130-139.

Lee, H.L., Hwang, S.C., Nah, J.W., Kim, J., Cha, B., Kang, D.H. and Jeong, Y. (2018) Redox- and pH-Responsive Nanoparticles Release Piperlongumine in a Stimuli-Sensitive Manner to Inhibit Pulmonary Metastasis of Colorectal Carcinoma Cells. *Journal of pharmaceutical sciences,* 107 (10), 2702-2712.

Lentz, T., Burrage, T., Smith, A., Crick, J. and Tignor, G. (1982) Is the Acetylcholine-Receptor a Rabies Virus Receptor. *Science,* 215 (4529), 182-184.

Lentz, T.L. (1990) Rabies virus binding to an acetylcholine receptor alpha-subunit peptide. *Journal of Molecular Recognition: JMR,* 3 (2), 82-88.

Lentz, T.L. (1991) Structure-function-relationships of curaremimetic neurotoxin loop-2 and of a structurally similar segment of rabies virus glycoprotein in their interaction with the nicotinic acetylcholine-receptor. *Biochemistry,* 30(45), 10949-10957.

Li, G., Simon, M.J., Cancel, L.M., Shi, Z., Ji, X., Tarbell, J.M., Morrison,Barclay,,III and Fu, B.M. (2010) Permeability of Endothelial and Astrocyte Cocultures: In Vitro Blood-Brain Barrier Models for Drug Delivery Studies. *Annals of Biomedical Engineering,* 38 (8), 2499-2511.

Li, H. and Qian, Z. (2002) Transferrin/transferrin receptor-mediated drug delivery. *Medicinal research reviews,* 22 (3), 225-250.

Li, H., Tong, Y., Bai, L., Ye, L., Zhong, L., Duan, X. and Zhu, Y. (2018) Lactoferrin functionalized PEG-PLGA nanoparticles of shikonin for brain targeting therapy of glioma. *International Journal of Biological Macromolecules,* 107 204-211.

Li, J., Feng, L., Fan, L., Zha, Y., Guo, L., Zhang, Q., Chen, J., Pang, Z., Wang, Y., Jiang, X., Yang, V.C. and Wen, L. (2011) Targeting the brain with PEG–PLGA nanoparticles modified with phage-displayed peptides. *Biomaterials,* 32 (21), 4943-4950.

Li, X., Hu, B., Jones, S.A., Zhang, Y., Lavaute, T., Du, Z. and Zhang, S. (2008a) Directed differentiation of ventral spinal progenitors and motor neurons from human embryonic stem cells by small molecules. *Stem cells,* 26 (4), 886-893.

Li, L., Guo, K., Lu, J., Venkatraman, S.S., Luo, D., Ng, K.C., Ling, E., Moochhala, S. and Yang, Y. (2008b) Biologically active core/shell nanoparticles self-assembled from cholesterol-terminated PEG-TAT for drug delivery across the blood-brain barrier. *Biomaterials,* 29 (10), 1509-1517.

Lie, D., Dziewczapolski, G., Willhoite, A., Kaspar, B., Shults, C. and Gage, F. (2002) The adult substantia nigra contains progenitor cells with neurogenic potential. *Journal of Neuroscience,* 22 (15), 6639-6649.

Lim, E., Kim, T., Paik, S., Haam, S., Huh, Y. and Lee, K. (2015) Nanomaterials for Theranostics: Recent Advances and Future Challenges. *Chemical reviews,* 115 (1), 327-394.

Lin, Q., Wong, H.L., Tian, F., Huang, Y., Xu, J., Yang, J., Chen, P., Fan, Z., Lu, C. and Zhao, Y. (2017) Enhanced neuroprotection with decellularized brain extracellular matrix containing bFGF after intracerebral transplantation in Parkinson's disease rat model. *International journal of pharmaceutics,* 517 (1-2), 383-394.

Lin, W.J., Juang, L.W. and Lin, C.C. (2003) Stability and release performance of a series of pegylated copolymeric micelles. *Pharmaceutical research,* 20 (4), 668-673.

Liu, J., Qiu, Z., Wang, S., Zhou, L. and Zhang, S. (2010) A modified double-emulsion method for the preparation of daunorubicin-loaded polymeric nanoparticle with enhanced in vitro anti-tumor activity. *Biomedical Materials,* 5 (6), 065002.

Liu, J., Xu, J., Zhou, J., Zhang, Y., Guo, D. and Wang, Z. (2017a) Fe3O4 -based PLGA nanoparticles as MR contrast agents for the detection of thrombosis. *International Journal of Nanomedicine,* 12 1113-1126.

Liu, M., Li, H., Luo, G., Liu, Q. and Wang, Y. (2008) Pharmacokinetics and biodistribution of surface modification polymeric nanoparticles. *Archives of Pharmacal Research,* 31 (4), 547-554.

Liu, Y., Huang, R., Han, L., Ke, W., Shao, K., Ye, L., Lou, J. and Jiang, C. (2009) Brain-targeting gene delivery and cellular internalization mechanisms for modified rabies virus glycoprotein RVG29 nanoparticles. *Biomaterials,* 30 (25), 4195-4202.

Liu, Y., Lu, Z., Mei, L., Yu, Q., Tai, X., Wang, Y., Shi, K., Zhang, Z. and He, Q. (2017b) Tandem Peptide Based on Structural Modification of Poly-Arginine for Enhancing Tumor Targeting Efficiency and Therapeutic Effect. *Acs Applied Materials & Interfaces,* 9 (3), 2083-2092.

Lo Bianco, C., Schneider, B.L., Bauer, M., Sajadi, A., Brice, A., Iwatsubo, T. and Aebischer, P. (2004) Lentiviral vector delivery of parkin prevents dopaminergic degeneration in an alpha-synuclein rat model of Parkinson's disease. *Proceedings of the National Academy of Sciences of the United States of America,* 101 (50), 17510-17515.

Lopez-Otin, C. and Matrisian, L.M. (2007) Tumour micro environment - Opinion - Emerging roles of proteases in tumour suppression. *Nature Reviews Cancer,* 7 (10), 800-808.

Lu, A., Salabas, E.L. and Schueth, F. (2007) Magnetic nanoparticles: Synthesis, protection, functionalization, and application. *Angewandte Chemie-International Edition,* 46 (8), 1222-1244.

Ma, Y., Zheng, Y., Liu, K., Tian, G., Tian, Y., Xu, L., Yan, F., Huang, L. and Mei, L. (2010) Nanoparticles of Poly(Lactide-Co-Glycolide)-d-a-Tocopheryl Polyethylene Glycol 1000 Succinate Random Copolymer for Cancer Treatment. *Nanoscale Research Letters,* 5 (7), 1161-1169.

Madhok, T., Matta, S. and Sharp, B. (1995) Nicotine Regulates Nicotinic Cholinergic Receptors and Subunit Messenger-RNAS in Pc-12 Cells through Protein-Kinase-a. *Molecular Brain Research,* 32 (1), 143-150.

Makadia, H.K. and Siegel, S.J. (2011) Poly Lactic-co-Glycolic Acid (PLGA) as Biodegradable Controlled Drug Delivery Carrier. *Polymers,* 3 (3), 1377-1397.

Makkouk, A., Joshi, V.B., Wongrakpanich, A., Lemke, C.D., Gross, B.P., Salem, A.K. and Weiner, G.J. (2015) Biodegradable Microparticles Loaded with Doxorubicin and CpG ODN for In Situ Immunization Against Cancer. *Aaps Journal,* 17 (1), 184-193.

Malhotra, M. and Prakash, S. (2011) Targeted Drug Delivery Across Blood-Brain-Barrier Using Cell Penetrating Peptides Tagged Nanoparticles. *Current Nanoscience,* 7 (1), 81-93.

Mandava, K. (2017) Biological and Non-Biological Synthesis of Metallic Nanoparticles: Scope for Current Pharmaceutical Research. *Indian Journal of Pharmaceutical Sciences,* 79 (4), 501-512.

Marras, C. and Chaudhuri, K.R. (2016) Nonmotor features of Parkinson's disease subtypes. *Movement Disorders,* 31 (8), 1095-1102.

Mathew, A., Fukuda, T., Nagaoka, Y., Hasumura, T., Morimoto, H., Yoshida, Y., Maekawa, T., Venugopal, K. and Kumar, D.S. (2012) Curcumin Loaded-PLGA Nanoparticles Conjugated with Tet-1 Peptide for Potential Use in Alzheimer's Disease. *Plos One,* 7 (3), e32616.

Maus, A.D.J., Pereira, E.F.R., Karachunski, P.I., Horton, R.M., Navaneetham, D., Macklin, K., Cortes, W.S., Albuquerque, E.X. and Conti-Fine, B.M. (1998) Human and rodent bronchial epithelial cells express functional nicotinic acetylcholine receptors. *Molecular Pharmacology,* 54(5), 779-788.

Mazarakis, N.D., Azzouz, M., Rohll, J.B., Ellard, F.M., Wilkes, F.J., Olsen, A.L., Carter, E.E., Barber, R.D., Baban, D.F., Kingsman, S.M., Kingsman, A.J., O'Malley, K. and Mitrophanous, K.A. (2001) Rabies virus glycoprotein pseudotyping of lentiviral vectors enables retrograde axonal transport and access to the nervous system after peripheral delivery. *Human molecular genetics,* 10 (19), 2109-2121.

McCarthy, D.J., Malhotra, M., O'Mahony, A.M., Cryan, J.F. and O'Driscoll, C.M. (2015) Nanoparticles and the Blood-Brain Barrier: Advancing from In-Vitro Models Towards Therapeutic Significance. *Pharmaceutical research,* 32 (4), 1161-1185.

McCall, R.L. and Sirianni, R.W. (2013) PLGA nanoparticles formed by single- or double-emulsion with vitamin E-TPGS. *Journal of visualized experiments: JoVE,* (82), 51015-51015.

McClure-Begley, T.D., Grady, S.R., Marks, M.J., Collins, A.C. and Stitzel, J.A. (2014) Presynaptic GABA(B) autoreceptor regulation of nicotinic acetylcholine receptor mediated [H-3]-GABA release from mouse synaptosomes. *Biochemical Pharmacology,* 91(1), 87-96.

Megard, I., Garrigues, A., Orlowski, S., Jorajuria, S., Clayette, P., Ezan, E. and Mabondzo, A. (2002) A co-culture-based model of human blood-brain barrier: application to active transport of indinavir and in vivo-in vitro correlation. *Brain research,* 927 (2), 153-167.

Meghana, S., Kabra, P., Chakraborty, S. and Padmavathy, N. (2015) Understanding the pathway of antibacterial activity of copper oxide nanoparticles. *Rsc Advances,* 5 (16), 12293-12299.

Meiser, J., Weindl, D. and Hiller, K. (2013) Complexity of dopamine metabolism. *Cell Communication and Signaling,* 11 34.

Meng, Z., Luan, L., Kang, Z., Feng, S., Meng, Q. and Liu, K. (2017) Histidine-enriched multifunctional peptide vectors with enhanced cellular uptake and endosomal escape for gene delivery. *Journal of Materials Chemistry B,* 5 (1), 74-84.

Merkus, P., Guchelaar, H., Bosch, A. and Merkus, F. (2003) Direct access of drugs to the human brain after intranasal drug administration? *Neurology,* 60 (10), 1669-1671.

Michalicova, A., Bhide, K., Bhide, M. and Kovac, A. (2017) How viruses infiltrate the central nervous system. *Acta Virologica,* 61 (4), 393-400.

Miller, D.S. (2015) Regulation of ABC Transporters at the Blood-Brain Barrier. *Clinical Pharmacology & Therapeutics,* 97 (4), 395-403.

Miura, Y., Takenaka, T., Toh, K., Wu, S., Nishihara, H., Kano, M.R., Ino, Y., Nomoto, T., Matsumoto, Y., Koyama, H., Cabral, H., Nishiyama, N. and Kataoka, K. (2013) Cyclic RGD-Linked Polymeric Micelles for Targeted Delivery of Platinum Anticancer Drugs to Glioblastoma through the Blood-Brain Tumor Barrier. *Acs Nano,* 7 (10), 8583-8592.

Modarres, H.P., Janmaleki, M., Novin, M., Saliba, J., El-Hajj, F., RezayatiCharan, M., Seyfoori, A., Sadabadi, H., Vandal, M., Minh Dang Nguyen, Hasan, A. and Sanati-Nezhad, A. (2018) In vitro models and systems for evaluating the dynamics of drug delivery to the healthy and diseased brain. *Journal of Controlled Release,* 273 108-130.

Mody, V.V., Siwale, R., Singh, A. and Mody, H.R. (2010) Introduction to metallic nanoparticles. *Journal of pharmacy & bioallied sciences,* 2 (4), 282-9.

Molhoek, E.M., van Dijk, A., Veldhuizen, E.J.A., Haagsman, H.P. and Bikker, F.J. (2011) Improved proteolytic stability of chicken cathelicidin-2 derived peptides by d-amino acid substitutions and cyclization*. Peptides,* 32(5), 875-880.

Moore, A.H., Bigbee, M.J., Boynton, G.E., Wakeham, C.M., Rosenheim, H.M., Staral, C.J., Morrissey, J.L. and Hund, A.K. (2010) Non-Steroidal Anti-Inflammatory Drugs in Alzheimer's Disease and Parkinson's Disease: Reconsidering the Role of Neuroinflammation. *Pharmaceuticals (Basel, Switzerland),* 3 (6), 1812-1841.

Mu, X., He, G., Yuan, X., Li, X. and Du, G. (2011) Baicalein protects the brain against neuron impairments induced by MPTP in C57BL/6 mice. *Pharmacology Biochemistry and Behavior,* 98 (2), 286-291.

Mukherjee, S., Ray, S. and Thakur, R.S. (2009) Solid Lipid Nanoparticles: A Modern Formulation Approach in Drug Delivery System. *Indian Journal of Pharmaceutical Sciences,* 71 (4), 349-358.

Mukhtar, M. and Pomerantz, R. (2000) Development of an in vitro blood-brain barrier model to study molecular neuropathogenesis and neurovirologic disorders induced by human immunodeficiency virus type 1 infection. *Journal of human virology,* 3 (6), 324-334.

Muller, R., Mader, K. and Gohla, S. (2000) Solid lipid nanoparticles (SLN) for controlled drug delivery - a review of the state of the art. *European Journal of Pharmaceutics and Biopharmaceutics,* 50 (1), 161-177.

Mundargi, R.C., Babu, V.R., Rangaswamy, V., Patel, P. and Aminabhavi, T.M. (2008) Nano/micro technologies for delivering macromolecular therapeutics using poly(d,l-lactide-co-glycolide) and its derivatives. *Journal of Controlled Release,* 125 (3), 193-209.

Mura, S., Nicolas, J. and Couvreur, P. (2013) Stimuli-responsive nanocarriers for drug delivery. *Nature Materials,* 12 (11), 991-1003.

Nair, L.S. and Laurencin, C.T. (2007) Biodegradable polymers as biomaterials. *Progress in Polymer Science,* 32 (8), 762-798.

Nakagawa, S., Deli, M.A., Kawaguchi, H., Shimizudani, T., Shimono, T., Kittel, A., Tanaka, K. and Niwa, M. (2009) A new blood-brain barrier model using primary rat brain endothelial cells, pericytes and astrocytes. *Neurochemistry international,* 54 (3-4), 253-263.

Nakagawa, S., Deli, M.A., Nakao, S., Honda, M., Hayashi, K., Nakaoke, R., Kataoka, Y. and Niwa, M. (2007) Pericytes from brain microvessels strengthen the barrier integrity in primary cultures of rat brain endothelial cells. *Cellular and molecular neurobiology,* 27 (6), 687-694.

Nam, J., Nam, H., Jung, S., Hwang, S., Wang, T., Hur, J., Im, K., Park, N., Kim, K.H. and Kim, S. (2012) Unique Photothermal Response and Sustained Photothermal Effect of pH-Responsive Gold-Nanoparticle Aggregates. *Chemphyschem,* 13 (18), 4105-4109.

National Institute for Health and Care Excellence (2017) *Parkinson's disease in adults* (NICE Guideline 71). Available at: https://www.nice.org.uk/guidance/ng33/resources/tuberculosis-1837390683589 [Accessed 24 November 2018].

Nayak, D., Minz, A.P., Ashe, S., Rauta, P.R., Kumari, M., Chopra, P. and Nayak, B. (2016) Synergistic combination of antioxidants, silver nanoparticles and chitosan in a nanoparticle-based formulation: Characterization and cytotoxic effect on MCF-7 breast cancer cell lines. *Journal of colloid and interface science,* 470 142-152.

Ngambenjawong, C., Gustafson, H.H., Pineda, J.M., Kacherovsky, N.A., Cieslewicz, M. and Pun, S.H. (2016) Serum Stability and Affinity Optimization of an M2 Macrophage-Targeting Peptide (M2pep). *Theranostics,* 6 (9), 1403-1414.

Nguyen, L.T., Chau, J.K., Perry, N.A., de Boer, L., Zaat, S.A.J. and Vogel, H.J. (2010) Serum Stabilities of Short Tryptophan-and Arginine-Rich Antimicrobial Peptide Analogs. *Plos One,* 5 (9), e12684.

Niidome, T., Shiotani, A., Mori, T. and Katayama, Y. (2010) Targeted delivery of gold nanorods modified with thermo-sensitive polymer. *Journal of Controlled Release,* 148 (1), E65-E66.

Nikanjarn, M., Gibbs, A.R., Hunt, A., Budinger, T.F. and Forte, T.M. (2007) Synthetic nano-LDL with paclitaxel oleate as a targeted drug delivery vehicle for glioblastoma multiforme. *Journal of Controlled Release,* 124 (3), 163-171.

Nimesh, S., Manchanda, R., Kumar, R., Saxena, A., Chaudhary, P., Yadav, V., Mozumdar, S. and Chandra, R. (2006) Preparation, characterization and in vitro drug release studies of novel polymeric nanoparticles. *International journal of pharmaceutics,* 323 (1-2), 146-152.

Noyce, A.J., Lees, A.J. and Schrag, A. (2016) The prediagnostic phase of Parkinson's disease. *Journal of Neurology Neurosurgery and Psychiatry,* 87 (8), 871-878.

Nur, M. and Vasiljevic, T. (2017) Can natural polymers assist in delivering insulin orally? *International Journal of Biological Macromolecules,* 103 889-901.

Obeso, J.A., Stamelou, M., Goetz, C.G., Poewe, W., Lang, A.E., Weintraub, D., Burn, D., Halliday, G.M., Bezard, E., Przedborski, S., Lehericy, S., Brooks, D.J., Rothwell, J.C., Hallett, M., DeLong, M.R., Marras, C., Tanner, C.M., Ross, G.W., Langston, J.W., Klein, C., Bonifati, V., Jankovic, J., Lozano, A.M., Deuschl, G., Bergman, H., Tolosa, E., Rodriguez-Violante, M., Fahn, S., Postuma, R.B., Berg, D., Marek, K., Standaert, D.G., Surmeier, D.J., Olanow, C.W., Kordower, J.H., Calabresi, P., Schapira, A.H.V. and Stoessl, A.J. (2017) Past, Present, and Future of Parkinson's Disease: A Special Essay on the 200th Anniversary of the Shaking Palsy. *Movement Disorders,* 32 (9), 1264-1310.

Oller-Salvia, B., Teixido, M. and Giralt, E. (2013) From Venoms to BBB Shuttles: Synthesis and Blood-Brain Barrier Transport Assessment of Apamin and a Nontoxic Analog. *Biopolymers,* 100 (6), 675-686.

Omidi, Y., Campbell, L., Barar, J., Connell, D., Akhtar, S. and Gumbleton, M. (2003) Evaluation of the immortalised mouse brain capillary endothelial cell line, b.End3, as an in vitro blood-brain barrier model for drug uptake and transport studies. *Brain research,* 990 (1-2), 95-112.

O'Reilly, E.J., Gao, X., Weisskopf, M.G., Chen, H., Schwarzschild, M.A., Spiegelman, D. and Ascherio, A. (2010) Plasma Urate and Parkinson's Disease in Women. *American Journal of Epidemiology,* 172 (6), 666-670.

Osaka, H., Wang, Y.L., Takada, K., Takizawa, S., Setsuie, R., Li, H., Sato, Y., Nishikawa, K., Sun, Y.J., Sakurai, M., Harada, T., Hara, Y., Kimura, I., Chiba, S., Namikawa, K., Kiyama, H., Noda, M., Aoki, S. and Wada, K. (2003) Ubiquitin carboxy-terminal hydrolase L1 binds to and stabilizes monoubiquitin in neuron. *Human molecular genetics,* 12 (16), 1945-1958.

Palm, C., Jayamanne, M., Kjellander, M. and Hallbrink, M. (2007) Peptide degradation is a critical determinant for cell-penetrating peptide uptake. *Biochimica Et Biophysica Acta-Biomembranes,* 1768 (7), 1769-1776.

Pan, R., Xu, W., Jafari, M., Chen, B., Sheinin, T. and Chen, P. (2015) DEGylation Enhanced the Stability of Peptide-siRNA Complexes in Serum. *Journal of Nanoscience and Nanotechnology,* 15 (12), 9982-9990.

Pandya, N.T., Jani, P., Vanza, J. and Tandel, H. (2018) Solid lipid nanoparticles as an efficient drug delivery system of olmesartan medoxomil for the treatment of hypertension. *Colloids and Surfaces B-Biointerfaces,* 165 37-44.

Panyam, J., Dali, M.M., Sahoo, S.K., Ma, W., Chakravarthi, S.S., Amidon, G.L., Levy, R.J. and Labhasetwar, V. (2003) Polymer degradation and in vitro release of a model protein from poly(d,l-lactide-co-glycolide) nano- and microparticles. *Journal of Controlled Release,* 92 (1–2), 173-187.

Paratcha, G., Ledda, F. and Ibáñez, C.F. (2003) The Neural Cell Adhesion Molecule NCAM Is an Alternative Signaling Receptor for GDNF Family Ligands. *Cell,* 113(7), 867-879.

Pardridge, W.M. (2005) The blood-brain barrier: bottleneck in brain drug development. *NeuroRx : the journal of the American Society for Experimental NeuroTherapeutics,* 2 (1), 3-14.

Pardridge, W.M. (2007) Blood-brain barrier delivery. *Drug discovery today,* 12 (1-2), 54-61.

Park, J., Fong, P.M., Lu, J., Russell, K.S., Booth, C.J., Saltzman, W.M. and Fahmy, T.M. (2009) PEGylated PLGA nanoparticles for the improved delivery of doxorubicin. *Nanomedicine-Nanotechnology Biology and Medicine,* 5 (4), 410-418.

Parkinson's UK (2017). *The Incidence and Prevalence of Parkinson's in the UK*. [online] Available at: https://www.parkinsons.org.uk/professionals/resources/incidence-and-prevalence-parkinsons-uk-report [Accessed 16 Nov. 2018].

Patel, T., Zhou, J., Piepmeier, J.M. and Saltzman, W.M. (2012) Polymeric nanoparticles for drug delivery to the central nervous system. *Advanced Drug Delivery Reviews,* 64 (7), 701-705.

Paterson, D. and Nordberg, A. (2000) Neuronal nicotinic receptors in the human brain. *Progress in neurobiology,* 61 (1), 75-111.

Peer, D., Karp, J.M., Hong, S., FaroKHzad, O.C., Margalit, R. and Langer, R. (2007) Nanocarriers as an emerging platform for cancer therapy. *Nature Nanotechnology,* 2 (12), 751-760.

Penichet, M., Kang, Y., Pardridge, W., Morrison, S. and Shin, S. (1999) An antibody-avidin fusion protein specific for the transferrin receptor serves as a delivery vehicle for effective brain targeting: Initial applications in anti-HIV antisense drug delivery to the brain. *Journal of Immunology,* 163 (8), 4421-4426.

Pfeiffer, R.F. (2016) Non-motor symptoms in Parkinson's disease. *Parkinsonism & related disorders,* 22 S119-S122.

Poller, B., Gutmann, H., Kraehenbuehl, S., Weksler, B., Romero, I., Couraud, P., Tuffin, G., Drewe, J. and Huwyler, J. (2008) The human brain endothelial cell line hCMEC/D3 as a human blood-brain barrier model for drug transport studies. *Journal of neurochemistry,* 107 (5), 1358-1368.

Pourcher, E., Remillard, S. and Cohen, H. (2010) Compulsive habits in restless legs syndrome patients under dopaminergic treatment. *Journal of the neurological sciences,* 290 (1-2), 52-56.

Price, A., Manzoni, C., Cookson, M.R. and Lewis, P.A. (2018) The LRRK2 signalling system. *Cell and tissue research,* 373 (1), 39-50.

Purkayastha, N., Eyer, K., Robinson, T., Dittrich, P.S., Beck, A.K., Seebach, D., Kolesinska, B. and Cadalbert, R. (2013) Enantiomeric and Diastereoisomeric (Mixed) L/D-Octaarginine

Derivatives - A Simple Way of Modulating the Properties of Cell-Penetrating Peptides. *Chemistry & Biodiversity,* 10 (7), 1165-1184.

Puschmann, A. (2017) New Genes Causing Hereditary Parkinson's Disease or Parkinsonism. *Current Neurology and Neuroscience Reports,* 17 (9), 66.

Qiao, R., Jia, Q., Huewel, S., Xia, R., Liu, T., Gao, F., Galla, H. and Gao, M. (2012) Receptor-Mediated Delivery of Magnetic Nanoparticles across the Blood-Brain Barrier. *Acs Nano,* 6 (4), 3304-3310.

Qosa, H., Miller, D.S., Pasinelli, P. and Trotti, D. (2015) Regulation of ABC efflux transporters at blood-brain barrier in health and neurological disorders. *Brain research,* 1628 298-316.

Quik, M. and Wonnacott, S. (2011) alpha 6 beta 2*and alpha 4 beta 2*Nicotinic Acetylcholine Receptors As Drug Targets for Parkinson's Disease. *Pharmacological reviews,* 63 (4), 938-966.

Räder, A.F.B., Reichart, F., Weinmüller, M. and Kessler, H. (2018) Improving oral bioavailability of cyclic peptides by N-methylation*. Bioorganic & Medicinal Chemistry,* 26(10), 2766-2773.

Ragnaill, M.N., Brown, M., Ye, D., Bramini, M., Callanan, S., Lynch, I. and Dawson, K.A. (2011) Internal benchmarking of a human blood-brain barrier cell model for screening of nanoparticle uptake and transcytosis. *European Journal of Pharmaceutics and Biopharmaceutics,* 77 (3), 360-367.

Rao, J.P. and Geckeler, K.E. (2011) Polymer nanoparticles: Preparation techniques and size-control parameters. *Progress in Polymer Science,* 36 (7), 887-913.

Rao, K.S., Reddy, M.K., Horning, J.L. and Labhasetwar, V. (2008) TAT-conjugated nanoparticles for the CNS delivery of anti-HIV drugs. *Biomaterials,* 29 (33), 4429-4438.

Rao, W., Wang, H., Han, J., Zhao, S., Dumbleton, J., Agarwal, P., Zhang, W., Zhao, G., Yu, J., Zynger, D.L., Lu, X. and He, X. (2015) Chitosan-Decorated Doxorubicin-Encapsulated

Nanoparticle Targets and Eliminates Tumor Reinitiating Cancer Stem-like Cells. *Acs Nano,* 9 (6), 5725-5740.

Rao, W., Zhang, W., Poventud-Fuentes, I., Wang, Y., Lei, Y., Agarwal, P., Weekes, B., Li, C., Lu, X., Yu, J. and He, X. (2014) Thermally responsive nanoparticle-encapsulated curcumin and its combination with mild hyperthermia for enhanced cancer cell destruction. *Acta Biomaterialia,* 10 (2), 831-842.

Regina, A., Romero, I., Greenwood, J., Adamson, P., Bourre, J., Couraud, P. and Roux, F. (1999) Dexamethasone regulation of P-glycoprotein activity in an immortalized rat brain endothelial cell line, GPNT. *Journal of neurochemistry,* 73 (5), 1954-1963.

Reichel, A. (2006) The role of blood-brain barrier studies in the pharmaceutical industry. *Current Drug Metabolism,* 7 (2), 183-203.

Reichel, A., Begley, D.J. and Abbott, N.J. (2003) An Overview of In Vitro Techniques for Blood-Brain Barrier Studies. *In:* Anon.*Methods in Molecular Medicine.* Humana Press, 307--324.

Reimold, I., Domke, D., Bender, J., Seyfried, C.A., Radunz, H. and Fricker, G. (2008) Delivery of nanoparticles to the brain detected by fluorescence microscopy. *European Journal of Pharmaceutics and Biopharmaceutics,* 70 (2), 627-632.

Rempe, R., Cramer, S., Huewel, S. and Galla, H. (2011) Transport of Poly(n-butylcyano-acrylate) nanoparticles across the blood-brain barrier in vitro and their influence on barrier integrity. *Biochemical and biophysical research communications,* 406 (1), 64-69.

Resende, R.R. and Adhikari, A. (2009) Cholinergic receptor pathways involved in apoptosis, cell proliferation and neuronal differentiation. *Cell Communication and Signaling,* 7 20.

Rodriguez, M., Rodriguez-Sabate, C., Morales, I., Sanchez, A. and Sabate, M. (2015) Parkinson's disease as a result of aging. *Aging Cell,* 14 (3), 293-308.

Rosborough, K., Patel, N. and Kalia, L.V. (2017) alpha-Synuclein and Parkinsonism: Updates and Future Perspectives. *Current Neurology and Neuroscience Reports,* 17 (4), 31.

Roux, F. and Couraud, P. (2005) Rat brain endothelial cell lines for the study of blood-brain barrier permeability and transport functions. *Cellular and molecular neurobiology,* 25 (1), 41-58.

Ruan, J., Ji, J., Song, H., Qian, Q., Wang, K., Wang, C. and Cui, D. (2012) Fluorescent magnetic nanoparticle-labeled mesenchymal stem cells for targeted imaging and hyperthermia therapy of in vivo gastric cancer. *Nanoscale Research Letters,* 7 309.

Ruckmani, K., Sivakumar, M. and Ganeshkumar, P.A. (2006) Methotrexate loaded solid lipid nanoparticles (SLN) for effective treatment of carcinoma. *Journal of Nanoscience and Nanotechnology,* 6 (9-10), 2991-2995.

Rupprecht, C., E. (1996) Rhabdoviruses: Rabies Virus. *In:* Baron, S., ed. *Medical Microbiology.* 4th ed. Texas: University of Texas Medical Branch at Galveston, Chapter 61.

Rychahou, P., Bae, Y., Reichel, D., Zaytseva, Y.Y., Lee, E.Y., Napier, D., Weiss, H.L., Roller, N., Frohman, H., Le, A. and Mark Evers, B. (2018) Colorectal cancer lung metastasis treatment with polymer–drug nanoparticles. *Journal of Controlled Release,* 275 85-91.

Sajjanar, B., Saxena, S., Bisht, D., Singh, A.K., Manjunatha Reddy, G.B., Singh, R., Singh, R.P. and Kumar, S. (2015) Effect of nicotinic acetylcholine receptor alpha 1 (nAChRα1) peptides on rabies virus infection in neuronal cells. *Neuropeptides,* 54, 59-64.

Salat, D. and Tolosa, E. (2013) Levodopa in the Treatment of Parkinson's Disease: Current Status and New Developments. *Journal of Parkinsons Disease,* 3 (3), 255-269.

Salomon-Ferrer, R., Goetz, A.W., Poole, D., Le Grand, S. and Walker, R.C. (2013) Routine Microsecond Molecular Dynamics Simulations with AMBER on GPUs. 2. Explicit Solvent Particle Mesh Ewald. *Journal of Chemical Theory and Computation,* 9 (9), 3878-3888.

Sanna, V., Pala, N. and Sechi, M. (2014) Targeted therapy using nanotechnology: focus on cancer. *International Journal of Nanomedicine,* 9 467-483.

Santra, S., Yang, H., Dutta, D., Stanley, J., Holloway, P., Tan, W., Moudgil, B. and Mericle, R. (2004) TAT conjugated, FITC doped silica nanoparticles for bioimaging applications. *Chemical Communications,* (24), 2810-2811.

Saraiva, C., Praca, C., Ferreira, R., Santos, T., Ferreira, L. and Bernardino, L. (2016) Nanoparticle-mediated brain drug delivery: Overcoming blood-brain barrier to treat neurodegenerative diseases. *Journal of Controlled Release,* 235 34-47.

Sarmento, B., Ribeiro, A., Veiga, F., Sampaio, P., Neufeld, R. and Ferreira, D. (2007) Alginate/chitosan nanoparticles are effective for oral insulin delivery. *Pharmaceutical research,* 24 (12), 2198-2206.

Schlosser, P.M., Bale, A.S., Gibbons, C.F., Wilkins, A. and Cooper, G.S. (2015) Human Health Effects of Dichloromethane: Key Findings and Scientific Issues. *Environmental health perspectives,* 123 (2), 114-119.

Schwarze, S., Ho, A., Vocero-Akbani, A. and Dowdy, S. (1999) In vivo protein transduction: Delivery of a biologically active protein into the mouse. *Science,* 285 (5433), 1569-1572.

Scott, C.J., Marouf, W.M., Quinn, D.J., Buick, R.J., Orr, S.J., Donnelly, R.F. and McCarron, P.A. (2008) Immunocolloidal targeting of the endocytotic siglec-7 receptor using peripheral attachment of siglec-7 antibodies to poly(lactide-co-glycolide) nanoparticles. *Pharmaceutical research,* 25 (1), 135-146.

Seabra, A.B. and Duran, N. (2015) Nanotoxicology of Metal Oxide Nanoparticles. *Metals,* 5 (2), 934-975.

Sezgin-bayindir, Z., Ergin, A.D., Parmaksiz, M., Elcin, A.E., Elcin, Y.M. and Yuksel, N. (2016) Evaluation of various block copolymers for micelle formation and brain drug delivery: In vitro characterization and cellular uptake studies. *Journal of Drug Delivery Science and Technology,* 36 120-129.

Shahar, A., Patel, K.V., Semba, R.D., Bandinelli, S., Shahar, D.R., Ferrucci, L. and Guralnik, J.M. (2010) Plasma Selenium is Positively Related to Performance in Neurological Tasks Assessing Coordination and Motor Speed. *Movement Disorders,* 25 (12), 1909-1915.

Shayan, G., Shuler, M.L. and Lee, K.H. (2011) The Effect of Astrocytes on the Induction of Barrier Properties in Aortic Endothelial Cells. *Biotechnology progress,* 27 (4), 1137-1145.

Sheikov, N., McDannold, N., Vykhodtseva, N., Jolesz, F. and Hynynen, K. (2004) Cellular mechanisms of the blood-brain barrier opening induced by ultrasound in presence of microbubbles. *Ultrasound in Medicine and Biology,* 30 (7), 979-989.

Shen, S. and Zhang, W. (2010) ABC Transporters and Drug Efflux at the Blood-Brain Barrier. *Reviews in the neurosciences,* 21 (1), 29-53.

Sheng, Y., Chen, X., Hou, X., Yuan, X., Yuan, B., Yuan, Y., Zhang, Q., Cao, X., Liu, C., Luo, W. and Hu, L. (2017) Urate promotes SNCA/alpha-synuclein clearance via regulating mTOR-dependent macroautophagy. *Experimental neurology,* 297 138-147.

Sian, J., Dexter, D.T., Lees, A.J., Daniel, S., Agid, Y., Javoyagid, F., Jenner, P. and Marsden, C.D. (1994) Alterations in Glutathione Levels in Parkinsons-Disease and Other Neurodegenerative Disorders Affecting Basal Ganglia. *Annals of Neurology,* 36 (3), 348-355.

Siepmann, J. and Siepmann, F. (2012) Modelling of diffusion controlled drug delivery. *Journal of Controlled Release,* 161 (2), 351-362.

Singer, H.S., Mink, J.W., Gilbert, D.L. and Jankovic, J. (2010) 1 - Basal Ganglia Anatomy, Biochemistry, and Physiology. *In:* Singer, H.S., Mink, J.W., Gilbert, D.L. and Jankovic, J., eds. *Movement Disorders in Childhood.* Philadelphia: W.B. Saunders, 2-8.

Snyder, E. and Dowdy, S. (2004) Cell penetrating peptides in drug delivery. *Pharmaceutical research,* 21 (3), 389-393.

Soddu, E., Rassu, G., Giunchedi, P., Sarmento, B. and Gavini, E. (2015) From naturally-occurring neurotoxic agents to CNS shuttles or drug delivery. *European Journal of Pharmaceutical Sciences,* 74, 63-76.

Son, S., Hwang, D.W., Singha, K., Jeong, J.H., Park, T.G., Lee, D.S. and Kim, W.J. (2011) RVG peptide tethered bioreducible polyethylenimine for gene delivery to brain. *Journal of Controlled Release,* 155 (1), 18-25.

Song, K.C., Lee, H.S., Choung, Y., Cho, K.I., Ahn, Y. and Choi, E.J. (2006) The effect of type of organic phase solvents on the particle size of poly(D,L-lactide-co-glycolide) nanoparticles. *Colloids and Surfaces A-Physicochemical and Engineering Aspects,* 276 (1-3), 162-167.

Song, Y., Du, D., Li, L., Xu, J., Dutta, P. and Lin, Y. (2017) In Vitro Study of Receptor-Mediated Silica Nanoparticles Delivery across Blood-Brain Barrier. *Acs Applied Materials & Interfaces,* 9 (24), 20410-20416.

Sorkin, A. and von Zastrow, M. (2002) Signal transduction and endocytosis: Close encounters of many kinds. *Nature Reviews Molecular Cell Biology,* 3 (8), 600-614.

Soudy, R., Gill, A., Sprules, T., Lavasanifar, A. and Kaur, K. (2011) Proteolytically Stable Cancer Targeting Peptides with High Affinity for Breast Cancer Cells. *Journal of medicinal chemistry,* 54 (21), 7523-7534.

Srinivasin, B; Kolli, A.R., Esch, M.B., Abaci, H.E., Shuler, M.L. and Hickman, J.J. (2015) TEER measurement techniques for *in vitro* barrier model systems. *Jala,* 20(2), 107-126.

St John, P.A. and Gordon, H. (2001) Agonists cause endocytosis of nicotinic acetylcholine receptors on cultured myotubes. *Journal of neurobiology,* 49 (3), 212-223.

St Pierre, C.A., Leonard, D., Corvera, S., Kurt-Jones, E.A. and Finberg, R.W. (2011) Antibodies to cell surface proteins redirect intracellular trafficking pathways. *Experimental and molecular pathology,* 91 (3), 723-732.

Stamatovic, S., Shakui, P., Keep, R., Moore, B., Kunkel, S., Van Rooijen, N. and Andjelkovic, A. (2005) Monocyte chemoattractant protein-1 regulation of blood-brain barrier permeability. *Journal of Cerebral Blood Flow and Metabolism,* 25 (5), 593-606.

Stanslowsky, N., Haase, A., Martin, U., Naujock, M., Leffler, A., Dengler, R. and Wegner, F. (2014) Functional differentiation of midbrain neurons from human cord blood-derived induced pluripotent stem cells. *Stem Cell Research & Therapy,* 5 35.

Starkstein, S.E., Brockman, S. and Hayhow, B.D. (2012) Psychiatric syndromes in Parkinson's disease. *Current Opinion in Psychiatry,* 25 (6), 468-472.

Stevanovic, M., Savic, J., Jordovic, B. and Uskokovic, D. (2007) Fabrication, in vitro degradation and the release behaviours of poly(DL-lactide-co-glycolide) nanospheres containing ascorbic acid. *Colloids and Surfaces B-Biointerfaces,* 59 (2), 215-223.

Suchowersky, O. (2002) Parkinson's disease: medical treatment of moderate to advanced disease. *Current neurology and neuroscience reports,* 2 (4), 310-316.

Sullivan, A.M. and Toulouse, A. (2011) Neurotrophic factors for the treatment of Parkinson's disease. *Cytokine & growth factor reviews,* 22 (3), 157-165.

Sun, H., Dai, H., Shaik, N. and Elmquist, W. (2003) Drug efflux transporters in the CNS. *Advanced Drug Delivery Reviews,* 55 (1), 83-105.

Surolia, R., Pachauri, M. and Ghosh, P.C. (2012) Preparation and Characterization of Monensin Loaded PLGA Nanoparticles: In Vitro Anti-Malarial Activity Against Plasmodium Falciparum. *Journal of Biomedical Nanotechnology,* 8 (1), 172-181.

Takayama, H., Ray, J., Raymon, H., Baird, A., Hogg, J., Fisher, L. And Gage, F. (1995) Basic Fibroblast Growth-Factor Increases Dopaminergic Graft-Survival and Function in a Rat Model of Parkinsons-Disease. *Nature medicine,* 1 (1), 53-58.

Tanaka, K.A., Key, N.S. and Levy, J.H. (2009) Blood Coagulation: Hemostasis and Thrombin Regulation. *Anesthesia and Analgesia,* 108 (5), 1433-1446.

Teixidó, M. and Giralt, E. (2008) The role of peptides in blood-brain barrier nanotechnology. *Journal of Peptide Science,* 14 (2), 163-173.

Tewari, A., Jog, R. and Jog, M.S. (2016) The Striatum and Subthalamic Nucleus as Independent and Collaborative Structures in Motor Control. *Frontiers in Systems Neuroscience,* 10 UNSP 17.

TG Study Grp (2017) Randomized Parkinson's trial of GDNF administered via intermittent intraputamenal convection-enhanced delivery. *Movement Disorders,* 32.

Thakkar, K.N., Mhatre, S.S. and Parikh, R.Y. (2010) Biological synthesis of metallic nanoparticles. *Nanomedicine-Nanotechnology Biology and Medicine,* 6 (2), 257-262.

Thavasu, P.W., Longhurst, S., Joel, S.P., Slevin, M.L. and Balkwill, F.R. (1992) Measuring Cytokine Levels in Blood - Importance of Anticoagulants, Processing, and Storage-Conditions. *Journal of immunological methods,* 153 (1-2), 115-124.

The Parkinson's Study Group (1993) Effects of Tocopherol and Deprenyl on the Progression of Disability in Early Parkinson's Disease. *N Engl J Med,* 328 (3), 176-183.

Thomsen, L.B., Burkhart, A. and Moos, T. (2015) A Triple Culture Model of the Blood-Brain Barrier Using Porcine Brain Endothelial cells, Astrocytes and Pericytes. *Plos One,* 10 (8), e0134765.

Thoulouze, M., Lafage, M., Schachner, M., Hartmann, U., Cremer, H. and Lafon, M. (1998) The neural cell adhesion molecule is a receptor for rabies virus. *Journal of Virology,* 72(9), 7181-7190.

Tietz, S. and Engelhardt, B. (2015) Brain barriers: Crosstalk between complex tight junctions and adherens junctions. *Journal of Cell Biology,* 209 (4), 493-506.

Tilling, T., Engelbertz, C., Decker, S., Korte, D., Huwel, S. and Galla, H. (2002) Expression and adhesive properties of basement membrane proteins in cerebral capillary endothelial cell cultures. *Cell and tissue research,* 310 (1), 19-29.

Timmer, M., Cesnulevicius, K., Winkler, C., Kolb, J., Lipokatic-Takacs, E., Jungnickel, J. and Grothe, C. (2007) Fibroblast growth factor (FGF)-2 and FGF receptor 3 are required for the development of the substantia nigra, and FGF-2 plays a crucial role for the rescue of dopaminergic neurons after 6-hydroxydopamine lesion. *Journal of Neuroscience,* 27 (3), 459-471.

Timmer, M., Grosskreutz, J., Schlesinger, F., Krampfl, K., Wesemann, M., Just, L., Bufler, J. and Grothe, C. (2006) Dopaminergic properties and function after grafting of attached neural precursor cultures. *Neurobiology of disease,* 21 (3), 587-606.

Toivonen, J.M., Olivan, S. and Osta, R. (2010) Tetanus Toxin C-Fragment: The Courier and the Cure? *Toxins,* 2 (11), 2622-2644.

Tomlinson, C.L., Stowe, R., Patel, S., Rick, C., Gray, R. and Clarke, C.E. (2010) Systematic Review of Levodopa Dose Equivalency Reporting in Parkinson's Disease. *Movement Disorders,* 25 (15), 2649-2653.

Tong, L., Wei, Q., Wei, A. and Cheng, J. (2009) Gold Nanorods as Contrast Agents for Biological Imaging: Optical Properties, Surface Conjugation and Photothermal Effects. *Photochemistry and photobiology,* 85 (1), 21-32.

Tooyama, I., Kawamata, T., Walker, D., Yamada, T., Hanai, K., Kimura, H., Iwane, M., Igarashi, K., Mcgeer, E.G. and Mcgeer, P.L. (1993) Loss of Basic Fibroblast Growth-Factor in Substantia-Nigra Neurons in Parkinsons-Disease. *Neurology,* 43 (2), 372-376.

Toth, A., Veszelka, S., Nakagawa, S., Niwa, M. and Deli, M.A. (2011) Patented in vitro blood-brain barrier models in CNS drug discovery. *Recent patents on CNS drug discovery,* 6 (2), 107-18.

Tsetlin, V. and Hucho, F. (2004) Snake and snail toxins acting on nicotinic acetylcholine receptors: fundamental aspects and medical applications. *FEBS letters,* 557 (1-3), 9-13.

Tuffereau, C., Benejean, J., Roque-Alfonso, A., Flamand, A. and Fishman, M. (1998) Neuronal cell surface molecules mediate specific binding to rabies virus glycoprotein expressed by a recombinant baculovirus on the surfaces of lepidopteran cells. *Journal of Virology,* 17(24), 7250-7259.

Tuffereau, C., Benejean, J., Roque-Alfonso, A., Flamand, A. and Fishman, M. (1998) *Neuronal cell surface molecules mediate specific binding to rabies virus glycoprotein expressed by a recombinant baculovirus on the surfaces of lepidopteran cells.* Journal of Virology: American Society for Microbiology.

Tuffereau, C., Schmidt, K., Langevin, C., Lafay, F., Dechant, G. and Koltzenburg, M. (2007) The rabies virus glycoprotein receptor p75(NTR) is not essential for rabies virus infection. *Journal of Virology,* 81(24), 13622-13630.

Tzeng, S.Y., Higgins, L.J., Pomper, M.G. and Green, J.J. (2013) Student award winner in the Ph.D. category for the 2013 society for biomaterials annual meeting and exposition, april 10-13,

2013, Boston, Massachusetts: Biomaterial-mediated cancer-specific DNA delivery to liver cell cultures using synthetic poly(beta-amino ester)s. *Journal of Biomedical Materials Research - Part A,* 101 A (7), 1837-1845.

Uhlig, T., Kyprianou, T., Martinelli, F.G., Oppici, C.A., Heiligers, D., Hills, D., Calvo, X.R. and Verhaert, P. (2014) The emergence of peptides in the pharmaceutical business: From exploration to exploitation. *EuPA Open Proteomics,* 4, 58-69.

Ul Ain, Q., Lee, J.H., Woo, Y.S. and Kim, Y. (2016) Effects of protein transduction domain (PTD) selection and position for improved intracellular delivery of PTD-Hsp27 fusion protein formulations. *Archives of Pharmacal Research,* 39 (9), 1266-1274.

Ulbrich, K., Hekmatara, T., Herbert, E. and Kreuter, J. (2009) Transferrin- and transferrin-receptor-antibody-modified nanoparticles enable drug delivery across the blood-brain barrier (BBB). *European Journal of Pharmaceutics and Biopharmaceutics,* 71 (2), 251-256.

Vajn, K., Viljetic, B., Degmecic, I.V., Schnaar, R.L. and Heffer, M. (2013) Differential Distribution of Major Brain Gangliosides in the Adult Mouse Central Nervous System. *Plos One,* 8 (9), e75720.

van den Berge, S.A., van Strien, M.E. and Hol, E.M. (2013) Resident adult neural stem cells in Parkinson′s disease—The brain′s own repair system? *European Journal of Pharmacology,* 719 (1), 117-127.

Verma, D.K., Singh, D.K., Gupta, S., Gupta, P., Singh, A., Biswas, J. and Singh, S. (2018) Minocycline diminishes the rotenone induced neurotoxicity and glial activation via suppression of apoptosis, nitrite levels and oxidative stress. *Neurotoxicology,* 65 9-21.

Veszelka, S., Pasztoi, M., Farkas, A.E., Krizbai, I., Dung, N.T.K., Niwa, M., Abraham, C.S. and Deli, M.A. (2007) Pentosan polysulfate protects brain endothelial cells against bacterial lipopolysaccharide-induced damages. *Neurochemistry international,* 50 (1), 219-228.

Veszelka, S., Toth, A., Walter, F.R., Toth, A.E., Grof, I., Meszaros, M., Bocsik, A., Hellinger, E., Vastag, M., Rakhely, G. and Deli, M.A. (2018) Comparison of a Rat Primary Cell-Based Blood-Brain Barrier Model With Epithelial and Brain Endothelial Cell Lines: Gene Expression and Drug Transport. *Frontiers in Molecular Neuroscience,* 11 166.

Vigerelli, H., Sciani, J.M., Jared, C., Antoniazzi, M.M., Medeiros Caporale, G.M., Rodrigues da Silva, A and Pimenta, D.C. (2014) Bufotenine is able to block rabies virus infection in BHK-21 cells. *Journal of Venomous Animals and Toxins Including Tropical Diseases,* 20 45.

Voigt, N., Henrich-Noack, P., Kockentiedt, S., Hintz, W., Tomas, J. and Sabel, B.A. (2014) Surfactants, not size or zeta-potential influence blood–brain barrier passage of polymeric nanoparticles. *European Journal of Pharmaceutics and Biopharmaceutics,* 87 (1), 19-29.

Vorbrodt, A. and Dobrogowska, D. (2004) Molecular anatomy of interendothelial junctions in human blood-brain barrier microvessels. *Folia Histochemica Et Cytobiologica,* 42 (2), 67-75.

Wagner, V., Dullaart, A., Bock, A. and Zweck, A. (2006) The emerging nanomedicine landscape. *Nature biotechnology,* 24 (10), 1211-1217.

Wang, H., Wan, G., Liu, Y., Chen, B., Chen, H., Zhang, S., Wang, D., Xiong, Q., Zhang, N. and Wang, Y. (2016) Dual-responsive nanoparticles based on oxidized pullulan and a disulfide-containing poly(beta-amino) ester for efficient delivery of genes and chemotherapeutic agents targeting hepatoma. *Polymer Chemistry,* 7 (41), 6340-6353.

Wang, J., Wang, Q., Zhou, F., Li, J., Li, Q., Zhou, H., Li, S., Ma, S. and Wen, T. (2018) The antitumor effect of TAT-DCF1 peptide in glioma cells. *Neuropeptides,* 71 21-31.

Wang, K., Wang, J., Wang, Y., He, Q., Wang, X. and Wang, X. (2004) Infusion of epidermal growth factor and basic fibroblast growth factor into the striatum of parkinsonian rats leads to in vitro proliferation and differentiation of adult neural progenitor cells. *Neuroscience letters,* 364 (3), 154-158.

Wang, S., Noberini, R., Stebbins, J.L., Das, S., Zhang, Z., Wu, B., Mitra, S., Billet, S., Fernandez, A., Bhowmick, N.A., Kitada, S., Pasquale, E.B., Fisher, P.B. and Pellecchia, M. (2013) Targeted Delivery of Paclitaxel to EphA2-Expressing Cancer Cells. *Clinical Cancer Research,* 19 (1), 128-137.

Watanabe, T., Dohgu, S., Takata, F., Nishioku, T., Nakashima, A., Futagami, K., Yamauchi, A. and Kataoka, Y. (2013) Paracellular Barrier and Tight Junction Protein Expression in the Immortalized Brain Endothelial Cell Lines bEND.3, bEND.5 and Mouse Brain Endothelial Cell 4. *Biological & pharmaceutical bulletin,* 36 (3), 492-495.

Watson, P.M.D., Paterson, J.C., Thom, G., Ginman, U., Lundquist, S. and Webster, C.I. (2013) Modelling the endothelial blood-CNS barriers: a method for the production of robust in vitro models of the rat blood-brain barrier and blood-spinal cord barrier. *Bmc Neuroscience,* 14 59.

Wender, P.A., Galliher, W.C., Goun, E.A., Jones, L.R. and Pillow, T.H. (2008) The design of guanidinium-rich transporters and their internalization mechanisms. *Advanced Drug Delivery Reviews,* 60 (4-5), 452-472.

Werle, M. and Bernkop-Schnurch, A. (2006) Strategies to improve plasma half life time of peptide and protein drugs. *Amino acids,* 30 (4), 351-367.

Wicki, A., Witzigmann, D., Balasubramanian, V. and Huwyler, J. (2015) Nanomedicine in cancer therapy: Challenges, opportunities, and clinical applications. *Journal of Controlled Release,* 200 138-157.

Wilhelm, I., Fazakas, C. and Krizbai, I.A. (2011) In vitro models of the blood-brain barrier. *Acta Neurobiologiae Experimentalis,* 71 (1), 113-128.

Wilson, B., Samanta, M.K., Santhi, K., Kumar, K.P.S., Paramakrishnan, N. and Suresh, B. (2008) Poly(n-butylcyanoacrylate) nanoparticles coated with polysorbate 80 for the targeted delivery of rivastigmine into the brain to treat Alzheimer's disease. *Brain research,* 1200 159-168.

Wisniewska-Kruk, J., Hoeben, K.A., Vogels, I.M.C., Gaillard, P.J., Van Noorden, C.J.F., Schlingemann, R.O. and Klaassen, I. (2012) A novel co-culture model of the blood-retinal barrier based on primary retinal endothelial cells, pericytes and astrocytes. *Experimental eye research,* 96 (1), 181-190.

Witt, K.A., Gillespie, T.J., Huber, J.D., Egleton, R.D. and Davis, T.P. (2001) Peptide drug modifications to enhance bioavailability and blood-brain barrier permeability. *Peptides,* 22 (12), 2329-2343.

Wolfbeis, O.S. (2015) An overview of nanoparticles commonly used in fluorescent bioimaging. *Chemical Society Reviews,* 44 (14), 4743-4768.

Wu, J., Zhang, E. and Fu, A. (2016) A novel cell-permeable RDP-p53 fusion protein for specific inhibition on the growth of cancerous neural cells. *Drug delivery,* 23 (7), 2464-2470.

Wu, J., Zhang, E. and Fu, A. (2016) A novel cell-permeable RDP-p53 fusion protein for specific inhibition on the growth of cancerous neural cells. *Drug delivery,* 23 (7), 2464-2470.

Xia, H., Gao, X., Gu, G., Liu, Z., Hu, Q., Tu, Y., Song, Q., Yao, L., Pang, Z., Jiang, X., Chen, J. and Chen, H. (2012) Penetratin-functionalized PEG-PLA nanoparticles for brain drug delivery. *International journal of pharmaceutics,* 436 (1-2), 840-850.

Xiang, Y., Liang, L., Wang, X., Wang, J., Zhang, X. and Zhang, Q. (2011) Chloride channel-mediated brain glioma targeting of chlorotoxin-modified doxorubicine-loaded liposomes. *Journal of Controlled Release,* 152 (3), 402-410.

Xiao, D., Jia, H., Zhang, J., Liu, C., Zhuo, R. and Zhang, X. (2014) A Dual-Responsive Mesoporous Silica Nanoparticle for Tumor-Triggered Targeting Drug Delivery. *Small,* 10 (3), 591-598.

Xiao, Y., Zhang, E. and Fu, A. (2017) Promotion of SH-SY5Y Cell Growth by Gold Nanoparticles Modified with 6-Mercaptopurine and a Neuron-Penetrating Peptide. *Nanoscale Research Letters,* 12 641.

Xicoy, H., Wieringa, B. and Martens, G.J.M. (2017) The SH-SY5Y cell line in Parkinson's disease research: a systematic review. *Molecular Neurodegeneration,* 12 10.

Xu, D., Jin, T., Zhu, H., Chen, H., Ofengeim, D., Zou, C., Mifflin, L., Pan, L., Amin, P., Li, W., Shan, B., Naito, M.G., Meng, H., Li, Y., Pan, H., Aron, L., Adiconis, X., Levin, J.Z., Yankner, B.A. and Yuan, J. (2018) TBK1 Suppresses RIPK1-Driven Apoptosis and Inflammation during Development and in Aging. *Cell,* 174 (6), 1477-1491.e19.

Xu, G., Yong, K., Roy, I., Mahajan, S.D., Ding, H., Schwartz, S.A. and Prasad, P.N. (2008) Bioconjugated quantum rods as targeted probes for efficient transmigration across an in vitro blood-brain barrier. *Bioconjugate chemistry,* 19 (6), 1179-1185.

Xu, L., Dan, M., Shao, A., Cheng, X., Zhang, C., Yokel, R.A., Takemura, T., Hanagata, N., Niwa, M. and Watanabe, D. (2015) Silver nanoparticles induce tight junction disruption and astrocyte neurotoxicity in a rat blood-brain barrier primary triple coculture model. *International Journal of Nanomedicine,* 10 6105-6119.

Xu, Y., Kim, C., Saylor, D.M. and Koo, D. (2017) Polymer degradation and drug delivery in PLGA-based drug-polymer applications: A review of experiments and theories. *Journal of Biomedical Materials Research Part B-Applied Biomaterials,* 105 (6), 1692-1716.

Yacoubian, T.A. and Standaert, D.G. (2009) Targets for neuroprotection in Parkinson's disease. *Biochimica et Biophysica Acta (BBA) - Molecular Basis of Disease,* 1792 (7), 676-687.

Yalcin, T.E., Ilbasmis-Tamer, S., Ibisoglu, B., Ozdemir, A., Ark, M. and Takka, S. (2018) Gemcitabine hydrochloride-loaded liposomes and nanoparticles: comparison of encapsulation

efficiency, drug release, particle size, and cytotoxicity. *Pharmaceutical development and technology,* 23 (1), 76-86.

Yamashita, T., Ninomiya, M., Acosta, P.H., Garcia-Verdugo, J.M., Sunabori, T., Sakaguchi, M., Adachi, K., Kojima, T., Hirota, Y., Kawase, T., Araki, N., Abe, K., Okano, H. and Sawamoto, K. (2006) Subventricular zone-derived neuroblasts migrate and differentiate into mature neurons in the post-stroke adult striatum. *Journal of Neuroscience,* 26 (24), 6627-6636.

Yameen, B., Choi, W.I., Vilos, C., Swami, A., Shi, J. and Farokhzad, O.C. (2014) Insight into nanoparticle cellular uptake and intracellular targeting*. Journal of Controlled Release*, 198, 485-499.

Yan, F., Zhang, C., Zheng, Y., Mei, L., Tang, L., Song, C., Sun, H. and Huang, L. (2010) The effect of poloxamer 188 on nanoparticle morphology, size, cancer cell uptake, and cytotoxicity. *Nanomedicine-Nanotechnology Biology and Medicine,* 6 (1), 170-178.

Yan, X.Z., Mohankumar, P.S., Dietzschold, B., Schnell, M.J. and Fu, Z.F. (2002) The rabies virus glycoprotein determines the distribution of different rabies virus strains in the brain. *Journal of Neurovirology,* 8(4), 345-352.

Yan, X.Z., Mohankumar, P.S., Dietzschold, B., Schnell, M.J. and Fu, Z.F. (2002) The rabies virus glycoprotein determines the distribution of different rabies virus strains in the brain. *Journal of neurovirology,* 8 (4), 345-352.

Yang, S., Jin, H. and Zhao, Z. (2018) An ECV304 monoculture model for permeability assessment of blood-brain barrier. *Neurological research,* 40 (2), 117-121.

Ye, D., Raghnaill, M.N., Bramini, M., Mahon, E., Aberg, C., Salvati, A. and Dawson, K.A. (2013) Nanoparticle accumulation and transcytosis in brain endothelial cell layers. *Nanoscale,* 5 (22), 11153-11165.

Yoshimura, S., Teramoto, T., Whalen, M.J., Irizarry, M.C., Takagi, Y., Qiu, J.H., Harada, J., Waeber, C., Breakefield, X.O. and Moskowitz, M.A. (2003) FGF-2 regulates neurogenesis and degeneration in the dentate gyrus after traumatic brain injury in mice. *Journal of Clinical Investigation,* 112 (8), 1202-1210.

Yuan, H., Zheng, J., Liu, P., Zhang, S., Xu, J. and Bai, L. (2007) Pathogenesis of Parkinson's disease: oxidative stress, environmental impact factors and inflammatory processes. *Neuroscience bulletin,* 23 (2), 125-30.

Zachrisson, O., Zhao, M., Andersson, A., Dannaeus, K., Haggblad, J.H., Isacson, R., Nielsen, E., Patrone, C., Ronnholm, H., Wikstrom, L., Delfani, K., McCormack, A.L., Palmer, T., Di Monte, D.A., Hill, M.P., Lang, A.M.J. and Haegerstrand, A. (2011) Restorative Effects of Platelet Derived Growth Factor-BB in Rodent Models of Parkinson's Disease. *Journal of Parkinsons Disease,* 1 (1), 49-63.

Zafar, K., Siddiqui, A., Sayeed, I., Ahmad, M., Salim, S. and Islam, F. (2003) Dose-dependent protective effect of selenium in rat model of Parkinson's disease: neurobehavioral and neurochemical evidences. *Journal of neurochemistry,* 84 (3), 438-446.

Zamboni, C.G., Kozielski, K.L., Vaughan, H.J., Nakata, M.M., Kim, J., Higgins, L.J., Pomper, M.G. and Green, J.J. (2017) Polymeric nanoparticles as cancer-specific DNA delivery vectors to human hepatocellular carcinoma. *Journal of Controlled Release,* 263 18-28.

Zeller, S., Choi, C.S., Uchil, P.D., Ban, H., Siefert, A., Fahmy, T.M., Mothes, W., Lee, S. and Kumar, P. (2015) Attachment of Cell-Binding Ligands to Arginine-Rich Cell-Penetrating Peptides Enables Cytosolic Translocation of Complexed siRNA. *Chemistry & biology,* 22 (1), 50-62.

Zeng, X., Geng, W. and Jia, J. (2018) Neurotoxin-Induced Animal Models of Parkinson Disease: Pathogenic Mechanism and Assessment. *Asn Neuro,* 10.

Zhan, C., Li, B., Hu, L., Wei, X., Feng, L., Fu, W. and Lu, W. (2011) Micelle-Based Brain-Targeted Drug Delivery Enabled by a Nicotine Acetylcholine Receptor Ligand. *Angewandte Chemie-International Edition,* 50 (24), 5482-5485.

Zhan, C., Yan, Z., Xie, C. and Lu, W. (2010) Loop 2 of Ophiophagus hannah Toxin b Binds with Neuronal Nicotinic Acetylcholine Receptors and Enhances Intracranial Drug Delivery. *Molecular Pharmaceutics,* 7 (6), 1940-1947.

Zhan, C., Yan, Z., Xie, C. and Lu, W. (2010) Loop 2 of Ophiophagus hannah Toxin b Binds with Neuronal Nicotinic Acetylcholine Receptors and Enhances Intracranial Drug Delivery. *Molecular Pharmaceutics,* 7 (6), 1940-1947.

Zhang, B., Sun, X., Mei, H., Wang, Y., Liao, Z., Chen, J., Zhang, Q., Hu, Y., Pang, Z. and Jiang, X. (2013) LDLR-mediated peptide-22-conjugated nanoparticles for dual-targeting therapy of brain glioma. *Biomaterials,* 34 (36), 9171-9182.

Zhang, B., Sun, X., Mei, H., Wang, Y., Liao, Z., Chen, J., Zhang, Q., Hu, Y., Pang, Z. and Jiang, X. (2013) LDLR-mediated peptide-22-conjugated nanoparticles for dual-targeting therapy of brain glioma. *Biomaterials,* 34 (36), 9171-9182.

Zhang, C., An, T., Wang, D., Wan, G., Zhang, M., Wang, H., Zhang, S., Li, R., Yang, X. and Wang, Y. (2016) Stepwise pH-responsive nanoparticles containing charge-reversible pullulan-based shells and poly(beta-amino ester)/poly(lactic-co-glycolic acid) cores as carriers of anticancer drugs for combination therapy on hepatocellular carcinoma. *Journal of Controlled Release,* 226 193-204.

Zhang, E. and Fu, A. (2015) A new strategy for specific imaging of neural cells based on peptide-conjugated gold nanoclusters. *International Journal of Nanomedicine,* 10, 2115-2124.

Zhang, J., Perry, G., Smith, M.A., Robertson, D., Olson, S.J., Graham, D.G. and Montine, T.J. (1999) Parkinson's Disease Is Associated with Oxidative Damage to Cytoplasmic DNA and RNA in Substantia Nigra Neurons. *The American Journal of Pathology,* 154 (5), 1423-1429.

Zhang, Q., Liu, Y., Yang, N., Wan, X. and Zuo, P. (2008) Nasal administration of cholera toxin B subunit-nerve growth factor improves the space learning and memory abilities in beta-amyloid protein(25-35)-induced amnesic mice. *Neuroscience,* 155 (1), 234-240.

Zhang, S., Wang, D., Li, Y., Li, L., Chen, H., Xiong, Q., Liu, Y. and Wang, Y. (2018) pH- and redox-responsive nanoparticles composed of charge-reversible pullulan-based shells and disulfide-containing poly(beta-amino ester) cores for co-delivery of a gene and chemotherapeutic agent. *Nanotechnology,* 29 (32), 325101.

Zhang, X., Du, L., Zhang, W., Yang, Y., Zhou, Q. and Du, G. (2017) Therapeutic effects of baicalein on rotenone-induced Parkinson's disease through protecting mitochondrial function and biogenesis. *Scientific Reports,* 7 9968.

Zhao, M., Zhao, M., Fu, C., Yu, Y. and Fu, A. (2018) Targeted therapy of intracranial glioma model mice with curcumin nanoliposomes. *International Journal of Nanomedicine,* 13 1601-1610.

Zhao, X., Shang, T., Zhang, X., Ye, T., Wang, D. and Rei, L. (2016) Passage of Magnetic Tat-Conjugated Fe3O4@SiO2 Nanoparticles Across In Vitro Blood-Brain Barrier. *Nanoscale Research Letters,* 11 451.

Zhao, Y., Li, X., Lu, C., Lin, M., Chen, L., Xiang, Q., Zhang, M., Jin, R., Jiang, X., Shen, X., Li, X. and Cai, J. (2014) Gelatin nanostructured lipid carriers-mediated intranasal delivery of basic fibroblast growth factor enhances functional recovery in hemiparkinsonian rats. *Nanomedicine-Nanotechnology Biology and Medicine,* 10 (4), 755-764.

Zhou, Y., Peng, Z., Seven, E.S. and Leblanc, R.M. (2018) Crossing the blood-brain barrier with nanoparticles. *Journal of Controlled Release,* 270 290-303.

Zhu, Q., Zhuang, X. and Lu, J. (2018) Neuroprotective effects of baicalein in animal models of Parkinson's disease: A systematic review of experimental studies. *Phytomedicine.*

Zhu, X. and Braatz, R.D. (2015) A mechanistic model for drug release in PLGA biodegradable stent coatings coupled with polymer degradation and erosion. *Journal of Biomedical Materials Research Part a,* 103 (7), 2269-2279.

Zhu, X., Pang, Z. and Shen, S. (2017) Tumor Microenvironment Responsive ACPP-Conjugated Micelles for Targeted Treatment of Brain Glioma. *Particle & Particle Systems Characterization,* 34 (2), UNSP 1600201.

Zou, L., Ma, J., Wang, T., Yang, T. and Liu, C. (2013) Cell-Penetrating Peptide-Mediated Therapeutic Molecule Delivery into the Central Nervous System. *Current Neuropharmacology,* 11 (2), 197-208.

Zucca, F., Giaveri, G., Gallorini, M., Albertini, A., Toscani, M., Pezzoli, G., Lucius, R., Wilms, H., Sulzer, D., Ito, S., Wakamatsu, K. and Zecca, L. (2004) The neuromelanin of human substantia nigra: Physiological and pathogenic aspects. *Pigment Cell Research,* 17 (6), 610-617.

Appendix 1

1.5 M Tris Buffer pH 6.8

18.17 g Tris base

70 mL double distilled water

Adjust to pH 6.8 with HCl

Make up to 100 mL

Laemmli sample treatment buffer (5x)

2 mL Tris buffer pH 6.8 (1.5 M)

5 mL glycerol

2.5 mL mercaptoethanol

1 g sodium dodecyl sulphate

0.5 mL bromophenol blue (1%)

Gel Stain

0.25 g Coomassie Brilliiant Blue

10 mL glacial acetic acid

45 mL methanol

45 mL water

Gel Destain

25 mL glacial acetic acid

150 mL methanol

325 mL water

Appendix 2

(A)

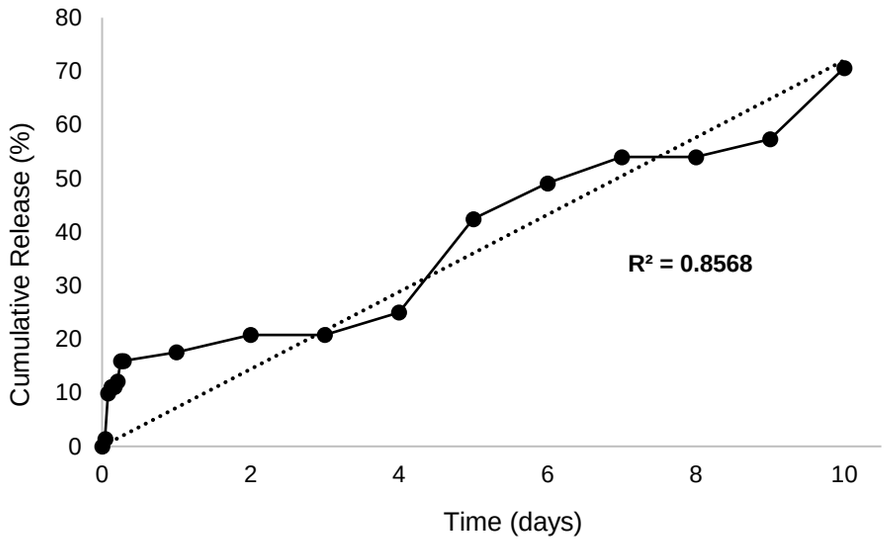

(B)

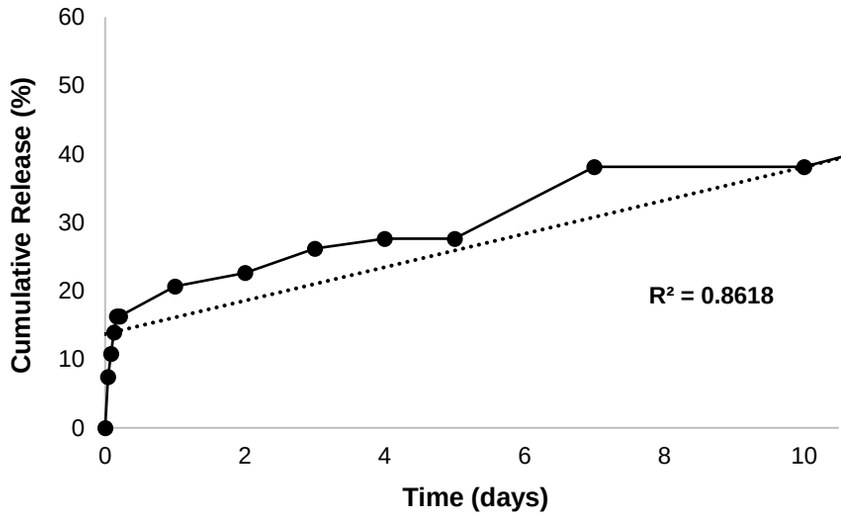

Figure A2.1. Zero order plot showing release kinetics of (A) myoglobin and (B) doxorubicin from PLGA NP at 37°C in PBS.

(A)

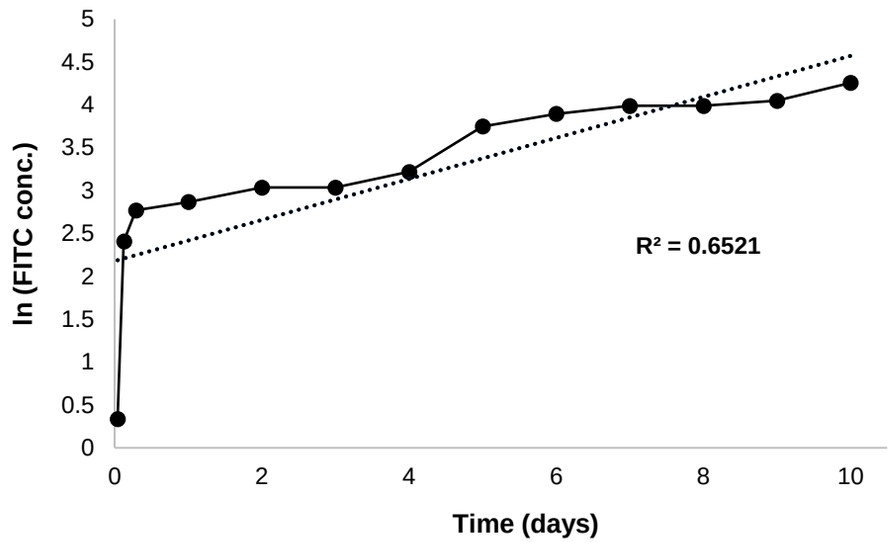

(B)

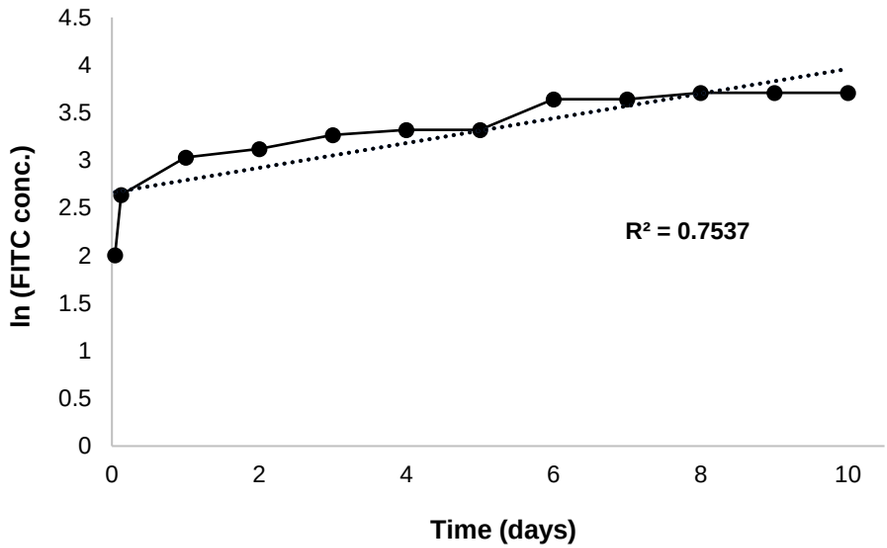

Figure A2.2. First order plot showing release kinetics of (A) myoglobin and (B) doxorubicin from PLGA NP at 37°C in PBS.

Appendix 3

JOURNAL OF DRUG TARGETING, 2017
VOL. 25, NO. 5, 379–385
http://dx.doi.org/10.1080/1061186X.2016.1223676

Taylor & Francis
Taylor & Francis Group

REVIEW ARTICLE

The potential use of rabies virus glycoprotein-derived peptides to facilitate drug delivery into the central nervous system: a mini review

Rachel Huey, Susan Hawthorne and Paul McCarron

School of Pharmacy and Pharmaceutical Sciences, Ulster University, Coleraine, UK

ABSTRACT

Rabies virus glycoprotein (RVG), a 505 amino acid type-1 glycoprotein, is responsible for the neurotrophic nature of the rabies virus infection. Despite varying reports in the literature as to which receptor is ultimately responsible for interaction of RVG with the nervous system, there is a strong argument for major nicotinic acetylcholine receptor (nAChR) involvement. Peptide derivatives of RVG, such as rabies virus-derived peptide (RDP) and RVG-29 are emerging as promising targeting ligands for the delivery of therapeutics to the central nervous system (CNS). The neurotrophic nature of RVG and indeed its derivatives may be due to interaction with ubiquitous nAChRs principally, but also association with other neural cell-specific molecules such as neural cell adhesion molecule (NCAM). It is possible that nAChR-mediated uptake of RVG-derived peptides may serve as an attractive new approach for targeting drug delivery to the brain. Potential application of this type of drug delivery system extends to many diseases affecting the CNS, where specific and effective drug delivery is normally a challenging process.

ARTICLE HISTORY
Received 20 June 2016
Revised 9 August 2016
Accepted 9 August 2016
Published online 1 September 2016

KEYWORDS
Rabies virus; glycoprotein; nicotinic acetylcholine receptor; peptide; targeted; delivery; central nervous system

Introduction

The emergence of peptides derived from the rabies virus glycoprotein (RVG) as targeting ligands for drug delivery to the brain, has shown promise as an effective way of non-invasively overcoming the blood brain barrier (BBB) for targeted therapy. RVG forms the part of the rabies virus which is responsible for this neural interaction and is ultimately responsible for the highly neurotrophic nature of the rabies virus itself, as it is the only surface protein expressed on the viral envelope [1]. Son et al. [2] described RVG as a potential "magic bullet" for the targeting of genes to the brain. Rabies Virus-derived peptide (RDP) is a 39 amino acid derivative of residues 330–357 of RVG, which has been determined as an important nerve binding region [3]. Due to this, RDP may retain the neurotrophic penetrating properties of RVG, acting as a facilitating ligand for neural cell entry of a conjugated payload. RDP has been utilised successfully to deliver therapeutic payloads to mouse brain *in vivo* [3], gaining effective entry into the central nervous system (CNS) and showing preferential accumulation in neural cells compared to non-neural, both *in vitro* and *in vivo* [4]. Likewise, it has been peripherally conjugated to gold nanoclusters for non-invasive brain screening, due to its observed ability to specifically accumulate in neurons *in vivo* [5]. Another derivative of RVG, RVG-29, allowed preferential accumulation of an Itraconazole payload in neural cells when conjugated to an albumin nanoparticle carrier [6]. Furthermore, Liu et al. [7] showed how nanoparticles coated with RVG-29 exhibited higher BBB crossing efficiency than unmodified nanoparticles.

Thus far, there has been conflicting evidence in the literature as to which receptor is utilised in these synthetic peptide-neural interactions and indeed by the RVG itself. Fu et al. [4] reports that the $GABA_{(a)}$ receptor is responsible for RDP uptake in neural cells, however RVG-29 has been linked to both the $GABA_{(b)}$ [7] and the nicotinic acetylcholine receptor (nAChR) [8,9]. There has been a wealth of work invested over the past three decades in elucidating which receptor is responsible for the highly neurotrophic nature of the rabies virus infection. To date, the evidence available in the literature does not allow a definitive conclusion to be made regarding one particular receptor being responsible for rabies virus infectivity. Rather, it appears likely that other factors are involved and should be considered in the interaction with neural cells.

This review will consider the RVG and the different receptors with which it has been linked. Given the abundance of evidence that would indicate major nAChR involvement, these receptors will also be discussed in regards to subtypes, typical structure and potential use as a target to mediate drug delivery into the CNS through exploitation of the hypothetical interaction with RVG. It may be possible to utilise this interaction to deliver therapeutic agents non-invasively across the BBB, with a view of treating neurodegenerative processes such as Parkinsons Disease (PD). It is therefore important that the receptor interaction of these RVG-derived peptides with neural cells is considered, if they are to be brought forward as potential drug-targeting moieties, to aid modelling and optimisation for *in vivo* success.

Rabies virus

The rabies virus is a pathogen of the mammalian nervous system, usually transferred from the saliva of an infected animal bite. The virus mostly affects motor neurons due to entry through the neuromuscular junction (NMJ) upon muscle infection [8], however Lycke & Tsiang [10] indicated that peripheral sensory neurons are also likely to be infected even though the receptor responsible for uptake had yet to be identified. Lewis et al. [11] studied rabies virus entry at the NMJ in chick nerve-muscle co-cultures as a major site of entry into neurons and consequently the CNS. Further supporting the evidence of both motor and sensory

CONTACT Dr. Susan Hawthorne s.hawthorne@ulster.ac.uk School of Pharmacy and Pharmaceutical Sciences, Ulster University, Cromore Road, Coleraine, UK
This article was originally published with errors. This version has been corrected. Please see Corrigendum. (http://dx.doi.org./10.1080/1061186X.2017.1302138)

neuron infection, this study also detailed how the virus travels throughout the nervous system via axonal retrograde transport. The retrograde pathway has been well established as the method of transport for the rabies virus as reviewed by Cherian et al. [12] and indeed other neurotoxins, from distal infection sites, such as the tetanus toxin [13]. Incidentally, the Tet-1 peptide has been looked at as a targeting peptide for the CNS by Kwon et al. [14], for the delivery of nucleic acids to neural cells in mice. This is another example of using an infective neuropeptide to direct a payload to a neural site, similar to the utilisation of RDP by Fu et al. [3,4].

Rabies virus glycoprotein (RVG)

RVG and the *nAChR*

RVG is a 505 amino acid type 1 membrane glycoprotein which is essential for infectivity of the Rabies Virus [15], as it is responsible for attachment to target cells. RVG facilitates entry of the virus specifically into neurons at the NMJ through interaction with neural cell receptor molecules. It was first proposed by Lentz et al. [16], that the acetylcholine receptor is a rabies virus receptor, based on the detection of the virus at or near acetylcholine sites in cultured chick myotubes. In this study, rhodamine-labelled alpha bungarotoxin (α-BTX) was used to detect the acetylcholine receptors, as this snake venom neurotoxin competitively binds to acetylcholine binding sites. Following a pre-incubation period, α-BTX was able to significantly reduce the number of chick myotubes that became infected by rabies virus. The authors acknowledged that other molecules may be involved as infection could not be totally prevented by blocking the acetylcholine receptor, but these must be closely associated with acetylcholine binding sites. The detection of dense clusters of acetylcholine receptors at the tips of junctional folds may serve to enhance uptake at the NMJ, allowing eventual transport into the CNS.

Lentz [17] later compared a segment of RVG with the structure of a loop 2 domain of the curaremimetic neurotoxin, King Cobra Toxin b, and their subsequent interaction with the nAChR. The loop 2 of snake venom neurotoxins share a few invariant amino acid residues, which are consistent amongst them all. Interestingly, these sequences resemble a related homology with those found in RVG. Snake venom neurotoxin is able to bind at or near the acetylcholine binding site of nAChRs and consequently block ligand binding. Based on this, it was shown how manipulating these residues on both a 20 residue derivative of the King Cobra Toxin b and a 29 residue derivative of RVG, displayed a similar response in that binding affinity was notably decreased, suggesting that these homologous sequences are responsible for interaction with the nAChR. It would appear that snake venom neurotoxins and RVG share the same binding mechanism to the nAChR, however an additional 10 amino acid sequence of RVG-29 peptide was identified which was important for maintaining a high binding affinity, unrelated to the neurotoxin structure. Similar work was carried out using the same neurotoxin by Zhan et al. [18], where a short 20 residue neurotoxin-peptide was produced to facilitate drug delivery to the brain, via nAChRs, on endothelial cells of the BBB. By successfully enhancing the accumulation of coumarin-6-loaded micelles in mouse brain, it was shown that this synthetic peptide bound with similar affinity to RVG derivative. This study inadvertently proved that a derivative of RVG binds to the neuronal-type nAChR, due to its inhibitory effect on α-BTX, which binds to residues 173–204 of the alpha subunit on nAChRs [19]. These studies prove that RVG has a very strong connection with the nAChR due to the similarities with snake venom neurotoxin residues.

Sajjanar et al. [20] found that synthesised peptides which have an homologous sequence with the α-1 subunit of the nAChR were able to bind rabies virus and prevent infection in N2A neuroblastoma cells. Vigerelli et al. [21] was also able to block rabies virus infection in BHK-21 (baby hamster kidney) cells using bufotenine, a tryptamine alkaloid from amphibian skin secretion. Based on the fact that other alkaloids such as nicotine and cytisine bind to the nicotinic receptor, the inhibitory effect of bufotenine on rabies virus would point toward this as the main surface receptor for cell entry. This recent research has come a long way from the work produced by Wunner et al. [22], where rabies virus infection of non-neuronal BHK-21 lead to a conclusion that the nAChR was not essential for cell entry. Of course it is now known, and supported by the aforementioned work of Vigerelli et al. [21], that these cells and indeed other non-neuronal cells may express the nicotinic receptor.

Kumar et al. [9] used a derivative of RVG to successfully target siRNA to mouse brain *in vivo* and showed that it specifically bound to neural N2A cells over non-neural HeLa cells. In this study, the authors suspected that receptor mediated endocytosis was the mechanism of uptake across endothelial cells of the BBB.

Work by Castaneda-Castellanos et al. [23] was based upon findings by Reagan & Wunner [24], that cells not expressing the nAChR can still become infected by rabies virus. They aimed at assessing the susceptibility of neuronal and non-neuronal cells, pre-treated with nicotinic agonists, to rabies virus infection. The viruses used in this study would be from two different sources, one replicated in BHK-21 cells and the other from adult mouse brain. It was found that both neuronal (dorsal root ganglia) and non-neuronal (Schwann, fibroblasts, etc.) cells became infected by both strains although neurotropism was observed, due to preferential accumulation in the neuronal cell type. At the time, the non-neuronal cell types were not believed to express nicotinic receptors and this lead to the conclusion that infectivity in non-neuronal cells was independent of this receptor, agreeing with previous research. It should be noted at the time of the work carried out by Wunner et al. [22] and by Reagan & Wunner [24], the method of nAChR detection was by α-BTX binding. It is now known that α-BTX does not bind to all nAChR subunits and more recently it has been shown that nAChRs are not restricted to neurons, in fact they are present throughout the CNS on microglia, [25], brain endothelial cells [26] and Schwann cells [27]. Taking this into consideration, there is a strong possibility that multiple cell types of neural origin can become infected with rabies virus via the nAChR and hence the neurotropism is not only due to neurons but glial cells too. It could be that cells of the central and peripheral nervous system express a higher number of, or a combination of, the right receptor molecules for glycoprotein binding. Care should therefore be taken when drawing conclusions, particularly when excluding nicotinic involvement. Castaneda-Castellanos et al. [23] considered that rabies virus strains can exhibit different behaviour *in vitro,* in that multiple cell types can become infected, which does not reflect what actually happens *in vivo*.

The above findings certainly indicate that the nAChR plays a major role in Rabies Virus infection, mediated by the glycoprotein and supports nicotinic interaction with glycoprotein peptide-derivatives. The strong preference of the Rabies Virus to neural cells *in vivo* compared to other cells also expressing nAChRs, implies that other factors or molecules are also involved at varying degrees.

Neural cell adhesion molecule and low affinity growth factor receptor

The involvement of Neural Cell Adhesion Molecule (NCAM) in cell attachment and uptake of the rabies virus is somewhat ambiguous and subsequently passed over in comparison to the nAChR. Also known as CD56, it is a glycoprotein from the immunoglobulin (Ig) superfamily with functions in cell adhesion and signalling [28]. NCAM plays a role in nervous system development by influencing cell migration, adhesion, neurite outgrowth and synaptic plasticity [29]. There has also been evidence to suggest that NCAM is required to maintain normal synaptic function at the NMJ following injury [30].

Thoulouze et al. [31] attempted to determine the role of NCAM in rabies virus infection, using NCAM-positive and NCAM-negative cells. It emerged that NCAM-negative cells transfected with the NCAM gene, showed enhanced susceptibility to the rabies virus infection and that blocking NCAM with a specific antibody and a heparin ligand reduced susceptibility. The authors believed this evidence would indicate that NCAM is a receptor for the rabies virus, certainly at the very least, it would suggest that NCAM plays a role in infection. Thoulouze et al. [31] considered that the nicotinic receptor and NCAM may both be closely involved or even synergistic in nature. The independence of NCAM from the acetylcholine receptor is questionable, as the *in vivo* work from this same study showed that the brains of NCAM deficient mice were still infected by rabies virus and equally so in the hippocampus, albeit far less efficiently than in the NCAM-positive wild-type mice. Furthermore, NCAM deficiency does not prevent rabies-induced death in mice but only delays it. The fact that NCAM is not essential for infectivity means that although it seems to play an important role, it cannot be classified as the main receptor.

Given the expression of NCAM throughout the central and peripheral nervous system in astrocytes, neurons and non-myelinating Schwann cells, it is quite possible that NCAM forms part of a receptor complex which is responsible for the neurotropism of RVG at the NMJ [8]. Thoulouze et al. [31], likened NCAM to the unidentified protein on BHK-21 cells, which binds to rabies virus, in work by Reagan & Wunner [24]. In addition to the nicotinic receptor, they detected rabies binding to an unknown protein, which similar to NCAM, was also a glycosylated integral membrane protein.

Hislop et al. [13] described how RVG associated with three types of receptor *in vitro*. These were the aforementioned nAChR, NCAM and the low-affinity nerve-growth factor/neurotrophin ($P75^{NTR}$) receptor. $P75^{NTR}$ is from the tumour necrosis factor (TNF) family of receptors and although it is responsible for neurotophin signalling pathways, it has also been implicated in neurodegenerative processes. It was proposed by Tuffereau et al. [32] that $P75^{NTR}$ could be a receptor for the rabies virus, after detecting association with RVG in infected cell lines *in vitro*. Almost a decade later, following doubts over association *in vivo*, Tuffereau et al. [33] revisited this work and concluded that $P75^{NTR}$ was not essential for rabies virus infection. It was also detailed that $P75^{NTR}$ expression alone, was not sufficient enough to infect cells *in vivo* and other factors are almost certainly implicated.

It should be noted that the interaction of RVG with $P75^{NTR}$ as accounted by Hislop et al. [13], was in a mouse hybrid cell line of neuroblastoma and spinal cord cells. This model was not representative of the *in vivo* NMJ and there appears to be no *in vivo* evidence of $P75^{NTR}$ presence at the NMJ [8]. Whether or not NCAM and $P75^{NTR}$ play a key role *in vivo* or merely an accessory role in the neurotropism of RVG remains unclear, as conclusions drawn from *in vitro* results have deviated from *in vivo* behaviour.

Nicotinic acetylcholine receptors-structure and subunit expression

There are two principal subtypes of Acetylcholine receptor in the human body, the metabotropic muscarinic acetylcholine receptor and the ionotropic nAChR. Both of these groups are activated by the endogenous ligand, acetylcholine, at neuronal and non-neuronal sites. The muscarinic subtype has been distinguished by its typical activation by muscarine, the mushroom toxin from *Amanita muscaria,* whereas the nicotinic subclass is prominently activated by the exogenous ligand, nicotine. nAChRs are a family of cationic channels and along with the muscarinic subtype, 5-Hydroxytryptamine (serotonin) receptors and γ-aminobutyric acid (GABA) $_{A/C}$ receptors, they form part of the Cys-loop gene superfamily commonly known as ligand-gated ion channels [34,35]. They have been classically further subdivided into neuronal-type nAChRs and muscle-type nAChRs, however more recently there has been evidence of "neuronal-type" nAChRs in other areas of the body besides the nervous system. Early studies and initial purification of this receptor was possible due to observations made of the Torpedo electric organ, where dense areas of nAChRs in the tail of these electric rays played a role in the stinging of prey. Alongside this, studies with α-BTX, a venom from the Taiwanese Krait (*Bungarus multicinctus*), competitively bound nAChRs at the NMJ, causing paralysis [36].

Neuronal-type nAChRs exist as homopentameric or heteropentameric subtypes. This means they are typically composed of five subunits surrounding a central pore, as depicted in Figure 1(a). Thus far, the subunits which have been identified in mammalian neuronal-type nAChRs are nine α (α1–α9) and three β (β2–β4) subunits. [37,38]. The homopentameric arrangement, also known as α-BTX sensitive, is composed of five identical α7 subunits and so five identical agonist binding sites. In the human central and peripheral nervous system, α7 homomeric receptors are one of the

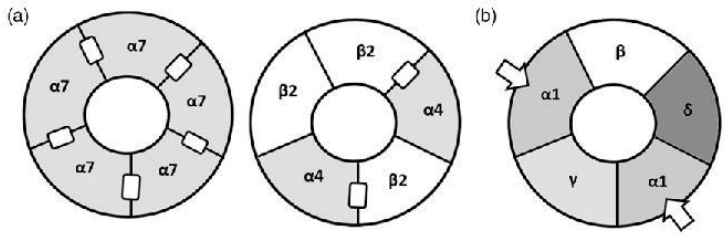

Figure 1. (a) An example of the neuronal-type nicotinic acetylcholine receptor subunit composition for the common (i) α7 homopentameric and (ii) $\alpha4\beta2^*$ heteropentameric subtypes. The ligand binding sites are displayed between alpha subunits (homopentameric) or alpha and beta subunits (heteropentameric). (b) Basic five subunit structure of the muscle-type nicotinic acetylcholine receptor with the acetylcholine binding site indicated on the alpha subunits. This example depicts subunits α, β, δ and γ in the ratio 2:1:1:1.

Table 1. Evidence of neuronal-type nAChR subunit detection and composition in different tissue types-both within and outside the central nervous system.

Organ/system	Location	Neuronal nicotinic acetylcholine receptor subunits
Brain	Unspecified	α3, α4, α5, α6, α7, β2, β3 and β4 [45]
	Hippocampus	Mainly α7 [51]
	Cerebellum	α3, α4, α7 and β2 [51]
	Striatum	α3, α4, α7 and β2 [51]
	Substantia Nigra	α3, α4, α7 and β2 [51]
	Cortex	α3, α4*, α7 and β2 [51]
	Microglia	α7 [44]
Blood brain barrier	Brain endothelial cells	α3, α5, α7, β2 and β3 [26]
Heart	Aortic endothelial cells	α3 and α7 [52]
Lung	Bronchial epithelial cells	α3, α5, α7, β2 and β4 [45,52]
Muscle	Muscle fibre (rat)	α7 [53]
Immune	Thymus	Human-α3, α5 & α7 [43,48]. Murine only- α2, α4, β2 & β4 [54]
	Peripheral macrophages	α7 [44]
Skin	Keratinocytes	α3, α5, α7, α9, β2 and β4 [46,47,55]

most commonly found, particularly in neurons of hippocampal origin. It is possible that α8 and α9 subunits also compose these homomeric receptors but so far the α8 subunit has not been identified in humans and the α9 subunit has presently not been isolated in neurons [34].

The heteropentameric arrangement is generally in the stoichiometry arrangement of $2\alpha3\beta^*$; where * signifies the possibility of a different additional α subunit in the complex [39]. These receptors will have two agonist binding sites, between α and β units, both of which must be occupied for activation of the receptor. These are also known as α-BTX insensitive but show a higher affinity in agonist binding compared to their homomeric counterparts. Although the α2, α3, α4, α6, β2 and β4 subunits play a role in binding and may be co-expressed by a particular neuron, only a few combinations may actually be formed. This also had led to the conclusion that α5 and β3 subunits merely play a supportive role rather than being involved in agonist binding [40].

The major nAChR subtypes in the mammalian CNS are $\alpha4\beta2^*$ and $\alpha7^*$, comprising approximately 90%. The structure of both these receptor subtypes and their respective binding sites are shown in Figure 1(a). Other brain areas such as the striatum, contain dopaminergic neurons which also widely express the $\alpha6\beta3^*$ subtype. Subsequently, the expression of these receptors is diminished in Parkinson's disease (PD), due to the loss of dopaminergic neurons [41,42]. In the CNS, nAChRs are widely expressed, as they form a major part of the cholinergic transmission pathways in the brain and peripheral ganglia. Their role in pre-synaptic neurotransmitter release and post-synaptic transmission means that central innervation gives rise to many different functions. These include cognition, reward, pain processing, arousal and motor activity [40]. These functions of nAChRs depend on brain location and indeed subunit composition.

It was previously mentioned, neuronal-type nAChRs may also be found on other body sites in non-neuronal roles. Table 1 details the particular subunits which have been detected thus far in the brain but also within other body systems, not involved in synaptic transmission. Lymphoid cells of the thymus [43], peripheral macrophages [44], lung epithelial cells [45], skin keratinocytes [46,47] and vascular endothelial cells [43] all express subunits which are capable of assembling functional nAChRs, which are thought to have roles in apoptosis and proliferation [48,49]. Sharma & Vijayaraghavan [50] reviewed the nicotinic subtype expression in these non-neural tissue types and in agreement with the data presented in Table 1, there is widespread indication that the α3, α5, α7, β2 and β4 subunits are the most common subtypes found outside the CNS. At the interface between the CNS and the blood circulation, there has been detection of nAChR subunits on brain endothelial cells of the BBB. These cells specifically express the α3, α5, α7, β2 and β3 subunits, as reported by Abbruscato et al. [26] in an immunoreactivity assay. Fischer et al. [53] detected the presence of the α7 subunit from nAChRs of neuronal origin in rat dennervated adult muscle. The role of these receptors in a non-neural capacity is unclear, although Gotti & Clementi [34] speculate about a gene expression role by altering calcium ion influx. On the contrary, muscle-type nAChRs are confined to muscle only [56]. In the muscle-type nAChRs, subunit composition of the receptor is not limited to only α and β subunits like those of neuronal origin. They are comprised of five different subunits – α1, β1, δ, γ and ε. Typical muscle-type nAChR subunit composition is shown in Figure 1(b), where subunits are usually in the ratio of 2:1:1:1 [39,57].

Castellanos et al. [58] found that mecamylamine and d-turbocurarine were the only nicotinic ligands of many, capable of reducing the ratios of rabies-infected neurons from primary culture. Conversely, at a similar time, Lentz et al. [59] found that only α-BTX, but neither mecamylamine nor d-turbocurarine, was capable of reducing rabies virus infection in IMR-32 neuroblastoma cells. Castaneda-Castellanos et al. [23] later explained that neuronal cells from primary culture may express different subunits to individual cell lines, offering an explanation for this inconsistency in results between the two studies involving nicotinic blocking agents. This explanation suggested that different nAChR subunit expression may potentially cause different binding affinities of the receptor with ligands such as α-BTX. The same may be true for RVG, in that it may only be able to bind to certain nAChR subunits.

Potential applications of RVG–nAChR interaction

The challenge of finding an effective treatment for neurodegenerative disorders is complicated by the difficulties posed by the BBB. It has been well established over many years how difficult drug delivery to the CNS can be, thus causing treatments to be of perceived limited efficacy *in vivo*. The specialised structure of the BBB is responsible for preventing the free passage of blood components from the general circulation into the CNS. Tight junctions composed of membrane proteins such as occludins and claudins between brain endothelial cells, prevent blood borne substances diffusing through paracellular space. This means only small (<400 Da), hydrophobic molecules such as oxygen and carbon dioxide can pass freely across the barrier [60]. Consequently, large or hydrophilic molecules require transcellular transport via energy-dependent mechanisms such as carrier mediated transport. The presence of *p*-glycoprotein efflux transporters together with low

endocytosis [61], makes drug delivery very difficult and ultimately is responsible for multi-drug resistance [62].

New strategies are required to conquer the problems of the BBB. One of these new methods in recent times has been to exploit molecules which are known to freely enter the CNS. Nicotine is the most well-known exogenous agonist of nAChRs due to its addictive nature through tobacco smoking. In fact, nicotinic activation has shown to promote neuronal survival and displayed neuroprotective properties in both *in vitro* and *in vivo* studies. There is sufficient evidence to suggest that disruption in transmission via nAChRs in the brain plays a significant role in age-related diseases [40]. This has led to the suggestion that nicotine and nicotinic drugs may be effective as a possible treatment for neurodegenerative disorders such as PD and Alzheimer's disease (AD).

Dunckley & Lukas [35], report changes in gene expression in SH-SY5Y neuroblastoma cells following nicotinic exposure. In this report, they discuss how some nAChR subtypes might be involved in intracellular signalling pathways which have certainly more than one type of effect. In other words, one receptor may modulate multiple pathways, such is the complexity of cholinergic transmission. This leads to a lack of efficacy and non-specificity, possibly explaining why nicotine and nicotinic drugs have not lived up to their clinical potential as a possible treatment for neurodegenerative disorders such as PD and AD. According to Gotti & Clementi [34], it is the α4 and α6 subunits that play a major role in dopamine release in the nigrostriatal pathway and the lack of selective activation by nicotinic agonists counters any desirable effects. This essentially rules out nicotinic treatment as a viable option in PD. In addition to this, the use of knockout mice have shown that nicotinic receptor subtypes in the brain are not essential for survival, but play a major part in the control of more complex behaviours. This supports the idea that their dysregulation is responsible in part for neural diseases such as schizophrenia, epilepsy, AD and PD [40].

Although nicotine has not been proved to be a viable option for the treatment of neurodegenerative disorders, this does not rule out the possibility of targeting the nAChR for a therapeutic purpose. Instead of activating these receptors to achieve a favourable biological response through signalling pathways, there is potential to use them as a means of improving entry and delivery of a therapeutic payload to the brain.

Due to the presence of neuronal nAChR s at the NMJ, it is possible that an RVG derivative may be utilised to target the delivery of drugs or drug carriers into the CNS, overcoming many problems of BBB crossing and neural cell entry. Lentz [63] established that the rabies virus can bind to residues 173–204 of the α1 subunit of muscle-type nAChRs present at the NMJ. This evidence was backed up by Gastka et al. [19], where rabies virus bound to the α1 subunit of muscle-type nAChR detected by Western Blotting. Here the authors concluded that the rabies virus shares a binding site with α-BTX, a competitive inhibitor of acetylcholine, which was able to inhibit rabies virus binding with the α1 subunit. Interestingly the aforementioned work by Lentz [63], also found that that the virus was able to bind to the α3 subunit, confirming that the rabies virus does in fact bind to neuronal-type nAChRs as well as muscle-type. It is however currently acknowledged that neuronal-type nAChRs are present at the NMJ too, meaning that additional subunits such as α7 are very likely to play a role in RVG binding and explain the ability of the rabies virus to traverse the CNS so readily.

RDP has been taken up by SH-SY5Y neuroblastoma cells *in vitro* but has also shown the capability to facilitate the delivery of therapeutics to mouse brain *in vivo* [4]. If the nAChR was responsible for RDP uptake, in order to cross the BBB it would have to bind to either the α3, α5 or α7 subunit as shown in Table 1. Likewise, SH-SY5Y neuroblastoma cells are known to express both the α7 and α3 subunits [35], also shown in Table 1. It could therefore be postulated that RDP has the potential to bind to more than one subtype of nAChR. However, to date, the major receptor responsible for RDP cellular uptake has not been elucidated for certain and hence the most important subtypes for brain entry have not yet been identified.

Taking advantage of the neurotrophic properties of RVG *in vivo* and the ubiquitous nature of nAChRs in the CNS may provide the basis for new brain targeting mechanisms, such as the work already mentioned, by Fu et al. [3,4] and Zhang & Fu [5] on RDP-conjugates. Mazarakis et al. [64], proposed that viral envelope glycoproteins such as RVG, may be utilised as a new approach for gene therapy, with a view of treating neurodegenerative disorders such as Parkinson's, Alzheimer's and Motor-Neuron diseases. Lewis et al. [11] confirmed the entry of rabies virus to the CNS via axonal retrograde transport and using endosomal tracers, found

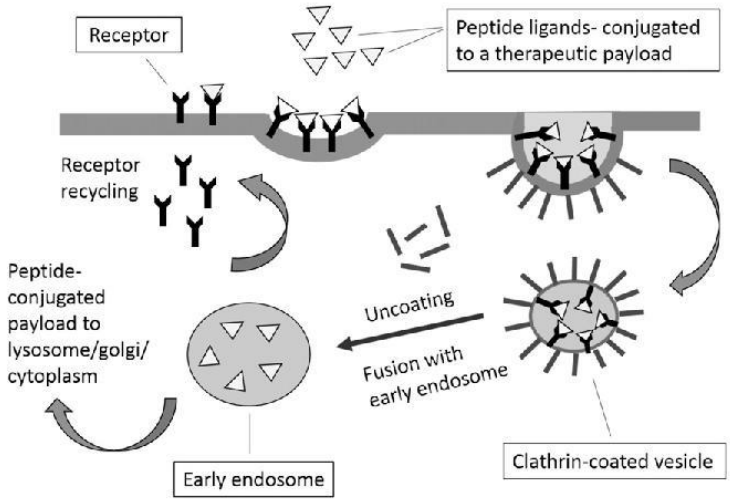

Figure 2. Hypothetical route of uptake of rabies virus-derived peptide (RDP) via clathrin-dependent receptor-mediated endocytosis.

evidence of receptor-virus endocytic uptake at the NMJ. This is possibly the mechanism by which RVG-conjugated vectors successfully delivered genetic material to motor neurons of rat spinal cord, hippocampus and striatum after intramuscular administration at the gastrocnemius muscle [64]. This study also showed that the vesicular stomatitis virus glycoprotein (VSV-G) was unable to target the vector to the CNS from the distal infection site. RVG therefore, shows better targeting capabilities to the CNS than VSV-G, allowing for specific accumulation of a therapeutic payload.

St. Pierre et al. [65] used a mouse neuroblastoma (MNA) cell line to detect RVG association with the endocytic pathway. RVG peptide derivatives such as RVG-29 and RDP are thought to gain cell entry via the endocytic pathway also. Liu et al. [7] reported that RVG-29 conjugated nanoparticles enter brain capillary endothelial cells via both clathrin and calveolae-dependent receptor-mediated endocytosis mechanisms. Fu et al. [4] related findings to further support the receptor-mediated endocytosis pathway as the main mechanism of RVG-derived peptide cell penetration, when it was shown that the endocytosis inhibitor, colchicine, was able to significantly prevent uptake of an RDP conjugate in SH-SY5Y neuroblastoma cells. Fu et al. hypothesised that clathrin-dependent endocytosis was most likely, regardless of whether the target surface receptor is the nAChR or GABA (A) receptor, as it is the most common endocytosis mechanism for both [4]. To date, there is no solid evidence of the type of endocytosis involved in the cellular uptake of RDP. A hypothetical diagram showing the proposed mechanism of uptake involving the clathrin-mediated endocytosis pathway is shown in Figure 2. It is therefore likely that RVG and its derivatives are internalised by a receptor-mediated endocytosis mechanism. The identity of this receptor is quite likely to be the nAChR, with a strong possibility of additional mechanisms such as association with NCAM, although areas of uncertainty exist. This is particularly true for the new RVG-derivatives such as RDP, where the GABA receptor has also been proposed as a potential candidate for binding.

The promise of these RVG-derived peptides for selectively targeting the CNS, could provide an exciting new way of non-invasively overcoming the challenges of the BBB and delivering a therapeutic cargo to the brain or spinal cord. Given the natural preference for neural cells *in vivo* and the lack of immune response reported thus far, the foundation for future work exists, to develop potential drug delivery systems for the fight against neurodegenerative disorders which are notoriously difficult to treat.

References

1. Yan XZ, Mohankumar PS, Dietzschold B, et al. The rabies virus glycoprotein determines the distribution of different rabies virus strains in the brain. J Neurovirol 2002;8:345–52.
2. Son S, Hwang DW, Singha K, et al. RVG peptide tethered bioreducible polyethylenimine for gene delivery to brain. J Control Release 2011;155:18–25.
3. Fu AL, Wang YL, Zhan LP, Zhou RM. Targeted delivery of proteins into the central nervous system mediated by rabies virus glycoprotein-derived peptide. Pharm Res 2012;29: 1562–9.
4. Fu AL, Zhao ZZ, Gao FY, Zhang MM. Cellular uptake mechanism and therapeutic utility of a novel peptide in targeted-delivery of proteins into neuronal cells. Pharm Res 2013;30: 2108–17.
5. Zhang E, Fu A. A new strategy for specific imaging of neural cells based on peptide-conjugated gold nanoclusters. Int J Nanomed 2015;10:2115–24.
6. Chen W, Zhan C, Gu B, et al. Targeted brain delivery of itraconazole via RVG29 anchored nanoparticles. J Drug Target 2011;19:228–34.
7. Liu Y, Huang R, Han L, et al. Brain-targeting gene delivery and cellular internalisation mechanisms for modified rabies virus glycoprotein RVG29 nanoparticles. Biomaterials 2009; 30:4195–202.
8. Lafon M. Rabies virus receptors. J NeuroVirol 2005;11:82–7.
9. Kumar P, Wu H, McBride JL, et al. Transvascular delivery of small interfering RNA to the central nervous system. Nature 2007;448:39–43.
10. Lycke E, Tsiang H. Rabies virus-infection of cultured rat sensory neurons. J Virol 1987;61:2733–41.
11. Lewis P, Fu YG, Lentz TL. Rabies virus entry at the neuromuscular junction in nerve-muscle cocultures. Muscle Nerve 2000;23:720–30.
12. Cherian S, Singh R, Singh A. Rabies glycoprotein: a benefit to the virus, us or both? J Vet Sci 2015;1:1–9.
13. Hislop JN, Islam TA, Eleftheriadou I, et al. Rabies virus envelope glycoprotein targets lentiviral vectors to the axonal retrograde pathway in motor neurons. J Biol Chem 2014;289:16148–63.
14. Kwon EJ, Lasiene J, Jacobson BE, et al. Targeted nonviral delivery vehicles to neural progenitor cells in the mouse subventricular zone. Biomaterials 2010;31:2417–24.
15. Etessami R, Conzelmann KK, Fadai-Ghotbi B, et al. Spread and pathogenic characteristics of a G-deficient rabies virus recombinant: an in vitro and in vivo study. J Gen Virol 2000;81:2147–53.
16. Lentz T, Burrage t, Smith A, et al. Is the acetylcholine receptor a rabies virus receptor? Science 1982;215:182–4.
17. Lentz TL. Structure-function-relationships of curaremimetic neurotoxin loop-2 and of a structurally similar segment of rabies virus glycoprotein in their interaction with the nicotinic acetylcholine-receptor. Biochemistry 1991;30:10949–57.
18. Zhan C, Yan Z, Xie C, Lu W. Loop 2 of ophiophagus hannah toxin b binds with neuronal nicotinic acetylcholine receptors and enhances intracranial drug delivery. Mol Pharm 2010;7:1940–7.
19. Gastka M, Horvath J, Lentz TL. Rabies virus binding to the nicotinic acetylcholine receptor alpha subunit demonstrated by virus overlay protein binding assay. J Gen Virol 1996;77:2437–40.
20. Sajjanar B, Saxena S, Bisht D, et al. Effect of nicotinic acetylcholine receptor alpha 1 (nAChRα1) peptides on rabies virus infection in neuronal cells. Neuropeptides 2015;54:59–64.
21. Vigerelli H, Sciani JM, Jared C, et al. Bufotenine is able to block rabies virus infection in BHK-21 cells. J Venom Anim Toxins Incl Trop Dis 2014;20:45.
22. Wunner WH, Reagan KJ, Koprowski H. Characterization of saturable binding sites for rabies virus. J Virol 1984;50:691–7.
23. Castaneda-Castellanos DR, Castellanos JE, Hurtado H. Differential use of the nicotinic receptor by rabies virus based upon substrate origin. J Neurovirol 2002;8:150–4.
24. Reagan KJ, Wunner WH. Rabies virus interaction with various cell lines is independent of the acetylcholine receptor. Arch Virol 1985;84:277–82.
25. Shytle RD, Mori T, Townsend K, et al. Cholinergic modulation of microglial activation by alpha-7 nicotinic receptors. J Neurochem 2004;89:337–43.
26. Abbruscato TJ, Lopez SP, Mark KS, et al. Nicotine and cotinine modulate cerebral microvascular permeability and protein expression of ZO-1 through nicotinic acetylcholine

receptors expressed on brain endothelial cells. J Pharm Sci 2002;91:2525–38.
27. Petrov KA, Girard E, Nikitashina AD, et al. Schwann cells sense and control acetylcholine spill-over at the neuromuscular junction by alpha 7 nicotinic receptors and butyrylcholinesterase. J Neurosci 2014;34:11870–83.
28. Paratcha G, Ledda F, Ibáñez CF. The neural cell adhesion molecule NCAM Is an alternative signaling receptor for GDNF family ligands. Cell 2003;113:867–79.
29. Hubschmann MV, Skladchikova G, Bock E, Berezin V. Neural cell adhesion molecule function is regulated by metalloproteinase-mediated ectodomain release. J Neurosci Res 2005; 80:826–37.
30. Chipman PH, Franz CK, Nelson A, et al. Neural cell adhesion molecule is required for stability of reinnervated neuromuscular junctions. Eur J Neurosci2010;31:238–49.
31. Thoulouze M, Lafage M, Schachner M, et al. The neural cell adhesion molecule is a receptor for rabies virus. J Virol 1998;72:7181–90.
32. Tuffereau C, Benejean J, Roque-Alfonso A, et al. Neuronal cell surface molecules mediate specific binding to rabies virus glycoprotein expressed by a recombinant baculovirus on the surfaces of lepidopteran cells. J Virol 1998;17:7250–9.
33. Tuffereau C, Schmidt K, Langevin C, et al. The rabies virus glycoprotein receptor p75NTR is not essential for rabies virus infection. J Virol 2007;81:13622–30.
34. Gotti C, Clementi F. Neuronal nicotinic receptors: from structure to pathology. Prog Neurobiol 2004;74:363–96.
35. Dunckley T, Lukas RJ. Nicotinic modulation of gene expression in SH-SY5Y neuroblastoma cells. Brain Res 2006;1116: 39–49.
36. Albuquerque E, Alkondon M, Pereira E, et al. Properties of neuronal nicotinic acetylcholine receptors: pharmacological characterisation and modulation of synaptic function. J Pharm Exp Ther 1997;280:1117–36.
37. Haddadian EJ, Cheng MH, Coalson RD, et al. In silico models for the human alpha 4 beta 2 nicotinic acetylcholine receptor. J Phys Chem B 2008;112:13981–90.
38. Quik M, Wonnacott S. $\alpha 6\beta 2^*$ and $\alpha 4\beta 2^*$ nicotinic acetylcholine receptors as drug targets for Parkinson's disease. Pharmacol Rev 2011;63:938–66.
39. Paterson D, Nordberg A. Neuronal nicotinic receptors in the human brain. Prog Neurobiol 2000;61:75–111.
40. Gotti C, Zoli M, Clementi F. Brain nicotinic acetylcholine receptors: native subtypes and their relevance. Trends Pharmacol Sci 2006;27:482–91.
41. Warpman U, Friberg L, Gillespie A, et al. Regulation of nicotinic receptor subtypes following chronic nicotinic agonist exposure in M10 and SH-SY5Y neuroblastoma cells. J Neurochem 1998;70:2028–37.
42. Posadas I, Lopez-Hernandez B, Cena V. Nicotinic receptors in neurodegeneration. Curr Neuropharm 2013;11:298–314.
43. Navaneetham D, Penn A, Howard J, ContiFine BM. Expression of the alpha 7 subunit of the nicotinic acetylcholine receptor in normal and myasthenic human thymuses. Cell Mol Biol 1997;43:433–42.
44. De Simone R, Ajmone-Cat MA, Carnevale D, Minghetti L. Activation of alpha 7 nicotinic acetylcholine receptor by nicotine selectively up-regulates cyclooxygenase-2 and prostaglandin E-2 in rat microglial cultures. J Neuroinflammation 2005;2:4.
45. Maus ADJ, Pereira EFR, Karachunski PI, et al. Human and rodent bronchial epithelial cells express functional nicotinic acetylcholine receptors. Mol Pharmacol 1998;54:779–88.
46. Grando SA, Zelickson BD, Kist DA, et al. Keratinocyte muscarinic acetylcholine receptors: immunolocalization and partial characterization. J Invest Dermatol 1995;104:95–100.
47. Grando SA, Horton RM, Mauro TM, et al. Activation of keratinocyte nicotinic cholinergic receptors stimulates calcium influx and enhances cell differentiation. J Invest Dermatol 1996;107:412–8.
48. Conti-Fine BM, Navaneetham D, Lei S, Maus ADJ. Neuronal nicotinic receptors in non-neuronal cells: new mediators of tobacco toxicity? Eur J Pharmacol 2000;393:279–94.
49. Egleton RD, Brown KC, Dasgupta P. Nicotinic acetylcholine receptors in cancer: multiple roles in proliferation and inhibition of apoptosis. Trends Pharmacol Sci 2008;29:151–8.
50. Sharma G, Vijayaraghavan S. Nicotinic receptor signaling in nonexcitable cells. J Neurobiol 2002;53:524–34.
51. Court JA, Martin-Ruiz C, Graham A, Perry E. Nicotinic receptors in human brain: topography and pathology. J Chem Neuroanat 2000;20:281–98.
52. Wang Y, Pereira EFR, Maus ADJ, et al. Human bronchial epithelial and endothelial cells express a7 nicotinic acetylcholine receptors. Mol Pharmacol 2001;60:1201–9.
53. Fischer U, Reinhardt S, Albuquerque EX, Maelicke A. Expression of functional alpha 7 nicotinic acetylcholine receptor during mammalian muscle development and denervation. Eur J Neurosci 1999;11:2856–64.
54. Kuo Y, Lucero L, Michaels J, et al. Differential expression of nicotinic acetylcholine receptor subunits in foetal and neonatal mouse thymus. J Neuroimmunol 2002;130:140–54.
55. Nguyen VT, Ndoye A, Grando SA. Novel human $\alpha 9$ acetylcholine receptor regulating keratinocyte adhesion is targeted by Pemphigus Vulgaris autoimmunity. Am J Pathol 2000;157: 1377–91.
56. Albuquerque EX, Pereira EFR, Alkondon M, Rogers SW. Mammalian nicotinic acetylcholine receptors: from structure to function. Physiol Rev 2009;89:73–120.
57. Galzi JL, Changeux JP. Neuronal nicotinic receptors: molecular organization and regulations. Neuropharmacology 1995; 34:563–82.
58. Castellanos JE, Castaneda DR, Velandia AE, Hurtado H. Partial inhibition of the in vitro infection of adult mouse dorsal root ganglion neurons by rabies virus using nicotinic antagonists. Neurosci Lett 1997;229:198–200.
59. Lentz TL, Fu YG, Lewis P. Rabies virus infection of IMR-32 human neuroblastoma cells and effect of neurochemical and other agents. Antiviral Res 1997;35:29–39.
60. Ballabh P, Braun A, Nedergaard M. The blood-brain barrier: an overview – structure, regulation, and clinical implications. Neurobiol Dis 2004;16:1–13.
61. Wilhelm I, Fazakas C, Krizbai IA. In vitro models of the blood-brain barrier. Acta Neurobiol Exp 2011;71:113–28.
62. Zlokovic BV. The blood-brain barrier in health and chronic neurodegenerative disorders. Neuron 2008;57:178–201.
63. Lentz TL. Rabies virus binding to an acetylcholine receptor alpha-subunit peptide. J Mol Recognit 1990;3:82–8.
64. Mazarakis ND, Azzouz M, Rohll JB, et al. Rabies virus glycoprotein pseudotyping of lentiviral vectors enables retrograde axonal transport and access to the nervous system after peripheral delivery. Hum Mol Genet 2001;10:2109–21.
65. St. Pierre CA, Leonard D, Corvera S, et al. Antibodies to cell surface proteins redirect intracellular trafficking pathways. Exp Mol Pathol 2011;91:723–32.

Appendix 4

International Journal of Pharmaceutics 525 (2017) 12–20

Contents lists available at ScienceDirect

International Journal of Pharmaceutics

journal homepage: www.elsevier.com/locate/ijpharm

Targeted drug delivery system to neural cells utilizes the nicotinic acetylcholine receptor

Rachel Huey[a], Barry O'Hagan[b], Paul McCarron[a], Susan Hawthorne[a,*]

[a] School of Pharmacy and Pharmaceutical Sciences, Ulster University, Coleraine, Northern Ireland, UK
[b] School of Biomedical Sciences, Ulster University, Coleraine, Northern Ireland, UK

ARTICLE INFO

Article history:
Received 9 February 2017
Received in revised form 7 April 2017
Accepted 10 April 2017
Available online 12 April 2017

Keywords:
Drug delivery system
Rabies virus
Targeted nanoparticles
Neural
Blood brain barrier (BBB)
Nicotinic acetylcholine receptor

ABSTRACT

Drug delivery to the brain is still a major challenge in the field of therapeutics, especially for large and hydrophilic compounds. In order to achieve drug delivery of therapeutic concentration in the central nervous system, the problematic blood brain barrier (BBB) must be overcome. This work presents the formulation of a targeted nanoparticle-based drug delivery system using a specific neural cell targeting ligand, rabies virus derived peptide (RDP). Characterization studies revealed that RDP could be conjugated to drug-loaded PLGA nanoparticles of average diameter 257.10 ± 22.39 nm and zeta potential of −5.51 ± 0.73 mV. In vitro studies showed that addition of RDP to nanoparticles enhanced drug accumulation in a neural cell line specifically as opposed to non-neural cell lines. It was revealed that this drug delivery system is reliant upon nicotinic acetylcholine receptor (nAChR) function for RDP-facilitated effects, supporting a cellular uptake mechanism of action. The specific neural cell targeting capabilities of RDP via the nAChR offers a non-toxic, non-invasive and promising approach to the delivery of therapeutics to the brain.

1. Introduction

1.1. Targeting peptides

New approaches are arising for the successful delivery of therapeutics to the central nervous system (CNS). Although notoriously challenging, the delivery of drug or gene payloads specifically to neural cells may be facilitated by the use of a targeting ligand or peptide. In recent times, peptide derivatives of rabies virus glycoprotein (RVG), such as RDP and RVG-29, have been successfully utilized as targeting ligands for drug delivery to the CNS. RVG is the only surface glycoprotein on the rabies virus envelope, which is responsible for the distinct neurotropism of the rabies virus infection (Yan et al., 2002). The use of RVG for specific neural targeting is therefore a promising concept, particularly in neurodegenerative medicine for conditions such as Parkinson's and Alzheimer's disease.

1.2. Rabies virus-derived peptide (RDP)

Rabies virus-derived peptide (RDP) has shown potential as a new targeting ligand for the specific and non-invasive delivery of therapeutics to the brain, due to its ability to cross the blood brain barrier (BBB). RDP is a 39 amino acid peptide derivative of RVG, which has not only been successful in safely directing therapeutic payloads to the brain in mice (Fu et al., 2012, 2013a,b), but also preferentially targets neural over non-neural cell types (Fu et al., 2013a).

The facilitated transport across the BBB enabled by RDP may be improved by encapsulating sensitive therapeutics in a protective delivery vehicle. So far, RDP has been conjugated to gold nanoclusters for non-invasively imaging mouse brain in vivo (Zhang and Fu, 2015). This type of facilitated delivery is possible as the surface of polymeric carriers such as nanoparticles (NP), can be easily modified (Delehanty et al., 2010). Polymeric drug delivery vehicles are usually composed of biodegradable polymers which are biocompatible and with an established safety profile, such as FDA-approved poly (lactic co-glycolic acid) (PLGA) or chitosan (Auffinger et al., 2013).

Abbreviations: RDP, rabies virus derived peptide; RVG, rabies virus derived peptide; BBB, blood brain barrier; NP, nanoparticles; PLGA, poly(lactic-co-glycolic acid); PDI, polydispersity index; ZP, zeta potential; EE, entrapment efficiency; CE, conjugation efficiency; SEM, scanning electron microscopy; DLS, dynamic light scattering; nAChR, nicotinic acetylcholine receptor.

* Corresponding author at: School of Pharmacy and Pharmaceutical Sciences, Ulster University, Coleraine, Northern Ireland BT52 1SA, UK.
E-mail address: s.hawthorne@ulster.ac.uk (S. Hawthorne).

http://dx.doi.org/10.1016/j.ijpharm.2017.04.023
0378-5173/

1.3. Receptors of rabies virus glycoprotein (RVG) derivatives

In order to optimize the characteristics and in vivo stability of RDP, it is important to know which receptor on neural cells is the target for interaction. There is strong evidence of RVG and other derivatives binding to the nicotinic acetylcholine receptor (nAChR) in a number of studies (Lentz, 1991; Gastka et al., 1996; Kumar et al., 2007; Sajjanar et al., 2015). Pilot studies by Fu et al. (2013a) however, suggested that the GABA(a) receptor subtype is most likely utilized for RDP cellular uptake by clathrin-mediated endocytosis. Liu et al. (2009) implicated the GABA(b) receptor subtype as being responsible for the cellular uptake of another RVG derivative, RVG-29. A lack of experimental data on RDP to date, means that the question of whether the nAChR or a GABA receptor subtype is responsible for cellular uptake cannot be answered with certainty. The aim of this study was to elucidate which receptor RDP binds to on a neural cell line.

This study details the preparation of PLGA NP incorporating the cytotoxic drug, doxorubicin, as a model payload. The effect of RDP conjugation to doxorubicin-loaded NP (RDP-Dox NP) is assessed for cytotoxicity in both neural and non-neural cell lines. Finally, the effect of blocking the nAChR, GABA(a) and GABA(b) receptors on RDP-Dox NP cytotoxicity is assessed.

2. Materials and methods

2.1. Materials

Acid terminated poly(lactic-co-glycolic) acid (PLGA)- MW 7000–17,000, dichloromethane (DCM), poly(vinyl) alcohol (PVA) 87–89% hydrolyzed- MW 85,000–124,000, doxorubicin hydrochloride, phosphate buffered saline (PBS), MES buffer, 1-ethyl-3-(3-dimethylaminopropyl)-carbodiimide (EDC), N-hydroxysuccinimide (NHS), 3,3-dimethylglutaric acid, 3-[4,5-dimethylthiazol-2-yl]-2,5 diphenyl tetrazolium bromide (MTT), hexamethonium, bicuculline, saclofen and mecamylamine were all purchased from Sigma-Aldrich (UK). RDP was synthesized by GL Biochem (Shanghai) Ltd. AChRα7 antibody was purchased from Santa Cruz Biotechnology, Inc. (USA).

All tissue culture reagents and media were purchased from Gibco®/Life Technologies. SH-SY5Y (human neuroblastoma) and HeLa (human cervical cancer) cell lines were both cultured in RPMI 1640 medium. MDA-MB-231 (human breast cancer) cells were cultured in DMEM medium. Finally, normal and non-neural epithelial CHO (Chinese hamster ovary) cells were cultured in Ham's F12 nutrient mixture. All tissue culture media was supplemented with 10% fetal bovine serum and 1% penicillin-streptomycin (5,000U ml^{-1}/5000 μg ml^{-1}). Cells were passaged using trypsin-EDTA 0.5%.

2.2. Preparation of nanoparticles (NP)

2.2.1. Preparation of blank NP

Acid terminated PLGA (100 mg) was dissolved in 4 ml of DCM. PVA was made up as a 1.25% solution in distilled water. The PLGA/DCM organic phase was added dropwise to 50 ml of 1.25% PVA solution and homogenized on full power for 6 min (Silverson LST homogenizer, Silverson, USA). The resulting o/w emulsion was left to stir overnight to evaporate any solvent. The NP emulsion was then centrifuged at 18809g for 30 min at 4 °C, before washing the pellet with distilled water three times for ten minutes each. The final pellet was resuspended in distilled water and freeze dried for 48 h (Labconco FreeZone 4.5 plus, USA).

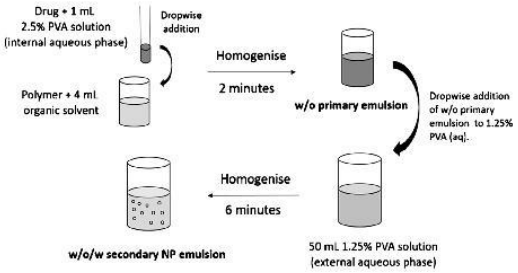

Fig. 1. Diagrammatic representation of the double emulsion technique used to prepare doxorubicin-loaded PLGA nanoparticles (NP).

2.2.2. Preparation of doxorubicin-loaded NP (Dox-NP)

The double emulsion technique (Fig. 1) was used to encapsulate doxorubicin in PLGA NP, similar to that detailed by Kalaria et al. (2009). Doxorubicin hydrochloride (5 mg) was dissolved in 1 ml of 2.5% PVA solution in distilled water. This was added dropwise to 100 mg PLGA/4 ml DCM and homogenized on full power for 2 min to produce the primary w/o emulsion (VDI 12 S2 homogenizer, VWR International Ltd., USA). This w/o emulsion was then added dropwise to 50 ml 1.25% PVA solution and homogenized for a further 6 min on full power to produce a w/o/w double NP emulsion. After allowing solvent to evaporate overnight, the NP formulation was centrifuged and freeze dried, as previously detailed. Supernatant from centrifugation was retained to analyze doxorubicin entrapment efficiency using UV–vis spectroscopy.

2.2.3. Conjugation of RDP to NP

Dox-NP (5 mg) were dispersed in 5 ml of 25 mM MES buffer (pH 5.0) to give a 1 mg ml^{-1} NP suspension. EDC and NHS reagents were prepared as 0.1 M and 0.7 M solutions, respectively, in 25 mM MES buffer. Aliquots of NHS (1 ml) and EDC (1 ml) were added to the NP suspension and allowed to stir at room temperature for one hour to activate the carboxyl group of acid terminated PLGA. The resultant suspension was centrifuged for 30 min and then washed three times with PBS for ten minutes at 18809g and at 10 °C. The final pellet was resuspended in 5 ml of PBS. RDP was made up in PBS to produce a 1 mg ml^{-1} RDP solution. RDP solution (100 μl) was added per 1 ml of the activated NP suspension and incubated overnight at 4 °C. The suspension was then centrifuged at 5 °C and washed three times, as before. The final pellet was dispersed in PBS to produce a 1 mg ml^{-1} RDP-conjugated doxorubicin-loaded NP suspension (RDP-Dox NP). Supernatant was retained for analysis of RDP conjugation efficiency using a bicinchoninic acid (BCA) assay.

2.3. Evaluation of NP

2.3.1. Dynamic light scattering (DLS)

Size, zeta potential and polydispersity measurements were carried out using dynamic light scattering (DLS) analysis (Zetasizer, Nano-series, Malvern Instruments, UK). Prior to DLS analysis, 1 mg of NP were dispersed in 1 ml of distilled water for measuring size and polydispersity index (PDI). For zeta potential (ZP) measurements, NP were dispersed in 1.0 mM KCl, pH 7.5, to maintain a constant ionic strength. Results were taken as an average of six measurements.

2.3.2. Determination of doxorubicin entrapment efficiency (EE)

Doxorubicin EE was calculated indirectly using supernatant from the formulation process, as detailed previously. A standard curve of doxorubicin concentration was prepared using absorbance spectrometry at 480 nm. Percentage EE was subsequently

calculated according to the following formula:

$$EE = \frac{Mass\ of\ drug\ in\ NP}{Mass\ of\ drug\ added} x100\%$$

2.3.3. Determination of RDP conjugation efficiency (CE)

RDP CE to PLGA NP was determined by a BCA assay. A standard curve was prepared from absorption of albumin standards at 562 nm, allowing the amount of unconjugated RDP in the supernatant from the peptide conjugation process to be determined. Using this value, the amount of RDP conjugated to NP was calculated based on the total amount added during formulation. The peptide CE was calculated according to the following formula:

$$CE = \frac{Mass\ of\ peptide\ conjugated\ to\ NP}{Mass\ of\ peptide\ added} x100\%$$

2.3.4. Scanning electron microscopy (SEM)

Blank PLGA NP preparations were prepared and re-suspended in distilled water. Samples were incubated at 37 °C for 0, 1, 4, 10, 30 and 60 days prior to freeze drying, to assess changes in polymeric NP characteristics at normal body temperature (36.5–37.5 °C). Small quantities of NP were mounted onto an aluminum stub and sputter coated in a Polaron E5100 sputter coater equipped with a gold/palladium target, prior to imaging under high vacuum in secondary electron mode (F.E.I Quanta Environmental). The use of distilled water was preferred over phosphate buffered saline (PBS) or indeed cell culture media, due to the possibility of salt deposits or other residual material causing decreased SEM image quality.

2.3.5. Drug release

Doxorubicin release was measured according to a method similar to that described by Betancourt et al. (2007). NP were incubated at 37 °C in both 0.1 M phosphate buffered saline (PBS) at pH 7.4 and 0.01 M dimethylglutaric acid (DMGA) buffer at pH 4.5. The acidic environment in DMGA buffer mimics the pH conditions of endocytic vesicles during cellular uptake, as late endosomes can have a pH of around 4.5 (Sorkin and von Zastrow, 2002). DMGA buffer (0.01 M) was prepared by addition of 3, 3-dimethylglutaric acid (6 mM), sodium hydroxide (3.9 mM) and sodium chloride (150 mM) to distilled water. Sodium hydroxide (2 M) was used to adjust the buffer to pH 4.5. PBS was prepared by dissolving one PBS tablet per 100 ml of distilled water. Dox-NP (15 mg) were added to a centrifuge tube and dispersed in 10 ml of either PBS or DMGA buffer before being incubated at 37 °C. Doxorubicin release was measured at various time points over 7 days by centrifuging the respective Dox-NP samples at 18809 *g* for 12 min and then transferring 200 μl aliquots of supernatant to a 96-well plate. Absorbance was measured at 480 nm (FLUOstar Omega microwell plate reader, BMG Labtech, Germany). The amount of doxorubicin in the supernatant was calculated using separate standard curves for doxorubicin in DMGA or PBS. Doxorubicin release was calculated as a percentage of maximum total doxorubicin in the NP, determined from the EE, with results expressed as percentage cumulative release.

2.4. In vitro evaluation

2.4.1. Cytotoxicity study

Cells were seeded into 96 well plates at a concentration of 1×10^{-4} cells ml^{-1} (100 μl per well) in the relevant culture media and incubated at 37 °C and 5% CO_2 for 24 h (Heraeus HERAcell, Thermo Fisher Scientific, UK). Dox NP and RDP-Dox NP were prepared as 1 mg ml^{-1} suspensions in sterile PBS and filter sterilized using a 450 nm filter. Blank PLGA NP with conjugated RDP (RDP-blank NP) were also prepared this way, to test for toxicity of the drug vehicle and RDP. NP treatment (100 μl) was added to each well, with six replicates for each of the treatment groups. Control groups were treated with 100 μl of serum-free media only.

Initially, SH-SY5Y cells were treated with RDP-blank NP, Dox NP and RDP-Dox NP for 30, 60 and 120 min to determine an appropriate treatment time. Following this, four different cell lines (HeLa, CHO, MDA-MB-231 and SH-SY5Y cells) were treated with the Dox NP and RDP-Dox NP formulations only, for a selected period of time to assess cytotoxicity. After the elapsed treatment time, all media was aspirated and replaced with 200 μl of the appropriate complete media. Cells were then incubated for a further 24 h before MTT assay. MTT solution (25 μl of 5 mg ml^{-1} in sterile PBS) was added on top of the media in each well and incubated at 37 °C for 2 h. The wells were then aspirated and purple formazan crystals dissolved by the addition of 70 μl of dimethyl sulfoxide (DMSO) per well. Absorbance was read at 570 nm (FLUOstar Omega microwell plate reader, BMG Labtech, Germany).

2.4.2. Receptor identification study

SH-SY5Y cells were seeded onto 96 well plates, as previously described. RDP-Dox NP 1 mg ml^{-1} in PBS were made up as a 20% suspension in serum-free media. Bicuculline and saclofen were first prepared as 1 mM stock solutions. Hexamethonium and mecamylamine were prepared as 10 mM stock solutions, with AChRα7 antibody diluted 1:10 with PBS. Final concentrations of inhibitors, once all treatments were added, were 100 μM for the GABA antagonists (bicuculline and saclofen), 1 mM for nAChR antagonists (hexamethonium and mecamylamine) and a 1:100 dilution of AChRα7 antibody.

SH-SY5Y cells were initially pre-treated for 30 min with either 20 μl of bicuculline, saclofen or hexamethonium prior to treatment with 100 μl of RDP-Dox NP treatment suspension (20 μg of NP per well). Cells were incubated as before for 120 min at 37 °C, 5% CO_2. Control wells were treated with serum-free media only. After incubation, wells were aspirated and 200 μl of fresh complete media added per well. After incubating for 24 h, an MTT assay was carried out, as before. This provided results for the first receptor identification assay, which was followed up by a second assay to block the nAChR only. The subsequent assay followed the same protocol, only 20 μl of mecamylamine or AChRα7 antibody solutions were allowed to incubate with SH-SY5Y cells for 60 min prior to RDP-Dox NP exposure. This was to ensure adequate time for the antibody to bind any homomeric α7 nAChRs.

2.5. Statistical analysis

All analysis carried out on cell viability values was determined using an unpaired *t*-test, with P values <0.05 indicating a statistically significant difference.

3. Results

3.1. Evaluation of NP

3.1.1. Dynamic light scattering (DLS)

NP were formulated according to the double emulsion method (Fig. 1) and characterized for size, zeta potential (ZP) and polydispersity index (PDI), the results of which are presented in Table 1. Using DLS analysis, it was determined that blank PLGA NP had an average particle diameter of 240.27 ± 14.72 nm, ZP of −18.4 ± 1.82 mV and PDI of 0.26 ± 0.04. Incorporation of a doxorubicin payload caused average NP diameter to increase to 242.73 ± 18.64 nm and the ZP to increase to −14.64 ± 1.32 mV. PDI also increased to 0.39 ± 0.05 upon introduction of a doxorubicin

Table 1
Characterization parameters of doxorubicin-loaded NP, with and without peripheral attachment of RDP.

NP Sample	Size (nm)	ZP[a] (mV)	PDI[b]	Dox EE[c] (%)	DC[d] (μg/mg)	RDP CE[e] (%)
Blank PLGA	240.27 ± 14.72	−18.40 ± 1.82	0.26 ± 0.04	–	–	–
Dox-NP	242.73 ± 18.64	−14.60 ± 1.32	0.39 ± 0.05	50.30	23.95	–
RDP-Dox-NP	257.10 ± 22.39	−5.51 ± 0.73	0.33 ± 0.06	50.30	23.95	62.0

[a] Zeta potential (mV) ± standard deviation.
[b] Polydispersity index ± standard deviation.
[c] Drug entrapment efficiency (%).
[d] Drug content (μg/mg).
[e] Peptide conjugation efficiency (%). Size, ZP and PDI as measured by dynamic light scattering are expressed as the average of three measurements (n = 3).

payload. Addition of RDP to the Dox-NP caused the average diameter to increase to 257.10 ± 22.39 nm, which was around 6% larger than the unlabeled Dox-NP. This difference in size was minimal compared to the effects on the ZP induced by RDP labelling, as it increased to −5.51 ± 0.73 mV. RDP conjugation did not have a significant effect on the PDI of the sample (0.33 ± 0.06), as it was similar to that of the unlabeled Dox-NP.

3.1.2. Determination of doxorubicin entrapment efficiency (EE) & RDP conjugation efficiency (CE)

The EE of doxorubicin was calculated using UV–vis absorbance at 480 nm to analyze the supernatant after centrifugation using indirect analysis. The EE was 50.30%, as shown in Table 1. The CE of RDP, which was attached to the acid-terminated PLGA by an EDC/NHS linker, was determined by a similar method only unconjugated peptide was detected by a BCA assay. RDP conjugation to the acid terminated PLGA NP was subsequently determined to be 62.0%, also shown in Table 1.

3.1.3. Scanning electron microscopy (SEM)

SEM images were obtained, as shown in Fig. 2, at ×24 000 magnification. Freeze dried sample with no prior incubation in Fig. 2(a) shows that NP are spherical in shape, with the presence of many sub-micron particles. Despite some of the largest particles within the sample measuring approximately 1 μm in size, the majority are 200–300 nm, supporting the data obtained from DLS analysis (Table 1). This explains the polydispersity within these NP, as seen from results in Table 1. Fig. 2(b)–(f) show NP which have been incubated at 37 °C for 1, 4, 10, 30 and 60 days in distilled water respectively. The same magnification for these images was used as for Fig. 2(a).

It is evident that incubation for 1 day caused the NP to swell and become slightly larger in diameter, with early signs of degradation due to minor surface pitting, as indicated in Fig. 2(b). There were some changes in shape and aggregation of material highlighted in Fig. 2(c), suggesting that after 4 days incubation at 37 °C, degradation processes were underway within the sample. After 10 days of incubation, much larger and aggregated particles were present within the sample, with more signs of structure irregularity in Fig. 2(d). By 30 days of incubation, in Fig. 2(e), most particles increased in size into the micrometer scale. There was continued loss of the regular spherical morphology of individual particles, with agglomeration more apparent. These larger particles were susceptible to breakdown under the beam of the microscope. Finally, in Fig. 2(f) after 60 days of incubation, there was complete loss of NP within the sample. Evidence of remaining larger spherical structures are highlighted in Fig. 2(f), as the remainder of the image shows only amorphous residual material.

3.1.4. Drug release study

Doxorubicin payload release was measured when NP were exposed to two different buffers. PBS buffer (10 mM) at pH 7.4 provided conditions similar to the neutral extracellular environment. DMGA buffer at pH 4.5 would mimic the acidic environment of late endocytic vesicles or indeed the lysosome. Fig. 3 shows that within the first hour in PBS buffer (pH 7.4), doxorubicin release was under 20% of the maximum payload, compared to the 60% released from the NP when in DMGA buffer (pH 4.5). After 5 h at pH 7.4, the cumulative doxorubicin release increased to 30%. However, there was no further notable release over the following 6 days. At pH 4.5, there was a sharp rise in the amount of doxorubicin released over the first 6 h of testing to 85%, but this noticeably levelled off at 90% over the following 5 days until 100% cumulative release was reached after 6 days of incubation. Over 7 days at 37 °C, the cumulative doxorubicin release at pH 7.4 reached a maximum of 31%.

3.2. In vitro evaluation

3.2.1. Cytotoxicity study

Fu et al. (2013a,b) reported no toxic reactions to RDP over experimental periods of three weeks, following repeated systemic administration in mice. Fig. 4 shows that the blank PLGA NP with peripherally attached RDP was not toxic to SH-SY5Y cells, as average cell viability remained at 96.0% (no significant difference) compared to control over 120 min. Results from Fig. 4 show that when the NP formulation was loaded with a cytotoxic payload, incubation of the cells for 60 min resulted in a significant decrease in SH-SY5Y neuroblastoma cell viability to 87.0% for Dox NP and 85.0% for RDP-Dox NP. After 120 min treatment time, toxicity of Dox NP did not increase any further. However, RDP-Dox NP toxicity was enhanced causing a reduction in SH-SY5Y cell viability to 75.0%. This treatment time was subsequently selected for further cell assays, due to the difference in cytotoxicity observed between RDP-Dox NP and Dox NP. It can, therefore, be concluded from Fig. 4 that any cell death observed was due to the effects of doxorubicin, as RDP attached to blank NP caused no significant cytotoxicity at any time point. After 120 min of exposure to SH-SY5Y cells, Dox NP caused 13% cytotoxicity when unconjugated and 25% cytotoxicity when conjugated with RDP.

Four different cell lines were treated with either Dox NP or RDP-Dox NP for 120 min and then incubated for 24 h at 37 °C and 5% CO_2. Results from Fig. 5 show that cell viability for the non-neural cell types- MDA-MB-231, CHO and HeLa cell lines remained similar following treatment with either NP formulation. The MDA-MB-231 and HeLa cell lines (non-neural) were not significantly affected by either NP treatment, although some toxicity was certainly observed compared to control. MDA-MB-231 cell line retained a cell viability of 91.9% after Dox-NP treatment and 92.6% following RDP-Dox NP treatment. For the HeLa cell group, cell viability reduced to 91.0% following Dox-NP exposure for 120 min and to 87.1% after RDP-Dox NP treatment (not significant). RDP, therefore, had no significant effect on the toxicity of the Dox-NP formulation. The normal, non-neural CHO cell line displayed cell viabilities of 83.4% and 86.7% following treatment with Dox-NP and RDP-Dox NP, respectively. Both of these values marginally turned out to have

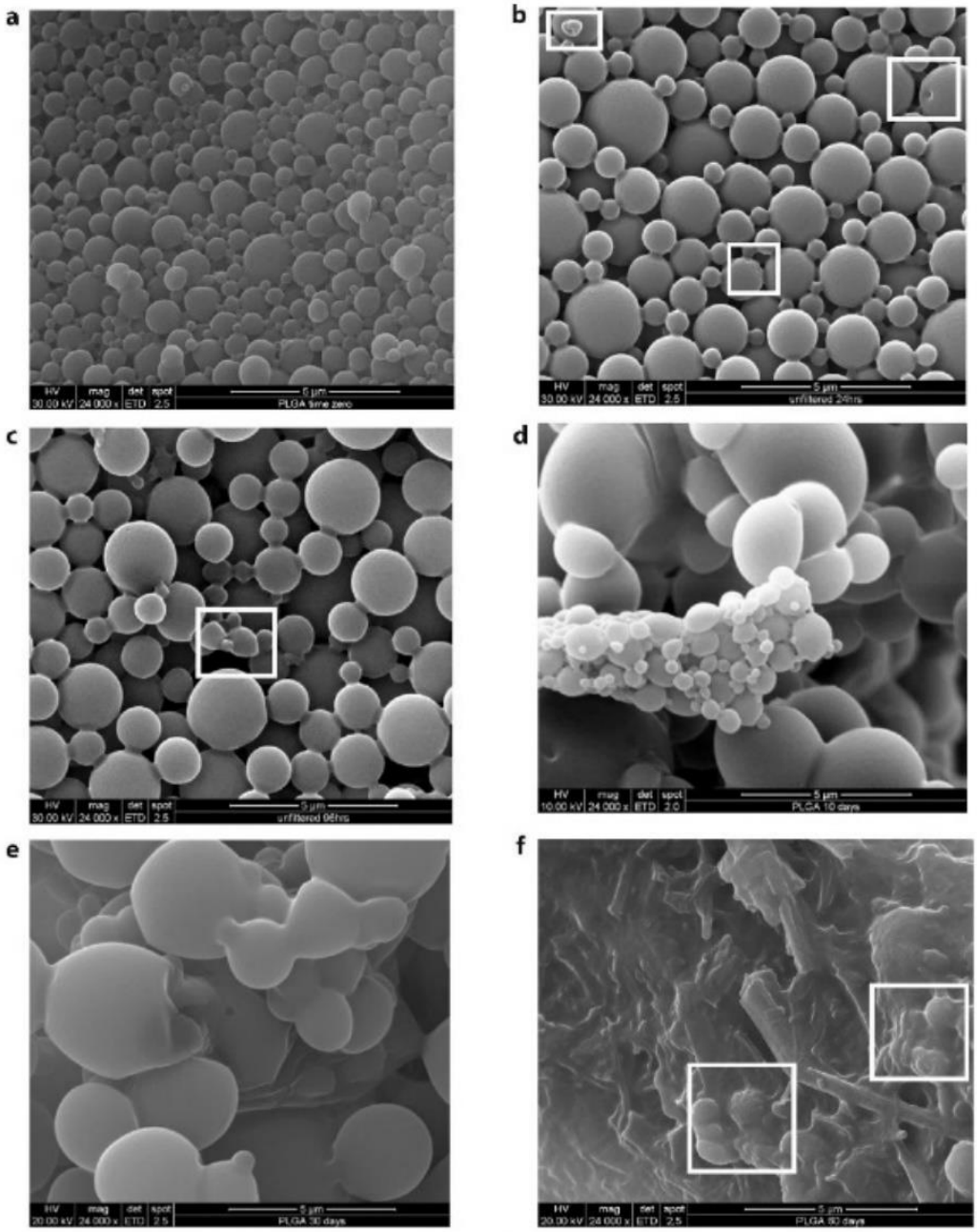

Fig. 2. SEM images of (a) lyophilized PLGA NP at room temperature and lyophilized PLGA NP after incubation at 37 °C for 1 day (b), 4 days (c), 10 days (d), 30 days (e) and 60 days (f). Early evidence of pitting on the NP surface (b) and loss of spherical morphology (c) are highlighted in the images for 1 day and 4 days incubation. Traces of spherical NP after 60 days incubation are highlighted in image (f). All SEM images (a)–(f) are at ×24 000 magnification.

a statistically significant P value (<0.05) compared to control, but not to each other. This means that RDP labelling did not have an effect on the toxicity of Dox-NP within the CHO cell line. This was not the case for the SH-SY5Y neuroblastoma cells, which had a significantly lower cell viability of 65.9%, when treated with the RDP-Dox NP compared to 78.3% when treated with the unlabeled Dox NP. The difference between these two treatment groups was approximately 13% and shown to be significant ($P < 0.05$), indicating alteration in cell viability due to RDP labelling.

3.2.2. Receptor identification study

In order to determine to which surface receptor RDP binds on neural cells, SH-SY5Y neuroblastoma cells were used alongside various inhibitors of the main neuron receptor types, namely the

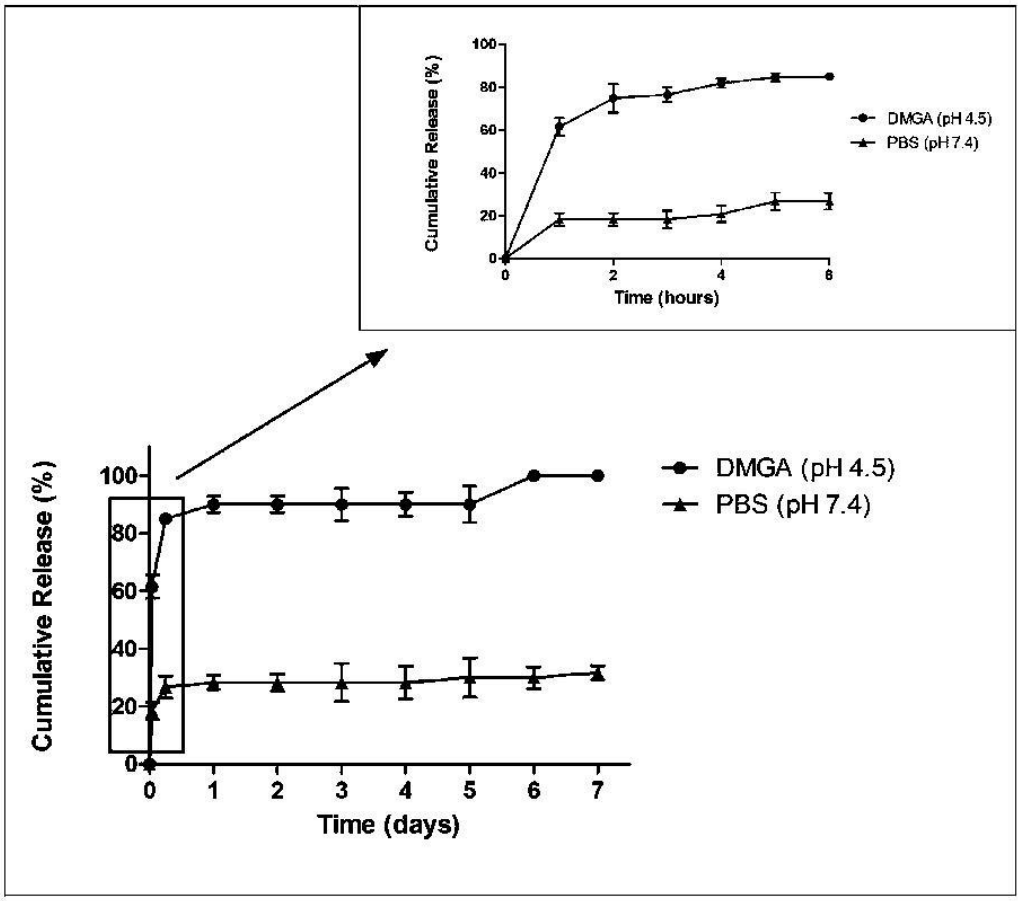

Fig. 3. In vitro doxorubicin release from PLGA NP at 37 °C measured over 7 days. Doxorubicin release was detected by UV–vis absorbance at 480 nm in either PBS at pH 7.4 or DMGA buffer at pH 4.5. Error bars represent ± standard error of the mean (n = 3).

GABA receptor and the nicotinic acetylcholine receptor (nAChR). Results from Figs. 4 and 5 provided evidence that RDP enhanced the cytotoxic effect of Dox NP on these cells specifically. SH-SY5Y cells were therefore an appropriate selection for receptor identification. Cells were pre-treated with either bicuculline or saclofen (competitive antagonists of the GABA receptor A and B subtypes, respectively) or hexamethonium (competitive antagonist of the nAChR).

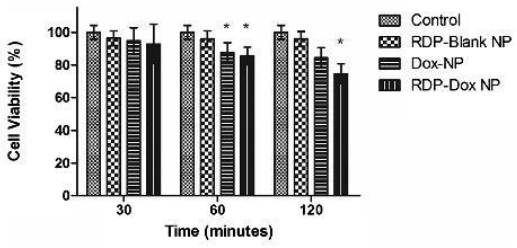

Fig. 4. Percentage cell viability of SH-SY5Y neuroblastoma cells following exposure to either serum free media (control), RDP-Blank NP, Dox-NP or RDP-Dox NP for 30, 60 and 120 min (20 μg of NP per each well of cells). Error bars represent ± standard error of the mean (n = 6). * Statistically significant difference compared to control (P value <0.05).

Results displayed in Fig. 6 shows that the hexamethonium pre-treated group was the only one to maintain a cell viability of 99.3%, compared to control. The GABA inhibitors bicuculline and saclofen were unable to prevent a significant decrease in cell viability, as

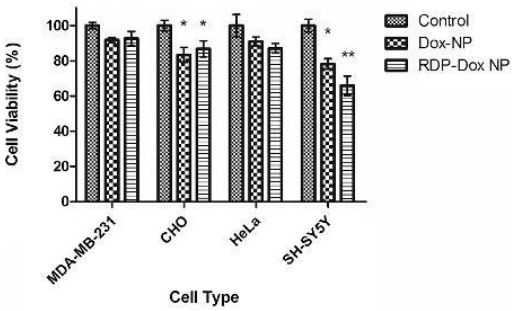

Fig. 5. Percentage cell viability of MDA-MB-231, CHO, HeLa and SH-SY5Y cells following treatment with either serum free media (control), Dox NP or RDP-Dox NP for 120 min (20 μg of NP per each well of cells). SH-SY5Y cells of neural origin, are the only cell line to show a statistically significant difference in cell viability between the Dox-NP group and RDP-Dox NP group (P value = 0.028, <0.05). Error bars represent ± standard error of the mean (n = 6). * Statistically significant difference compared to control; ** statistically significant difference compared to Dox-NP treatment.

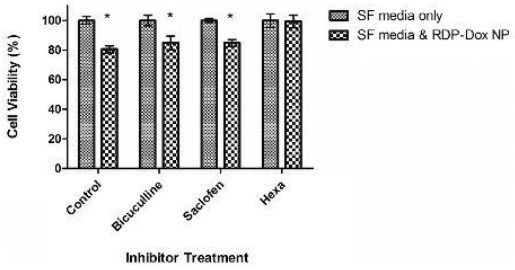

Fig. 6. Percentage cell viability of SH-SY5Y neuroblastoma cells following treatment with RDP-Dox NP (20 μg) for 120 min, to assess the effect of 30 min pre-treatment with different receptor inhibitors on RDP-facilitated NP uptake. Inhibitors were not toxic to cells, as percentage cell viability remained at 100.0% compared to control when treated with serum free (SF) media only. Hexamethonium (Hexa), the competitive nAChR antagonist, was the only inhibitor able to block the effect of NP treatment. Error bars represent ± standard error of the mean (n = 6). *Statistically significant difference compared with control; P value <0.05.

RDP-Dox NP treatment for 120 min caused cell viability to decrease to 84.8% ($P < 0.05$ compared to control) for both groups. This suggested that RDP did not depend on either GABA receptor subtypes for gaining cell entry, conflicting with the findings of Fu et al. (2013a). Treatment with hexamethonium, saclofen or bicuculline alone did not cause any cell death and so any decreases in cell viability was due to RDP-Dox NP treatment. The SH-SY5Y cell viability of the RDP-Dox NP treated cells with no prior treatment with a receptor inhibitor was 80.5%. This level of cell death was similar to the bicuculline and saclofen pre-treated groups, where there was approximately 16% cell death. In contrast, the hexamethonium pre-treated cells were significantly different to those with no prior inhibitor treatment ($P < 0.05$).

Fig. 7 shows that pre-treatment of SH-SY5Y cells with either AChRα7 antibody or the non-competitive nAChR antagonist mecamylamine prevented RDP-Dox NP-induced SH-SY5Y cell death, as cell viability remained at 100.0% compared to control. None of the inhibitors used in the experiments of both Figs. 6 and 7 are cell permeable, but rather bind to extracellular receptors. The lack of effect caused by RDP-Dox NP in the presence of hexamethonium, mecamylamine and AChRα7 antibody indicated a receptor-dependent mechanism of RDP cellular uptake.

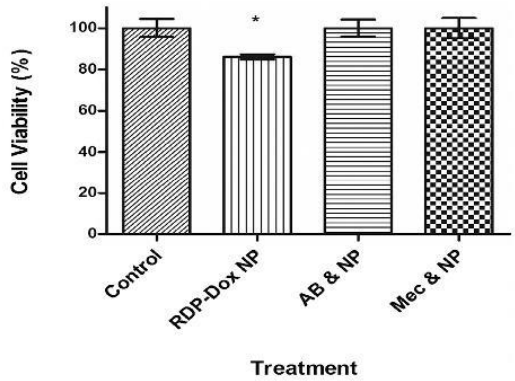

Fig. 7. Percentage cell viability of SH-SY5Y neuroblastoma cells following pre-treatment with different nAChR inhibitors and exposure to RDP-Dox NP (20 μg) for 120 min. Mecamylamine (Mec) and AChRα7 antibody (AB) both blocked the effect of RDP-Dox NP. Error bars represent ± standard error of the mean (n = 6). * Cell Viability = 86.1%; statistically significant difference compared to control (P value = 0.027, <0.05). NP = RDP-Dox NP treatment.

4. Discussion

In order for RDP to be advanced as a therapeutic CNS targeting ligand, it is necessary to know which neural surface receptor the peptide targets. This study aimed to determine which receptor RDP binds to on a neural SH-SY5Y neuroblastoma cell line following conjugation to a doxorubicin-loaded NP vehicle. The cytotoxicity of this formulation in neural and non-neural cell lines was also tested.

4.1. Evaluation of NP

Doxorubicin-loaded PLGA NP were successfully prepared with an EE of 50.30%, similar to that reported by Kalaria et al. (2009). The difficulty in achieving a high entrapment of doxorubicin is possibly owing to the high water solubility of doxorubicin hydrochloride (Cohen-Sela et al., 2009), causing partition of the drug to the outer aqueous phase of the double emulsion.

4.1.1. Dynamic light scattering (DLS)

Successful conjugation of RDP to the acid terminated PLGA caused average NP diameter to increase by no more than 20 nm compared to the blank and doxorubicin-loaded formulations, as shown in Table 1. RDP conjugation did however, have a considerable impact on the ZP measurement, as it increased to −5.51 mV. This can be explained by the amino acid sequence of the peptide- KSVRTWNEIIPSKGCLRVGGRCHPHVNGGGRRRRRRRRR, which is cationic due to the presence of two lysine residues and twelve arginine residues in total (Fu et al., 2012).

4.1.2. Scanning electron microscopy (SEM)

SEM was carried out on PLGA NP to visualize the effects of incubating in distilled water at 37 °C over various periods of time. Obvious swelling caused by water absorption through the NP polymer matrix lead to a progressive increase in NP diameter over time, with complete loss of nano-sized particles after 60 days (Fig. 2a–f). These NP have shown the ability to swell, form aggregates and develop pits over time, following a similar pattern of degradation to those imaged by Panyam et al. (2003), Stevanovic et al. (2007) and Hussein et al. (2013). This is advantageous, as the ideal drug delivery vehicle would not accumulate in the body over a long period of time.

4.1.3. Drug release

Receptor mediated endocytosis is the proposed mechanism of RDP cellular uptake (Fu et al., 2013a) and indeed for most NP modified with targeting ligands (Danhier et al., 2012). Resembling the endocytic process, data in Fig. 3 reveal how release of doxorubicin in DMGA buffer (pH 4.5) within the first hour was 40% greater than that released in PBS (pH 7.4). It could be postulated that the acidic environment at pH 4.5 is increasing the rate of drug diffusion out of the NP polymer matrix, possibly due to fully ionized doxorubicin (Ayen et al., 2011), which has a pK_a of 8.2 (Makkouk et al., 2015). Alternatively, the polymer may be undergoing faster degradation under acidic conditions (Fredenberg et al., 2011). Either one of these possibilities is likely to cause more doxorubicin payload release, compared to that observed at pH 7.4.

It is most likely that the mechanism of drug release in PBS (pH 7.4) over this 7-day period is largely by drug diffusion through water-filled pores in the PLGA polymer (Fredenberg et al., 2011). This is supported by the SEM data presented in Fig. 2, which generally indicates swelling of the NP rather than erosion in distilled water up to 10 days, at 37 °C. Hypothetically, it would only be when the NP are exposed to the progressively acidified environment of the endocytic pathway (Abdul-Hammed et al., 2010), that the full doxorubicin payload has the potential to be

released inside the cell. The low pH environment of the stomach means that oral administration would not be feasible for this type of NP formulation, but rather another form of systemic administration would be required for future *in vivo* studies.

4.2. In vitro evaluation

4.2.1. Cell cytotoxicity assay

SH-SY5Y neuroblastoma cells were treated with RDP- blank NP, Dox NP and RDP-Dox NP to assess cytotoxic effects over varying exposure times (Fig. 4). Treatment time of 120 min was sufficient to observe the effects of RDP in initial studies and so longer incubation of NP was not necessary. RDP conjugated to blank PLGA NP (RDP-blank NP) showed no significant cytotoxicity over this time period. This result showed that RDP can be used as a non-toxic targeting ligand in vitro and was in accordance with the in vivo findings by Fu et al. (2012, 2013a,b) on lack of RDP adverse effects.

Dox NP imparted 13% cytotoxicity on SH-SY5Y cells over both 60 and 120 min. This toxicity would be expected due to an initial release of cell permeable doxorubicin from the NP, according to the release data in Fig. 3. This was in contrast to the RDP-Dox NP formulation, where the amount of toxicity in SH-SY5Y cells was almost doubled to 25% after 120 min. Due to the fact that RDP itself does not appear toxic, this enhancement of cytotoxicity must be due to an increased accumulation of doxorubicin inside the cell. These results imply that RDP conjugation to the NP causes enhanced cellular uptake in a short period of time.

RDP has been previously shown to target preferentially neural cells, both in vitro and in vivo (Fu et al., 2012, 2013a,b). Results from Fig. 5 show that RDP significantly enhanced the cytotoxicity of the doxorubicin-loaded NP treatment in the SH-SY5Y neural cell type as opposed to the non-neural cell types (CHO, MDA-MB-231 & HeLa). It is clear from these findings that RDP enhanced cellular uptake of an attached nanocarrier within the neural cell line exclusively. It has already been conclusively shown by Fu et al. (2012, 2013a) that RDP does enter neural cells and this is an energy-dependent mechanism. If doxorubicin was causing local effects, results for Dox NP and RDP-Dox NP treatments would be similar for SH-SY5Y cells, as seen with the CHO, MDA-MB-231 and HeLa cell lines. To this end, it would appear that RDP retains the neurotropism of the parent glycoprotein, RVG.

4.2.2. Receptor identification

In order to determine which receptor is responsible for cellular interaction with RDP, different antagonists of the nAChR, GABA(a) and GABA(b) receptors were utilized to test the effect on RDP- Dox NP treatment of SH-SY5Y cells. Results from Figs. 6 and 7 revealed that the nAChR is necessary for RDP-Dox NP to have any significant effect on SH-SY5Y cell viability. A competitive nAChR antagonist (hexamethonium), a non-competitive nAChR antagonist (mecamylamine) and a specific antibody of the nAChR all prevented RDP-facilitated effects on SH-SY5Y cells. Conversely, blocking either GABA(a) or GABA(b) receptor subtypes had no effect in preventing a significant decrease in SH-SY5Y cell viability (Fig. 6). It can, therefore, be concluded from this work that the nAChR most definitely plays an important role in cellular interaction with RDP. It is most likely that via this receptor, RDP facilitates the internalization of a conjugated payload, leading to the specific effects observed in SH-SY5Y cells.

These findings conflict with Fu et al. (2013a), who reported that GABA itself prevented cellular uptake of RDP. It is possible that high concentrations of GABA causes desensitization of nAChRs through negative feedback mechanisms to control acetylcholine-mediated GABA release (McClure-Begley et al., 2014). If this were the case, it would falsely appear as though GABA is preventing RDP uptake via a GABA receptor rather than the desensitizing effect on the nAChR. In this instance, the nAChR may not be able to bind RDP and consequently undergo receptor-mediated endocytosis. This, however, does not explain why Fu et al. (2013a) found that nicotine was unable to prevent RDP uptake, unless RDP was able to outcompete the nicotinic agonist in a concentration dependent manner.

5. Conclusion

Early success and the attractive properties of this novel peptide for targeting neural cells can be attributed to inheritance of the strong neurotropism displayed by the parent glycoprotein, RVG. For the first time, a biodegradable doxorubicin-loaded NP formulation was prepared, with peripherally attached RDP. These conjugated NP impart increased cytotoxicity on SH-SY5Y neural cells but not to two non-neural malignant cell lines (MDA-MB-231 and HeLa cells) or a non-neural normal cell line (CHO cells). This study showed that RDP alone is non-toxic in vitro and in identifying the nAChR as necessary for RDP uptake, progression can be made in the development of this ligand for use in targeted drug delivery systems. The use of RDP within polymeric drug carrier formulations may provide a safe and valuable approach to neural cell-targeting, protecting sensitive therapeutics from enzymatic degradation whilst enabling BBB passage. This work provides a basis for the future development of RDP as part of a non-invasive, brain-targeted drug delivery system for use across a range of various disease states.

Acknowledgements

This work was supported by The Dowager Countess Eleanor Peel Trust [grant number- MBE/12005960.1] and the Department of Employment and Learning (DEL) Northern Ireland. Thanks to Dr Deborah Lowry (Ulster University) for proof-reading this manuscript.

References

Abdul-Hammed, M., Breiden, B., Adebayo, M.A., Babalola, J.O., Schwarzmann, G., Sandhoff, K., 2010. Role of endosomal membrane lipids and NPC2 in cholesterol transfer and membrane fusion. J. Lipid Res. 51 (7), 1747–1760.

Auffinger, B., Morshed, R., Tobias, A., Cheng, Y., Ahmed, A.U., Lesniak, M.S., 2013. Drug-loaded nanoparticle systems and adult stem cells: a potential marriage for the treatment of malignant glioma? Oncotarget 4 (3), 378–396.

Ayen, W.Y., Garkhal, K., Kumar, N., 2011. Doxorubicin-loaded (PEG)(3)-PLA nanopolymersomes: effect of solvents and process parameters on formulation development and *in vitro* study. Mol. Pharm. 8 (2), 466–478.

Betancourt, T., Brown, B., Brannon-Peppas, L., 2007. Doxorubicin-loaded PLGA nanoparticles by nanoprecipitation: preparation, characterization and in vitro evaluation. Nanomedicine 2 (2), 219–232.

Cohen-Sela, E., Chorny, M., Koroukhov, N., Danenberg, H.D., Golomb, G., 2009. A new double emulsion solvent diffusion technique for encapsulating hydrophilic molecules in PLGA nanoparticles. J. Control. Release 133 (2), 90–95.

Danhier, F., Ansorena, E., Silva, J.M., Coco, R., Le Breton, A., Preat, V., 2012. PLGA-based nanoparticles: an overview of biomedical applications. J. Control. Release 161 (2), 505–522.

Delehanty, J.B., Boeneman, K., Bradburne, C.E., Robertson, K., Bongard, J.E., Medintz, I.L., 2010. Peptides for specific intracellular delivery and targeting of nanoparticles: implications for developing nanoparticle-mediated drug delivery. Ther. Deliv. 1 (3), 411–433.

Fredenberg, S., Wahlgren, M., Reslow, M., Axelsson, A., 2011. The mechanisms of drug release in poly(lactic-co-glycolic acid)-based drug delivery systems-A review. Int. J. Pharm. 415 (1–2), 34–52.

Fu, A.L., Wang, Y.L., Zhan, L.P., Zhou, R.M., 2012. Targeted delivery of proteins into the central nervous system mediated by rabies virus glycoprotein-derived peptide. Pharm. Res. 29 (6), 1562–1569.

Fu, A.L., Zhao, Z.Z., Gao, F.Y., Zhang, M.M., 2013a. Cellular uptake mechanism and therapeutic utility of a novel peptide in targeted-delivery of proteins into neuronal cells. Pharm. Res. 30 (8), 2108–2117.

Fu, A., Zhang, M., Gao, F., Xu, X., Chen, Z., 2013b. A novel peptide delivers plasmids across blood-brain barrier into neuronal cells as a single-component transfer vector. PLoS One 8 (3), e59642.

Gastka, M., Horvath, J., Lentz, T.L., 1996. Rabies virus binding to the nicotinic acetylcholine receptor alpha subunit demonstrated by virus overlay protein binding assay. J. Gen. Virol. 77, 2437–2440.
Hussein, A.S., Abdullah, N., Ahmadun, F., 2013. In vitro degradation of poly (D: L-lactide-co-glycolide) nanoparticles loaded with linamarin. IET Nanobiotechnol. 7 (2), 33–41.
Kalaria, D.R., Sharma, G., Beniwal, V., Kumar, M.N.V.R., 2009. Design of biodegradable nanoparticles for oral delivery of doxorubicin: *in vivo* pharmacokinetics and toxicity studies in rats. Pharm. Res. 26 (3), 492–501.
Kumar, P., Wu, H., McBride, J.L., Jung, K., Kim, M.H., Davidson, B.L., Lee, S.K., Shankar, P., Manjunath, N., 2007. Transvascular delivery of small interfering RNA to the central nervous system. Nature 448 (7149), 39–43.
Lentz, T.L., 1991. Structure-function-relationships of curaremimetic neurotoxin loop-2 and of a structurally similar segment of rabies virus glycoprotein in their interaction with the nicotinic acetylcholine-receptor. Biochemistry 30 (45), 10949–10957.
Liu, Y., Huang, R., Han, L., Ke, W., Shao, K., Ye, L., Lou, J., Jiang, C., 2009. Brain-targeting gene delivery and cellular internalization mechanisms for modified rabies virus glycoprotein RVG29 nanoparticles. Biomaterials 30 (25), 4195–4202.
Makkouk, A., Joshi, V.B., Wongrakpanich, A., Lemke, C.D., Gross, B.P., Salem, A.K., Weiner, G.J., 2015. Biodegradable microparticles loaded with doxorubicin and cpg odn for in situ immunization against cancer. Aaps J. 17 (1), 184–193.
McClure-Begley, T.D., Grady, S.R., Marks, M.J., Collins, A.C., Stitzel, J.A., 2014. Presynaptic GABA(B) autoreceptor regulation of nicotinic acetylcholine receptor mediated [H-3]-GABA release from mouse synaptosomes. Biochem. Pharmacol. 91 (1), 87–96.
Panyam, J., Dali, M.M., Sahoo, S.K., Ma, W., Chakravarthi, S.S., Amidon, G.L., Levy, R.J., Labhasetwar, V., 2003. Polymer degradation and *in vitro* release of a model protein from poly(d, l-lactide-co-glycolide) nano- and microparticles. J. Control. Release 92 (1–2), 173–187.
Sajjanar, B., Saxena, S., Bisht, D., Singh, A.K., Manjunatha Reddy, G.B., Singh, R., Singh, R.P., Kumar, S., 2015. Effect of nicotinic acetylcholine receptor alpha 1 (nAChRα1) peptides on rabies virus infection in neuronal cells. Neuropeptides 54, 59–64.
Stevanovic, M., Savic, J., Jordovic, B., Uskokovic, D., 2007. Fabrication, in vitro degradation and the release behaviours of poly(DL-lactide-co-glycolide) nanospheres containing ascorbic acid. Colloids Surf. B-Biointerfaces 59 (2), 215–223.
Yan, X.Z., Mohankumar, P.S., Dietzschold, B., Schnell, M.J., Fu, Z.F., 2002. The rabies virus glycoprotein determines the distribution of different rabies virus strains in the brain. J. Neurovirol. 8 (4), 345–352.
Zhang, E., Fu, A., 2015. A new strategy for specific imaging of neural cells based on peptide-conjugated gold nanoclusters. Int. J. Nanomed. 10, 2115–2124.

Appendix 5

Design, Stability and Efficacy of a New Targeting Peptide for Nanoparticulate Drug Delivery to SH-SY5Y Neuroblastoma Cells

Rachel Huey[a], Dan Rathbone[b], Paul McCarron[a] & Susan Hawthorne[a]*

[a] School of Pharmacy & Pharmaceutical Sciences, Ulster University, Coleraine, UK.

[b] Aston Pharmacy School, Aston University, Aston Triangle, Birmingham, UK.

* Corresponding author- E-mail: s.hawthorne@ulster.ac.uk; School of Pharmacy and Pharmaceutical Sciences, Ulster University, Coleraine, Northern Ireland BT52 1SA, UK

Abstract

In recent years, rabies virus-derived peptide (RDP) has shown promise as a specific neural cell targeting ligand, however stability of the peptide in human serum was unknown. Herein, we report the molecular modelling and design of an optimised peptide sequence based on interactions of RDP with the α7 subunit of the nicotinic acetylcholine receptor (nAChR). The new sequence, named DAS, designed around a 5-mer sequence which demonstrated optimal nAChR binding *in silico*, showed greatly improved stability for up to 8 hours in human serum in comparison to RDP, which degraded within 2 hours at 37 °C. *In vitro* analysis using SH-SY5Y neuroblastoma cells showed that DAS-conjugated nanoparticles containing the cytotoxic drug doxorubicin (DAS-Dox-NP) displayed significantly enhanced cytotoxicity compared with untargeted doxorubicin-loaded nanoparticles (Dox-NP). DAS-Dox-NP had no significant effect on non-neural cell types, confirming its neural-specific targeting properties.

In this manuscript, we report the design and testing of an optimised peptide ligand, conjugated to a nanoparticulate delivery vehicle and specifically targeted to neural cells.. Future impact of an innovative targeting peptide ligand combining the ability to selectively identify the target and facilitate cellular internalisation could enable the successful treatment of many neural cell disorders.

Key words: peptide targeting, nanoparticle, drug delivery, neural cell, RDP

Abbreviations

DAS – newly designed targeting peptide

DOX- doxorubicin

DOX-NP – unlabelled doxorubicin-loaded nanoparticles

α7 nAChR - nicotinic acetylcholine receptor alpha 7 subunit

NP- nanoparticles

PLGA- poly (lactic-co-glycolic) acid

RDP- rabies virus derived peptide

RDP-DOX-NP – RDP-labelled doxorubicin-loaded nanoparticles

DAS-DOX-NP – DAS-labelled doxorubicin-loaded nanoparticles

sc-DAS – scrambled version of the newly designed targeting peptide

sc-DAS-DOX-NP – scrambled DAS-labelled doxorubicin-loaded nanoparticles

Introduction

Specific targeting of therapeutics is a growing area of research for a number of different disease states. The benefits of this over conventional drug delivery are numerous, including improved bioavailability of the drug at the target organ, reduction of unwanted side effects and smaller dosages required for therapeutic effect. Cell penetrating peptides (CPPs) can greatly enhance the intracellular uptake of conjugated cargo across biological membranes in a non-invasive, non-disruptive manner. However, due to lack of tissue specificity, CPPs such as TAT (transactivating transcriptional activator) peptide, penetratin and polyarginine are not as efficient when aiming to deliver expensive or toxic drugs [1]. One group of diseases which are difficult to treat and may benefit from targeted delivery methods are neural cell disorders such as neuroblastoma [2-4] and neurosarcoma [5].

Neural cell-specific peptide targeting ligands have been explored in the past decade to deliver therapeutic agents in animal studies with success [6-10]. Many promising neural cell-specific targeting peptides take advantage of native receptors, transporters or enzymes to deliver therapeutic cargoes. Derivatives from natural neurotoxic agents have been utilised due to their highly efficient transport abilities to nervous systems, such as tetanus toxin fragment C [11], neurotropic virus glycoproteins and fragments of snake, scorpion and bee venoms [10]. Thus far, promising results with these ligands are still surrounded with concerns of immune reactions and true specificity for neural cells only. Kumar et al. [6] first showed that a derivative of rabies virus glycoprotein (RVG), RVG-29, utilised nicotinic acetylcholine receptor (nAChR) transport to safely and non-invasively deliver siRNA to neuro-2a cells and mouse brain. Following this success, derivatives of RVG have since been utilised to take advantage of this property for drug delivery to the CNS to treat a range of brain disorders [12-14].

RVG found in the rabies virus envelope, is responsible for viral entry into the nervous system [15]. Rabies virus-derived peptide (RDP) is a 39-amino acid derivative of RVG, which has shown early success as a neural cell-targeting ligand both *in vitro* and *in vivo* [16-19]. In previous work [20], we reported that RDP is dependent upon interaction with the nAChR and activity was inhibited by blocking the homomeric α7 subtype of this receptor, commonly found throughout the nervous systems. An obstacle in the development of many peptide targeting ligands is the issue of serum instability due to proteolysis, hence breakdown of the peptide upon systemic administration. This is particularly true for larger sequences of amino acids, which may be more susceptible to enzymatic degradation *in vivo*. Fu et al. [16] reported that the approximate *in vivo* half-life of an RDP fusion protein in mice is only one hour. The stability of RDP ligand alone in human serum has not yet been reported, however given its relatively large size it could be subject to stability issues in future studies.

In this study, we report the molecular modelling, design and development of an optimised neural cell-targeting sequence, which we have termed DAS, based on interactions of RDP with the neural α7 nAChR subunit. Furthermore, we report the enhanced stability of DAS in human serum compared to RDP and highlight its ability to

specifically target neural cells with concomitant release of active nanoparticulate payloads.

Materials and Methods

Materials

Resomer® RG 502 H, Poly(D,L-lactide-*co*-glycolide)-PLGA, **acid terminated (**MW 7,000-17,000), dichloromethane (DCM), poly(vinyl) alcohol (PVA) 87-89% hydrolysed- MW 85,000-124,000, MES hydrate, 1-ethyl-3-(3-dimethylaminopropyl)-**carbodiimide** (EDC), N-hydroxysuccinimide (NHS), trichloroacetic acid (TCA), human serum from male AB plasma (USA origin), α-cyano-4-hydroxycinnamic acid (CHCA) matrix, 3-[4,5-dimethylthiazol-2-yl]-2,5 diphenyl tetrazolium bromide (MTT), hexamethonium and mecamylamine were all purchased from Sigma-Aldrich (UK). RDP, DAS and scrambled DAS (sc-DAS) peptides were synthesised by GL Biochem (Shanghai) Ltd. Nicotinic acetylcholine receptor-α7 antibody was purchased from Santa Cruz Biotechnology, Inc. (USA). Doxorubicin hydrochloride was obtained from VWR International (Pennsylvania, USA). Tissue culture reagents and media were purchased from Gibco®/ Life Technologies. Human cancer cell lines, SH-SY5Y (human neuroblastoma) and HeLa (human cervical cancer), were cultured in RPMI 1640 medium as were the normal CHO (Chinese hamster ovary) cell line. MDA-MB-231 (human breast cancer) cells were cultured in DMEM medium. Both RPMI 1640 and DMEM media were supplemented with 10% foetal bovine serum and 1% penicillin-streptomycin (5,000U ml^{-1}/5,000 µg ml^{-1}). All other chemicals were of analytical grade.

Design of novel targeting peptide

Step 1 Protein-ligand docking

Potential interactions between RDP and the α7 homomeric nAChR were explored, using α-subunit residues 173-204 as a starting point in this study. Original rabies virus glycoprotein (RVG) is reported to bind to these residues of the α1 nAChR subunit found at the neuromuscular junction (NMJ), hence facilitating the entry of the rabies virus into the nervous system [21, 22]. The coordinates of the neuronal nAChR α7 subunit, acetylcholine-binding protein were obtained from the Protein Databank entry 3SQ6, chain A [23]. This was imported into CACHe Worksystem Pro (version 7.5.0.85; Fujitsu Ltd). Hydrogen atoms were added using the default settings in line with presumed protonation states for ionisable amino acid side-chains. The positions of the added hydrogen atoms were optimised by locking the coordinates of all the non-hydrogen atoms and subjecting the system to a molecular mechanics (MM2) geometry optimisation. The 30-mer of RDP, KSVRTWNEIIPSKGCLRVGGRCHPHVNGGG, was divided into all possible contiguous ten amino acid fragments (residues 1-10; 2-11; 3-12 etc.) and each docked four times, using CACHe Worksystem Pro, into the

prepared protein structure from 3SQ6 where the potential active site was defined as residues 173 – 204. The amino acid side-chains in the defined active site were allowed to be flexible as were all rotatable bonds in the 10-mer proteins. The genetic algorithm settings for the docking protocol included population size 50, maximum generations 3000, crossover rate 0.8, mutation rate 0.2 and convergence when the RMSD population fitness was less than 1.

Step 2 Molecular dynamics simulations

The input files for molecular dynamics simulations of the docked protein-ligand complexes were prepared using the Antechamber module of the AMBER Tools package (Version 14) [24], implementing the ff14SB force field. Disulphide bonds were enforced between the receptor residue pairs 125 & 138 and 186 & 187. The system was neutralised by addition of sodium ions and then solvated within a truncated octahedron of TIP3P water molecules extending 8 Å from the surface of the protein. Using the Amber 14 molecular dynamics package CUDA version [25-27], the system was energy-minimised for 2,000 cycles using a non-bonded cut-off of 12 Å and then heated under constant volume to 300 K over 25 ps under Langevin dynamics (time step = 1 fs). The heating was continued at 300 K for a specified period under constant pressure also using Langevin dynamics (SHAKE on, time step = 2 fs) using the Particle–Mesh–Ewald (PME) method to treat the long range electrostatic interactions with a 12 Å non-bonded cut-off.

Step 3 Peptide design

Residues of interest from RDP (GCLRV) were identified from the work carried out in section 2.2.1- 2.2.2 and were subsequently incorporated into the design of a new peptide. A widely used flexible linking sequence -GGGGS- was subsequently added to the GCLRV sequence as a spacer in the design of a new peptide [28], to allow freedom of movement once conjugated to PLGA NP. Finally, two glycine residues followed by an arginine tail consisting of 6 alternating L- and D- arginine residues –GGRrRrRr- were also added to the sequence for enhanced stability and resistance to metabolic processes [29]. The new D-arginine-containing 18-amino acid sequence, which we have termed DAS, was NH_2-GGGGSGCLRVGGRrRrRr-COOH.

Serum stability of RDP and DAS peptides

Peptide stability testing in human serum was carried out according to a previously detailed method [30]. Briefly, human serum was diluted to 25% with phosphate buffered saline (PBS) and subsequently centrifuged at 18809 *g* for 10 minutes to remove lipids, before incubating at 37°C. RDP and newly derived peptide, DAS, were prepared so that final serum peptide concentration was 10 µM prior to incubation at

37°C. A 200 µL aliquot was removed from each serum-peptide mixture at various time points and reacted with 40 µL of 15% TCA for 15 minutes at 4°C to remove larger serum proteins. The collected samples were centrifuged at 18809 g to remove precipitated serum proteins for 10 minutes and supernatant collected for storage at -20°C. Samples were analysed by MALDI-TOF mass spectrometry (PerSeptive Biosystems Voyager-DE Biospectrometer, Herefordshire UK). A 10 µL aliquot of serum sample was mixed with 10 µL of CHCA matrix (10 mg/mL fully dissolved), 1.5 µL of which was used for analysis. The mass/charge ratio (m/z) was plotted against relative abundance.

Preparation of nanoparticles and conjugation of peptide to nanoparticles

Doxorubicin-loaded PLGA nanoparticles (Dox-NP) were prepared by a double emulsion technique and characterised according to methods previously described by this group [20]. FITC-Dextran-loaded PLGA nanoparticles (FITC-NP) for confocal fluorescence imaging were also prepared and characterized using the method previously described in [20] using 4 mg of FITC-Dextran per 100 mg of PLGA polymer. Entrapment efficiency (EE) of FITC-Dextran and doxorubicin in NP was determined using fluorescence spectroscopy (excitation 485 nm, emission 520 nm) and UV-Vis absorbance (480 nm) respectively, on a FLUOstar Omega microwell plate reader (BMG Labtech, Germany).

$$EE = \frac{Mass\ of\ drug\ in\ NP}{Mass\ of\ drug\ added}\ x\ 100\%$$

Peptides were conjugated to nanoparticles according to methods previously described by this group [20].

In vitro *assays*

Initial studies suggested that the presence of serum in the cell-based assay medium had minimal influence on the results of DAS-conjugated NP treatment (see Appendix 3). Therefore all assays were carried out in serum free medium to minimise possible interference associated with serum proteins in in vitro assays.

In vitro *cellular uptake study*

Cellular uptake of FITC-NP preparations were evaluated in SH-SY5Y and HeLa cell lines using a Leica SP5 confocal microscope (x 63,000 magnification). Cells were seeded onto 13 mm glass coverslips at a concentration of $1x10^5$ cells/mL (500 µL) and

cultured in complete RPMI media at 37°C/5% CO_2 overnight. All existing media was aspirated and the cells were treated with 1 mg/mL (500 µL) of either FITC-NP, RDP-FITC NP or DAS-FITC NP in serum free media (SFM) for 24 hours whilst incubating at 37°C/5% CO_2. Prior to imagining, all cells including controls were treated with 75 nM Lysotracker red in serum free media (SFM) for 30 minutes to visualise lysosomes in cells and track potential co-localisation with NP along the cellular internalisation pathway. FITC fluorescence emission was collected between 510- 550 nm (excitation wavelength 490 nm). Lysotracker emission was collected separately between 590-650 nm (excitation wavelength 580 nm).

In vitro *cytotoxicity study*

SH-SY5Y cells were plated out at a concentration of $1x10^5$ cells/mL (96 well plate) in complete RPMI media and incubated at 37°C/5% CO_2 for 16 hours. A range of DAS Dox-NP concentrations were initially tested to determine the most effective concentration to use for subsequent assays. All existing media was aspirated and the cells were then treated with 100 µL of serum free media (SFM) and either 60 µL of a 4 mg/mL NP suspension (final concentration 1.5 mg/mL) or an equivalent concentration of free peptide. Control wells were treated with serum-free media only. Cell viability was assessed after incubating for 24 hours (37°C/5% CO_2), using an MTT assay. To calculate cell viability, 25 µL of MTT (5 mg/ml) in PBS was added to each well on top of media and incubated at 37°C/5% CO_2 for 2 hours. After this, all media was aspirated and cells solubilised with 70 µL of DMSO per well. UV-Vis absorbance was read at 570 nm and cell viability calculated. To assess targeting specificity to neural cells, NP treatment was also added to non-neural cell lines CHO, HeLa and MDA-MB-231 according to the same protocol. The cytotoxic effect of a scrambled version of DAS (NH_2-RVGGCSGGGGGLRrRrRr-COOH) conjugated to Dox-NP (scDAS-Dox NP) was also assessed in SH-SY5Y cells.

We demonstrated previously that RDP function could be blocked with nAChR inhibitors [20]. To determine whether nAChR antagonists would affect the activity of DAS, SH-SY5Y cells were first preincubated for 30 minutes with either 1 mM hexamethonium (competitive), 1 mM mecamylamine (non-competitive) or anti-AChRα7 antibody (1:100 dilution), all in serum-free medium, prior to addition of Dox-NP or DAS-Dox NP, using the method described above.

Statistical Analysis

All results reported were statistically analysed using an unpaired t-test. A p value of < 0.05 was considered statistically significant.

Results

Design of novel targeting peptide

A model of the receptor was built using the X-ray crystal structure coordinates from the Protein Databank, entry 3SQ6, chain A [23]. For the purposes of the docking experiments the active site was defined as residues 173 – 204. The 30-mer RDP peptide was divided into all possible contiguous ten amino acid fragments (residues 1-10; 2-11; 3-12 etc.) and docked into the receptor. The 10-mer fragments were allowed full rotational flexibility as were the side-chains of the amino acids in the receptor active site. Each fragment was docked four times using a genetic algorithm protocol and the complexes were scored using potential of mean force (PMF: given in kcal/mol). Since the genetic algorithm uses an initial random number seed, the best (lowest energy) result only is reported for each 10-mer fragment in Table 1. [Table 1 near here]. The 10-mer fragment that gave the best binding enthalpy score (PMF energy) comprised residues 9-18 (IIPSKGCLRV). The best-scoring complex from this fragment was subjected to molecular dynamics in explicit water for 100 ns. After the first 50 ns of simulation it was noticed that not all of the 10-mer was interacting with the receptor. Residues 9 – 12 (IIPS) in particular were positioned on average orthogonal to the receptor surface and engaged with water molecules. A snapshot at 92 ns is shown in Figure 1 [Figure 1 near here]. .

Consequently, the initial receptor IIPSKGCLRV complex was cut down to a version containing residues 14-18 (GCLRV) and this complex was subjected to molecular dynamics in explicit water for 100 ns. After a settling period of approximately 60 ns, the GCLRV fragment adopted a fairly stable conformation (RMSD plot shown in Appendix 1) on the surface of the receptor with each amino acid, except for the N-terminal glycine, making hydrogen bonding interactions. Hydrophobic interactions with the receptor were also observed for the leucine and the valine residues in this fragment. A two-dimensional view of the receptor-GCLRV interactions can be found in Appendix 2. A new peptide (DAS) incorporating the GCLRV fragment from RDP was designed accordingly, consisting of 18 amino acids (GGGGSGCLRVGGRrRrRr) as described earlier in this report.

Serum stability of RDP and DAS peptides

RDP and DAS were incubated in 25% human serum at 37°C and then analysed by MALDI-TOF mass spectrometry to determine stability (Figure 2) [Figure 2 near here]. . RDP with no prior incubation (Figure 2B) gave rise to a peak consistent with its molecular weight of 4.6 kDa. Upon incubation in serum for 2 hours intact RDP was no longer detectable, however a new signal was detected between 2.7-3.2 kDa, most likely to be RDP breakdown fragments (Figure 2C). A minimal trace of RDP remained in Figure 2D, suggesting RDP and its degradation products had continued to degrade over 8 hours. Fully intact DAS expectedly gave rise to a peak at around 1.9 kDa indicated in Figure 2E, prior to incubation at 37°C. After 2 hours of incubation, approximately 60%

of the signal remained, as shown in Figure 2F. After 8 hours in serum, a small amount of intact DAS remained as indicated (Figure 2G). Over the time course observed the new 18-mer peptide, DAS, was more resistant to degradation by serum proteases than RDP.

Characterisation of NP preparations

Particle size, zeta potential, drug content and peptide conjugation efficiency of the formulations are shown in Table 2. PLGA NP were successfully loaded with either cytotoxic doxorubicin or FITC-Dextran with entrapment efficiencies of 64% and 77% respectively. [Table 2 near here].

In vitro cellular uptake

Visualisation of FITC-NP uptake by confocal fluorescence microscopy (Figure 3) demonstrates the ability of both RDP and DAS to preferentially target SH-SY5Y neural cells and promote cellular uptake compared to the untargeted FITC-NP [Figure 3 near here]. . In contrast, detected fluorescence signal was low in Hela cells and no notable difference in cellular uptake was observed between all formulations, indicating that RDP and DAS do not function as targeting peptides in this non-neural cell line. Furthermore, the signal detected by Lysotracker red indicates that there may be co-localisation of lysosomes and internalised FITC-NP in SH-SY5Y cells.

In vitro *cytotoxicity study*

The IC_{50} of DAS Dox-NP was calculated to be 0.9 mg/mL (Figure 4) [Figure 4 near here]. Figure 5 A shows the effect of DAS conjugation to Dox-NP in SH-SY5Y neural cells. Treatment with DAS-Dox NP caused a significant enhancement in SH-SY5Y cytotoxicity, as cell viability decreased to 60.0% (± 6.0% SD) compared with 82.7% (± 4.0% SD) when treated with untargeted Dox-NP. Figure 5 A also shows that neither free RDP nor free DAS peptides caused any significant decrease in cell viability. In addition, when a scrambled version of the DAS peptide was conjugated to Dox NP (sc-DAS-Dox NP), there was no significant decrease in cell viability compared to untargeted Dox-NP treatment [Figure 5 near here]. .

Figure 5 B shows the effect of preincubating SH-SY5Y cells with the nAChR antagonists hexamethonium, mecamylamine and anti- AChRα7 antibody. Pretreatment with all of the antagonists inhibits the cytotoxic effects of DAS-DOX-NP. These results suggest that DAS is facilitating uptake of cytotoxic NP through mechanisms involving the nAChR.

The effects of DAS-DOX-NP on the non-neural cell lines HeLa, MDA-MB-231 and CHO are shown in Figure 6 [Figure 6 near here]. . The cell viabilities for the normal, non-neural CHO cells and the cancer cell lines HeLa and MDA-MB-231 ranged narrowly from 62%-75% between all NP-treated groups. In the neural cell line SHSY-5Y however, both RDP and DAS promote susceptibility of the cells to the cytotoxic effects of Dox-NP showing a statistically significant decrease in cell viability for both RDP-Dox NP (59.7% ± 4.7% SD) and DAS-Dox NP (62.0% ± 9.8% SD) formulations compared to the untargeted Dox-NP (75.0% ± 7.1% SD).

Discussion

RDP is a peptide with a molecular weight of 4.6 kDa and, as such, its size may make it prone to proteolysis by serum proteases, which would severely limit its *in vivo* targeting ability and application. Therefore, design of a smaller and more proteolytically resistant peptide, which retains the sequence essential for binding to the nAChR, could be very beneficial. In earlier work, we reported that RDP requires the nAChR for function [20]. In this current work we modelled for interactions between RDP and the α7 nAChR subunit (which is specific to neural nAChR) [31] and uncovered a 5-amino acid section of the RDP sequence, -GCLRV-, which displays strong interactions with the α7 nAChR subunit and has potential for development as a new targeting sequence. The addition of poly-arginine residues to a peptide has shown to promote water solubility and confer highly effective cell penetrating properties to a conjugated cargo whilst prolonging circulation time [29,32], therefore we included six arginine residues at the C terminal of the new peptide and included half of them as the protease-resistant D amino acid. In doing this, the whole peptide should be less vulnerable to serum proteases and negatively charged plasma proteins, an effect which Liu et al. reported as similar to pegylation [32]. We also added the linker sequence -GGGGS- to the N terminal of the peptide, as described in the methods section, to allow free movement of the peptide once conjugated to the NP.

The reported use of RDP as a neural cell-specific targeting ligand both *in vitro* and *in vivo* has been a promising step towards facilitating delivery of therapeutics to neural cells [16-19]. However, there have been no reports on the stability of RDP in serum, with a previous stability study looking at RDP-conjugated nanoparticles concentrating on the stability of the payload and not the targeting peptide [33].

In this report, we have shown for the first time that RDP breaks down when incubated with human serum at 37°C within 2 hours (Figure 2C). Although this may be long enough to demonstrate an effect *in vivo*, it would be desirable to optimise the peptide sequence to make it less prone to enzymatic degradation in serum. If serum half-life could be extended then potential *in vivo* dosing would be lower and less frequent, which is preferable when utilising expensive or toxic therapeutic payloads. Our findings show that the new DAS peptide displays a considerable improvement in stability

characteristics compared to RDP, with mass spectrometry analysis detecting intact DAS peptide up to 8 hours after incubation in human serum at 37°C (Figure 2G). D-amino acids, such as the D-arginine residues incorporated into DAS, have been used to improve the proteolytic resistance of peptides successfully within the area of drug delivery due to their ability to avoid quick metabolism [29,34]. There have also been many reports in the literature on the use of D-amino acid substitutions to promote serum stability of targeting peptides which aligns with the results reported here [35-39].

In a previous publication, we demonstrated the use of RDP as a targeting ligand which enhanced the uptake of a conjugated nanoparticulate payload to induce cytotoxic effects in SH-SY5Y cells [20]. These findings are further supported by the confocal fluorescence images presented in Figure 3, which show RDP and DAS both facilitate NP uptake into neural cells specifically. It has been suggested by Fu et al. [17], that the cellular uptake mechanism of RDP may involve energy-dependent internalisation pathways such as clathrin-dependent endocytosis. Indeed, observations of co-localisation between RDP and DAS conjugates with lysosomes in our findings support this idea (Figure 3). In addition, we have also demonstrated that, like RDP, DAS significantly enhances cytotoxicity of Dox-NP in SH-SY5Y cells compared to untargeted DOX-NP and both free RDP and DAS peptides, which are non-toxic (Figure 5 A). When a scrambled version of DAS was conjugated to Dox NP (sc-DAS-Dox NP), there was no enhancement in cytotoxicity compared to untargeted Dox-NP treatment (Figure 5 A) demonstrating the necessity to retain the original –GCLRV- targeting sequence derived from RDP.

We also reported previously that nAChR antagonists prevented RDP action in SH-SY5Y cells [20] and the same inhibitors were employed to observe their effect on DAS peptide action. Mecamylamine, hexamethonium and antibody against α7 subunit of homomeric neuronal nAChR were able to block the effects of DAS-DOX-NP confirming that DAS does indeed bind to neuronal nAChR in the same way as RDP (Figure 5 B).

The results displayed in Figure 6 confirm the specific action of DAS as a neural cell-targeting ligand as it had no significant effect in three non-neural cell lines (HeLa, MDA-MB-231 and CHO).

In conclusion, the results described herein demonstrate that using molecular modelling and peptide design we have created a novel, bespoke neural cell nAChR targeting peptide, which we have termed DAS. This peptide displays an enhancement in serum stability whilst retaining neural cell specificity, and aids efficient cellular uptake and release of nanoparticle payloads. This targeted delivery system has potential for use in delivering therapeutics in a more specific manner to neural cells.

Acknowledgements

Special thanks to the Dowager Countess Eleanor Peel Trust and the Department of Employment and Learning (DEL) Northern Ireland for their financial support of this work.

Declarations of interest

Authors have no conflict of interest.

Funding

The Dowager Countess Eleanor Peel Trust [grant number- MBE/12005960.1] and the Department of Employment and Learning (DEL) Northern Ireland funded this work. Neither funding source was involved in the preparation or submission of this manuscript.

References

[1] Malhotra M, Prakash S. Targeted drug delivery across blood-brain-barrier using cell penetrating peptides tagged nanoparticles. Current Nanoscience. 2011;7(1):81-93.

[2] Louis C, Shohet J. Neuroblastoma: molecular pathogenesis and therapy. Ann. Rev. Med. 2014;66;49-63

[3] Whittle S, Smith V, Doherty E, Zhao S, McCarty S, Zage P. Overview and recent advances in the treatment of neuroblastoma. Expert Rev. Anticancer Ther. 2017;17:369-386

[4] Coughlan D, Gianferante M, Lynch C, Stevens J, Harlan L. Treatment and survival of childhood neuroblastoma: Evidence from a population-based study in the United States. Pediatric Hematology and Oncology. 2017;34:320-330

[5] Zehou O, Fabre E, Zelek L, Sbidian E, Ortonne N, Banu E, Wolkenstein P, Valeyrie-Allanore L. Chemotherapy for the treatment of malignant peripheral nerve sheath tumors in neurofibromatosis 1: a 10-year institutional review. Orphanet Journal of Rare Diseases. 2013;8:127-133

[6] Kumar P, Wu H, McBride JL, Jung K, Kim, MH, Davidson BL, Lee SK, Shankar P, Manjunath N. Transvascular delivery of small interfering RNA to the central nervous system. Nature. 2007;448(7149):39-43.

[7] Kwon EJ, Lasiene J, Jacobson BE, Park I, Horner PJ, Pun SH. Targeted nonviral delivery vehicles to neural progenitor cells in the mouse subventricular zone. Biomaterials. 2010;31(8):2417-2424.

[8] Zhang B, Sun X, Mei H, Wang Y, Liao Z, Chen J, Zhang Q, Hu Y, Pang Z, Jiang X. LDLR-mediated peptide-22-conjugated nanoparticles for dual-targeting therapy of brain glioma. Biomaterials. 2013;34(36):9171-9182.

[9] Gao Y, Wang Z, Zhang J, Zhang Y, Huo H, Wang T, Jiang T, Wang S. RVG-peptide-linked trimethylated chitosan for delivery of siRNA to the brain. Biomacromolecules. 2014;15(3):1010-1018.

[10] Soddu E, Rassu G, Giunchedi P, Sarmento B, Gavini E. From naturally-occurring neurotoxic agents to CNS shuttles or drug delivery. European Journal of Pharmaceutical Sciences. 2015;74:63-76.

[11] Toivonen JM, Olivan S, Osta R. Tetanus toxin C-fragment: The courier and the cure? Toxins. 2010;2(11):2622-2644.

[12] Liu Y, Huang R, Han L, Ke W, Shao K, Ye L, Lou J, Jiang C. Brain-targeting gene delivery and cellular internalization mechanisms for modified rabies virus glycoprotein RVG29 nanoparticles. Biomaterials. 2009;30(25):4195-4202.

[13] Chen W, Zhan C, Gu B, Meng Q, Wang H, Lu W, Hou H. Targeted brain delivery of itraconazole via RVG29 anchored nanoparticles. J Drug Target. 2011;19(3):228-234.

[14] Son S, Hwang DW, Singha K, Jeong JH, Park TG, Lee DS, Kim WJ. RVG peptide tethered bioreducible polyethylenimine for gene delivery to brain. J Controlled Release. 2011;155(1):18-25.

[15] Yan XZ, Mohankumar PS, Dietzschold B, Schnell MJ, Fu ZF. The rabies virus glycoprotein determines the distribution of different rabies virus strains in the brain. J Neurovirol. 2002;8(4):345-352.

[16] Fu A, Wang Y, Zhan L, Zhou . Targeted delivery of proteins into the central nervous system mediated by rabies virus glycoprotein-derived peptide. Pharm Res. 2012;29(6):1562-1569.

[17] Fu A, Zhao Z, Gao F, Zhang M. Cellular uptake mechanism and therapeutic utility of a novel peptide in targeted-delivery of proteins into neuronal cells. Pharm Res. 2013;30(8):2108-2117.

[18] Fu A, Zhang M, Gao F, Xu X, Chen Z. A novel peptide delivers plasmids across blood-brain barrier into neuronal cells as a single-component transfer vector. Plos One. 2013;8(3):e59642.

[19] Wu, J., Zhang, E. and Fu, A. A novel cell-permeable RDP-p53 fusion protein for specific inhibition on the growth of cancerous neural cells. Drug delivery. 2016, 23 (7), 2464-2470.

[20] Huey R, O'Hagan B, McCarron P, Hawthorne S. Targeted drug delivery system to neural cells utilizes the nicotinic acetylcholine receptor. Int J Pharm. 2017;525(1):12-20.

[21] Lentz TL. Rabies virus binding to an acetylcholine receptor alpha-subunit peptide. J Mol Recognit. 1990;3(2):82-88.

[22] Gastka M, Horvath J, Lentz TL. Rabies virus binding to the nicotinic acetylcholine receptor alpha subunit demonstrated by virus overlay protein binding assay. J Gen Virol. 1996;77:2437-2440.

[23] Li SX, Huang S, Bren N, Noridomi K, Dellisanti CD, Sine SM, Chen L. Ligand-binding domain of an α7-nicotinic receptor chimera and its complex with agonist. Nature Neuroscience. 2011;14:1253–1259.

[24] Case DA, Cheatham TE, Darden T, Gohlke H, Luo R, Merz KM, Onufriev A, Simmerling C, Wang B, Woods RJ. The Amber biomolecular simulation programs. J Chem Theory Comput. 2005;26:1668-1688.

[25] Salomon-Ferrer R, Goetz AW, Poole D, Le Grand S, Walker RC. Routine microsecond molecular dynamics simulations with AMBER - Part II: Particle Mesh Ewald. J Chem Theory Comput. 2013;9:3878-3888.

[26] Goetz AW, Williamson, MJ, Xu D, Poole D, Le Grand S, Walker RC. Routine microsecond molecular dynamics simulations with AMBER on GPUs. 1. Generalized born. J Chem Theory Comput. 2012;8:1542-1555.

[27] Le Grand S, Goetz AW, Walker RC. SPFP: Speed without compromise - a mixed precision model for GPU accelerated molecular dynamics simulations. Comput Phys Commun. 2013;184:374-380.

[28] Chen X, Zaro JL, Shen W. Fusion protein linkers: Property, design and functionality. Adv Drug Deliv Rev. 2013;65(10):1357-1369.

[29] Wender PA, Galliher WC, Goun EA, Jones LR, Pillow TH. The design of guanidinium-rich transporters and their internalization mechanisms. Adv Drug Deliv Rev. 2008;60(4-5):452-472.

[30] Nguyen LT, Chau JK, Perry NA, de Boer L, Zaat SAJ, Vogel HJ. Serum stabilities of short tryptophan-and arginine-rich antimicrobial peptide analogs. Plos One. 2010;5(9):e12684.

[31] Gotti C, Zoli M, Clementi F. Brain nicotinic acetylcholine receptors: Native subtypes and their relevance. Trends Pharmacol Sci. 2006;27(9):482-491.

[32] Liu Y, Lu Z, Mei L, Yu Q, Tai X, Wang Y, Shi K, Zhang Z, He Q. Tandem peptide based on structural modification of poly-arginine for enhancing tumor targeting efficiency and therapeutic effect. Acs Applied Materials & Interfaces. 2017;9(3):2083-2092.

[33] Gao Y, Wang Z, Zhang J, Zhang Y, Huo H, Wang T, Jiang T, Wang S. RVG-peptide-linked trimethylated chitosan for delivery of siRNA to the brain. Biomacromolecules. 2014;15(3):1010-1018.

[34] Purkayastha N, Eyer K, Robinson T, Dittrich PS, Beck AK, Seebach D, Kolesinska B, Cadalbert R. Enantiomeric and diastereoisomeric (mixed) L/D-octaarginine derivatives - A simple way of modulating the properties of cell-penetrating peptides. Chemistry & Biodiversity. 2013;10(7):1165-1184.

[35] Soudy R, Gill A, Sprules T, Lavasanifar A, Kaur K. Proteolytically stable cancer targeting peptides with high affinity for breast cancer cells. J Med Chem. 2011;54(21):7523-7534.

[36] Wang S, Noberini R, Stebbins JL, Das S, Zhang Z, Wu B, Mitra S, Billet S, Fernandez A, Bhowmick NA, Kitada S, Pasquale EB, Fisher PB, Pellecchia M. Targeted delivery of paclitaxel to EphA2-expressing cancer cells. Clinical Cancer Research. 2013;19(1):128-137.

[37] Di Grazia A, Cappiello F, Cohen H, Casciaro B, Luca V, Pini A, Di YP, Shai Y, Mangoni ML. D-amino acids incorporation in the frog skin-derived peptide esculentin-1a(1-21)NH2 is beneficial for its multiple functions. Amino Acids. 2015;47(12):2505-2519.

[38] Ngambenjawong C, Gustafson HH, Pineda JM, Kacherovsky NA, Cieslewicz M, Pun SH. Serum stability and affinity optimization of an M2 macrophage-targeting peptide (M2pep). Theranostics. 2016;6(9):1403-1414.

[39] Meng Z, Luan L, Kang Z, Feng S, Meng Q, Liu K. Histidine-enriched multifunctional peptide vectors with enhanced cellular uptake and endosomal escape for gene delivery. Journal of Materials Chemistry B. 2017;5(1):74-84.

Table 1. PMF docking scores for the 10-mer fragments ranked in order of score.

Fragment	PMF Docking Score (kcal/mol)
9_18	-815.10
17_26	-804.66
10_19	-791.05
12_21	-779.10
16_25	-767.22
11_20	-763.91
14_23	-754.99
8_17	-753.55
4_13	-752.98
21_30	-742.21
1_10	-728.43
18_27	-728.35
7_16	-723.68
13_22	-723.66
2_11	-721.83
6_15	-712.65
19_28	-703.93
20_29	-702.34
5_14	-693.11
3_12	-682.99
15_24	-639.01

Table 2. PLGA nanoparticle characterisation parameters.

NP sample	Size[a] (d.nm)	ZP[a] (mV)	DC[b] (µg/mg)	RDP[c] (µg/mg)	DAS[d] (µg/mg)
Dox-NP	242.7 ± 18.6	-14.6 ± 1.3	12.8	53.6	23.2
FITC-NP	286.5 ± 11.3	-10.3 ± 1.0	30.8	97.2	43.9

[a]Size and zeta potential (ZP) reported as average of three measurements ± standard deviation. [b]DC= drug content per 1 mg of NP based on entrapment efficiencies of 64% (Dox) and 77% (FITC); [c]RDP content per 1 mg of NP based on conjugation efficiency of 54% to Dox-NP and 73% to FITC-NP. [d]DAS content per 1 mg of NP based on conjugation efficiency of 58% to Dox-NP and 88% to FITC-NP.

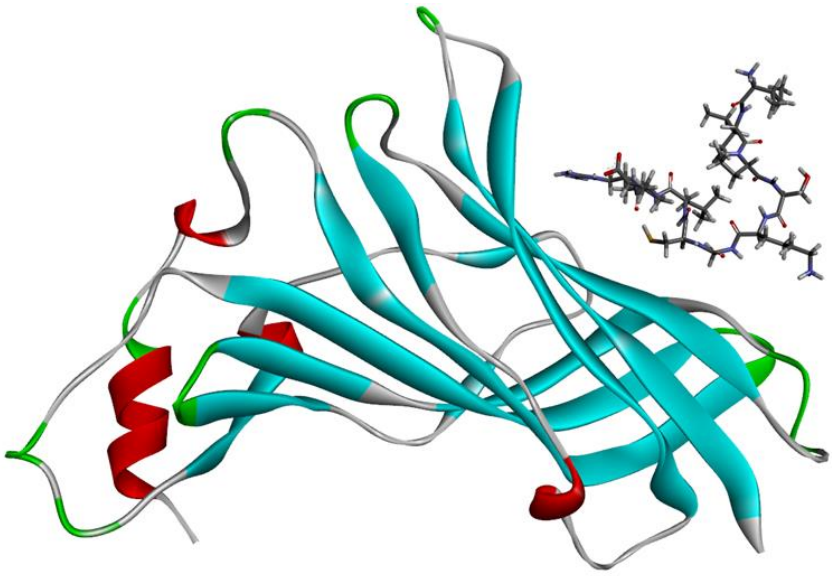

Figure 1. Snapshot at 92 ns from the molecular dynamics simulation of fragment IIPSKGCLRV (stick form) with the nicotinic acetylcholine receptor (ribbon form). Residues IIPS are not in contact with the receptor surface.

(A) Serum

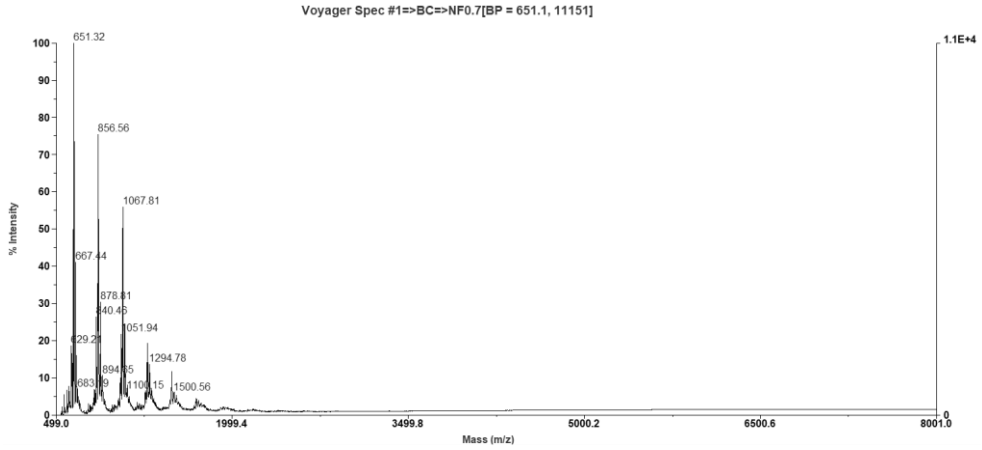

(B) RDP- T=0

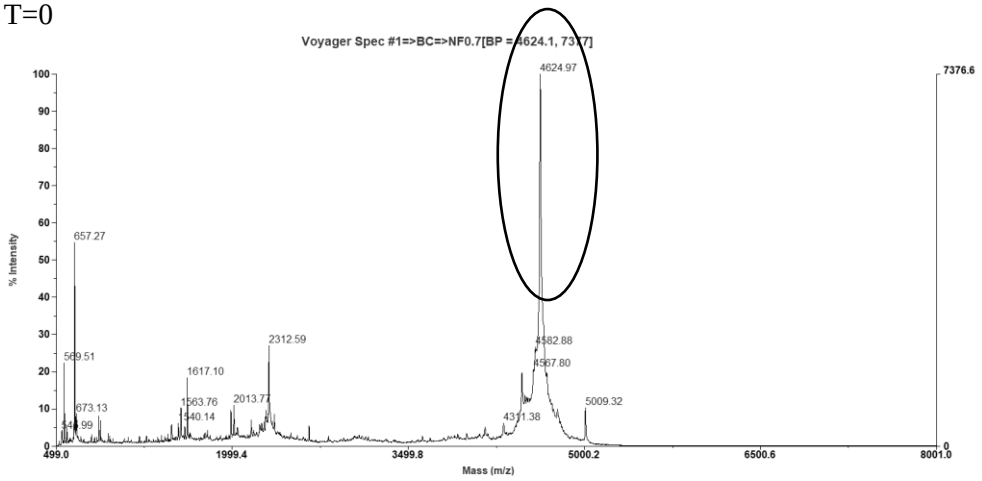

(C) RDP- T=2h

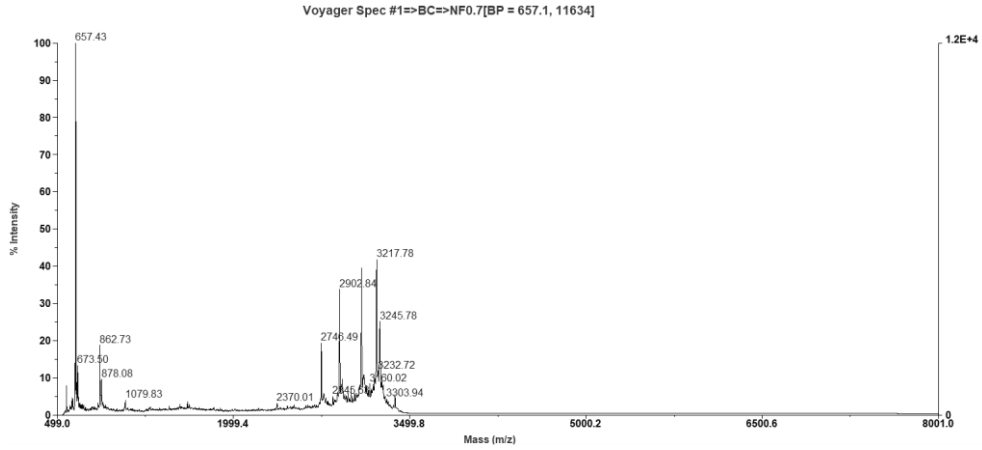

(D) RDP- T=8h

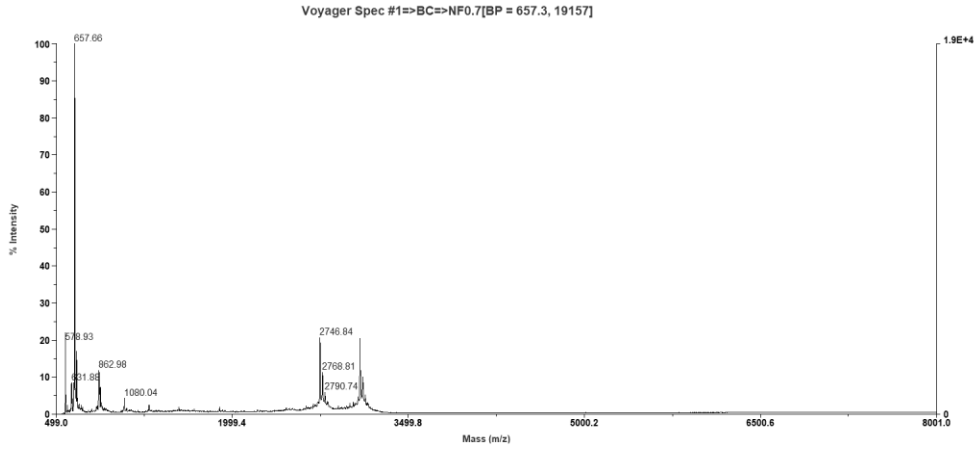

(E) DAS- T=0

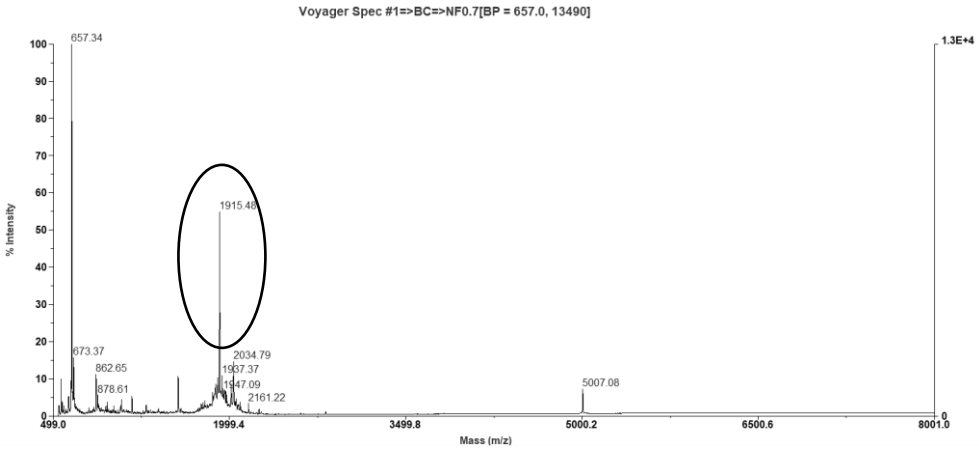

(F) DAS- T=2h

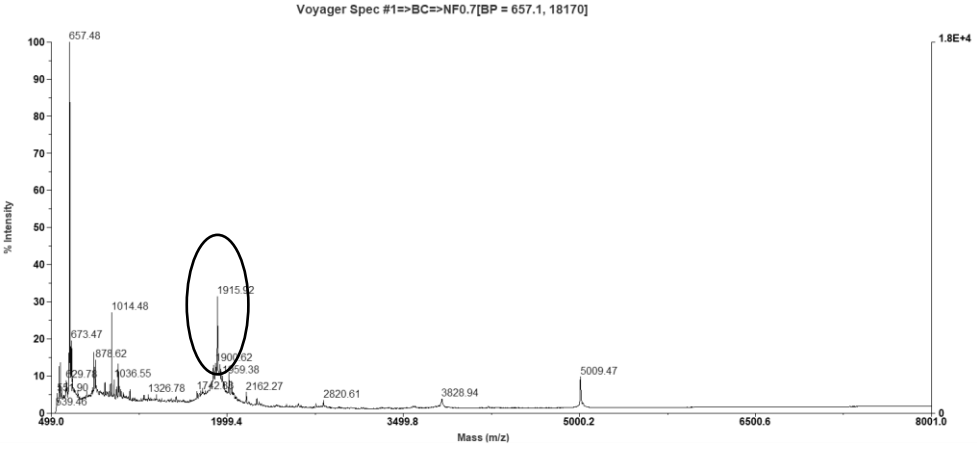

(G) DAS- T=8h

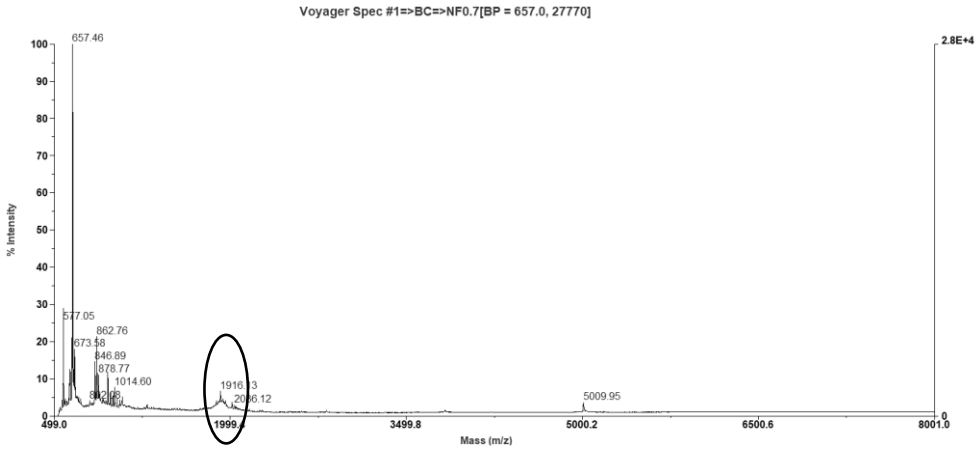

Figure 2. MALDI-TOF mass spectrometry analysis of peptide stability in 25% human serum at 37°C for various periods of time. (A) Human serum with no peptide. Profile detected for RDP (MW approx. 4.8kDa) in serum at time zero (B), 2 hours (C) and 8 hours (D) post incubation. Peaks for intact peptide are indicated by a circle on the intensity/mass traces. DAS peaks (MW approx. 1.9kDa) for the same time points are shown (E)-(G) respectively.

(A)

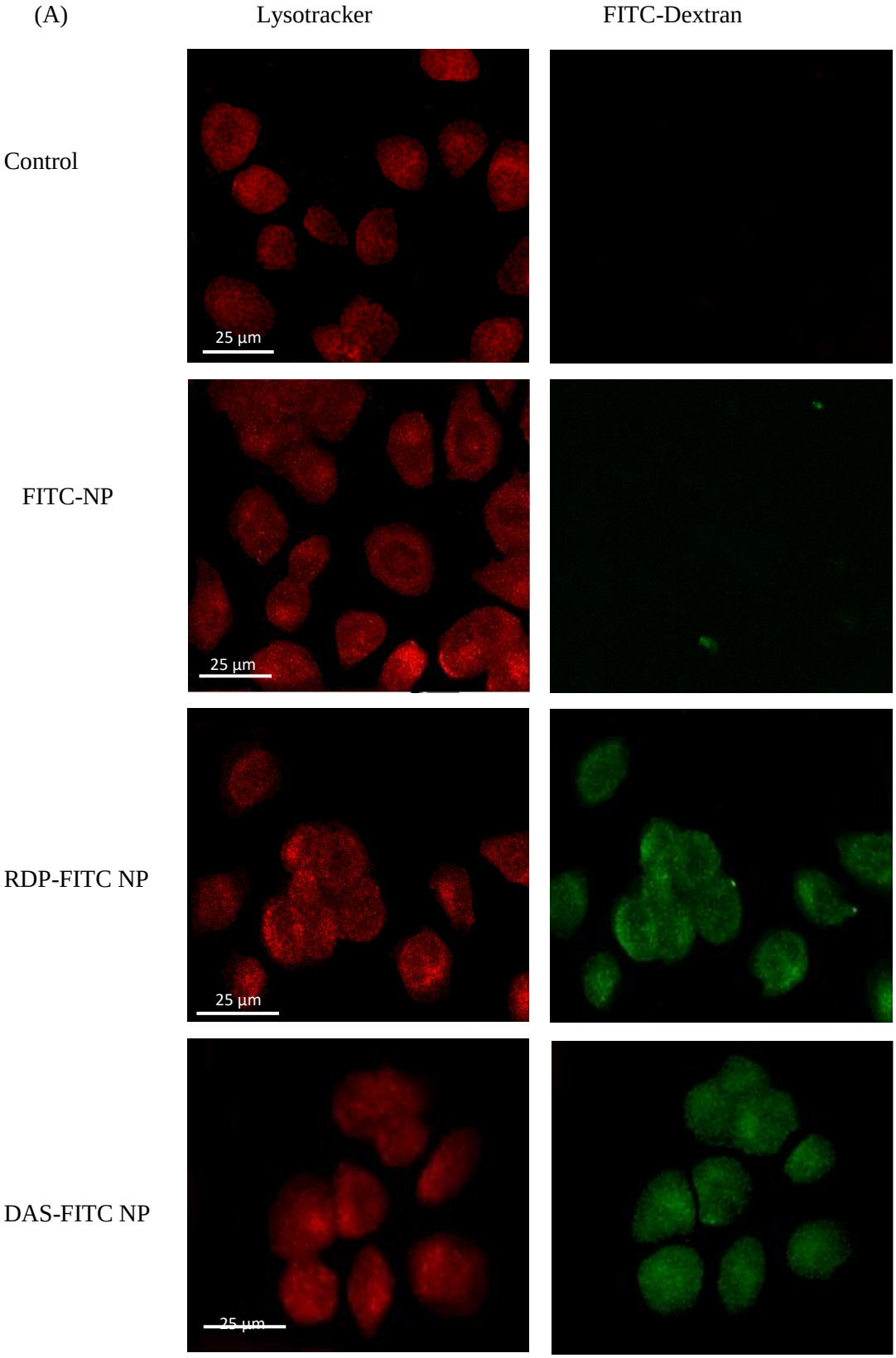
Lysotracker
FITC-Dextran
Control
FITC-NP
RDP-FITC NP
DAS-FITC NP
25 µm
25 µm
25 µm
25 µm

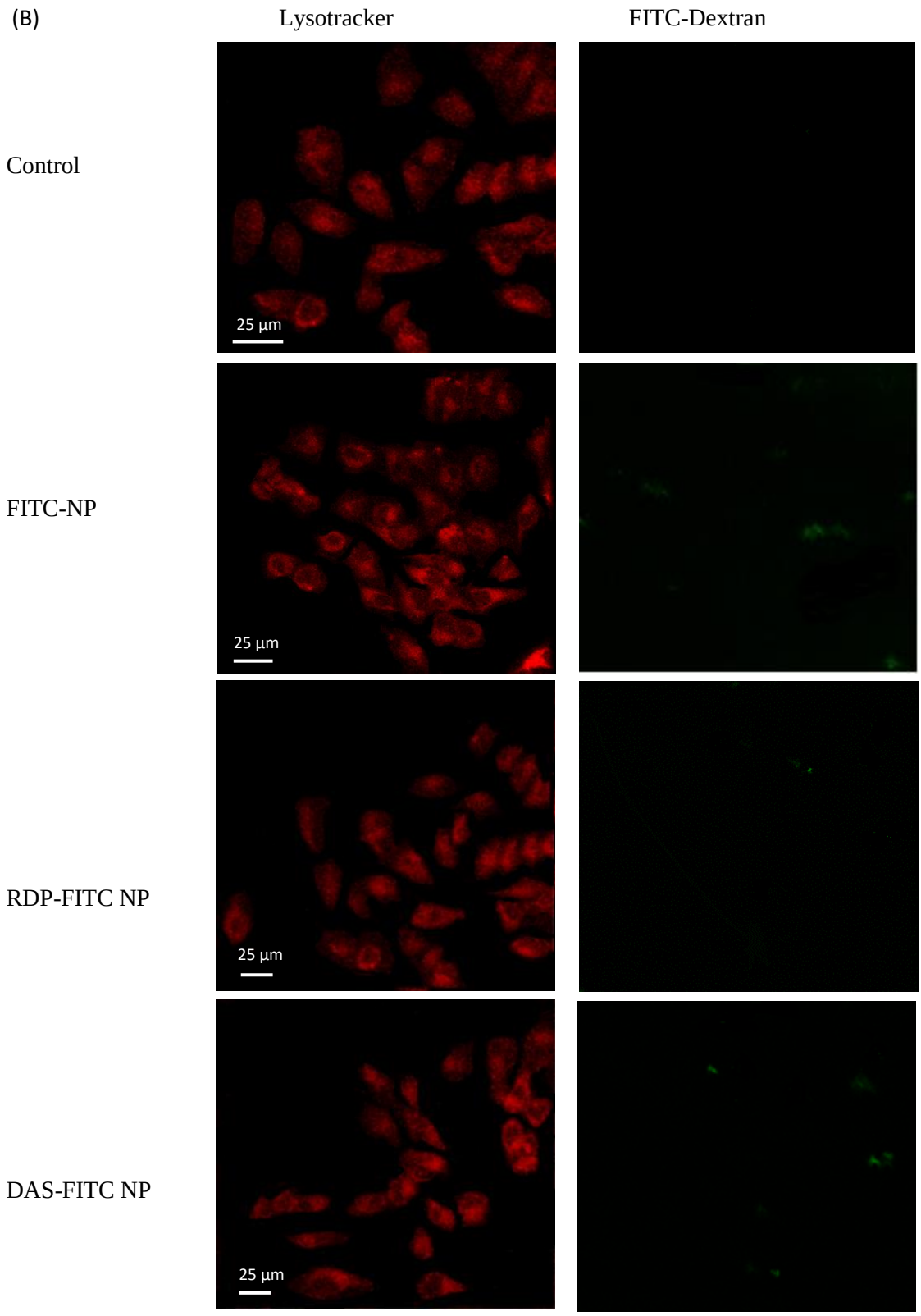

Figure 3. Confocal images showing the effect of RDP and DAS labelling on the cellular uptake of FITC-NP (green) in (A) SH-SY5Y cells and (B) HeLa cells.

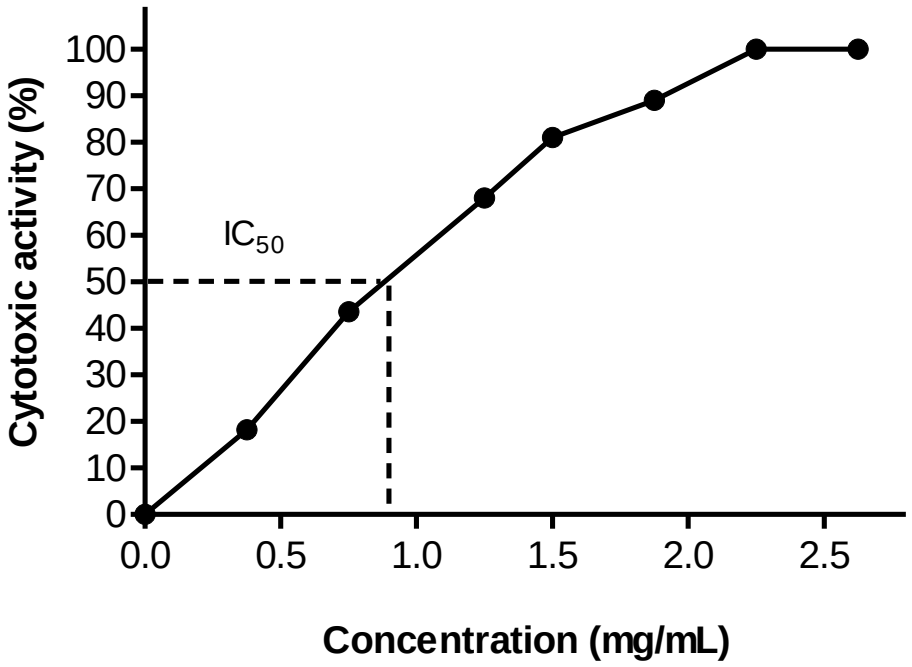

Figure 4. Determination of IC_{50} of DAS-DOX-NP on SHSY-5Y cells.

(A)

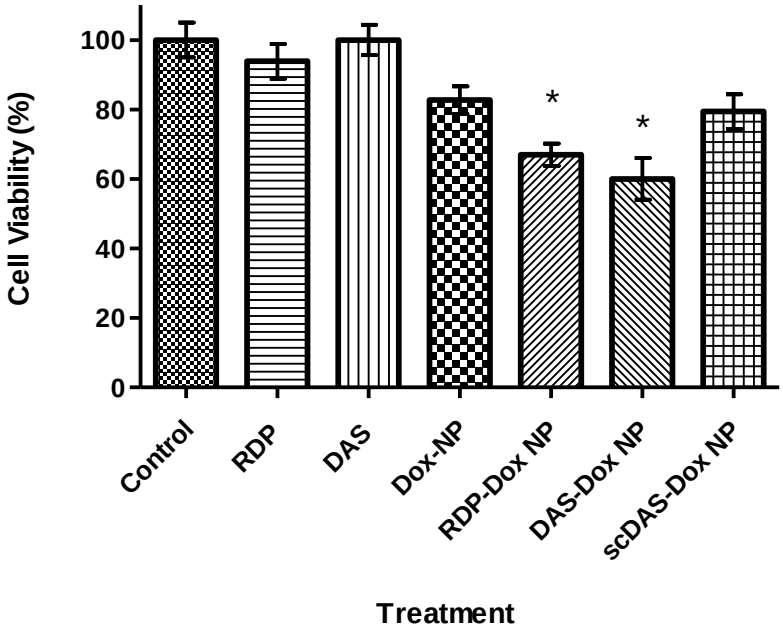

(B)

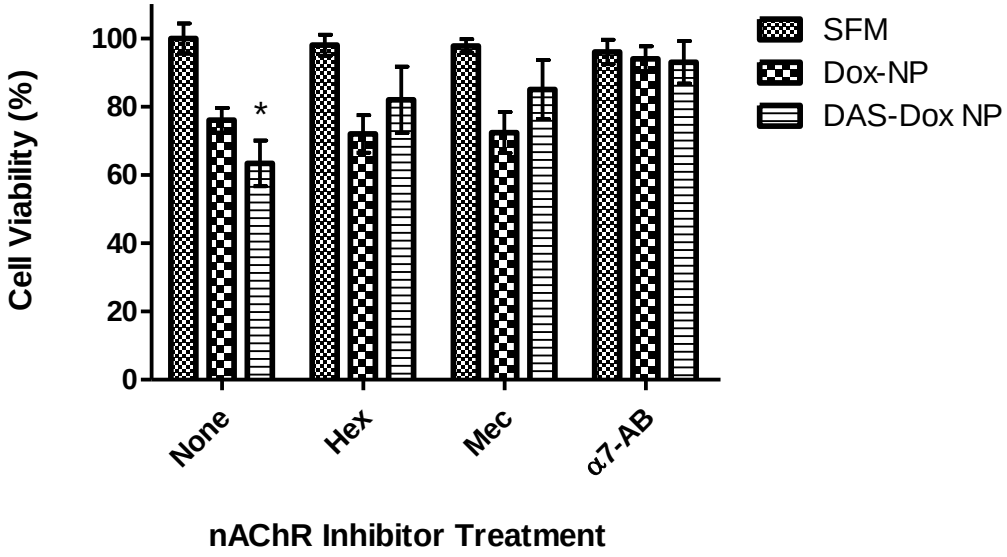

Figure 5. SH-SY5Y human neuroblastoma cell viability following treatment with (A) DAS-conjugated doxorubicin-loaded NP (DAS-Dox NP) compared to free peptide and unlabelled doxorubicin NP (Dox-NP) and scrambled DAS NP. Control samples were treated with serum-free media only. (B) Effect of nAChR antagonists hexamethonium (Hex) and mecamylamine (Mec) and antibody directed against alpha-7 subunit of homomeric neuronal nAChR (α7-AB) on DAS ligand activity on SH-SY5Y neural cells. * Statistically significant difference compared to Dox-NP (P value < 0.05).

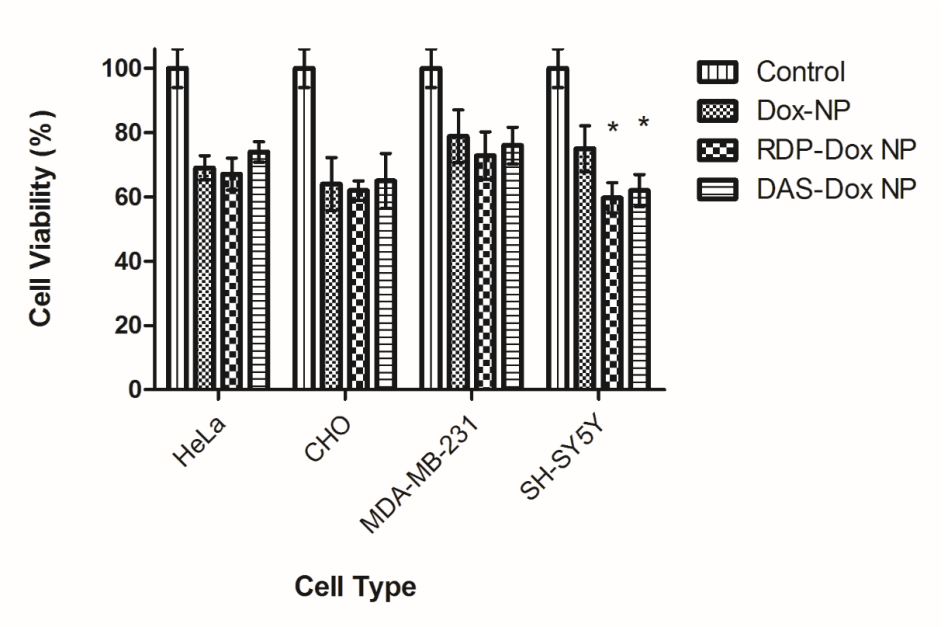

Figure 6. Effect of peptide targeting ligands RDP and DAS on doxorubicin-loaded NP toxicity towards non-neural cell lines HeLa, CHO and MDA-MB-231 compared to SH-SY5Y neural cells. Control groups were treated with serum-free media only. * Statistically significant difference compared to Dox-NP (P value < 0.05).

Appendix 1

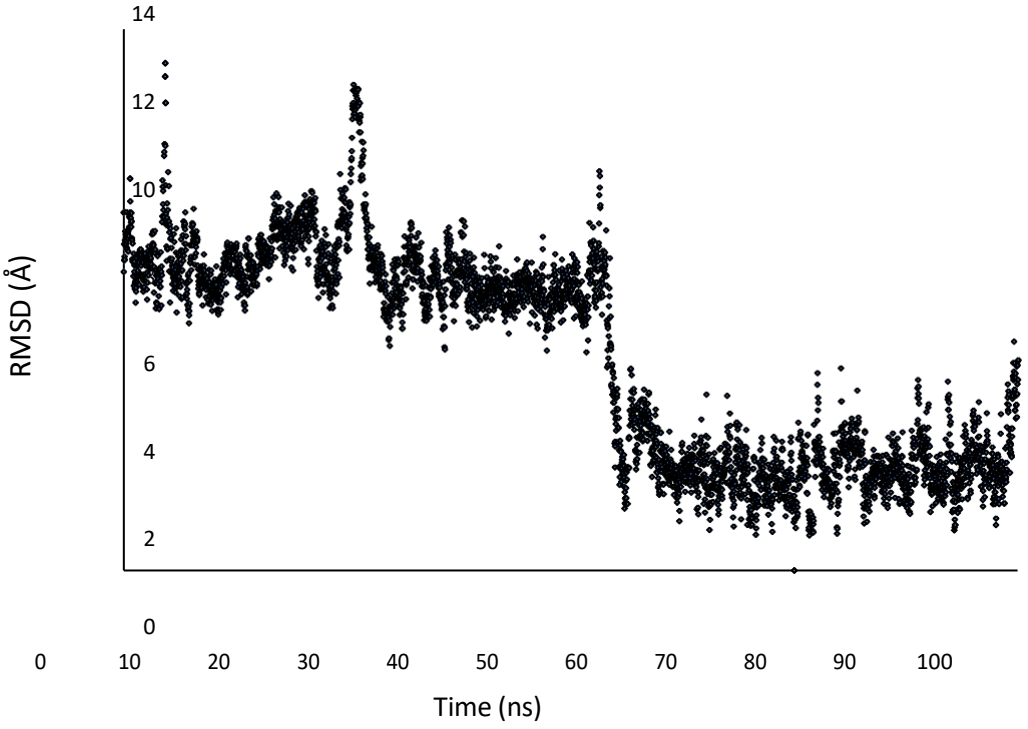

RMSD (Å) of the fragment GCLRV throughout a 100 ns molecular dynamics simulation in complex with the receptor, referenced to the simulation frame at 75 ns.

Appendix 2

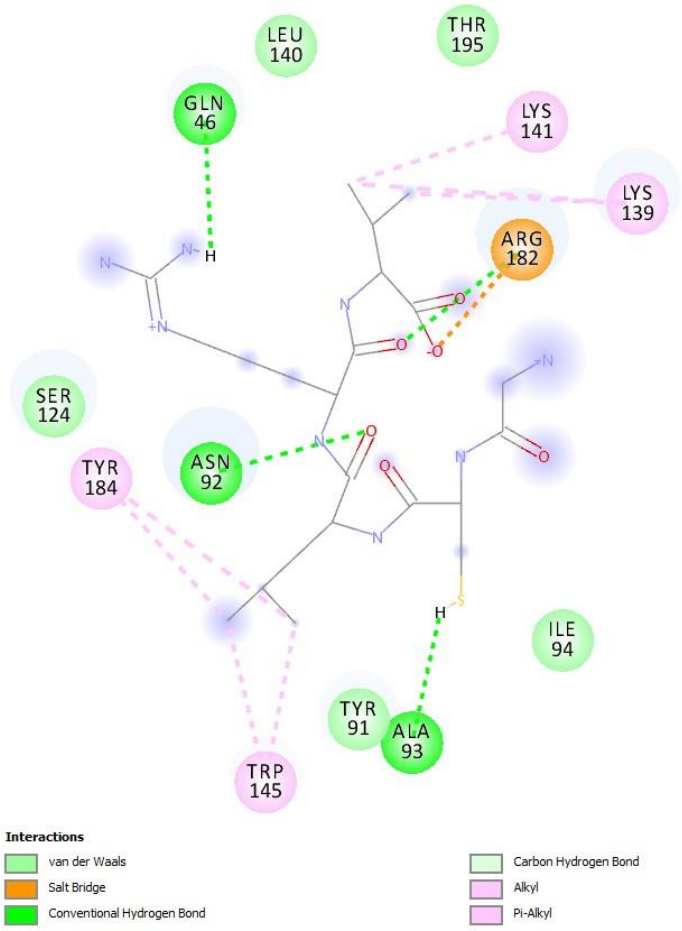

Two-dimensional view of the receptor-ligand interactions for GCLRV at 74 ns in the molecular dynamics simulation

Appendix 3

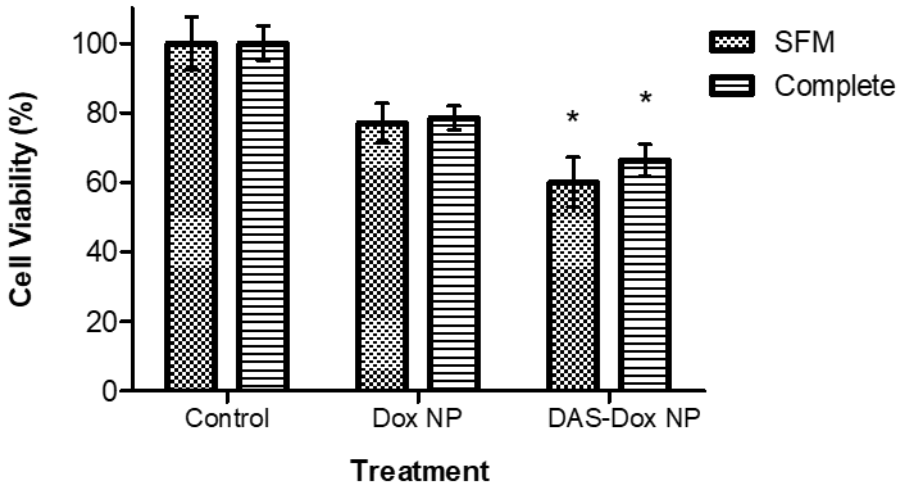

Cell viability of SH-SY5Y neuroblastoma cells following NP treatment in either serum-free medium (SFM) or with medium containing foetal bovine serum (complete). Control groups were treated with either SFM or complete media only. Cell toxicity was assessed by MTT assay following 24 hours of treatment at 37°C. *Statistically significant difference compared to Dox NP treatment (P value <0.05, n=6).